Ultrasonic atomisers for reducing pollution from petrol engines.

by

TERJE ALMÅS

A Thesis submitted to the University of Warwick

for the degree of Doctor of Philosophy

November 1975.

SUMMARY.

This thesis opens with a review of present knowledge about pollution from internal combustion engine exhaust, covering the formation of pollutants in the engine, some of the effects of emission on man, and the influence of various engine parameters on exhaust emission. The thesis describes the development and application of ultrasonic atomisers operating at approximately 100 kHz, the investigation of the formation of droplets in a liquid layer on a vibrating surface and the measurement of droplet size using liquid wax and microphotography.

Chapter 4.3 presents the results of calculations of eigenvalues and vibration amplitudes in an ultrasonic atomiser, using a three dimensional finite element programme.

Chapter 6.2 and 6.3 describes experiments on a two-stroke and a four-stroke engine which demonstrate the improvment in engine emissions which can be achieved using ultrasonic atomisers, particularly at low load.

Experiments were carried out with ultrasonic atomisers mounted in a novel carburettor unit, and the result were compared with the engine performance using a normal carburettor. A special manifold intended to achieve the best possible utilisation of the atomiser was designed and tested.

PREFACE.

Research on pollution from I.C. engines in the Department of Engineering of the University of Warwick started with the work described in this thesis.
Although no previous pollution research had been carried out in the Department, some of the necessary instruments and test equipment were available.

The test equipment for exhaust gas quality measurement was assembled from parts produced by well known firms. In order to collect information in this field I visited research institutes such as Shell Research Centre in Thornton, Ford Motor Company Central laboratory Laindon, SU-carburettors, Birmingham, British Leyland Motor Corporation, Coventry and the Royal Inst. of Aeronautical Engineering, Cranfield. I am pleased to acknowledge the valuable help and advice which I received from many specialist workers in these and other organisations.

Among the members of staff of the Engineering Department I would like to mention especially Dr. P.W. Johnson and Dr. C.J.N. Alty who were supervisors of the project.

I am also grateful to members of the Mechanical Technicians Pool and the University Workshops who have been involved in manufacturing parts and preparing experiments. I would like to mention especially Mr. A.E. Webb's support during the first two years of the work.

A Ford Pinto test engine was loaned to the Engineering Department by the Ford Motor Company for the project. Shell has also supported the project by providing equipment and also funds to cover travel expenses.

I am grateful to the Technical University in Trondheim for granting me sabbatical leave for the first year and to the Royal Norwegian Council for Scientific and Industrial Research for support during the second year of study. During the third year I received support from the British Council to whom I express my thanks.

CONTENTS

CONTENTS

NOMENCLATURE AND TERMINOLOGY

b.m.e.p. = brake mean effective pressure
CVS = Constant volume sampler
CPU = Computer processing unit
Curie temp. = temperature where magnetostriction is lost in transducers
Crystal = ceramic, piezoelectric material
DISA = Dansk Industri Syndikat A/s
ECE = Economic commission for Europe
FID = Flame Ionisation Detector
I.C. = Internal Combustion
NDIR = Non Dispersive Infrared analyser
p.p.m = parts per million
PCV = Positive crankcase ventilation
Transformer (velocity) = concentrator, horn
Transducer = arrangement to produce vibration

A = Area (m^2)
a = radius (m)
B = Transfer number
c = specific heat (J/kg K) (thermodyn.)
c = speed of sound in actual medium (m/s)
c_o = speed of sound in a rod (m/s)
c_B = speed of sound in infinite medium (B=Bulk) (m/s)
D = diameter (of droplet μm) (m)
d = piezoelectric constant $\left(\frac{\text{coul/m}^2}{\text{N/m}^2}\right)$ $\left(\frac{\text{strain}}{\text{field at c. stress}}\right)$ or $\left(\frac{\text{charge density}}{\text{stress at c. el. field}}\right)$
E = Youngs modulus (N/m^2)
F = force (N)
f = frequency (Hertz)
G = shear modulus (N/m^2)
g = piezoelectric constant $\left(\frac{\text{v/m}}{\text{N/m}^2}\right)$ $\left(\frac{\text{el field}}{\text{stress at c. charge}}\right)$ or $\left(\frac{\text{strain}}{\text{charge density at c. stress}}\right)$
h = heat transfer coefficient (W/m^2K)
I = acoustic intensity W/s (W/m^2)
i = nodal number
K = dielectric constant (clamped or free) (farad/m)
k = coupling coefficient (%)

κ = polytropic exponent
L = length (m)
M = magnification factor
M = total mass (kg)
m = mass (kg)
N = number
P = power (W)
P = sound pressure (N/m^2)
Q = Quality factor
Q = latent heat (J/kg K)
q = heat (J)
Re = Reynolds Number
S = Area normal to sound wave (m^2)
Sc = Schmidt Number
T = Temperature (K) (^oC)
t = time (s)
u = particle velocity (m/s)
v = particle velocity (m/s)
v = Specific volume (m^3/kg)
Y = Youngs modulus (N/m^2)
Z_{ae} = acoustic impedance

α = part of energy transmitted
λ_e = evaporation constant
λ = wavelength (m)
λ_c = capillary wave length (m)
ρ = density (kg/m^3)
ν = Poisson's ratio
ν = kinematic viscosity (m^2/s)
μ = dynamic viscosity (NS/m^2)
σ = surface tension (N/m^2)
σ = stress (N/m^2)
τ = shear stress (N/m^2)
Δ ="small part of"
ε = compression ratio
ε_o = permittivity constant of vacuum
ξ, ζ, η = displacement

Suffix: ac = acoustic; t = transmitted; r = refected; L = fuel; g = gas; s = surface; M = manifold; X,Y,Z = in direction (-)

LIST OF FIGURES

1 Introduction

The rapid growth of motor traffic over a relatively short period of time has caused much concern about motor vehicle emissions. In Britain alone the number of cars now exeeds 15 million. In recent years much research has been carried out to determine how dangerous the exhaustemissions from internal combustion (I.C.) engines are to human life and to nature in general. Although there is little evidence that the present level of pollution from engines represents a threat to health in Europe, the experience obtained in other countries, especially America and Japan, has led to the introduction of legislation which will reduce the level of pollutants from I.C. engines significantly if it can be met. Car manufacturers in Europe, Japan and the USA are endeavouring to find economical and good technical solutions that will make it possible to meet the legislation enacted in the various countries.
There is no "world standard" for acceptable levels of the different gas components in the exhaust stream. Various countries have enacted controls according to their environment and pollution characteristics. The legislation in the US, and in California in particular, is far more severe than in Europe.

The research described in this thesis is intended as a contribution to the solution of the problem of reducing pollution from I.C. engines without too much loss of power or efficiency. The author has tried to choose solutions which, if successful, could easily be adopted in commercial production of petrol en-

gines, and in particular has chosen to investigate the use of ultrasonic atomisation as a means of improving inlet system characteristics.

Ultrasonic atomisers used in the inlet systems of internal combustion engines have many advantages compared with conventional carburation or fuel injection systems. Low cost, small dimensions, very low power requirements and the fact that they do not need high pressure fuel feed are some of their main merits. However, when one starts from the very beginning in a field there are many elementary problems which take time to solve. In the field of ultrasonic atomisation very little previous work has been done and therfore there are few publications available to assist in the design of an atomiser. The first step of the project, namely to make a suitable and reliable atomiser, took a long time: its application in the actual engine inlet system still needs to be investigated further in order to find the best possible arrangement.
It is hoped that this thesis will assist the research which will surely be carried out in the future in this field.

1.1 Review of pollution from I.C. engines

1.1.1 Definition of pollution

When substances are added to the environment in such amounts that humans, animals, vegetation or materials are affected we are speaking of pollution.
Pollution is mostly regarded as waste emitted by man, but nature

is itself a source of pollution. For instance nitric oxides and hydrocarbons from I.C. engines are regarded as pollutants, although nature produces about 80% of the total volume of those gases emitted into the atmosphere. Furthermore it is necessary to look at the pollution problem both locally and globally.
The concentration of road vehicles causes pollution problems in certain areas, although seen globally there appears to be no reason for alarm.
It takes time for wind to remove the waste, for the vegetation to inspire gases or for soot to settle. The problem is that of disturbing the balance of nature. Where this balance is disturbed in the atmosphere and adverse effects arise we have air pollution.

Air pollution and water pollution are very closely related, and it would not be correct to discuss air pollution without also considering water pollution.
The oceans and our lakes and rivers play a very important part in the cleaning procedure of nature. Often the gases emitted into the atmosphere cause much more harm to life and vegetation when they enter the water than they cause by their presence in the air. Power stations burning fuels with high sulphur content can be a source of damage to fish in waters many hundreds of miles away.

As mentioned above, it is important to consider the effects of pollution both locally and globally.
In relation to pollution from I.C. engines the formation of carbon oxides shows this clearly. Carbon monoxide (CO) is perhaps the most dangerous gas emitted by gasoline engines. It is well

known that an engine running in a closed garage will cause certain death within a few minutes. Globally however, CO is not a problem. CO will oxidise in the atmosphere to carbon dioxide CO_2, which is not (yet) considered to be a pollutant as carbon dioxide plays a most important part of photosynthesis and the associated production of oxygen.

However, the increase in the atmospheric concentration of CO_2 of nearly 1 ppm per year is somewhat alarming. Although the effect of a change in atmospheric carbon dioxide content on the radiation balance is not fully clear, it has been shown (1) that the temperature at the earth's surface will rise because of the so-called greenhouse effect.

The most difficult part of the pollution problem concerns the partly unknown secondary effects. It is much easier to discover and understand primary effects, such as when poisonous gases are emitted into the atmosphere and cause a health danger.

A typical secondary effect of automotive pollution is smog. Smog in the atmosphere is a product of hydrocarbons, nitrogen oxides and sunlight.

There are several such hazardous secondary products of gasoline engine exhaust, many of which are not well understood. An even more dangerous secondary effect not related directly to I.C. engines is experienced in water, where micro-organisms can change nearly harmless compounds into a highly dangerous poison. Discoveries like those have been a warning to all research workers in pollution, in air or water, and have forced upon us a certain reluctance to regard an emittant as harmless.

1.1.2 Components in I.C. engine exhaust which are pollutants

The fuel used in combustion engines is a very complicated mixture of various hydrocarbons. In order to simplify the chemical reactions it is useful to consider the standardised fuel indolene.

Indolene is made mainly for petrol engine emission testing and has an average 1.86 atoms of hydrogen for each atom of carbon. The chemical formula for indolene can be written $C_7 H_{13.02}$.

If the combustion is complete the oxidation will give CO_2 and water (H_2O) as combustion products, beside nitrogen (N_2) which is not an active component in the combustion reaction itself.

$$C_7 H_{13.02} + 10.3\ O_2 + 38.7\ N_2 \rightarrow 7\ CO_2 + 6.51\ H_2O + 38.7\ N_2$$

according to this equation one mole of indolene requires for total oxidation 49 mole of air, and produces 7 moles of carbon dioxide and 6.51 moles of water. This means, in terms of mass, 1410.2 kg of air for every 97.0 kg of fuel. The correct air-fuel ratio for indolene is therefore 14.5 : 1. However, the real combustion process is more complex than that shown above. In practice it seems impossible to achieve complete oxidation, so that carbon monoxide is formed in considerable quantities. Additionally oxides of nitrogen are formed in the engine, owing to reactions which occur at the high temperatures present during combustion. Hydrogen is emitted only in small quantities. Some of the fuel will pass through the engine almost unchanged: other parts will be converted into very complicated organic compounds and be emitted as so-called unburned hydrocarbons.

Ordinary commercial petrol is not a clean product. Various components such as lead and other substances are added to the fuel to improve combustion properties, but there can also be other organic compounds present containing such elements as sulphur and nitrogen, which derive from the crude oil and are not completely removed during the distillation process. The content of sulphur in gasoline is regarded as not significant whereas it is often important in the combustion of the heavier diesel fuels. Components which are considered as pollutants in the gasoline engine exhaust are therefore:

Unburned hydrocarbons (HC) and oxides of HC

Nitric oxides (NO, NO_2 etc)

Carbon monoxide (CO)

Lead compounds

Smoke (carbon particles)

Additionally, there is some sulphur dioxide and traces of heavy metals, other than lead, added to the fuel and oil to give desired properties.

Sulphur dioxide and nitrogen dioxide are the only pollutants which are fully oxidised (burned).

For this project the lead compounds are not of particular interest. The most sensible thing one can do about lead seems to be to remove it from the petrol and design the engines to tolerate lower grade fuel (i.e. fuel with lower octane number). A reduction of lead content from 0.8 gram/litre to 0.4 gram/litre is already decided in many countries. Some countries have decided to reduce to 0.15 gram/litre These reductions are not ex-

pected to give the engine manufacturer any difficulties. Elimination of lead, however, could increase wear of the engine valves, but this problem could also certainly be dealt with. Even if the content of lead is reduced, there is no fundamental need to lower the compression ratio. The content of TEL (tetra ethyl lead) can be compensated for by the use of higher octane number aromatics.

However, instead of lead components in the exhaust the aromatics would increase the emission of polynuclear aromatics and aldehydes. Combustion engines with lower compression ratios seems to be the most obvious answer. However, the thermal efficiency is lower and therefore the specific fuel consumption higher. One can argue that, in the context of world fuel shortage, this is not desirable.

Some lead particle traps to be inserted in the exhaust system have been developed and are said to be effective.

1.1.3 The known effects on nature and man

Many of the gases mentioned in the context of engine exhaust pollution occur naturally and can be found all over the world.

The average concentrations in the atmosphere of gases of interest in connection with automotive pollution, are at sea level:

CO	0.1 ppm	HC (CH_4)	1.5 ppm
CO_2	320 ppm	O_3	0.02 ppm
NO_2	0.001ppm	SO_2	0.0002 ppm
N_2O	0.3 ppm	NH_3	0.01 ppm

Carbon dioxide

The level of carbon dioxide is 320 ppm. It is estimated that half of the carbon dioxide emitted to the atmosphere via combustion of fossil fuel remains in the atmosphere.
The rate of increase of CO_2 concentration is about 0.2% of the present total level per year. The concentration of CO_2 in the atmosphere influences the weather and it may ultimately be considered a pollutant. CO_2 is only poisonous to human beings at very high concentrations (15 000 ppm). It is, maybe, the irony of fate that the most important gas for oxygen production in the future has to be considered as a pollutant, although only about 10% of the total volume of CO_2 produced is man-made. 90% is due to biological decay, respiration and release from the oceans.

Carbon monoxide

Because of the uncertainty about the residence time of CO in the atmosphere it has been difficult to predict how big the natural production is, compared with the man-made sources. Recent research (3) carried out by a team from the US Argonne National Laboratory concludes that the natural emission of CO is many times greater than that from combustion engines. The combustion engine is, however, by far the biggest source of man-made carbon monoxide (90%).
As stated earlier CO-pollution is not a global danger but a local one. Cities with heavy road traffic can have considerable concentrations. On a traffic island in London a five minute average of 50 ppm has been measured. The average over a day on

the same island was about 35 ppm.

According to air quality standards of 1971 in the United States, the 8 hour level is 9 ppm and the 1 hour level 35 ppm. The emergency level is however as high as 240 ppm for one hour. At 240 ppm CO concentration there is said to be danger of acute sickness or risk of death in groups of sensitive persons.

Carbon monoxide is no doubt the most widespread pollutant from combustion engines, but there are only a few cities in the world where an 8 hour average is measured higher than 9 ppm. The toxicity of CO is due to the fact that the haemoglobin in the blood that carries oxygen to various parts of the body has a higher affinity for carbon monoxide than for oxygen. In air polluted by carbon monoxide the haemoglobin gradually gets "occupied" by CO until an equilibrium value is reached, depending upon the CO concentration in the air. Insufficient oxygen transport may result.

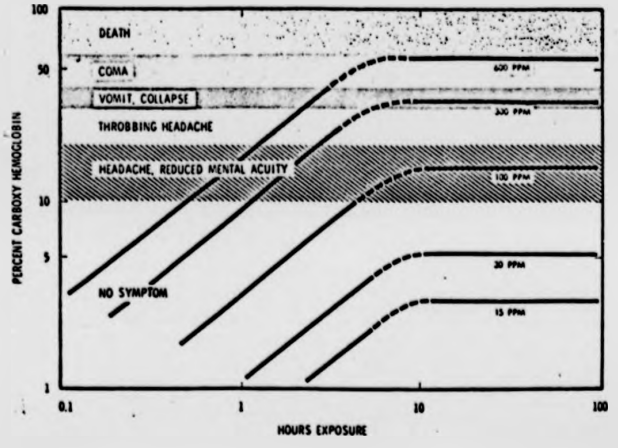

Fig. 1 Toxicity of carbon monoxide

Figure 1 shows (2) that a person will eventually get a warning of a dangerous CO-level at approximately 100 ppm after 5-8 hours exposure. This varies of course from person to person. A smoker for instance has far more carboxy- haemoglobin in the blood than a non-smoker (up to 5% COHb) and would react differently. (Cigarete smoke contains about 400 ppm CO when inhaled into the lungs.)

Little is known about the effects of exposure to low concentrations of CO over very long periods of time. Research must be used to test allegations that even 15 ppm reduces the oxygen supply to the brain sufficiently to affect brain function. The removal mechanism for CO in nature is not known with certainty, but it is thought that CO oxidises to CO_2 by means of a radical chain reaction giving the CO lifetime in the surface atmosphere as low as 2-3 months (3).

Unburned hydrocarbons (HC)

More than 80% of the hydrocarbons emitted into the atmosphere is from natural sources.
The main hydrocarbon produced in nature is methane (CH_4). The removal occurs by means of reactions with NO, NO_2 and O_3. It is believed that oxidation of CH_4 (by OH) in the troposphere is the main producer of natural CO (as much as 4×10^9 tonnes annually) (3,4) (Pollution is calculated as 0.22×10^9 tonnes) (6).
There is no evidence that the hydrocarbons emitted to the atmos-

phere by combustion engines are directly harmful to health even at the concentrations measured in areas with heavy road traffic. Some (partly) oxidised hydrocarbons , in particular aldehydes, cause eye irritation and odour (especially formaldehyde and acrolin).

More important is the role HC plays together with nitric oxides (NO_x) to generate photochemical smog and peroxy- nitrates (e.g. PAN). The undesirable effects of smog include damage to plants, material damage, poor visibility in the atmosphere, eye irritation and toxic effects, most of which are believed to be coused by oxidising agents such as ozone, nitrogen dioxide and PAN.

Many different types of hydrocarbon can occur in exhaust gas and their tendency to form smog is not uniform. The unsaturated hydrocarbons have the highest reactivity, with the reactivity depending upon the location of double or triple bonds. The reactions are very complicated and are not fully understood. The presence of NO_x is, however, just as important in smog formation as HC. The hydrocarbon acts as fuel for the photochemical reaction and the NO_x as both fuel and catalyst.

However, it is maintained that there is enough NO_x in the air, without vehicle exhaust emission, for photochemical reactions to occur. This is certainly one of the reasons why legislation has been enacted to reduce HC before reduction of NO_x. As will be discussed later, the HC component is much easier to remove from the exhaust gases than is NO_x.

Nitrogen oxides NO_x

Nature produces approximately ten times as much NO_x as is caused by man-made pollution sources. Of the nitrogen oxides found in combustion engine exhaust only nitrogen dioxide is toxic at low concentrations. NO_2 is more toxic than CO and the US federal air quality standard is set as low as 0.05 ppm (annual exposure.)

Concentrations in excess of 10 ppm can cause death. Experiments shows that a concentration of 0.5 ppm produces loss of eye lashes and causes chronic disorder of the lung tissues and the respiratory system. For normal urban levels of NO_2 there is no evidence that exposure is a health hazard. Nitrogen oxides (NO_x) are present in the exhaust mainly as nitric oxide (NO). Only about 2 to 3% is NO_2.

Nitric oxide mixed with oxygen in the air will oxidize rapidly to NO_2.

$$2\ NO + O_2 = 2\ NO_2$$

The oxidation process is dependent on oxygen concentration. In normal ambient O_2 concentration, 10 minutes are required to oxidize half of the NO at a concentration of 500 ppm, but lack of oxygen will slow down the process considerably. Also in still conditions in the atmosphere the oxidation process is very slow. In polluted areas the concentration of NO_2 is very seldom higher than 0.1 ppm.

Nitrogen dioxide absorbs solar radiation (wavelength between 0.6 and 0.38 µm) which causes dissociation:

$$NO_2 \rightarrow NO + O$$

The result is that oxygen in the air together with the oxygen produced by dissociation form ozone (O_3).
This reaction is similar to the ozone production in the stratosphere.
Ozone O_3 and NO will on the other hand produce NO_2 and O_2:

$$NO + O_3 = NO_2 + O_2$$

It is evident that until equilibrium is established, reactions which involve NO_2, NO, O_2 and solar energy proceed in intense sunlight, the O_3 level will increase, and a rapid change of hydrocarbons into other types of organic molecules occurs. The result is that HC and NO_2 will be removed and secondary pollutants are formed, some as aerosols. An important control strategy in smog-type pollution is to reduce the possibility for the formation of the most reactive types of hydrocarbons. The total removal of hydrocarbons from the exhaust gases is not likely to suceed without the use of expensive devices. It would have been a major improvement, however, if the structure of the emitted hydrocarbons had not allowed the formation of very reactive products.
In the future it might be possible to look at emission control more from this aspect and eventually to achieve a better balance between cost and outcome.
The most volatile hydrocarbons in the alkene group, the olefines, are most important in the production of photochemical smog. Olefines are not an important group in ordinary gasoline, but exist in cracked gasoline, produced for better utilization of crude oil. Cracking also takes place in the engine combustion

chamber. Up to 50% of hydrocarbons in the exhaust can belong to the alkene group.

As we know that smog formation is restricted to a few big cities in the world it is perhaps possible to confine limits on the use of certain fuel types to these areas. Heavy cracked gasoline, for instance, could be used in areas where smog does not present a problem.

1.1.4 How pollutants in I.C. engines are formed

Hydrocarbons

There are four main sources of hydrocarbon emission.

1. Evaporation and crankcase ventilation
2. Incomplete combustion throughout the mixture in the cylinder
3. Quench zone
4. Scavenging losses

Evaporation and crankcase ventilation

Most combustion engines in the U.S.A now have control of evaporation losses. Before these controls were introduced the evaporation from the carburettor and fuel tank caused up to 20% of the total hydrocarbon loss from the car. Crankcase ventilation could be responsible for another 20%. Evaporation from the carburettor and tank is directly related to the fuel volatility. In newer models of cars the crankcase is vented back to the carburettor so that the oil vapour is burned in the engine. The major part of the fuel vapour from the tank and the carburettor float chamber is prevented from escaping by improved design. For instance, a carbon-filled container can be used to absorb the vapour when

the engine is stopped and recycle the condensate back to the engine after starting. This modification reduces the vapour loss from a given vehicle by about 90%.

Incomplete combustion

The reasons for incomplete combustion can be divided into two main groups: (i) reasons fundamentally associated with fuel preparation and combustion in the cylinder, and (ii) those which arise because of imperfections in components, incorrect timing or bad maintenance, etc.

We will not discuss the latter reasons for incomplete combustion beyond stating that with regard to hydrocarbon emission the engine condition is very important. Research on pollution from engines must be done on engines in the best condition, and it must be realised that a worn engine or an engine not properly maintained will have considerably increased HC emissions.

This is one of the difficulties of the work on pollution from Internal Combustion engines. It might be possible to keep a low level of HC emissions from a new engine, but as the engine gets worn this low level can not generally be maintained.

A pollution-controlled engine could be a very bad polluter if a cylinder is misfiring because of a faulty sparking plug etc. However, even the very best conditioned I.C. engine emits some hydrocarbons in the exhaust.

Flame quenching

First of all we have "flame quenching" near the walls of the combustion chamber. The combustion tends to be very incom-

plete near cold surfaces and in between liner and piston. Although the quench zone is only about 0.10 mm thick (7), the volume of unburned hydrocarbons from this region is the main source of HC emission via the exhaust gases.

The thickness of the quench zone is dependent upon air-fuel ratio, cylinder temperature and pressure and is measured to be about 0.08 mm at full throttle and about 0.4 mm at idle, at stoichiometric air-fuel ratio.

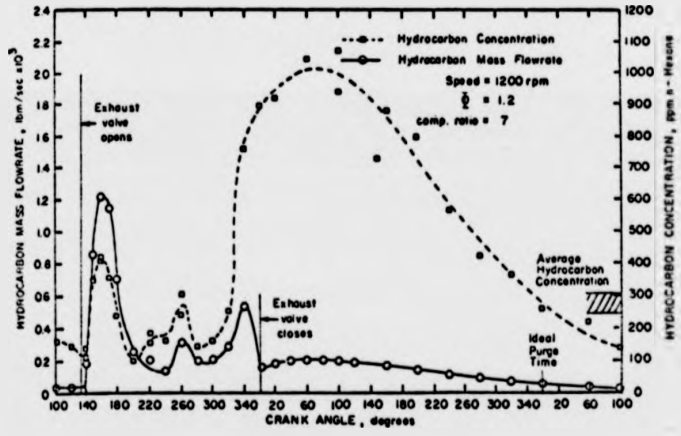

Fig. 2 HC-concentration in exhaust

Figure 2 shows the hydrocarbon concentration in the exhaust measured by Daniel and Wentworth (8). As the piston scrapes off the boundary layers on the walls containing unburned hydrocarbons the concentration increases. The concentration is highest at the end of the stroke (shortly before the exhaust valve closes). The high concentration measured before the exhaust valve opens is partly due to HC residues in the exhaust system from the previous cycle.

In the quench zone and the quench crevices over two hundred types of organic compound have been identified, arising from heated, but not completely burned, fuel.

In transient engine operation there are additional sources of HC which are even more difficult to detect. It is shown that during deceleration residual gases can cause misfiring. Residuals can also create a locally incombustible mixture in the cylinder.

Scavenging losses

Scavenging losses occur due to the fact that parts of the charge to the cylinder escape during the scavenging period . Especially for 2-stroke engines is such short circuiting of charge significant, but also some high performance 4-stroke engines might have such losses.

Aldehydes

The formation of aldehydes in the combustion chamber occurs during low temperature periods of combustion, and is more important for compression ignition (Diesel) engines. It has been observed that in gasoline engines the formation of aldehydes such as formaldehyde and acrolin (HCHO and C_2H_3CHO) increases shortly before knocking occurs (auto-ignition caused by excessive pressure in the cylinder). It is belived that there is a close connection between the oxidation that leads to knocking and the formation of aldehydes. Formation of aldehydes also occurs when air is injected into the exhaust system to remove hydrocarbons and carbon monoxide from the exhaust.

Carbon monoxide

Carbon monoxide is formed during the combustion of hydrocarbon fuels at high temperatures. With complete combustion CO

will oxidise to CO_2.

If, during the combustion especially in the expansion period, there is locally or overall lack of oxidants, low gas temperature, or not sufficient time for oxidation available, CO will remain in the exhaust gases.

As Figure 3 shows the air-fuel ratio is a most important parameter for CO formation.

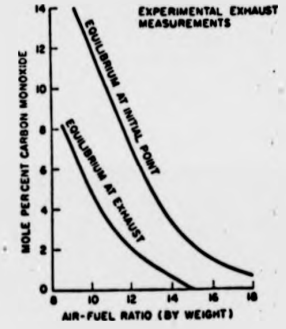

Fig. 3

Even if the air-fuel ratio is sufficently high it is, still possible for CO to be formed locally in the cylinder.

Oxides of Nitrogen

As mentioned previously about 97% of all oxides of nitrogen in the exhaust emission from I.C. engines is nitric oxide. NO is formed mainly at high temperatures.

Although the peak temperature is sufficiently high for NO formation in the combustion chamber, there is insufficient time to allow the NO level to reach the equilibrium value;furthermore the cooling down process occurs so rapidly that the NO formed has insufficient time to decompose to N_2 and O_2. NO is "frozen" in and remains in the exhaust at a concentration near to the maximum level occurring during the combustion process (as shown in fig. 4).

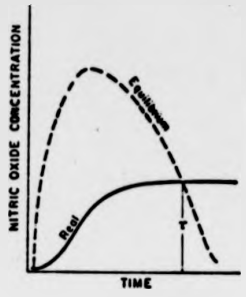

Fig. 4

According to this, NO formation would be relatively high in slow speed, heavy load conditions of operation.

In the formation of NO, the air-fuel ratio is also an important factor. Maximum NO concentration occurs at a slightly lean mixture, at more lean mixtures:the NO formation falls as a result of lower combustion temperatures. With very rich mixtures the NO level also decreases rapidly because less oxidants are available.

1.1.5 The effect of engine parameters on exhaust emission

In research on pollution from internal combustion engines, especially where experiments are involved, it is very important to know about the various factors which influence the concentrations of the different gases in the exhaust.

When the influences of changes in design of engine or components are investigated a comparision is worthless if the operating parameters which affect the exhaust gas composition are not controlled. A series of measurements must be repeated,changing only the parameter that is to be investigated.

Factors of importance in investigations on a particular engine are:

1. Air/fuel ratio
2. Ignition

3. Exhaust back pressure
4. Intake manifold pressure
5. Temperatures
6. Output power
7. Engine speed

When comparing different engines we have in addition

8. Combustion chamber surface to volume ratio
9. Combustion chamber design
10. Cylinder displacement and stroke/bore ratio (S/B)
11. Compression ratio (ε)
12. Valve timing

Air/fuel ratio

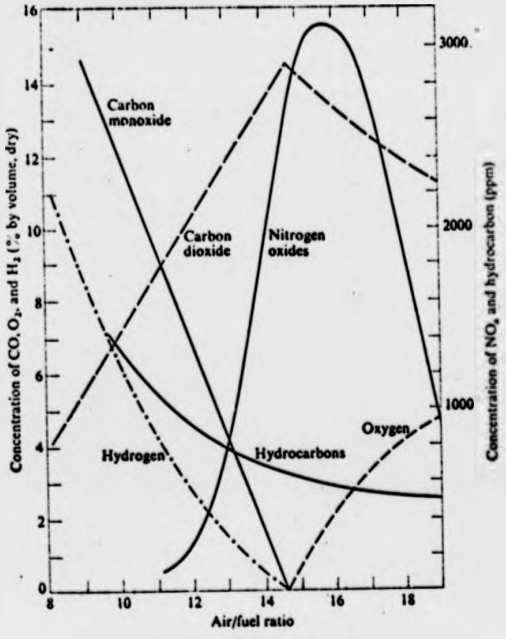

Fig. 5

The effect of air-fuel (A/F) ratio on emissions has been closely studied since work on engine emission control began about twenty years ago.
Engines without pollution control devices, as built before 1968, have an air-fuel ratio normally slightly rich, typically 12 to 14:1.
As can be seen in Figure 5 the level of hydrocarbons and CO is then higher than at weak mixtures (A/F more than 14.7:1).

For reducing carbon monoxide it has proved very successful to run at lean mixture, that is at air-fuel ratios higher than 14.7:1.

Modern carburettors are normally tuned to an air-fuel ratio of about 13.5:1. At higher A/F ratios than approximately 15.5 unstable engine operation can cause poor driveability of the car and an increase of HC. Laboratory tests show, however, that the hydrocarbon concentration may continue to decrease up to an A/F ratio of about 17:1. At higher ratios the engine starts to misfire because either overall or locally there is too lean a mixture in the cylinder. The flame propagation is incomplete or slows down.

Air-fuel ratios higher than 16 normally cause a major drop in engine maximum power.

As figure 5 shows, the NO_x level peaks at an air-fuel ratio of about 16. An engine adjusted to an air-fuel ratio of about 16 for lowest possible carbon monoxide concentration will normally have a high rate of NO_x emission. As discussed previously this is caused by the higher concentrations of oxidants in the cylinder in combination with high combustion temperatures. As the curve for NO_x in Fig. 5 shows, there is a rapid drop of NO_x at very lean mixtures (A/F ratios up to 20). However research on engines shows that to achieve 40% reduction on NO_x the engine maximum power had to be reduced by 30%. This is a typical result from engines with conventional inlet systems. The atomisation and distribution of fuel in the conventional carburettor inlet system is not very good, especially in transient conditions and at low speeds. It is hoped that, through better atomisation vaporisation and distribution of the fuel,the engine-performance

at higher air-fuel ratios can be considerably improved. Several fuel injection systems have been developed with this as their aim.

Inlet systems and fuel atomisation will be discussed in a later chapter.

Ignition timing

Changes in an engine that give higher exhaust temperatures tend to give lower emission of hydrocarbons and carbonmonoxide. If the timing is retarded such an effect can be achieved. The manufacturer sets the timing according to the best overall performance and economy, retarded ignition will normally mean a reduced fuel economy at the same power. The decrease in HC accompanying retarded ignition is thought to be caused also by the lower surface to volume ratio during combustion. Surface to volume ratio will be discussed later. If the ignition is retarded very much, the CO level after combustion will increase because the time available for oxidation is too short. Retarded ignition gives however a higher temperature of the exhaust gases and the oxidation activity in the exhaust system increases. Part of CO in the exhaust will burn in the exhaust system before being emitted to the atmosphere.

Ignition retardation alone is not considered to be a satisfactory means to control emissions, because of the unacceptable loss of power and fuel econnomy, but is an important means to control emission at low load and idle. Accurate ignition timing control is very important and it is necessary to minimise timing tolerances in the production of engines.

Exhaust back pressure

As discussed in an earlier chapter, it is the last part of the charge to be exhausted from the cylinder which contains the largest concentration of hydrocarbons. If the exhaust back pressure increases to such a level that the last part of the charge remains in the cylinder, the hydrocarbon emission may decrease. However, if the backpressure is too high the residuals in the cylinder will cause incomplete combustion in subsequent cycles. Raising the back pressure always has a bad influence on both economy and power.

A higher back pressure is favourable in relation to NO_x. The temperature in the cylinder will drop without addition of oxidants. A high back pressure has no advantage at low speed or idle, because under those conditions the charge is already diluted with exhaust gas owing to bad scavenging, and higher dilution leads to bad running of the engine.

Intake manifold pressure

The metering system in an ordinary carburettor engine is based on the depression in the venturi.

At a constant A/F ratio and with the optimum timing for maximum power, power output level at constant speed has little influence on emission of CO and HC, when we are speaking of concentration and not weight. Higher power output would however give increased temperature during combustion and cause a higher NO_x level.

An increase in inlet manifold pressure would have a supercharging effect. On an engine running under load at constand speed, the inlet manifold pressure can be varied by changing the throttle position. However, this will generally lead to a change in air-fuel ratio and the emission levels change accordingly.

Temperature

A higher temperature level is advantageous for HC and CO emissions. Higher temperature of the combustion chamber walls has the effect of decreasing the quench zone thickness.According to J.I. Wentworth (9), the HC reduction is 0.35 - 0.58 ppm (as Hexane) per degree Fahrenheit. A higher exhaust temperature increases the cleaning up process in the exhaust system. For obvious reasons, increased temperature is not of advantage for NO_x emissions.

An increased temperature of the inlet system gives better evaporation of the fuel, but a temperature higher than that necessary for vaporisation under all engine conditions is not desirable . Higher temperature requires fuel with higher octane number, and because of the lower charge density a worse volumetic efficiency (and consequently lower output) is to be expected.

Output power

If the air-fuel ratio is assumed constant, one would expect a lower concentration of hydrocarbons at higher power output at constant speed because the combustion temperature increases. However, other factors tends to increase the level of HC, so that it remains approximately constant with increased power at constant speed. A factor which tends to raise the HC level is the effect of reduced residence time defined as:

$$t_{res} = \frac{\text{Volume of system } [m^3]}{\text{Volumetric gas flow } [m^3/sec]}$$

The effect of output power on CO emission at constant air-fuel ratio is also not significant, but the NO_x concentration increases. It is very important to remember that we are speaking of concentration in ppm and not mass flow rate of emission. The mass of emitted gases will of course increase with the load, in proportion to the exhaust gas weight emitted.

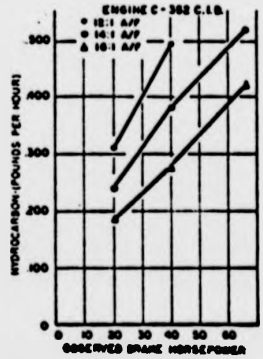

Figure 6 shows the mass flow of HC at different air-fuel ratios versus engine power output (9).

Fig. 6

Engine speed

Increased engine speed at the same power output normally reduces all pollutants in the exhaust. The turbulence promotes

oxidation reactions as a result of better mixing, both in the combustion chamber and in the exhaust system.
Higher speed at the same power output will cause a drop in the engine b.m.e.p. and also in the combustion temperature. The lower combustion temperature will tend to build up a higher HC level, but normally there is an overall reduction of hydrocarbon emission.

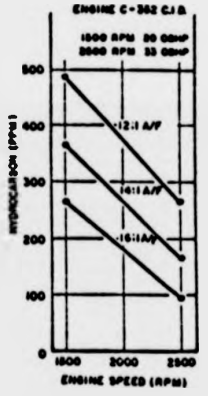

Fig. 7

The Figure 7 showes the drop in hydrocarbon concentration for an engine, measured at 3 different air-fuel ratios. The engine power was rated from 15 KW at 1500 rpm upto 25 KW at 2500 rpm.

Surface to volume ratio (S/V)

The influence of the quench zone on the formation of HC has already been mentioned, in the chapter concerned with the formation of hydrocarbons. It is obviously an advantage to keep the surface area in contact with the combustion flames as small as possible. Figure 8 shows the influence of S/V ratio measured for different engines. (Figure from reference 10).

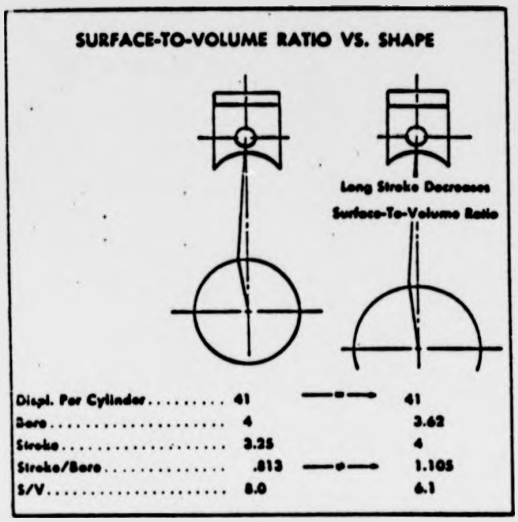

Fig. 8

The CO level is not significantly influenced by S/V ratio whereas the HC level is greatly influenced.

The S/V ratio has become an important parameter which is used in designing combustion chambers and in choosing cylinder dimensions.

Combustion chamber design

Figure 9 shows S/V values of some combustion chamber designs.

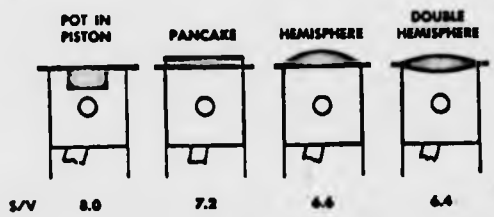

Fig. 9

The double hemisphere gives the lowest S/V ratio and is shown on the right in Figure 9. As factors other than S/V ratios must be considered, combustion chamber are not shaped as simply as those in the figure. The designer must take into account the

position of the sparkplugs and valves, how the heat is transported from the hot parts to the cooling channels, etc.

Stroke / Bore ratio

Modern engines have S/B ratios close to, or even lower than, 1.0. The reason for this is that long stroke engines are less economical, more expensive to produce and need more space under the bonnet. Higher S/B ratio gives however reduction in s/v ratio, because longer stroke more closely approaches the minimum area spherical chamber.

Compression ratio

In recent years there has been a tendency to lower the compression ratio to enable the engine to run on fuels of lower octane number. A reduced compression ratio lowers the thermal efficiency and subsequently increases the exhaust temperature of the engine. The surface to volume ratio (s/v) decreases when the clearance volume is bigger. Both those things tend to decrease the concentration of emitted hydrocarbons.

Valve timing

Valve timing is a very important parameter in an engine. The designer's aim when dimensioning the valve gear is to provide for the highest possible volumetric efficiency in order to achieve high performance and low specific fuel consumption. Since the formation of nitrogen oxides is temperature dependent, a change in valve timing which gives incomplete scavenging and lower combustion temperatures will lower the level of NO_x.

We have discussed earlier that the last part of the combustion gases to be exhausted from the cylinder contains a high level of hydrocarbons. If the change of valve timing ensures that this HC-rich exhaust remains in the cylinder and reburns, a reduction of hydrocarbons may be attained.

There are several possible strategies for changes in valve timing. Early closing of the exhaust valve, somewhat before top centre, would cause the last portion of the exhaust gas to be trapped in the cylinder. Late closing of the exhaust valve will draw exhaust back into the cylinder when the piston is moving downwards. Early inlet valve opening causes exhaust to enter into the inlet manifold : a low load condition with higher vacuum makes this most effective.

Increased overlap (that is the time when the exhaust valve and the inlet valve are both open) would be achieved by a combination of early inlet valve opening and late exhaust valve closing. Camshaft advance (early exhaust close + early inlet open) or camshaft retard would be a way to solve the technical problems of achieving timing changes.

Reduction of emissions by recirculation of exhaust will always give loss of maximum power and efficency. If the amount of dilution reaches a certain level, misfiring occurs and an increase of hydrocarbons is inevitable.

1.1.6 The Measurement of vehicle exhaust and legislation

The table shows types of instruments which are widely used for measuring vehicle exhaust emissions. The instruments used in this project are underlined and their operation is described briefly in this chapter.

CO	NDIR	Although CO_2 emission is not regarded as pollution, it is of great value to measure the CO_2 level. Knowing the CO_2 concentration the air-fuel ratio can be calculated (11), using for instance the Shell method TRC II.
CO_2	NDIR	
NO	NDIR	
	PDS	
	Ozone chemiluminescence	
	Polarographic cell	
	Salzman	
	Mass Spectrometer	
HC	NDIR	
	FID	
	GLC	

A more exact determination of air-fuel ratio by means of gas analysis involves additionally either the measurement of O_2 or an after-oxidation of the exhaust in a furnace. In the present research it was necessary to have simultaneous measurement of the airflow into the engine, for reasons which we will discuss later. As the fuel consumption is a very important parameter in all research on engines, the fuel flow rate is normally measured. If this is done the obvious way to calculate the air-fuel ratio is to divide the air flow rate by the fuel flow rate. For petrol engines this is certainly the most accurate method. For diesel engines, however the air-fuel ratio would be overestimated because of the short circuiting air during the scavenging process.

The most commonly used instrument for analysing exhaust gases from combustion engines is the Nondispersive Infrared Analyzer (NDIR). NDIR analyser works on the principle of selective absorption. Many gases have the property of absorbing infrared radiation of certain wavelengths (λ) and transmitting other

wavelengths in the range 4.5 to 5.0 µm. For CO_2 the range is 4.0 to 4.5 µm. In a NDIR analyser there are two identical sources of infrared light. One source serves as a reference and directs a beam through a pipe filled with a reference gas which does not absorb the radiation. The other beam is led through a similar pipe which can be filled with the sample gas. (Figure 10) Residual radiation of the relevant frequency is then absorbed in the live side of the detector cell. The absorption of the infrared radiation in the sample tube gives a lower temperature in the detector at the end of the sample tube. The difference of temperatures can be measured and relates to the amount of gas present in the sample. The sample tube receives a constant stream of the gas to be analyzed.

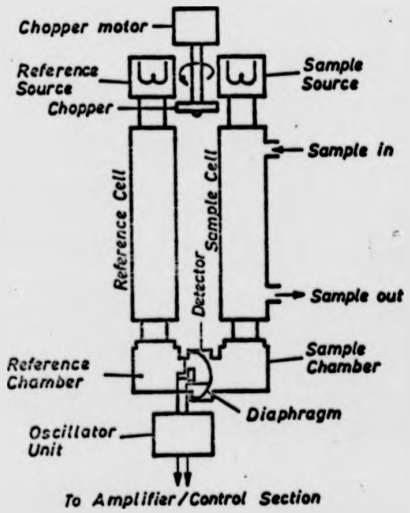

Fig. 10

The detector has two chambers one for each tube. The chambers are separated by a diaphragm carrying a capitance plate, to register the movment of the diaphragm. The capacitance change, sets up an AC signal in the amplifier. A shutter that alternately block and unblocks the radiation causes the diaphragm to move from its position with no radiation to a certain amplitude with radiation, depending on the pressure difference in the two compartments of the detector. This reduces the drift in response of the system.

NDIR is also used for nitrogen oxides, but at very low concentrations, as in the CVS procedure (see p.35), the NDIR method must be replaced by more sensitive instruments. NDIR is now only rarely used for measuring hydrocarbons, because the response is very different for different types of HC (for example NDIR gives a low reading for aromatics). Also it is found that an HC - NDIR responds to gases other than HC, such as CO and CO_2.

Flame ionization detectors (FID) are very much in use for detecting hydrocarbons.

FID is based upon the fact that the hydrocarbons in a flame of pure hydrogen and air produce ions at a rate proportional to the number of carbon atoms present. Almost all types of hydrocarbons are measured with the same response.

An electrostatic field near the burning flame attracts positive ions to a collector and electrons to a cathode. The DC-current that flows is amplified in a sensitive amplifier whose output signal can be recorded.

As will be described in a later chapter, the FID is very sensitive to the rate of flow of hydrogen, air and sample gas, so those flowrates need to be kept under close control.

Figure 11 (page 33) shows a FID burner schematically.

Measurement of NO and NO_x by the ozone chemiluminescence analyser is based upon the chemiluminescent reactions between nitric-oxide and ozone.

If ozone is present in excess, the intensity of the light produced when nitric oxide is introduced is proportional to the amount of NO present in the reactor. A photomultiplier detects the light intensity. By means of an amplifier and a calibration unit, the NO concentration is registered on an indicator, direct-

ly in vpm (parts per million in volume).

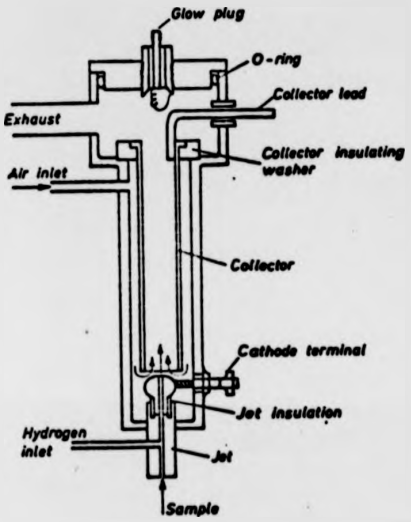

Fig.11

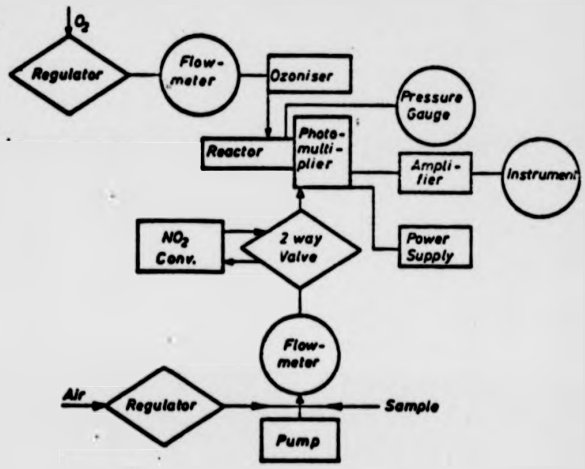

Fig.12

In order to permit measurements of NO_2, an in line converter decomposes NO_2 into NO.

When the converter is used the sum NO + NO_2 can be read on the meter.

A chemiluminescent analyser is a complicated and expensive instrument capable of measuring concentrations as low as 0.01 vpm. The interference from other gases in the exhaust is negligible. Figure 12 shows schematically the sample flow through the instrument.

Sampling

Investigations of emissions from engines on test beds are almost always comparative measurements. Concentrations of gas mixtures are measured and compared with the concentration after changes have been made to components or other parameters on the

engine. Emission tests carried out in order to measure the pollution level according to exhaust gas quality standards, must be carried out following special procedures, so arranged that a representative sample of the exhaust is taken. All procedures for governmental tests incorporate the use of a chassis dynamometer and specially approved test eqipment. In early test procedures a probe was inserted into the tail pipe and the gas to be analysed could be sucked continuously into the analysers. This method is very similar to the methods used on engine test beds. Later test procedures, however, involve one or more plastic bags. The plastic bag collects a representative portion of the exhaust gas after a test run in which acceleration, speed and time are closely specified. By the use of bags it is not necessary to have continuously running analysers. The preparation of the result is much easier because an average value of the testcycle can be recorded directly, sampled from the middle of the bag.

The European ECE method, shown schematically on fig. 13 involves a large PVC bag to collect the exhaust gases emitted during a cycle. A flowmeter allows the measurement of the exhaust gas volume.

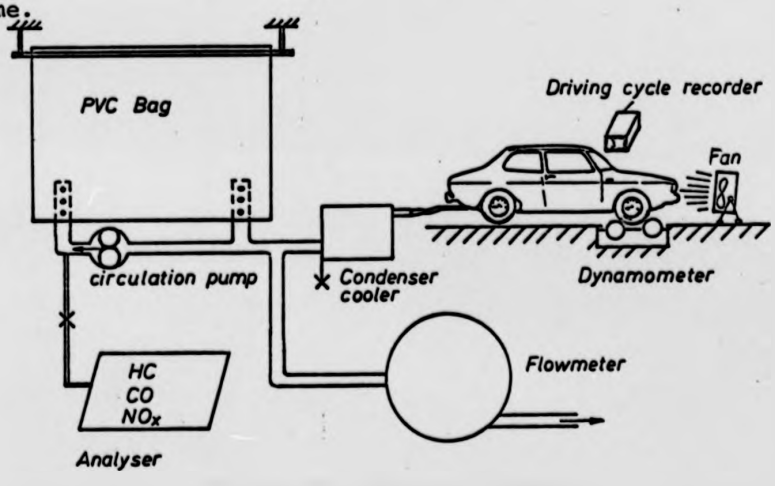

Fig.13 ECE test method

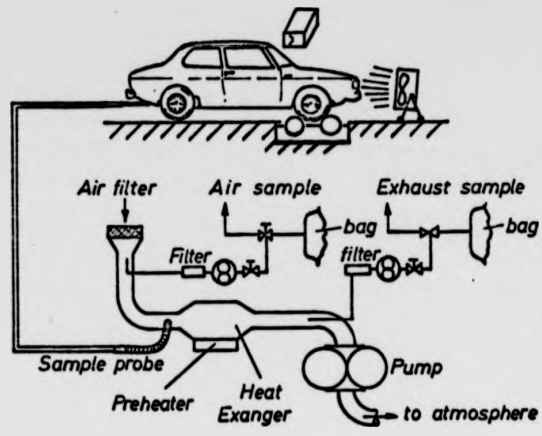

Fig.14 US method CVS 1

The US CVS-1 system dilutes the exhaust gas with air to avoid vapour condensation, and is designed to measure true mass emissions.

As mentioned earlier, measurement of very low concentration requires sensitive instruments.

Based on the CVS-1 tests, the emission US. standards for 1974 are

Hydrocarbons	3.4 g/mile.
Carbon monoxide	39 g/mile.
Oxides of nitrogen	3 g/mile.

However, after 1975 the CVS-1 procedure is extended to involve 3 sampling bags CVS-3, then it is possible to weight cold start periods separately. This new method is similar to CVS-1 and uses the same cycle. After 1976 the US standards measured with CVS-3 are

Hydrocarbon	0.4 g/mile.
Carbon monoxide	3.4 g/mile.
Nitric oxide	0.4 g/mile (deferred until 1977).

The last requirement, 0.4 g/mile NO_x, is a very difficult stan-

dard to meet and this level, originally proposed for 1976, is now deferred to 1977.

The US standards are much more severe than the ECE requirements: however some European countries are considering a strengthening of the regulations up to the level of the US standards. Figure 15 shows a comparison between the ECE standards and the US standards. The US standards are converted to ECE cycle.

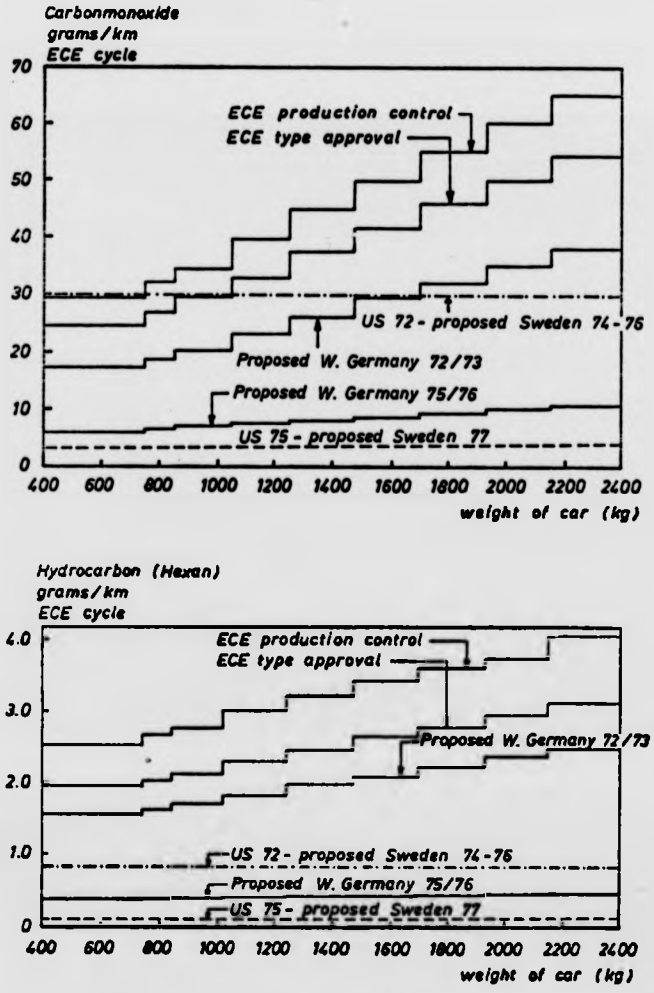

Fig.15

1.1.7 Methods for reducing emission of pollutants

For the reasons stated in paragraph 1.1.4, it is easier to reduce the levels of emitted hydrocarbons and carbon monoxide than those of nitrogen oxides. One could argue that a reduction of NO_x would be easier if there were no legislation governing hydrocarbons and carbon monoxide. That is, if the concentrations of HC and CO are reduced by means of improved completion of combustion, the concentration of NO_x tends to rise owing to the higher temperatures and the presence of more oxidants during combustion. During the first years of the work on pollution control on engines there were no standards for nitrogen oxides. The work done in those years concentrated, therefore, on reduction of HC and CO. A large reduction in those pollutants was achieved by inexpensive changes in engine equipment. The crankcase emission, caused by blowby from the cylinders into the crankcase, was estimated to contribute up to 25% of all HC emission from the uncontrolled vehicle. An internal crankcase ventilation system eliminates all blowby emissions. In this system the vent pipe from the crankcase is directly connected to the air intake of the engine. This is called positive crankcase ventilation (PCV) and is shown in Fig.16. A valve reduces the suction at high vacuum but allows enough ventilation of the crankcase.

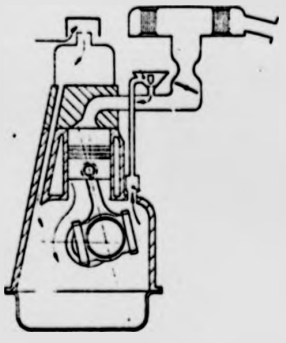

Fig.16

In some engines the vent pipe from the crankcase has a separate filter (breather). This is called a open PVC system. Carburettor and tank vapour control have also been introduced. On the carburettor all direct

external ventilation is eliminated, and the temperature of the fuel bowl is reduced by means of heat shields and insulating gaskets. The tank and carburettor vapours may be vented to a storage system or retained internally in the carburettor or induction system. Some manufacturers use the crankcase as a storage chamber. Others use a container fitted with activated carbon as a hold up for vapour.

To reduce the hydrocarbon and carbon monoxide emission in the exhaust, the carburettor is carefully designed to maintain a sufficiently lean mixture under all driving conditions. The ignition timing is retarded and the idle speed is increased to prevent misfiring. Automatic choking for cold starts combined with heated air inlet due to diversion of the exhaust reduces the HC and CO emissions in the warmup period. When the engine has reached normal working temperature a bimetallic element operates a valve in the inlet system so that normal ambient air is sucked into the engine.

In some vehicles there is a built-in mechanism that reduces emissions by allowing no advanced timing in the acceleration period at lower gears. Only in direct drive is the advanced timing mechanism in operation.

As stated in an earlier chapter this retarded timing will reduce hydrocarbon as well as nitrogen oxide emissions. But of course in lower gears the fuel economy is impaired, especially in stop and go driving.

The carburettor of an emission controlled engine has become a very complicated device. In order to have satisfactory fuel metering under all driving conditions there are carburettors in use having 3 and 4 venturies (barrels).

The need for exact metering has led to the development of sophis-

ticated petrol injection systems, involving electronic metering of air-fuel ratio. There are also some simpler mechanical metering systems in use. Electronic petrol injection involves normally the use of electromagnetically operated injectors which inject fuel into the inlet manifold, close to the valves. Most systems work with pulsed injection. The pulse duration is controlled electronically to give the right amount of fuel in response to signals from sensors for temperature, atomosheric and manifold pressure, and speed. Petrol injection is expensive and can be used only in expensive cars. The system is also generally difficult to repair when faults occur, and special equipment is needed to service it. The main advantage of petrol injection is no doubt improved atomisation and distribution of fuel. A carburettor is normally situated away from the cylinder inlet ports to give space for the manifold branches to the different cylinders. This separation causes the fuel from the carburettor to impact on the inlet manifold walls, especially at low speed when the venturi air speed is low and the fuel is badly atomised. Impaction in the inlet system is widely believed to be the major reason why choking is necessary when the engine is cold. For obvious reasons, there is a close connection between manifold temperature and impaction. A hot manifold improves the vaporisation of the "droplets" from the carburettor. If the fuel is vaporised and condensation can be avoided on the way to the engine, there will be no liquid fuel resident in the inlet system, and a more uniform distribution to the cylinders will result.
However, a heated inlet manifold will increase the charge temperature and so a decrease in maximum power output is inevitable.

Most gasoline engines have the manifolds heated either by water circulated from the engine cooling water system (used by cross-

flow engines) or by heat transfer from the exhaust manifold. On engines with inlet and exhaust on the same side, the exhaust manifold and the inlet manifold can be clamped together for better heat transfer (hot spot).

As discussed earlier, the last part of the charge scavenged from the cylinder is highest in hydrocarbons and is also the coolest. A higher temperature of the exhaust gases increases the after-reactions in the exhaust system.

We have seen that a method to get higher exhaust temperatures is to make the combustion less perfect. Another way is to insulate the exhaust system to prevent heat from getting lost and to fabricate exhaust ports with heat resistant steel liners as shown in Figure 17.

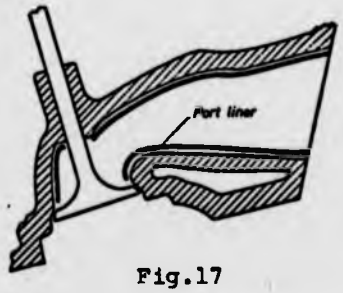

Fig.17

Enlarged exhaust manifold volume gives lower exhaust gas speed and therefore more time is available for after-reactions. A more effective way to increase exhaust after-reactions is to inject air into the exhaust system. Air injection has been investigated on several types of cars and the results are promising. However air injection alone is not enough to fulfil the most severe legislation. Air injection will reduce the HC and CO emissions, but oxides of nitrogen are not reduced: in fact they might be increased according to whether the temperature is sufficiently high. The temperature is again dependent upon the air-fuel ratio during combustion. Rich mixtures have a higher hydrocarbon level in the exhaust gas, which keeps the after-reactions going and creates a higher temperature. Thermal reactors have been developed for after-oxidation of HC and CO. Also catalysts are able to promote oxi-

dation of hydrocarbons and carbon monoxide.
A catalytic converter could be shaped as a silencer and filled with a noble metal, (platinum or an oxide) shaped to give high surface area per unit volume. Alumina pellets covered with the catalyst material are often used.
Catalytic reduction of NO is also possible, and scientists all over the world are involved in research to find catalysts which are able to reduce the three main pollutants emitted effectively and inexpensively.
Some catalysts have been found to produce toxic compounds: others emit metallic compounds,or quickly deteriorate. Deterioration is often accelerated by the presence of lead compounds in the fuel.

It is likely that an exhaust treatment device able to fulfil the most severe legislation must be a two stage system - a catalytic converter and a thermal reactor to reduce NO to N_2 and O_2.
The ideal catalyst would of course reduce all three components.
It seems that future pollution control systems will probably make combustion engines less efficient.
The principal method known today to reduce NO_x is to lower the combustion temperature. This will reduce the NO_x level but increase the HC and CO concentration. Thermal or catalytic reactors then enable the exhaust to be after-oxidised or decomposed.

The US goverment has realised the difficulties involved in the reduction of NO_x to the proposed level of 0.4 ^{g}/mile and has given the car manufacturers another year (until 1977) to try to solve the problems.
From an economical point of view neither exhaust after-treatment nor recirculations of exhaust gases for reduction of NO_x (and consequent decrease of engine thermal efficiency) is desireable.

The methods an engineer would like should

1. be inexpensive in production and use
2. not involve much maintenance
3. not give higher fuel consumption
4. not reduce maximum power or driving performance.

After-treatment would, as far as can be seen now, mean a worsening of all the above factors. Pollution reduction in the engine itself, by improved design and techniques, is the only attractive way for an idealistic engineer.

Looking at the problem from this viewpoint there seems to be only one method: to get the engine to perform well at very lean mixtures.

As shown in the Figure 5 the level of NO_x and CO will be reduced at very lean mixtures. The hydrocarbon level tends to increase mainly because of misfiring, but also because of the formation of a thicker quench zone.

Very lean operation can only be achieved by very good fuel preparation in the engine inlet system. Maldistribution and an inhomogeneous mixture increase misfiring and cause the engine to perform badly. Very lean operation is therefore not attainable using an ordinary carburettor. Injection systems or combined injection and carburettor (the so-called stratified charge system) are more likely to succeed.

In a stratified charge system there is often a petrol injection system that gives a rich mixture close to the spark in order to start the combustion of an overall lean mixture. A stratified charge system is expensive but so far most successful. A stratified charge can not be incorporated into an existing engine, but would mean a redesign.

The basis for all lean operation of conventional engines however, is an overall homogeneous mixture. In order to obtain this, fine atomisation of the fuel is necessary. Fuel atomised to small droplets will be more easily vaporised in the manifold.
The project described in this thesis deals with a device developed for better atomisation of the fuel.

2 The Aims of the research carried out at the University of Warwick

The present knowledge of the influence of combustion engine design on emission permits certain modifications to be made to reduce pollution emission on the engine itself. Examples of such modification are the reduction of surface to volume ratio in the combustion chamber, the avoidance of "dead" volumes which create increase of hydrocarbons, retarded ignition timing (especially at idle) and better carburettors which operate with leaner mixtures.
We have seen from a previous chapter that another means of reducing pollutants could be the use of so-called "hang-on" devices, which reduce components in the exhaust gases when incorporated as a part of the exhaust system.

2.1 To assess what can be achieved by good preparation of fuel

Most modern production engines with emission control for cars work at air-fuel ratios near to 14. However, at this mixture strength the NO_x formation in the engine is close to its maximum. Figure 5 page 20 shows the trends of pollutant formation in the engine at air-fuel ratios up to 19.
Research carried out in several places confirms that at constant load the formation of pollutants drops with increasing air-fuel ratio from 16 up to approximately 18. At even leaner operation the level of hydrocarbons tends to rise again. As mentioned previously one of the reasons for this is the increased thickness of the quench layer. With decreasing combustion temperature, as a result of higher air-fuel ratio, the combustion close to the surface of combustion chamber is very poor. Increasing the air-fuel ratio above approximately 17-18 tends to cause unsteady flame propagation even in the charge further away from the walls. If the concentration near the spark plug is locally too lean, the charge will not ignite and the whole unburned charge of hydrocarbons is emitted in the exhaust. Extra lean mixture operation is very often limited by poor preparation of the fuel-air mixture before it enters the engine cylinder. Very little can be done with the hydrocarbons formed in the quench zone, but improved mixture preparation should reduce hydrocarbon emission

produced in the charge remote from the walls.
The figure 5 page 20 shows the emissions at part load. Experiments indicate that the curves at idle have similar characteristics. Significant reduction of all pollutants may occur at air-fuel ratio above 18.
Full throttle conditions however tend to reduce the gain on NO_x emissions. The explanation for that must be that the temperature during combustion is higher at full load, and the amount of air corresponding to air-fuel ratio of, for instance, 19 is not enough to keep the temperature level low enough to avoid increase in NO_x formation.
Because of the reduction in pollutant, very lean operation is the most interesting aspect of pollution control. But looking at the formula for thermal efficency shows another interesting feature of extra lean mixtures in gasoline engines.
In the ideal process for combustion engines with constant volume energy addition, as is approximately the case for gasoline engines, the thermal efficiency can be expressed as:

$$\eta_0 = 1 - \frac{q_0}{q} = 1 - \left(\frac{V_2}{V_1}\right)^{K-1}$$

$$\eta_0 = 1 - \frac{1}{\varepsilon^{K-1}}$$

For stoichiometric mixture the value for κ is calculated to be 1.3 For pure air κ is 1.402. As the mixture becomes leaner the exponent (κ-1) increases and consequently the thermal efficiency of the process improves.
Reports on over-lean operation show that air-fuel ratios above 18 are very difficult to achieve in ordinary production engines, and special care has to be taken over fuel preparation.

2.2 The causes of imperfect fuel preparation

The following factors make the fuel preparation imperfect in the inlet system of an engine.

1. Variations in the effective fuel flow rate
2. Maldistribution between cylinder
3. Inhomogeneous mixture

1. The ordinary carburettor for combustion engines may be a very good device for mixture metering but it certainly has limitations.

The carburettor is not a very good atomiser, especially at low air speeds. Also the fact that the throttle is situated after the venturi will cause maldistribution of mixture into the manifold.
The instability of fuel flow in the carburettor, the escape of big droplets from the carburettor feed tube and the presence of impacted fuel in the system cause variations of mixture strength withtime, and can cause misfiring of the charge when the carburettor setting is very lean. In transient operation the variation of mixture strength is especially apparent. Transient operation at very lean mixture is of course very difficult: very lean operation is probably limited to constant speed conditions. Even at " constant speed ", small changes of power, and therfore of mixture delivery, must be tolerated. At very high air-fuel ratios this could cause instability of the fuel delivery and cause the engine to run badly. Systems where fuel is metered individually to the cylinders may improve the distribution: the residence time of the droplets however, is short and could cause only partly evaporated droplets and therefore inhomogeneous charge in the cylinder.

2. Maldistribution between cylinders is also very common. In fact measurements of exhaust composition show very clearly that on a multi-cylinder engine there are large variations of mixture strength from cylinder to cylinder. Differences of air-fuel ratios of 2 and more are often measured.
The maldistribution is most apparent on engines with 6 cylinders or more. 8-cylinder in-line engines as produced for large U.S. cars are often extremely bad. The difference in length of the branches from the carburettor inevitably causes large differences of mixture strength at the different cylinders. Even 4-cylinder engines suffer from significant maldistribution.
The geometry of the inlet manifold is of course very important, but there seems to be only one way to solve the problem with single carburettor arrangements, namely to evaporate the fuel before it enter the manifold branches. Geometrical maldistribution seems to be almost eliminated if the fuel is vaporised beforehand.

3. As mentioned above the ordinary carburettor set-up will at times produce a very inhomogeneous mixture of vapour and drop-

lets of various sizes. The droplets produced in the venturi have very different masses and will also therefore have different vaporisation rates.

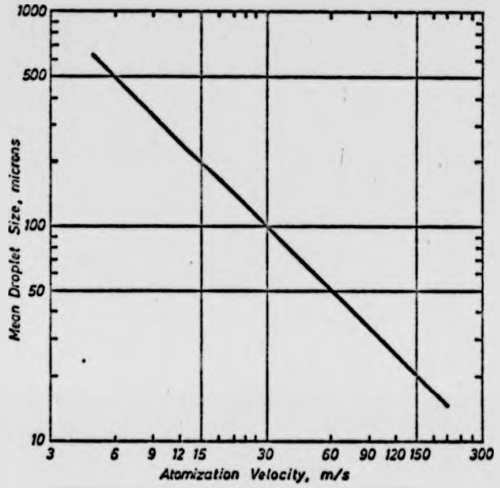

Fig.18

At low engine speeds it is extremely unlikely that the biggest droplets formed are completely vaporised in the inlet system. Photographs taken on glas manifolds show that even for a hot engine the impaction is heavy: the fuel burned in the engine cylinder is evaporated from the warm manifold walls or is sucked into the cylinder as big drops.

As figure 18 shows, mean droplet size falls with increasing airspeed in the venturi. At a venturi air-speed of 65 m/s the mean droplet size is calculated according to the Nukiyama-Tanasawa equation, to be approximately 60 µm. According to figure 18 under idling condition the mean droplet size will be well abowe 500 µm.

Carburettors with constant venturi area have to be dimensioned according to maximum power performance. Obviously there is a limit to the magnitude of losses that can be tolerated in the venturi at full speed. Even a venturi dimensioned for very high pressure drop at full load is too big to give high enough airspeeds at low load.

The constant depression carburettor has advantages here: the " venturi " area is adjusted according to air flow in order to keep the air-speed at a high level even at idle.

2.3 The impaction of droplets and droplet evaporation

Theoretical investigations on droplet size and impaction in inlet manifolds show very clearly that most of the fuel droplets produced in the carburettor impact in the first bend on the manifold (12).

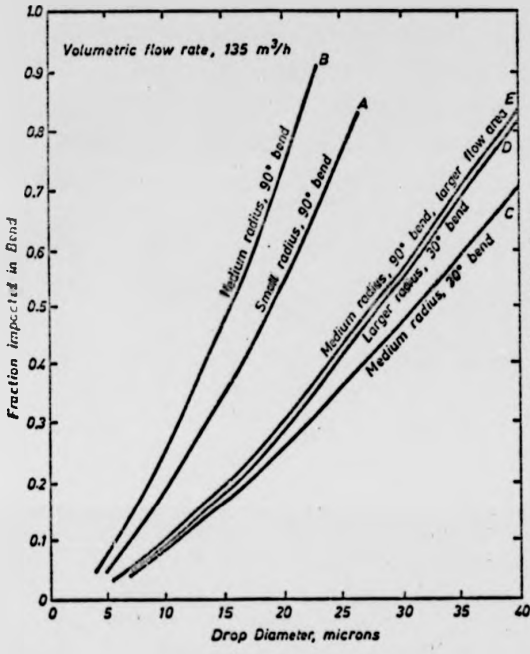

Fig.19

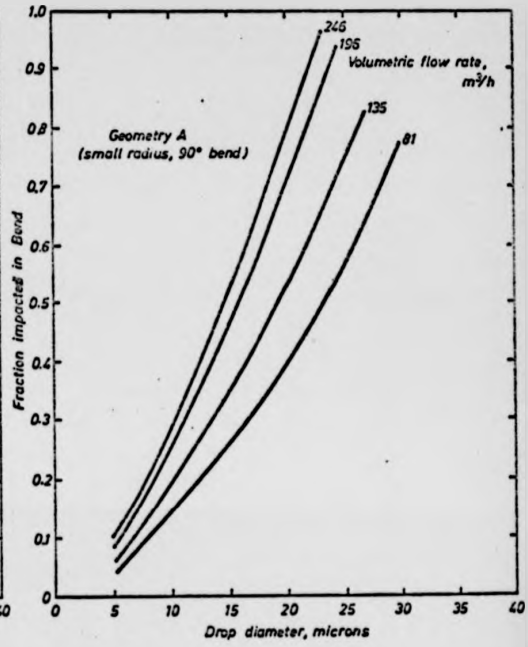

Fig.20

According to figure 19, which shows the fraction of impaction on 90° and 30° bends, there is very little chance for droplets bigger than 30 µm to avoid collision with the bottom wall of the runner of the inlet manifold in a downdraught carburettor mounting.
At higher flowrates (and therefore higher air speeds) the impaction rate increases.
Even in a 30° bend of the same diameter, half of the 30 µm droplets will impact at the same flowrate (Figure 19 (12)).
The calculations of droplet impaction do not take into account the effect of the throttle butterfly valve. As the valve is situated after the venturi, it will cause an asymmetrical flow, besides collecting droplets. The impaction in the manifold of an engine is certainly even worse than the results from an idealized calculation predict. The impacted fuel on the surface in the manifold will be moved owing to aerodynamic forces from the air stream in the manifold. Only at very slow flow rates is the liquid film in laminar flow. Instabilities at higher air-speed cause the fuel to be thrown off the surface. In the warm manifold, evaporation from the surface accounts for a major part of the fuel vapour produced in the inlet system, especially at slow speed.

The liquid film on the walls in the manifold causes maldistribution of the mixture and delay in the transport from the carburettor to the cylinder.

Several experiments with vapour generators have shown that the response and driveability of an engine running on completely vaporised fuel are improved, and that there is no need for enriching the mixture for acceleration (13).

The problem in using vapour generators or other devices which evaporate the fuel before the inlet manifold is the response time of the device. When the load on the engine changes, the vaporiser has to produce the mixture at the right air-fuel ratio immediately. If a high temperature of the mixture is to be avoided this is only possible by using a vaporiser of large volume or a by pass system, where a part of the mixture produced is recycled when the engine is running at lower load. In such a system the energy used to produce the recycled mixture would be lost. The temperature of the mixture must be kept higher than the dew point of the mixture to avoid condensation in the inlet manifold branches. This will cause a drop of maximum power output. The lean mixture operation also influences the power output considerably. Figure 21 shows the maximum power from an engine at different air-fuel ratios, with ordinary carburettor (A) and with a vaporiser which heats the metered mixture from the carburettor using heat pipes from the exhaust (13).

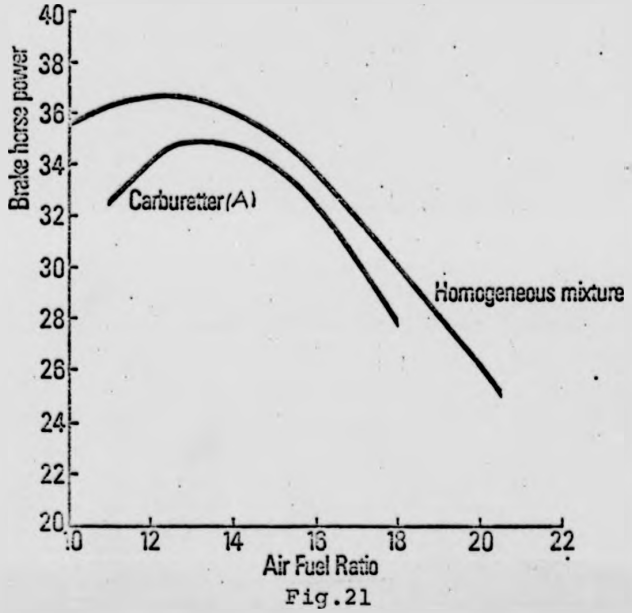

Fig.21

A part of the drop in power at higher air-fuel ratio is thought to be caused by the high temperature of the charge. When the vaporisation of the fuel is achieved in a unit placed after the carburettor it is necessary to produce a considerable amount of heat in order to obtain full vaporisation at all load conditions, because very little time is

available for vaporisation at high mixture flow.
An improvement to this system is to use a by pass system so that only a small part of the air together with the fuel is treated in the vaporiser.

In the conventional inlet system the manifold is heated by contact with the exhaust manifold: in modern cross flow engines the heating is by means of a water jacket which is connected to the cooling system of the engine.
Vaporisation occurs from droplets in the air or from the fuel film on the walls of the manifold. To vaporise 1kg of gasoline approximately 350 kJ of heat is needed. The vaporised fuel will remain as vapour as long as the temperature is higher than the dew point of the mixture. The dew point for gasoline mixture is shown in the following table for air-fuel ratios of 15:1 and 20:1.

Vacuum mm Hg	Dewpoint in °C for A/F 15	A/F 20
0	46.5	40.5
50	45.0	39.5
250	38.4	33.4
370	34	29.0
500	32.2	22.0

At higher air-fuel ratios the dewpoint decreases. According to this table it is possible to get vaporisation in the manifold of an engine at about 40°C if there is sufficient time for the droplets to absorb the heat.
Vaporisation occurs from the surface and smaller droplets have a bigger surface to volume ratio, as the following figure 22 shows. The total surface and the diameter sum of the droplets increases with increasing number of droplets, assuming constant volume, as illustrated in the figure 22. Area shown in curve A.
As expected both curves show an increasing gradient when the droplet-diameter approaches zero.
Droplets formed from 1 cm^3 of fuel would have an increase in surface area of 820 cm^2 at a reduction in droplet size from 26 µm to 5.7 µm. Furthermore the existence of a large number of droplets would ease the heat transfer to the fuel mass.

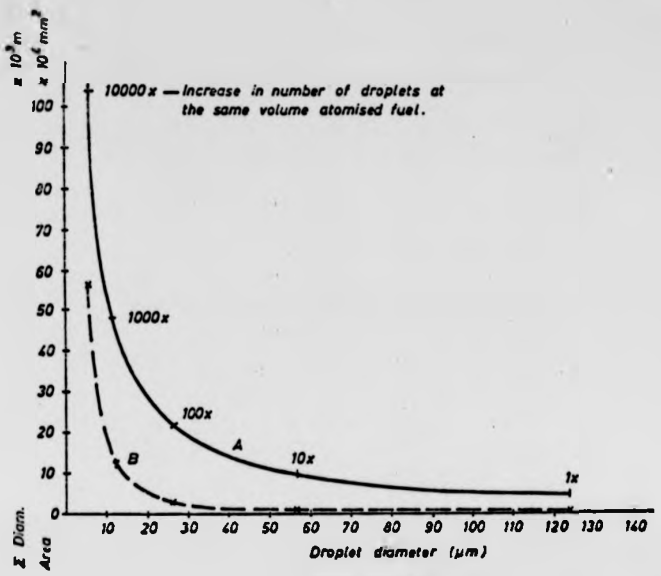

Fig.22

The diameter sum of the droplets would be extended approximately 20 times.

Several scientists have carried out research on evaporation of droplets in an air-stream. Normally the evaporation rate from a liquid surface is expected to be proportional to the surface area. If the heat transfer were by radiation this would be the case but, because the vaporisation rate is principally controlled by the conduction of heat through the gas film surrounding the droplet, scientists seem to agree that the vaporisation mass rate is more nearly proportional to the droplet diameter.

According to Mc Adams (14) the following expression can be written.

$$-\frac{dm}{dt} = \frac{\pi}{4} \cdot \rho \cdot \lambda_e \cdot D \qquad (1)$$

m = mass of evaporated fuel
ρ = density of fuel
D = droplet diameter
λ_e = evaporation constant

This equation defines an air evaporation constant dependent on the conditions under which the evaporation takes place.

The mass of fuel in a droplet can be expressed as

$$m = \rho \cdot \pi \cdot D^3/6 \quad \text{or} \quad \frac{dm}{dt} = \frac{1}{2}\pi \cdot D^2 \cdot \rho \frac{dD}{dt}$$

This expression gives us in (1) the droplet reduction according to: $D = D_0 - \lambda t$

In an induction system, the heat transfer is controlling at relatively high evaporation rate and the evaporation constant is found to follow the expression

$$\lambda_e = \frac{4\lambda}{c_p \rho_L} \ln(1+B) \cdot Nu \tag{2}$$

where B is the transfer number and Nu the Nusselt number which for mass transfer is a function of Reynolds and Schmidt number according to:

$$Nu = 2 + 0.6 \cdot Re^{1/2} \cdot Sc^{1/3} \tag{3}$$

The transfer number is for evaporation without combustion is

$$B_{nocomb} = \frac{c_p(T_g - T_s)}{Q} \tag{4}$$

The expression for the evaporation constant is then:

$$\lambda_e = \frac{4 \cdot \lambda}{c_p \rho_L} \ln\left(1 + \frac{c_p(T_g - T_s)}{Q}\right)(2 + 0.6 \sqrt{Re}\ \sqrt[3]{Sc}) \tag{5}$$

λ	:	thermal conductivity of gas or vapour
c_p	:	specific heat of vapour
ρ_L	:	density of fuel
T_g, T_s	:	temperature of air and vaporising surface, resp.
Q	:	latent heat of vaporisation + enthalpy increase before vaporisation
Re	:	Reynolds number
Sc	:	Schmidt number
ν	:	kinematic viscosity

μ : dynamic viscosity
ρ : density

In order to calculate the evaporation constant λ_e it is necessary first to find a value for the transfer number B. The transfer number is dependent on the heat transfer to the air-fuel mixture in the manifold and on the temperature of the mixture. **The heat flow rate from the manifold to the gas is given by:**

$$q = h\ A(T_M - T_g)$$

where:
- A = area of manifold transfering heat
- T_M = temperature of manifold wall
- T_g = gas temperature
- h = heat transfer coefficient

Few experiments have been carried out to measure the heat transfer coefficient in gasoline engine inlet manifolds. McAdams (14) suggests an equation based on studies of correlations for pipes, where h is a function of Reynolds number (Re), Prandtl number (Pr) the manifold diameter (Dm), length (L) and branch radius (Rb) and mass (M), as follows:

$$h = 0.023\left(1 + \frac{7\ Dm}{L}\right)\left(1 + \frac{3.5\ Dm}{2\ Rb}\right)Re^{-0.2}\ Pr^{-0.67}\ M\ c_p$$

Because of the liquid film in the manifold and the complicated shape, the h-values computed from this equation do not correspond very well with values reported from measurements on manifolds.

Measurements carried out in diesel engine inlet ports (15) give values in the range of 426 to 540 kJ / m^2 h ^oC.
If the first straight part of the inlet manifold is considered, the Dittus-Boelter correlation, $Nu = 0.023\ Re^{0.8}\ Pr^{0.4}$, can be used in the range $0.6 < Pr < 100$ according to (16). According to this formula the heat transfer coefficient would vary from approximately 42 kJ/m^2h^oC at idle to a maximum of 250 kJ/m^2h^oC. at maximum power. (Re from $\approx$2000 to $\approx$20 000).
Sharp bends and the branches to the different cylinders will probably give higher h- values close to the inlet ports. However, as it is of interest to find out more about the evaporation of

droplets in the first part of the induction system and before the distribution of the charge to the different cylinders takes place, the values h_{idle} = 42 kJ/m²h°C. and h_{load} = 250 kJ/m²h°C. are used in the following estimation.

The equation $$M\, c_p(T_g - T_s) = h\, A(T_M - T_g)$$

gives the connection between the heat transferred from the walls to the charge at different flowrates and heat transfer coefficients.
T_M is in the following estimation 80 °C.
If the gas temperature (T_g) is assumed to be 50 °C, the first 100 mm of the manifold could raise the mixture temperature to only 50.8 °C at idle, and to only 50.4 °C at maximum load.
The transfer number would accordingly be as low as B_{idle} = 0.04 and B_{max} = 0.01 when the assumption is made that the temperature of the vaporising surface is at dew point. This gives an evaporation constant of approximately $\lambda_{idle} = 1.28 \times 10^4\ \mu m^2/s$ and $\lambda_{max} = 3.20 \times 10^3\ \mu m^2/s$
This would again suggest an evaporation time according to equation 2 of:

Droplet Diam µm	evapor. time sec. IDLE	evapor. time sec. Maxload 6000 rpm
10	7.8×10^{-3}	3.12×10^{-2}
30	7.03×10^{-2}	2.8×10^{-1}
60	2.8×10^{-1}	1.12
120	1.12	4.5

If the volume of the inlet system allows a residence time equal the time for one revolution the total residence time in the manifold would be 0.16×10^{-1}s at idle (1000 rpm) and 10^{-2}s at 6000 rpm.
In the example above droplets of approximately 15 µm diameter would have time to evaporate at idle, at full speed the droplets would have to be smaller than 6 µm.
The assumption that the droplets are surrounded by gas at dew point temperature is very doubtful, but makes the calculation simpler. Without adding heat to the system there is normally very little chance that complete evaporation takes place so early in the manifold system that no droplets impact in the bends.

With an air-speed of say 15 $^{m}/s$ (medium load) the time for evaporation within the first 100 mm of the manifold is 6×10^{-3}s. Under the conditions assumed in the example, only droplets in the range up to 10 µm would have time to evaporate.
Calculations of this kind can only give an estimate of what happens in the manifold. Turbulence and the presence of liquid fuel make the heat transfer very difficult to calculate, and the formulae are of very doubtful validity. However analytic investigations do give us a better understanding, which allows us when designing the system to take steps to improve the fuel preparation. Possible strategies are listed below.

1. The fuel droplets must be as finely atomised as possible. Reduction of droplet size increases the surface area and, as we have seen, improves vaporisation. The vaporisation should occur as early as possible after atomisation, to avoid impaction and maldistribution.

2. The inlet system flow paths should be as straight as possible. No bends or restrictions such as the butterfly valve should occur closely after where the droplets are formed.

3. Very little vaporisation is posible without heat input. Heat must therefore be applied in the area where the fuel is atomised, but control is necessary to avoid applying too much heat, especially at part load.

4. A large cross-sectional area of the manifold gives a lower air speed and more time for evaporation to occur.

5. Bends close to the engine inlet should have large radii and be shaped to avoid impaction, because some large droplets are likely to be formed even in the best system, especially during transient operation of the engine.

The size of the fuel droplets is the most important factor of those mentioned abowe.
It was therefore decided to work with ultrasonic atomisers for atomisation of the fuel.

Unfortunately no ultrasonic atomising equipment was available, because the technology of ultrasonic atomisers is very little known and hardly in use yet.
Consequently it was necessary first to develop an ultrasonic atomiser able to give small enough droplets, and shaped suitably to be situated in an engine inlet system. The power needed for the atomiser had to be within the range of what is available in the electrical system of a car.
The design had to be uncomplicated and as inexpensive as possible so that if the project were successful the new system could easily be adopted and used by the industry.
Of course the development of a new device is not finished after approximately two years of experiments. Endurance tests and optimisation require much more time, but one of the aims has been to make the atomiser good enough to permit tests on an engine so that the results may be compared with those from the engine with the original equipment.
It is important to find out if an ultrasonic atomiser arrangement, replacing the carburettor, can improve the engine performance parameters such as power, fuel consumption and exhaust gas emissions.
In view of the difficulty of producing engine parts of complex shape it was decided, as a first step, to modify an inlet manifold produced for the engine, and to use the experience gained from this investigation to design a new, more suitable manifold.
The metering system is a very complicated part of the emission-controlled engine and it is not considered to be an aim of this project to develop such a system.
For comparative investigations it is necessary to carry out the metering by means of hand operated valves for both air and fuel because, if the effect of improved atomisation of fuel on engine performance is to be investigated, important engine parameters such as air-fuel ratio must be kept as constant as possible.

3 Test facilities and instruments

3.1 4-stroke engine

For the purpose of the experiments, a Ford Pinto 1600 cm^3 engine was loaned by the Ford Central laboratory in Laindon.
This Pinto engine represented the 1974 US export model, equipped with pollution control devices including a carburettor giving a lean mixture and retarded ignition timing at idle.
The carburettor had a thermostatically regulated hot-air inlet and thermostatic choke control.
There was evaporation control on the float chamber, whereby the vapour was fed into the manifold of the engine, and the engine had the crankcase ventilation led to the clean side of the air filter. The engine was fitted to the testbed on its original rubber mounts, lined up with the dynamometer and connected to it through a shaft with two universal joints and a splined coupling. In order that the engine could be idled the gearbox and clutch were used as in the car. The dynamometer was of the DC type capable of motor or generator operation and coupled to a Ward-Leonard AC to DC converter. The installation was controlled in such a way that it operated with a constant speed characteristic. The load was regulated by varying the dynamometer field current. A schematic diagram of the testbed is shown in Appendix I, together with a description and user's instructions. The load torque was measured with a load cell of strain gauge type and a strain gauge bridge of DC type.
In order to increase the sensitivity at low load two instruments were used in parallel: the most sensitive instrument could be switched off at higher torques.
Drawings of the load cell with the electric circuits are also to be found in Appendix I.
All normal accessories belonging to the engine were fitted, except the cooling fan.
The fan would make the test cell unnecessarily uncomfortable. Instead of the radiator cooling system of a car, a special cooler using the laboratory cooling water circuit was designed and produced. Drawing of the cooler are also shown in Appendix I. The cooler was built together with a cooling water reservoir for the engine and the original pressure cap was used to maintain the correct water pressure and temperature. The exhaust system was

of course slightly different from that in the car. Although the same exhaust silencer was used, there was a sharp bend close to the exhaust manifold to save space in the test cell. The exhaust pipe was also somewhat longer than in the car with the exhaust emitted directly to the atmosphere outside the laboratory.
As is often the case at laboratory installations the exhaust system tended to be hotter than in the car because of the absence of air flow relative to the engine. For the oil sump the air flow is necessary to keep the oil temperature down. A fan can be used to cool the sump but it is somewhat more difficult to cool the exhaust system on a testbed, in order to obtain the same exhaust temperature along the exhaust pipe as in the vehicle. A long very hot exhaustpipe will cause after-oxidation of the exhaust gases. Exhaust gas analyses from testbed engines are often different from those taken from the car by sampling in the tailpipe. This does not reduce the value of comparative measurements.

3.2 Instrumentation

As mentioned above, the engine power was measured by means of a load cell which indicated the torque which the dynamometer absorbed from the engine. A static calibration related the torque to the load on the load cell. There were two tachometers, one counted the engine speed and the other the speed of the dynamometer. In order to obtain more accurate measurement of speed, a stroboscope mounted in front of the engine could be used.
The revolution counter on the dynamometer was of the 3 phasetype and accurate enough for the experiments. To indicate the ignition timing a timing light triggered from the high tension lead of cylinder No 1 was used. For comparative emission tests the ignition timing is of fundamental importance and must be kept constant.
The air filter was replaced with a Ricardo Alcock Viscous flowmeter type: 476 H for air flow measurements. There is always a danger that the change of the inlet system caused by the flowmeter causes change in the engine characteristics. Inlet systems are often tuned to give the best possible performance. A flowmeter can change this tuning considerably.
Fuel consumption was measured with volume flowmeter and stopwatch. This method is accurate but the adjustment to a chosen air-fuel

ratio is difficult or at least time consuming. A simultaneous reading of flow rate would have been better. However, continuous reading fuel flowmeters are not geneally very accurate. An average value given by volumemeter is more representative for a given load. An ordinary mercury in glass thermometer was used to measure ambient air temperatures. The air temperature in the inlet manifold and in the air filter were recorded at every setting. Exhaust temperature and the temperatures of cooling water and oil are also interesting, the latter especially, because the lack of air-speed could lead to high oil temperature. Oil temperatures above 110 ^{o}C were avoided. Above 90 ^{o}C a cooling fan was in operation to cool the engine oil sump.
The exhaust thermometer was of thermoelectric type, based on chromel-alumel wire.
A vacuum gauge was used to register the pressure in the inlet-manifold.

3.3 2-stroke engine

The two-stroke unit was intended for use only in pilot studies of how the ultrasonic atomisers perform in an engine inlet system.
These studies revealed many difficulties at an earlier stage and more easily than if they had been carried out on the 4-cylinder engine. A single cylinder two stroke 2.0 HP engine is very small and uncomplicated and experiments on it are less time consuming. This two stroke engine was fitted to an 60 A, 12 V alternator. In order to absorb the engine power over the whole operating range, the voltage was increased to 25 V. The power was measured with a wattmeter.
The alternator was regulated by using an external field current from a 12 V battery. The generated current was removed in the form of heat in wire-wound high watt resistances. Although the alternator was up to 70% overloaded there were no complications. More information about the two-stroke testbed is shown in Appendix I. Because the efficiency of the alternator was not known, the measured power output could not be converted to exact engine power output. Fuel consumption could therefore not be related to power. Because of this a calculation of specific fuel consumtion and emissions in grammes per kW was not attempted.

The measured power output of the two-stroke unit is only of value as a comparative figure and tells little about the engine performance and the quality of the engine.
There was no free shaft on the engine or alternator for connection to a mechanical revolution counter. A stroboscope triggered from the generator coils in the flywheel of the engine was used to measure the rpm very satisfactorily.
For the measurement of air and fuel consumption the same system was used as for the Ford engine. Smaller air-flowmeters have greater resistance and may cause changes in output power. Therefore the Ricardo flowmeter was used also in the experiments with the smaller unit.
Two-stroke engines are much more sensitive to inlet system changes than are 4-stroke engines. The accuracy of the Ricardo flowmeter at very low flow rates is of course not very good but because of the influence on the engine, a bigger flowmeter with less restricted flow is preferred to a more accurate flowmeter that gives higher restrictions.

3.4 Exhaust gas quality measurements

As was seen in an earlier paragraph, the most interesting gases to be measured in connection with exhaust products are carbon monoxide, carbon dioxide, nitric oxides, and hydrocarbons. Carbon monoxide and carbon dioxide were measured with NDIR. These instruments require much space and are heavy. In order to have as short a sample line as possible from the engine exhaust manifold to the analysers, and because the equipment may be required for other testbeds, it was decided to mount the NDIR-analysers together with the hydrocarbon FID on a trolley. All three instruments could then have a common sample system and related flow regulation on a front panel. A back panel could be used for flowmeters, pressure gauges, electric controls and switches.

There was separate calibration input to the analysers. This enables quick calibration checks before or after a measurement on the engine, if necessary.
The figure 23 shows the flow diagram of the CO, CO_2 and HC analysers on the trolley.
The sample gas is led from the exhaust pipe of the engine through stainless steel pipes into the " cooler " of the analyser.

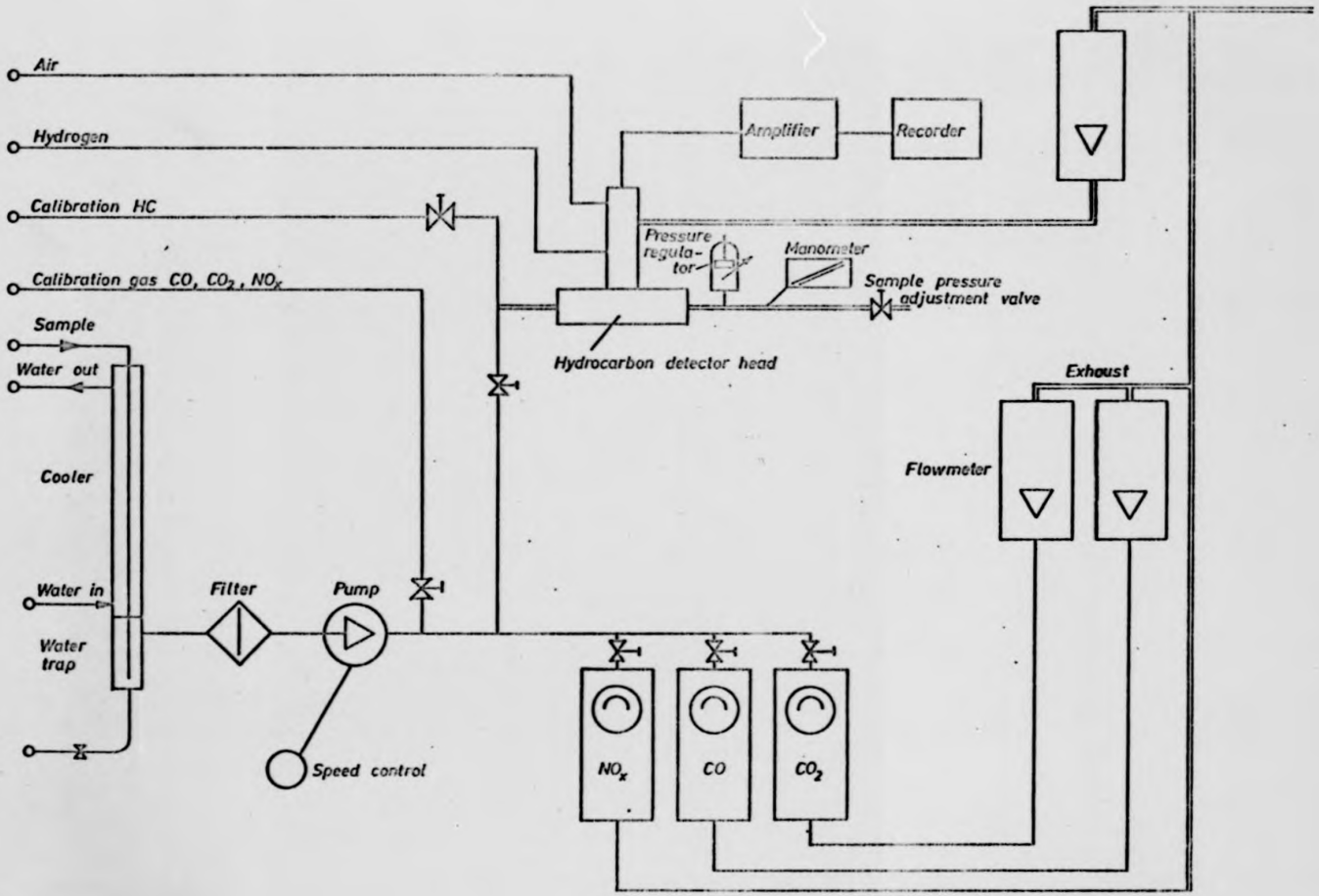
Air
Hydrogen
Calibration HC
Calibration gas CO, CO_2, NO_x
Sample
Water out
Cooler
Water in
Water trap
Filter
Pump
Speed control
Amplifier
Recorder
Pressure regulator
Manometer
Sample pressure adjustment valve
Hydrocarbon detector head
Exhaust
Flowmeter
NO_x
CO
CO_2

Fig.23

The cooler prevents the water in the sample gas from condensing in the system. All pipes after the cooler are insulated.
If the sample gas has its lowest temperature in the cooler, no condensation will take place elsewhere in the flow through the analysers. The filter is especially constructed for easy change of filter paper.
More details and a drawing of the filter can be found in Appendix II.
A diaphragm pump with speed control delivers the sample gas at pressure to all analysers.
Neither the NDIR analysers nor the NO-NO_x analyser is very sensitive to variations in the flow rate. The flowrate of the sample through each NDIR analyser was adjusted to approximately 1.5 litre/min.
The HC analyser is more sensitive to pressure differences. Even a water bubbler would give pulsations of the output reading of the recorder. As an extra " safety " pressure control a petroleum filled bubbler was used, but the main pressure regulator was a pressure cylinder with a plunger. The weight of the plunger regulates the pressure as the plunger is lifted up to a " leak hole" in the cylinder. This " plunger " regulator governs the pressure without pulsation. It is also easy to check that the pressure is correct when the pressure regulated from the " plunger regulator " is very near to the pressure governed from the bubbler. If the bubbler is in operation the signal from the HC analyser pulsates. Also the manometer shows clearly when the pressure is too high and the bubbler is functioning. Petroleum has less surface tention and the pressure pulsation is not so disturbing as with water. (Details in Appendix II).
The flowmeter on the exhaust side of the FID burner is only in use at start-up and when the air and hydrogen flows are adjusted. Experiments were carried out to find the best setting. The exhaust from the FID burner has a high water content and condensation easily takes place in the pipe and in the flowmeter. Water in the exhaust line causes the FID flame to be unsteady. A condenser in the system was successful but as the sensitivity of the FID analyser improves very much at " free exhaust " all measurements were carried out with the flowmeter disconnected.
The FID analyser is very sensitive to the flow rates of hydrogen and air. Several experiments show that a hydrogen flow rate of 15 ml/min and an air flow rate of 230 ml/min was most successful.

This gives an air-hydrogen ratio of 15.33 measured with the same flowmeter calibrated for air. Measurements of hydrocarbon concentrations are often inaccurate because of residues of hydrocarbons which settle down in the system. If for instance the filter is not frequently changed, hydrocarbons remaining in the filter cause the instrument to show a hydrocarbon reading even with a clean air sample. The hydrocarbon residues have to be " washed " out of the system first. In order to have comparable results the paper filter was changed before every series of measurements, and the system was drained to give a zero reading on the recorder. Although the HC analyser is partly " homemade " the repeatability and sensitivity are extremely good.

Calibration gases give the same reading even after long periods of time. The sensitivity of the analyser is very good and an output of 2mm/ppm can be recorded without disturbing noise. In order to avoid reactions which could influence the accuracy of the measurements, stainless steel tubes were used for all connections between the various components or analysers. Thermal insulation of the tubes and fittings was achieved by using thick insulation tape. More details of the FID - analyser can be found in Appendix II.

The use of an FID - analyser requires experience if exact measurements are to be obtained. Analysers produced by skillful manufacturers are easier to handle than analysers made on a one-off basis. The FID-analyser described in greater detail in Appendix II, has a chromatograph detector head and the amplifier produced by PYE, so that the important components are produced by a well known firm. However, as long as the rest of the arrangement is " homemade " the FID analyser cannot be used commercially or to produce results for comparison with standard requirements. For use in research, where measurements are to be compared, such a homemade analyser is very suitable and, with skillful use, may even be more accurate than " easy to use " analysers from manufacturers because more control mechanisms may be built in.

The NO - NO_x chemiluminescent analyser was purchased as a complete unit. The experience with this analyser is very good and it caused very little difficulty.

This analyser also was checked on calibration before every series of measurements, but the reading was always stable and varied only a little. The NO - NO_x analyser is calibrated to read vpm directly on the meter. There is only a very small proportion of

NO_2 in the exhaust (about 2 to 5%). Almost all nitric oxides are NO.
It was therefore decided to measure only NO. The exact measurement of total NO_x content would require a constant check of the converter efficiency.

3.5 Instrument calibration

The power from the engine measured in Watts is defined as

$$P = F\, ds/dt = F\, v$$

when P and v in same direction. If the torque is defined as tangentialforce × radius we can write $P = Fr\omega$.
The force F is the force measured on the load cell and the radius r the distance from the load cell to the centre of the dynamometer.When n in rpm:

$$P = \pi/30 \quad n\ F\ r \qquad [W]$$

For the calibration of the load cell a lever was fixed on the opposite side of the dynamometer and the calibration force placed at an exact measured distance from dynamometer centre. The known torque on the load cell was then related to the instrument reading as shown in the calibration curve figure 24.
The formula for Power is then

$$P = 0.1047 \frac{n}{1000} M \qquad [kW]$$

M according to scale deflection on instrument and calibration curve.
Load cells based on strain gauges are very reliable and stable. The only operating problem is to adjust the strain gauges correctly. To make adjustment easier, a permanent set-up for checking the calibration was built, consisting of a spring balance placed on a jib near the dynamometer.
By means of the spring balance a known smaller torque can very easily be put on the load cell to check that the calibration is correct before use. As the calibration curve Figure 24 shows, the plot of meter reading against torque is, as expected, a straight line. For the check only one point is necessary to test whether the calibration is correct.
Another important value necessary for determining the power is

the speed. Both revolution counters were calibrated against a stroboscope(Figure 25).
The accuracy of these measurements should be good enough for the purpose of comparing different experiments on the inlet system. Furthermore measurements on combustion engines are always limited in accuracy more by the unsteadiness of the engine caused by variations in the fuel flow and ignition timing than by inaccuracy of instruments or meter reading.

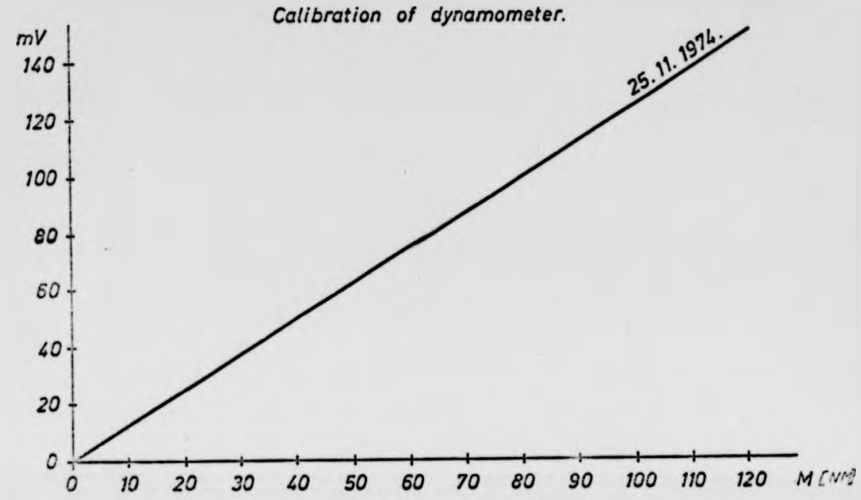
Calibration of dynamometer.
mV
140
120
100
80
60
40
20
0
25.11.1974.
0
10
20
30
40
50
60
70
80
90
100
110
120
M [NM]

Fig.24

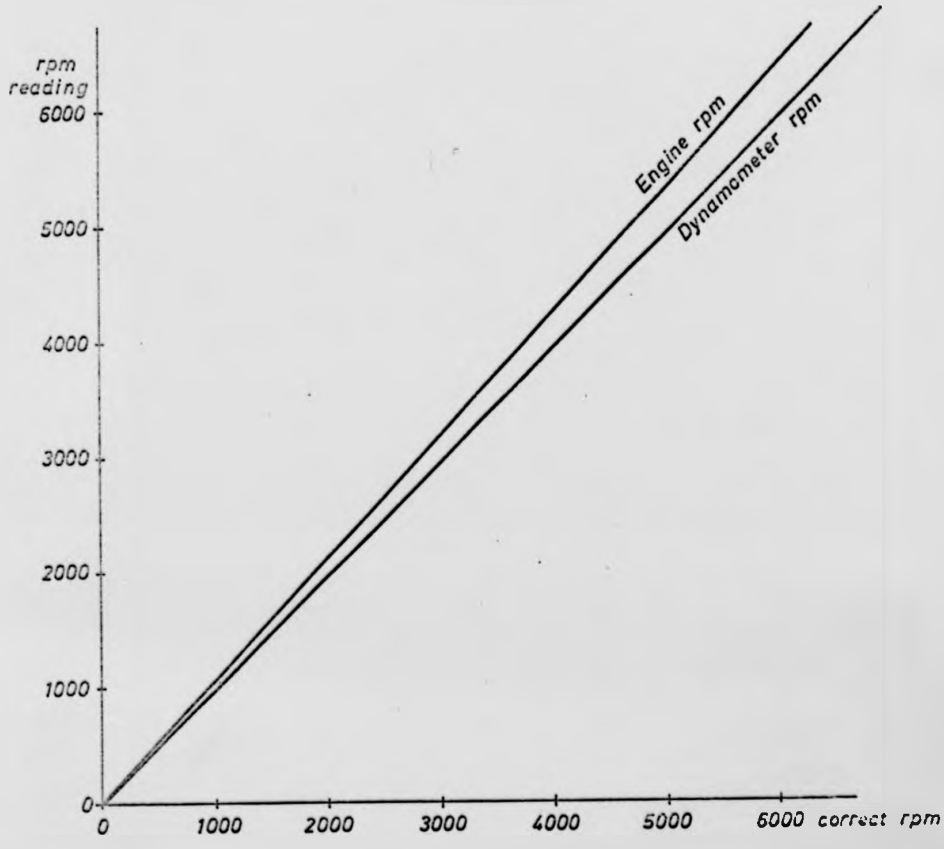
rpm
reading
6000
5000
4000
3000
2000
1000
0
Engine rpm
Dynamometer rpm
0
1000
2000
3000
4000
5000
6000 correct rpm

Fig25

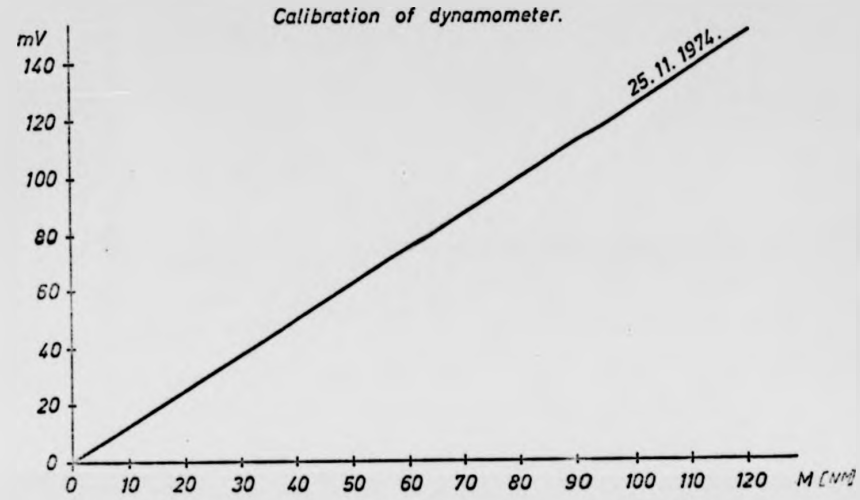
Calibration of dynamometer.
mV
140
120
100
80
60
40
20
0
25.11.1974.
0
10
20
30
40
50
60
70
80
90
100
110
120
M [Nm]

Fig.24

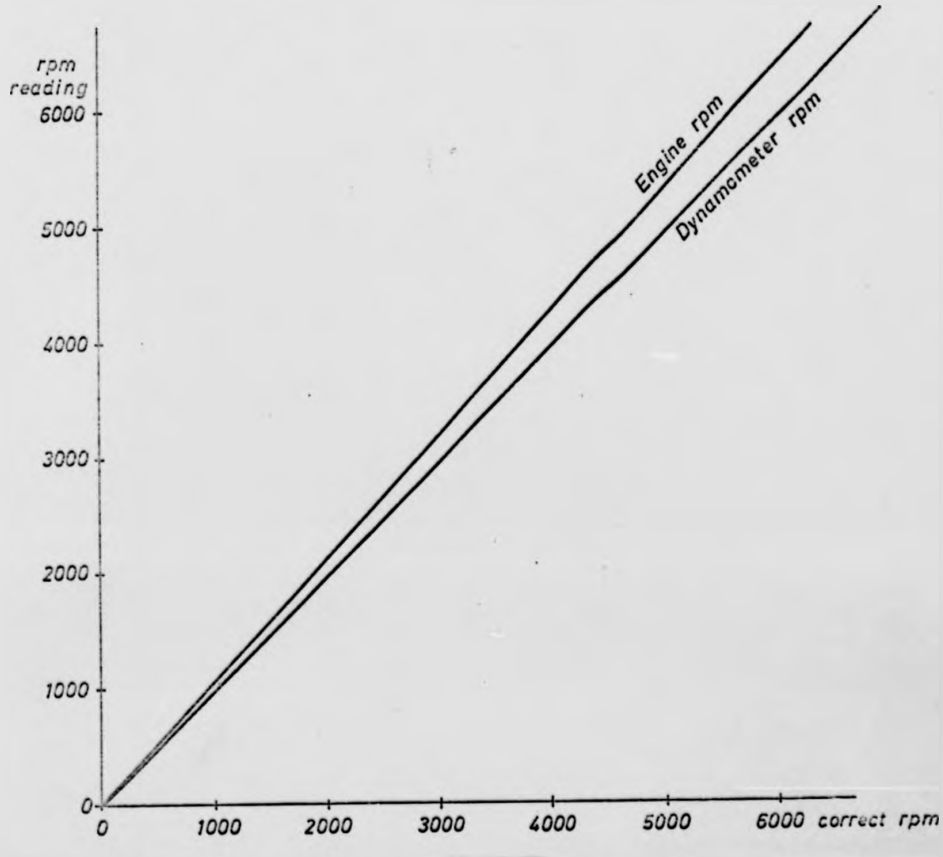
rpm
reading
6000
5000
4000
3000
2000
1000
0
Engine rpm
Dynamometer rpm
0
1000
2000
3000
4000
5000
6000 correct rpm

Fig25

Calibration of exhaust gas analysers

Both CO and CO_2 analysers have a built-in sensitivity check. On pressing a button situated on the analyser panel, a calibration wire is inserted in the radiation beam of the instrument: this causes a deflection on the meter. If this deflection is much different from the standard value the instrument calibration has changed and it should be recalibrated or re-adjusted.
The calibration curves for these analysers are not linear and it is necessary to use several gases or to blend gases to cover the whole range.
For the calibration of CO-CO_2 NDIR analysers two calibration gas bottles were used. Those gases were mixtures of 2% CO plus 8% CO_2 in nitrogen, and 4% CO plus 12% CO_2 in nitrogen. Those two bottles were obviously not enough to calibrate the whole instrument range from 0-12%. The gases were therefore blended to give other mixtures. In order to get an accurate mixture of the two gases two different methods were used.
The arrangement of two flowmeters and a blending vessel is shown in Figure 26

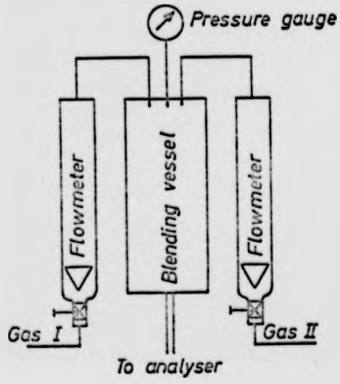

Fig.26

This set-up allows continuous readings of blends, by adjusting the flowrate, and represents a very quick way to calibrate. The method is exact enough for most measurements. The calibration curve for the CO analyser was found to be exactly the same as determined by the manufacturer of the analyser before delivery which suggests that this calibration method is sufficiently accurate. However, the calibration curve for the CO_2 analyser is different and it changed during the research programme. The reason for this is probably a leak of gas from the detector. The sensitivity loss of the CO_2 analyser was progressive and therefore a calibration check was necessary before every series of measurements. It was not considered to be necessary to compensate for this drift by increasing the sensitivity of the instrument. If

the sensitivity is increased on the instrument the calibration curve changes over the whole range. Figures 27 and 28 show the calibration curves from the manufacturer and at different times during the research.

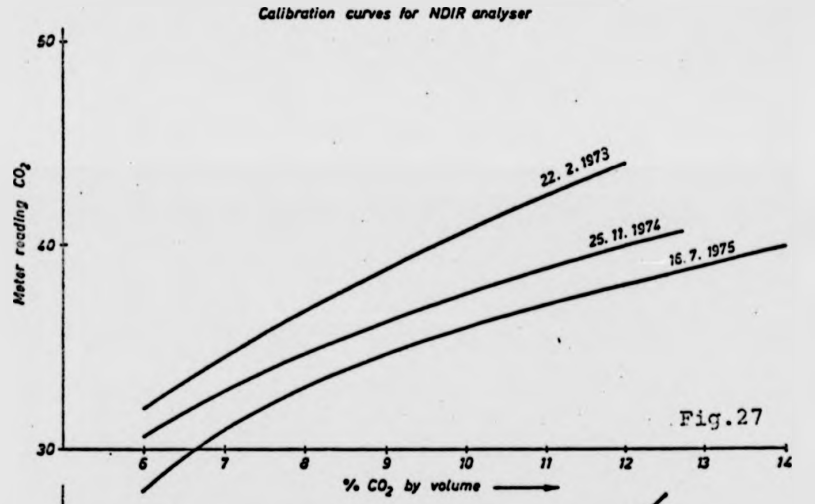

Fig.27

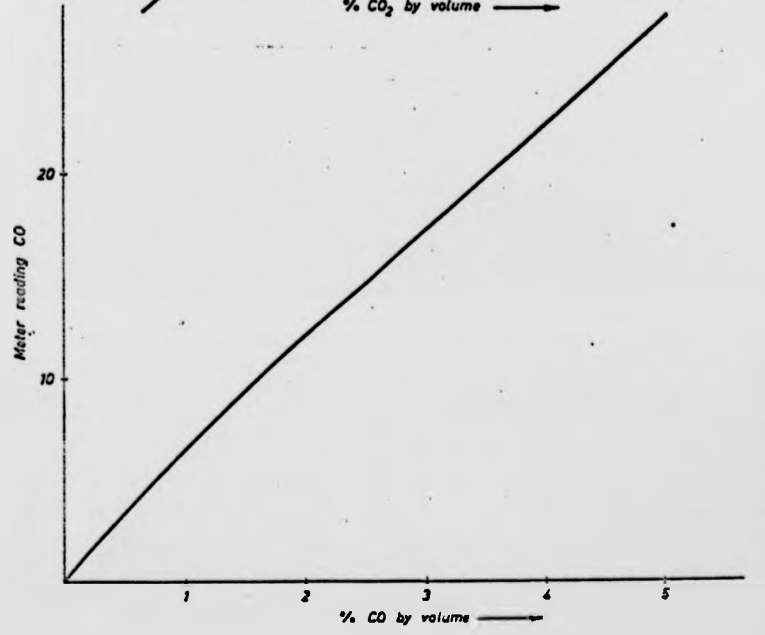

Fig.28

Calibration of Luminox analyser

The NO - NO_x analyser is a linear instrument. When the correct sensitivity is set with a calibration gas (spangas) the whole range is correct. A calibration could show that this is the case. A calibration gas, with 1000 vpm NO was used to set the instrument. It then gave at 100 vpm calibration gas 99,5 vpm on the meter. Such a small discrepancy is not significant because the NO level changes more than that in the engine during a test.
Obviously the spangas used should be as close to the expected level of NO as possible to avoid unnecessary incorrectness. The range of the instrument is from 0 vpm to 10 000. Measurements on IC engine exhaust would need only a small part of that range, maybe up to 4000 vpm.

Calibration of FID-Analyser

The sensitivity of the hydrocarbon analyser is mainly dependent upon the following factors.

1. Air-hydrogen ratio
2. Exhaust back pressure of burner
3. Sample pressure
4. Gain set on recorder and ionisation amplifier.

The air-hydrogen ratio has to be chosen to give a stable flame in the burner under all conditions, and good sensitivity.
A too lean or too rich mixture tends to cause the flame to blow out when switching from calibration gas to sample, or the flame blows out simply because of accidental variations of the sample flow rate. In normal operation, after ignition and a heating up period, the air-hydrogen ratio was adjusted to maximum sensitivity of the analyser. Although the burner would not ignite at this setting, the flame was stable after ignition. The sensitivity decreases especially if the air-hydrogen ratio is too low. At leaner operation than approximately 15.3 the influence on the sensitivity is less significant until the flame blows out.
The air hydrogen ratio of 15.3 is not the true ratio as the flowrates are measured with a flowmeter calibrated for air. The stoichiometric air-fuel ratio is determined as 34 according to the equation:

$$H_2 + \frac{1}{2}\times O_2 + \frac{1}{2}\times 3.76\ N_2 = H_2O + \frac{1}{2}\times 3.76\ N_2$$

or in terms of mass:

$$2 + 16 + \frac{1}{2}\times 3.76\times 28 = 2 + 16 + \frac{1}{2}\times 3.76\times 28$$

D.J Patterson, NA Henein (17 p 316) gives a value of 15.4 for the ratio for best sensitivity.

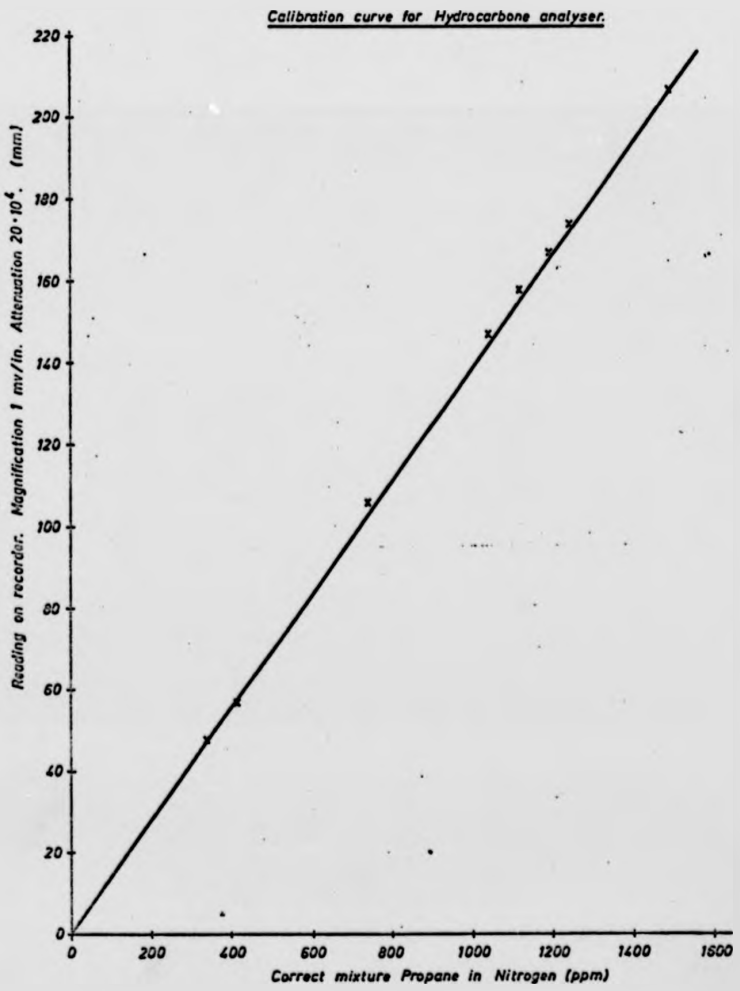

Fig.29

During ignition and warm-up the mixture was adjusted slightly richer. At leaner mixture it was very difficult to get ignition and the flame when ignited was very unstable.
The exact measurement of hydrocarbons is very difficult. Hydrocarbons are very easily trapped in the system. Condensed water contains hydrocarbons which then escape the analyser. Also the filtering necessary to prevent clogging of the sample jet will trap a certain amount of hydrocarbons. Previous work on hydrocarbons remaining in the water when the engine exhaust is emitted under water, as is the case with most boat engines, shows that hydrocarbons, even if they are not soluble in water, are dispersed in water for a considerable time before they settle. Some lighter hydrocarbons are also soluble to a certain extent (18).
The calibration curve for an FID analyser is linear. This makes it very easy to take quick calibration checks. To do this check there is an separate input on the analyser so that the sample flow from the engine need not be disconnected. For the calibration, propane in nitrogen was used.
Propane is much more convenient to use than hexane because hexane can condense at ambient temperature in a laboratory, giving different mixture strength at different temperatures.
The FID reads the amount of carbon in the sample. Propane ($C_3 H_8$) gives approximately half of the reading for hexane ($C_6 H_{14}$) because the ratio of number of carbon atoms is 1:2.
To check for linearity, four different mixture strengths were used namely 1000 ppm, 500 ppm, 100 ppm and 50 ppm.
As the calibration curve Fig.29 shows the linearity is good.
Because of the many factors influencing the sensitivity it is good practice to check one point of this curve every day before taking observations. This check can be done in 5 to 10 seconds. FID analysers bought as complete units are in this respect better because sophisticated pressure controls are built-in to ensure less variation in the flowrates of gases and sample. A " home made " analyser with mainly hand operated valve control and pressure gauges need somewhat more attention. If for instance the sample flow is too high the analyser output could be non-linear and in this case the one point calibration check would not necessarily indicate the fault.

4 Ultrasonic Atomisers

4.1 Possible methods for droplet formation

In paragraph 2.3 there is discussion of the importance of fine atomisation of the fuel for achieving quick evaporation in the inlet system. It seems to be very difficult to avoid impaction of even the smallest droplets in conventional systems, but the situation could be helped by heat input to vaporise the droplets so quickly after formation in the manifold that impaction is avoided. It would also be helpful to change the design of the inlet system so that no sharp bends or other restrictions, such as a butterfly valve, are situated closely after the atomiser. Some heat must be provided in this area, without increasing the charge temperature so much that a significant loss of volumetric efficency is caused. A suitable atomiser must therefore not only give small droplets, but must also be small enough to fit in the inlet system. Also the power source for the atomiser must be considered as well as the price of the whole device.

Many types of fuel atomiser have been developed. Many of these are able to give droplets of the size aimed for in the inlet system of an engine. However, these atomisers are expensive and need higher pressures than are easily possible with gasoline, the atomisers having been developed for diesel or heating fuel. In order to obtain higher pressures the use of piston type pumps is necessary. These piston pumps have small tolerances and the pumping of gasoline creates difficult lubrication problems. The pressure used in petrol injection systems is in the range 2 to 20 bar. Compared with the pressure in a diesel engine injector, up to 1000 bar and more, this pressure is very low. A swirl type atomiser operating at 20 bar would give droplets of approximately 75 µm diameter (19). Such droplets are still too large to reduce impaction and to obtain quick evaporation.

Mechanical atomisers also exist. A spinning disc atomiser has a cup or disc rotating at high speed, so that fuel spread on to the surface will be thrown off the lip and caught up by the surrounding air. Such atomisers are very difficult to incorporate into a inlet manifold design as the rotating disc needs bearings and must be driven by the airflow or by a separate electric motor. A spinning disc atomiser driven from the air sucked into the engine will have a low speed at idle and will perform very badly at start. Some of the pressure jets also perform badly at low speed because they are dimensioned for a much higher flow rate (de-

pending however upon the design of the pump and the injectors). Modern electronic injection systems often employ an electrically driven fuel pump (pressure 2 - 5 bar approx) and solenoid type injectors. The quantity of fuel delivered to the cylinder is metered by the length of the opening period of the injector valve. The pressure available for atomisation 2 - 5 bar would according to (19) give droplets in excess of 100 µm diameter.

The advantage of fuel injection systems, even those working at low pressure, is that the fuel is injected close to the hot inlet valve and even large droplets evaporate quickly because of the heat available.

The air metered for combustion can be kept cool and as no venturi is necessary there is less restriction to the flow into the cylinder. This gives a higher volumetric efficiency and a greater output power. There is however the question of whether the very short residence time of the droplets in the inlet system is enough to give the best possible fuel preparation especially at high engine speed. Smaller droplets should improve this condition by evaporating more rapidly. As we have stated previously, fuel injection systems, like carburettors, give an increase in the hydrocarbon emission at air-fuel ratios above 16 to 18.

The other aspect of incomplete combustion, maldistribution between cylinders, can be improved by the use of fuel injection systems because each injector can be adjusted separately to give the same amount of fuel.

Inhomogeneous mixture is a very difficult problem but some improvement would be achieved through better atomisation and the turbulent mixing of fuel and air.

Considering all these problems there seems to be no atomiser available which has all the features one could wish. In particularly the demand for low price and simplicity is difficult to fulfil with present systems.

Atomisation by ultrasonic vibrations has been known for nearly 50 years. Although the possibility of using ultrasonics as a tool to atomise fuel in engine inlet systems has been discussed in many papers concerned with pollution problems, very little has been published about research in this area.

This apparent lack of interest is very surprising since many scientists have predicted and shown by experiments that droplets of dimensions down to 1 µm can be obtained if the frequency is high enough. Obviously vibrations of such high frequency that 1 µm dia-

meter droplets are formed are difficult to obtain, especially with fuel flow rates high enough to be interesting for use in combustion engines. Also the electronics necessary to drive the vibrator was complicated and expensive before power transistors were available. Research carried out by Norster (20) shows this clearly.

There are two theories which attempt to explain the mechanism of droplet formation on a vibrating surface, the capillary wave theory and the cavitation theory. A standing sound-wave normal to a surface forms a wave pattern in a liquid film on the surface, and if the vibration amplitude is sufficently large, the capillary waves on the liquid surface cause liquid to break off and form droplets.

The wavelength of the capillary waves decreases with increasing frequency, which explains why the droplet diameter decreases with increasing exciting frequency. The cavitation theory explains the break off of droplets by pressure variations on the surface. According to this theory the pressure variations create cavities in the liquid film which cause droplets to be thrown off the surface.

Studies of a liquid film on a vibrating surface under a microscope show clearly that a wave pattern is formed that supports the capillary wave theory. Increasing the thickness of the liquid film changes this wave pattern and causes larger droplets to be thrown off the surface. This could support the idea that both the capillary wave theory and the cavitation theory are correct.

In a later chapter this problem is dealt with in more detail and relevant photographs are shown.

To produce droplets of one micron diameter an exciting frequency of up to 200 kHz would be needed. There are various methods of creating high frequency vibrations, but at frequencies higher than 100 kHz the piezoelectric ceramic seems to be the only and obvious choice. Magnetostrictive transducer needs more power and is far bigger and more difficult to incorporate in the inlet system of an engine.

The piezo-electric ceramics used for ultrasonic cleaning, underwater echo soundings, etc, are very compact devices and can create high frequency vibrations effectively.

Unfortunately there are no ultrasonic atomisers available on the market and research on ultrasonic atomisation in combustion engine

inlet systems must start with the development of ultrasonic vibrators capable of atomising at least 5 litres per hour to droplets of the smallest possible size.
5 litres per hour would be the maximum consumption of one cylinder of any gasoline engine on the market. It seems to be a better idea to develop an atomiser of that size and then to consider using several atomisers working together in an engine rather than one bigger atomiser capable of atomising, for instance, 20 litre per hour (for a 4-cylinder engine). Having one atomiser for each cylinder would make it possible to do investigations with atomisers mounted close to the inlet valve, as in injection systems.
Later research has established that the size of a " 20 litre " atomiser would make it very difficult to obtain the droplet size one is aiming for. This is because such a high flow rate makes it necessary to have a large diameter of the atomiser body. As we shall see later, there are limitations on the diameter/wavelength ratio because of special properties concerning the propagation of sound in solids. Very little is known about sound propagation in solids when the diameter/wavelength ratio approaches unity. Theory valid when the wavelength is much longer than the diameter of the speciman seems to collapse, and research carried out on diameter/wavelength ratios of approximately 0.5 shows that the sound propagation is not uniform and the soundwaves are impossible to direct.Much power is lost and atomisers built with this ratio do not perform efficiently.

4.2 The theory of piezoelectric ultrasonic vibration

Ultrasound belongs to the field of acoustics and can in many respects be compared with electromagnetic radiation and electricity. Ultrasonic waves travel in a medium, and obey the general wave equation, are reflected from surfaces, and are refracted when travelling from one medium to another. Ultrasonic energy can be scattered from surfaces just like light.
The comparison with electricity is that the force (or pressure) in the ultrasonic wavemotion acts like voltage, and the particle velocity is analogous to current.
The ratio pressure/velocity at a given point in the wave field is an acoustic impedance by analogy with the electrical impe-

dance, which is the ratio voltage/current. Like the electrical impedance in electricity, the acoustic impedance is a useful quantity to consider when the aim is to match different components to give the smallest possible losses in a transmission line, or to tune a vibrator to give a low loss standing wave of a certain frequency.

An ultrasonic wave which propagates in solid generates particle motion and creates strain and stress in the material. If the strain is within the elastic range of the material the wave motion is sinusoidal at any point in the system.

In ultrasonic vibrators of the type developed in the project there are several modes of different types of waves to consider but only the longitudinal waves in direction normal to the vibrating surface can be used effectivly to produce surface vibration of the kind used for atomisation.

All the other types of wave such as shear waves and surface waves must be regarded as disturbances which dissipate energy in the vibrator and make it less effective. The presence of the other types of waves makes the designing of ultrasonic vibrators difficult especially at higher frequencies. It is necessary to reduce the influence as much as possible of these " parasitic " wave forms at least in the resonance area of the vibrator.

It is not possible in any vibrator to avoid excitation of unwanted waveforms completely but some designs are better than others.

Figure 30 shows how longitudinal waves propagate in a rod with radius much smaller than the wave length of the frequency concerned ($a/\lambda \approx 0$). The waves cause the rod material to be compressed and expanded in the way illustrated in the figure. As long as the rod is slender the motion of the particles in a given cross section normal to the axis is uniform, that is the vibration amplitude is independent of radial or azimuthal position.

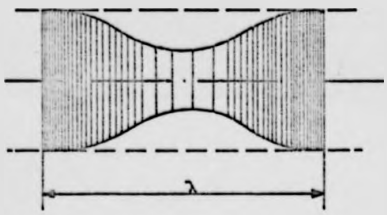

Fig.30

The speed c_o of the propagating wave is defined as $c_o = \frac{Y}{\rho}$ where Y is the Youngs Modulus and ρthe density of the material. (For

aluminium $c_o = 5.2 \times 10^3$m/s. In an" infinite " body the propagation of the sound is influenced by the surrounding material, and the expression for sound speed c_B incorporates a function of Poisson's ratio ν:

$$c_B = c_o \sqrt{(1-\nu)/(1+\nu)(1-2\nu)}$$

If the radius/wavelength ratio is in the range 0.05 to 1.1 (approximately) the speed of sound can not be defined by simple equations any more: in fact the soundspeed becomes almost unpredictiable Publication by L.Y. Tu and others (21) shows the longitudial wave velocity in rods as a function of radius wavelength ratio a/λ for different materials (figure 31). For aluminium c_B is 6.3×10^3m/s and for a/λ ratios smaller than 2.5 the sound speed drops considerably.

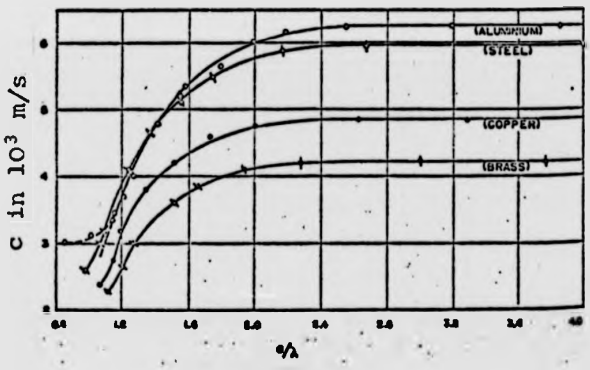

Fig.31

Figure 32 (21) shows more clearly the instability at a/λ ratios lower than 1.0 for an aluminium rod. The Figure shows the relative velocity $c/c_B = \frac{\text{Velocity in actual rod}}{\text{Velocity in infinite medium}}$ as a function of the radius-wavelength radio a/λ.

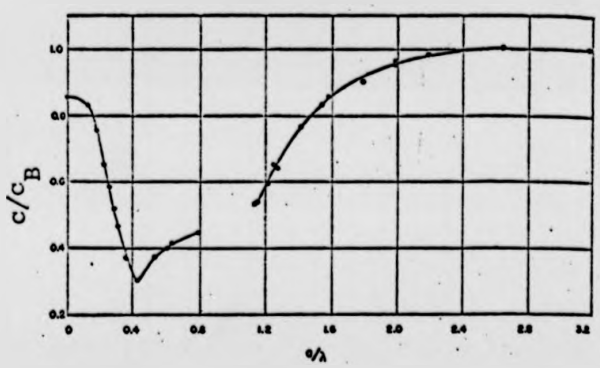

Fig.32

As can be seen there are no reliable results in the area $a/\lambda \approx 1.0$, and from $a/\lambda = 0.4$ to $a/\lambda = 0$ the velocity in the rod increases from approx 2.5×10^3 to 5.2×10^3m/s where the value 5.2×10^3m/s represents the velocity c_o in a slender rod.

The results shown in Figure 31 and 32 for aluminium agree well with

what was discovered during the present experiments with different types of vibrators. A vibrator shaped to give an increased amplitude of vibration may be called a concentrator or a velocity transformer, the shape of a velocity transformer is not a simple cylinder and the sound speed is dependent upon the actual geometry. Difficult shapes cause different types of waveform to be excited and this complicates the problem.

According to the frequency - wavelength relation, $\lambda = c/f$, velocity transformers working at 100 kHz would have a wavelength based on c_o, of approximately 52 mm. It is therefore not possible at such high frequency to avoid a/λ ratios in the region of $a/\lambda = 0$ to 1.0. In fact for this application of ultrasonics, one is quite likely to be working in the neighbourhood of $a/\lambda = 0.5$. All efforts to get a concentrator to perform well at approximately this ratio have been unsuccessful.

As we shall see later the one-dimensional theory of wavepropagation is not valid at a/λ ratios below approximately 2.5. However in the search for a mathematical model it is interesting to look at the one dimensional theory first.

4.2.1 One-dimensional wave equations

An elastic medium may be considered to consist of homogeneous elements of density ρ, Young's Modulus Y, thickness dx and cross sectional area S. When a compressive force F_x is applied to the element the material allows a displacement ζ.

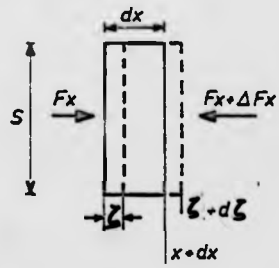

Fig.33

The force $$F_x = - Y S \frac{\partial \zeta}{\partial x} \quad (1)$$

at (x + dx) the force is

$$F_x + dF_x = F_x + \frac{\partial F_x}{\partial x} dx \quad (2)$$

(1) gives $\frac{dF_x}{dx} = -Y\ S\ \frac{\partial^2 \zeta}{\partial x^2}$

or in (2) $$F_x + dF_x = F_x - Y\ S\ \frac{\partial^2 \zeta}{\partial x^2}\ dx \qquad (3)$$

The net force acting on the element x is therefore

$$F_x - F_x - Y\ S\ \frac{\partial^2 \zeta}{\partial x^2}\ dx = - Y\ S\ \frac{\partial^2 \zeta}{\partial x^2}\ dx$$

The acceleration force of the element is

$$F_A = M\ \frac{\partial^2 \zeta}{\partial t^2} \quad \text{where } M = S\ \rho\ dx \text{ is mass of element}$$

$$F_A = S\ \rho\ dx\ \frac{\partial^2 \zeta}{\partial t^2}$$

For loss-less vibration the elastic forces and the inertia forces are equal.

$$\rho\ \frac{\partial^2 \zeta}{dt} + Y\ \frac{\partial^2 \zeta}{\partial x^2} = 0 \qquad (4)$$

This equation can also be written in the form

$$\frac{\partial^2 \zeta}{dt} + \frac{Y}{\rho}\ \frac{\partial^2 \zeta}{\partial x^2} = 0$$

or, since $c_o^2 = Y/\rho$,

$$\frac{\partial^2 \zeta}{\partial t^2} + c_o^2\ \frac{\partial^2 \zeta}{\partial x^2} = 0$$

This equation is only valid for a slender bar with uniform cross-sectional area at very small a/λ ratios.
If the area changes with x the equation of motion in the element can be derived as follows:

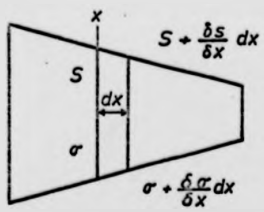

Fig.34

At (x + dx) is the stress

$$\sigma = Y\ \frac{\partial \zeta}{\partial x}$$

and the cross-sectional area is:

$$(S_x + dS_{xx}) = S_x + \frac{S}{x}\ d_x$$

Therefore the equation 4 changes to:

$$Y\,S\,\frac{\partial^2\zeta}{\partial x^2}\,dx + S\,\rho\,dx\,\frac{\partial^2\zeta}{\partial t^2} - Y\,\frac{\partial\zeta}{\partial x}\,\frac{\partial S}{\partial x}\,dx = 0$$

or:

$$\frac{1}{c_o^2}\,\frac{\partial^2\zeta}{\partial t^2} - \frac{1}{S}\,\frac{\partial S}{\partial x}\,\frac{\partial\zeta}{\partial x} + \frac{\partial^2\zeta}{\partial x^2} = 0 \qquad (5)$$

This differential equation can be solved using the general solution $\zeta = f_1(ct - x) + f_2(ct + x)$.

L.G Merkulov (22) has calculated magnification factors and stress for concentrators of different shape and has shown (22) how the results can be used as a tool for designing transformers. However, the assumption that the sound propagation is one-dimensional is not valid for transformers of the type and size which are of interest in this project.

Many experiments carried out during the development period show clearly that the work carried out by L.G. Merkulov and others (22) is not very useful in the design of concentrators with small dimensions and high frequency.

4.2.2 Two-dimensional wave equation

The two-dimensional equations are written for axi-symmetric bodies with the assumption that the stress-strain relation is linear. The vibration is assumed to be undamped.

The positions of the vibrating particles are defined in a cylindrical polar coordinate system (r, θ, x) in terms of u, the displacement in x-direction, and v, the displacement in radial direction. Because of the axi-symmetry there is no displacement in the θ - direction. Figure 36 shows an element at position (r,θ,x) in the coordinate system. The thickness of an element is dr and the depth is dx. By symmetry σ_θ is independent of θ so that there is no shear stress in the σ_θ direction therefore:

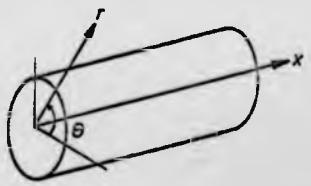

Fig.35

$$\tau_{\theta r} = 0, \quad \tau_{r\theta} = 0, \quad \tau_{\theta x} = 0, \quad \tau_{x\theta} = 0$$

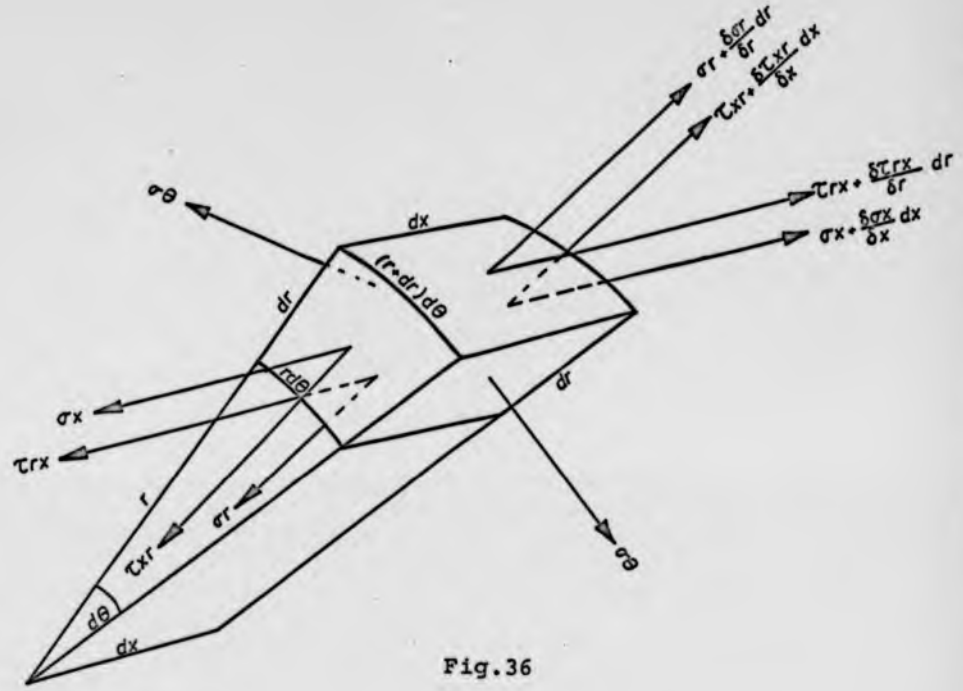

Fig.36

For the radial motion:

$$\left(\sigma_r + \frac{\partial \sigma_r}{\partial r}\, dr\right) dx\ (r+dr)d\theta - \sigma_r\, dx\ r\, d\theta$$

$$+ \left(\tau_{xr} + \frac{\partial \tau_{xr}}{\partial x}\, dx - \tau_{xr}\right) dr\ r\, d\theta - 2\sigma_\theta\, dr\, dx \sin\frac{d\theta}{2}$$

$$= dr\, dx\, r\, d\theta\, \rho\, \frac{d^2v}{dt^2}$$

or

$$\left(\frac{\partial \sigma_r}{\partial r} + \frac{\partial \tau_{xr}}{\partial x}\right) + \left(\frac{\sigma_r - \sigma_\theta}{r}\right) = \rho\, \frac{\partial^2 v}{\partial t^2} \qquad (1)$$

Equation (1) represents the equation of motion in the radial direction.

For axial motion the equation is:

$$\left(\sigma_x + \frac{\partial \sigma_x}{\partial x} dx - \sigma_x\right) dr\, r\, d\theta + \left(\tau_{rx} + \frac{\partial \tau_{rx}}{\partial r} dr\right)(r+dr)\, d\theta\, dx$$

$$- \tau_{rx}\, r\, d\theta\, dx = dr\, dx\, r\, d\theta\, \rho \frac{d^2u}{dx^2}$$

That is

$$\left(\frac{\partial \sigma_x}{\partial x} + \frac{\partial \tau_{xr}}{\partial r}\right) + \frac{\tau_{rx}}{r} = \rho \frac{\partial^2 u}{\partial x^2}$$

The three-dimensional stress-strain relationships are:

$$\sigma_x = \frac{E}{1+\nu}\left[\varepsilon_x + \frac{\nu}{1-2\nu}(\varepsilon_x+\varepsilon_r+\varepsilon_\theta)\right] \qquad (3)$$

$$\sigma_r = \frac{E}{1+\nu}\left[\varepsilon_r + \frac{\nu}{1-2\nu}(\varepsilon_x+\varepsilon_r+\varepsilon_\theta)\right] \qquad (4)$$

$$\sigma_\theta = \frac{E}{1+\nu}\left[\varepsilon_\theta + \frac{\nu}{1-2\nu}(\varepsilon_x+\varepsilon_r+\varepsilon_\theta)\right] \qquad (5)$$

$$\tau_{rx} = \tau_{xr} = G\, \sigma_{xr} = \frac{E}{2(1+\nu)} \gamma_{xr} \qquad (6)$$

Also

$$\varepsilon_x = \frac{\partial u}{\partial x}, \qquad \varepsilon_r = \frac{\partial v}{\partial r}, \qquad \varepsilon_\theta = \frac{v}{r}, \qquad \gamma_{xr} = \frac{\partial u}{\partial r} + \frac{\partial v}{\partial x} \qquad (7 - 10)$$

Equations 1 and 3-10 (2) give the following relation for radial motion in terms of displacement.

$$\frac{E}{1-\nu}\left[\frac{\partial^2 v}{\partial r^2} + \frac{\nu}{1-2\nu}\left(\frac{\partial^2 u}{\partial x \partial r} + \frac{\partial^2 v}{\partial r^2} + \frac{1}{r}\frac{\partial v}{\partial r} - \frac{v}{r^2}\right)\right] + \frac{E}{2(1+\nu)}\left[\frac{\partial^2 v}{\partial r \partial x} + \frac{\partial^2 v}{\partial x^2}\right]$$

$$+ \frac{E}{r(1+\nu)}\left[\frac{\partial v}{\partial r} - \frac{v}{r}\right] = \rho \frac{\partial^2 v}{\partial t^2}$$

or

$$\left(\frac{1-\nu}{1-2\nu}\right)\frac{\partial^2 v}{\partial r^2} + \left(\frac{1}{2(1-2\nu)}\right)\frac{\partial^2 u}{\partial r \partial x} + \left(\frac{1-\nu}{1-2\nu}\right)\left(\frac{1}{r}\right)\frac{\partial v}{\partial r} - \left(\frac{1-\nu}{1-2\nu}\right)\frac{v}{r^2} + \frac{1}{2}\frac{\partial^2 v}{\partial x^2}$$

$$= \rho \frac{(1+\nu)}{E} \frac{\partial^2 v}{\partial t^2}$$

Similarly the equation for axial motion in terms of displacement is

$$\frac{E}{1+\nu}\left[\frac{\partial^2 u}{\partial x^2} + \frac{\nu}{1-2\nu}\left(\frac{\partial^2 u}{\partial x^2} + \frac{\partial^2 v}{\partial x \partial r} + \frac{1}{r}\frac{\partial v}{\partial x}\right)\right] + \frac{E}{2(1+\nu)}\left[\frac{\partial^2 u}{\partial r^2} + \frac{\partial^2 v}{\partial x \partial r}\right]$$

$$+ \frac{E}{2(1+\nu)r}\left[\frac{\partial u}{\partial r} + \frac{\partial v}{\partial x}\right] = \rho \frac{\partial^2 u}{\partial t^2}$$

Simularly the equation for axial motion in terms of displacement is

$$\left(\frac{1-\nu}{1-2\nu}\right)\frac{\partial^2 u}{\partial x^2} + \left(\frac{1}{2(1-2\nu)}\right)\frac{\partial^2 v}{\partial x \partial r} + \left(\frac{1}{2(1-2\nu)}\right)\left(\frac{1}{r}\right)\frac{\partial v}{\partial x} + \frac{1}{2r}\frac{\partial u}{\partial r}$$

$$+ \frac{1}{2}\frac{\partial u}{\partial r} = \rho \frac{1+\nu}{E} \frac{\partial^2 u}{\partial t^2}$$

The equations have three independent variables and the relations are very complex and difficult to solve. After consultations with mathematicians at the University of Warwick, it was finally decided that the use of the finite element method would require less time and would have better chance of success.

4.2.3 The analysis of vibrations using finite element computer programme

During the last few years the finite element method has become widely accepted as a very valuable method of analysis for temperature, stress and displacement problems.
Programmes for steady state analysis of axi-symmetric and plane structures are already common, but the techniques are now being applied to time-varying problems (23).
The programmes available for axi-symmetric structures are not suitable for longitudinal vibrations of the kind present in ultrasonic concentrators. To rewrite those programmes would take a very long time, and it seemed to be a better idea to use the part of Norsk Veritas SESAM 69 programme package which is made to deal with eigenvalue problems in the structure of ships. SESAM 69 (24) stands for " Super Element Structural Analysis program Modulus " and is a computer programme based on the Finite Element Method, especially adapted for use in the multilevel super-element technique. A super-element is an element created from bacic elements due to reduction of certain degrees of freedom.
For the analysis of free vibration and to calculate eigenvalues and diplacements in solids of the kind considered in this project, the part-programme NV 333 for solving three dimensional problems can be used.A three dimensional finite element programme needs long computer time and is expensive to use. In order to reduce the computer time as much as possible the nodes of the elements were fixed in the tangential direction and the displacements at the same radius and same position on the x-axis were made linearly dependent.
In this way the number of degrees of freedom could be reduced significantly.

The computer programme is based on the displacement method and works with twenty-node isoparametric hexahedron elements.
Such elements permit adjustment of the shape to fit the structure more accurately depending of course upon the number of element used.
Figure 37 shows a typical element.

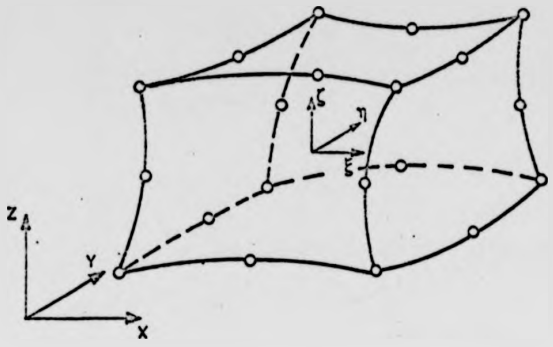

Fig.37

A shape function matrix of second degree defines the displacements at the nodes. The same function is used to describe the geometry of the element.
The displacements within the element are given by:

$$u_x = [N]\ (\delta_x)^e$$

$$u_y = [N]\ (\delta_y)^e$$

$$u_z = [N]\ (\delta_z)^e$$

Where u_x, u_y, u_z are the displacements in x, y and z direction respectively. N is the matrix containing the shape function N_i (i = 1 to 20) and $(\sigma_x)^e$, $(\sigma_y)^e$, $(\sigma_z)^e$ are nodal displacement vectors in the three directions.

The shape functions are

for corner nodes:

$$N_i = \frac{1}{8}(1 + \zeta\zeta_i)(1 + \eta\eta_i)(1 + \xi\xi_i)(\xi\xi_i + \eta\eta_i + \zeta\zeta_i - 2)$$

for mid edge nodes:

$$N_i = \frac{1}{4}(1 - \xi^2)(1 + \eta\eta_i)(1 + \zeta\zeta_i)$$

where $\xi_i = 0$

where $n_i = 0$

$$N_i = \frac{1}{4}(1 + \xi\xi_i)(1 - \eta^2)(1 + \zeta\zeta_i)$$

where $\zeta_i = 0$

$$N_i = \frac{1}{4}(1 + \xi\xi_i)(1 + \eta\eta_i)(1 - \zeta^2)$$

Here ξ_i, ζ_i, η_i are nodal values of ξ, ζ and η respectively.

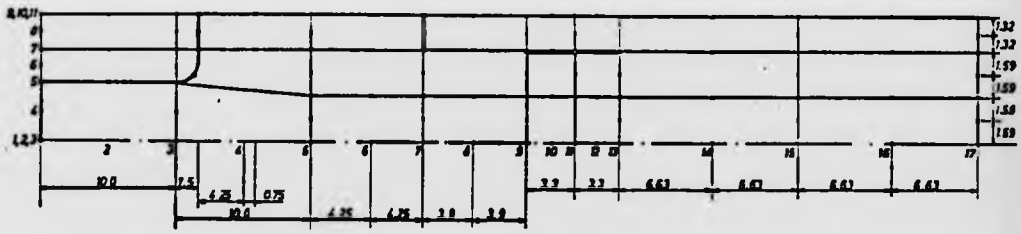

Fig.38

Figure 38 shows the element mesh in the half section of the atomiser of type 22 described later in this report. The mesh is quite coarse in order to save computer time. In the three-dimensional programme the number of degrees of freedom is 672. This would mean an execution time of approximately 1/2 hour at the Univac 1108 computer. However, by fixing the movement in the y-direction (angular) and specifying linear dependence on some nodes in z-direction, the number of degrees of freedom was reduced to 188 and the computer time cut to about 15 minutes.
The element mesh is built up of nine planes in the z-direction and four planes in the x-direction giving 11 and 17 nodal planes respectively. The nodal planes 9,11,13 in the z-direction are positioned on the surface of the transducers. In the interface between the transducers and the compressional member of the atomiser body (sleeve), as well as at the end of the sleeve some extra nodes had to be defined in order to ensure separation of the transducers from the atomiser body. This part of the structure represents the most diffi-

cult part in the mesh, and some assumptions had to be made. Instead of making a very complicated geometry, the elasticity of the material was adjusted in inverse proportion to the cross-sectional area of the sleeve. This takes into account that the 1.5 mm clearence between the transducers and the sleeve is not provided for.

Figure 39 shows the three-dimensional plot of the mesh.
The numbers represents the nodal number.
The accuracy of the calculation is very much dependent on the relation between the size of elements and the wavelength of the sound wave. The wavelength in aluminium at 98.5 kHz is, for the chosen geometry about 49.5 mm which is considerably longer than the length 10 mm of the biggest element, but for higher harmonics the accuracy is not expected to be good.
The computer programme calculates amplitudes of movment in axial and radial directions.
Resonances will be registered in both directions although mainly resonances in axial directions are of interest for this project.
The following table contains the print-out of the eigenvalues for the first 20 modes. The figure in brackets gives the correct measured average value for the atomiser of type 22.
As can be seen the accuracy of the calculation is surprisingly good, especially at the working resonance of the atomiser where the discrepancy is 1.79% between the calculated and measured value.

S U M M A R Y O F F R E Q U E N C I E S

MODE NO.	FREQ(KHERTZ)	MODE NO.	FREQ(KHERTZ)
1	.000	11	193.039
2	42.546 (38.0)	12	199.930
3	75.714 (72.2)	13	203.366
4	100.371 (98.6)	14	214.703
5	127.125 (123.0)	15	219.214
6	151.844	16	235.733
7	163.696	17	239.556
8	168.606	18	247.508
9	174.171	19	258.173
10	183.102	20	267.134

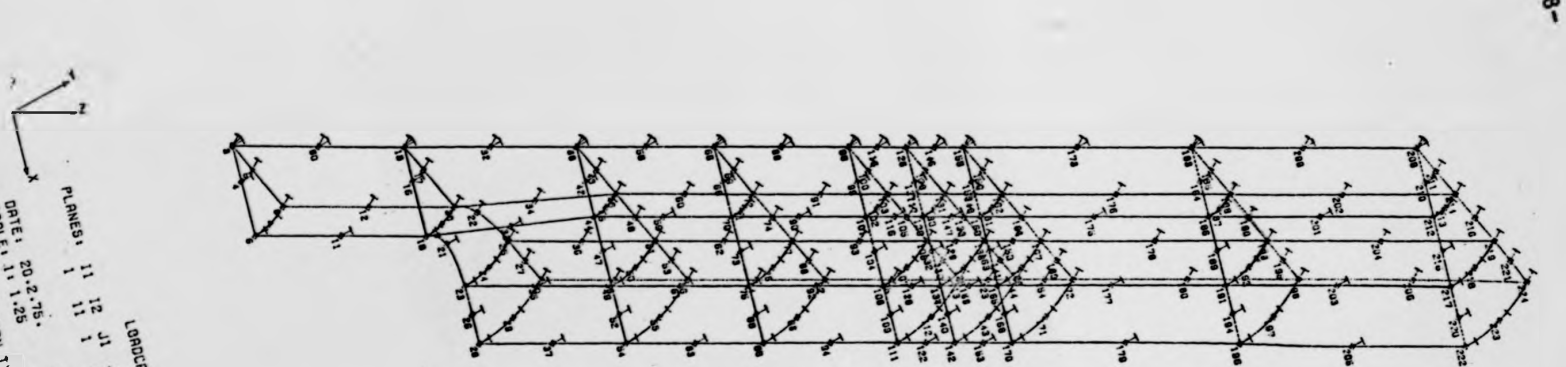
Y
Z
X
PLANES: I1 I2 J1 J2 K1 K2
1 11 1 3 1 17
LOADCASE: 1.
DATE: 20.2.75.
SCALE: I: 1.25
ULTRASONIC HORN TYPE 22

Fig.39

The fact that the calculated values are higher than the measured ones gives reason to believe that a finer element mesh would improve the accuracy of the calculation.
The displacement method of the finite element programme causes decrease of stiffness if the element mesh is finer: this is the reason why the calculated values are higher than the correct ones. It is encouraging that the coarse element mesh used gives such good results.
Figure 40 shows the displacements of the nodes in the 4 main planes along the x-axis. As can be seen the vibration amplitude of the atomiser tip smaller end is approximately 10 times bigger than the amplitude of the larger end. Where the displacement curves cross the x-axis represent nodes in the structure. The countour lines run on the atomiser body (Figure 40) shows how the propagation of the wave varies across the diameter.
The three contour lines represent the nodes of the standing wave and the location of the nodes at the surface of the body are almost exactly where they can be detected on the surface of the body by means of a microscope. This will be discussed in more detail in a later chapter.

If the element mesh is made fine enough the calculation would show in more detail the wave-pattern in the transducer region. This would be a very useful help for optimising the atomiser to best possible efficiency.
For a series of calculations a three dimensional programme is too complicated and expensive to use. The calculation presented in this thesis shows, however, that the use of finite element methods can be extremely valuable as an aid in design of ultrasonic concentrators. Obviously a two dimensional programme based on an axi-symmetrical method would cut the computer execution time (CPU-Time) considerably, and it would be worth while to write such a programme if further investigations are to be carried out. The work involved in writing a programme for axi-symmetrical bodies is estimated to take more than one year and would be outside the scope of this project.

Appendix III gives the computer print-out of the linear displacements at mode 4 and a flow diagram of the programme, showing the basic steps in the calculation.

Fig.40, to page 89

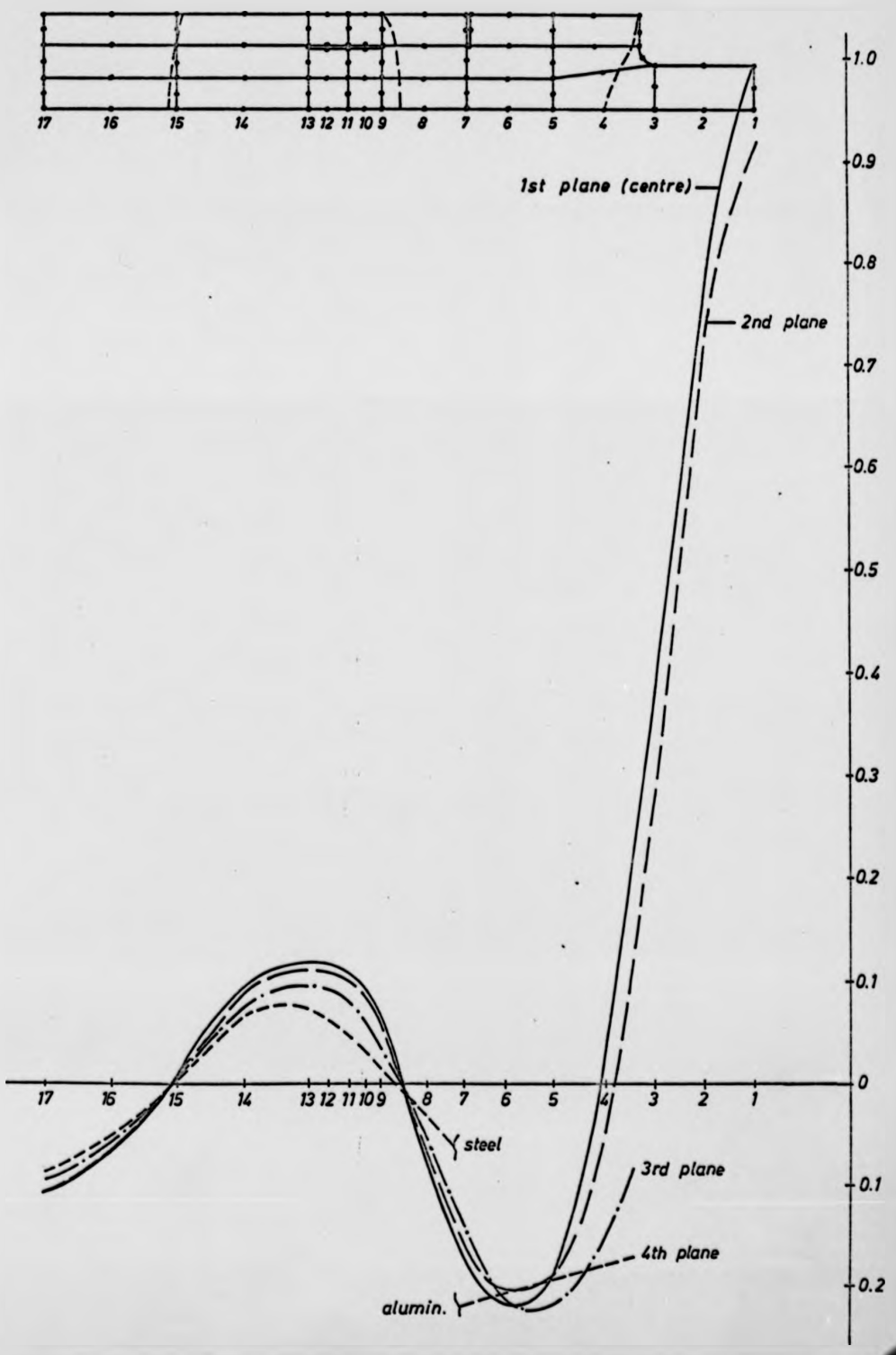

4.3 Some properties of ultrasonics

As we have heard, the attenuation of ultrasonic waves is dependent upon two factors, namely the geometrical factor and the energy absorption or scattering characteristics of the media involved. The geometrical factor takes into account the size of the sound source and the wavelength of the sound waves as well as the presence of reflecting surfaces near to the propagating wave. The maximum rate of decrease of intensity occurs when a point source is located far from any reflecting surface in a infinite medium. The acoustic intensity is defined as $I = W/S$, where W is energy of the sound wave and S the area at right angles to the direction of the wave propagation. In the case of a point source and maximum rate of intensity decrease $I = W/4\pi r^2$, where r is the distance from the source.

Energy absorption in solids is dependent upon frequency: a higher frequency increases the losses in most cases.

Losses in solids are explained as a non elastic phenomenon, and other imperfections in the structure of the material. The absorption in solids varies from 1/1000 dB/metre in homogeneous material to 100 dB/metre in plastics and cast iron ($dB=10 \log_{10}(\frac{I}{I_0})$.

To quantify the transmission of sound waves in different solids acoustic impedance is defined as:

$$Z_{ac} = \frac{\text{sound pressure}}{\text{volume velocity}}$$

The volume velocity is the particle velocity multiplied by the area in which the sound pressure acts.

An important factor is the characteristic impedance $R = \rho c$ (c = speed of sound, ρ density). The characteristic impedance explains acoustic properties of a medium, and is an important parameter in determining how a sound wave acts when propagating into another medium.

When a sound wave is propagating normally through a boundary between two media, part of the energy of the wave will be reflected and the other part transmitted according to the properties of the two media.

The part of energy transmitted (α_t) or reflected (α_r) can be described in terms of the characteristic impedances of the two media as follows.

$$\alpha_t = \frac{I_t}{I_i} = \frac{4\rho_2 \cdot c_2 \cdot \rho_1 \cdot c_1}{(\rho_2 \cdot c_2 + \rho_1 \cdot c_1)^2} \qquad \alpha_r = \frac{I_r}{I_i} = \left(\frac{\rho_2 \cdot c_2 - \rho_1 \cdot c_1}{\rho_2 \cdot c_2 + \rho_1 \cdot c_1}\right)^2$$

where I_t and I_r are intensity of the transmitted and reflected waves respectively and I_i is the intensity of the incident wave. It is important to note that if the characteristic impedance of two media is the same, the sound wave would theoretically be transmitted without reflection, and the intensity of the transmitted wave would equal I_i. The equations for sound power reflection or transmission coefficients (α_r and α_t) show also that if $\rho_2 c_2 > \rho_1 c_1$ the reflected wave has the same phase as the incident wave. If $\rho_1 c_1 > \rho_2 c_2$ a phase shift occurs.

Figure a and b shows water with $\rho c = 1.48 \times 10^6$ kg/m^{2}s and steel with $\rho c = 46.7 \times 10^6$kg/m^{2}s characteristic impedance.

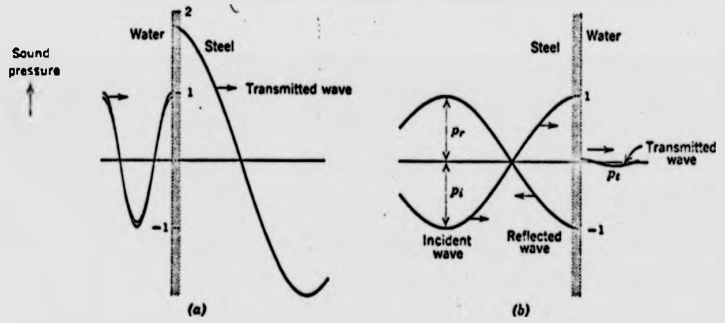

The sound pressure wave transmitted from steel to water is very much reduced in amplitude.

The amplitudes for reflected or transmitted soundpressure (P) can be calculated using the relations

$$I = \frac{p^2}{2\rho c}$$

or $$\frac{P_r}{P_i} = \frac{\rho_2 \cdot c_2 - \rho_1 \cdot c_1}{\rho_2 \cdot c_2 + \rho_1 \cdot c_2} \quad \text{and} \quad \frac{P_t}{P_i} = \frac{2\rho_2 \cdot c_2}{\rho_2 \cdot c_2 + \rho_1 \cdot c_1}$$

Standing waves are formed as a result of interference of waves of the same frequency. Longitudinal waves which are reflected at a surface will produce a resultant wave of amplitude dependent upon the phase. At " in phase " condition the amplitude is at maximum. Out of phase condition will represents a sum of the incident and the reflected wave. If the two sound waves are 180° out of phase there is a cancellation and a standing wave is formed. For a standing wave there is no flow of energy along the axis of the sound wave and particles in distance $\lambda/2$ never move. A

standing wave has nodes and antinodes. At the antinode the displacement of the particles is maximum (ξ max). All ultrasonic devices working with high intensity vibrations are tuned to give sound waves which reflect on a surface and produces waves in the opposite direction exactly in phase. This condition is called resonance. The resonance length of a solid bar depends upon the sound speed and the frequency according to $c = \lambda f$, where c is the speed of sound, λ the wavelength and f the frequency.

A solid bar would be in resonance if the length of the bar $l = \frac{\lambda}{2} = \frac{c}{2f}$. A cylindrical bar would have the same maximum displacement at each end $\xi o = \xi e$. As we shall see, the shape of the body in which ultrasound travels can make ξe different. If the body is designed to increase the amplitude we are speaking of a velocity transformer or concentrator.

Equation 5 page 80 describes the displacement in transformers and the term $\frac{1}{S}\frac{\partial S}{\partial x}\frac{\partial \xi}{\partial x}$ takes the change in shape into account if one dimensional propagation is assumed.

Investigation of different shapes leads to the conclusion that stepped horns or double cylindrical shapes give the most advantages in our case, taking production, size and the special application into account.

The equation on page 80 describes the propagation of sound waves in solids in which the cross-sectional area changes along the axis of motion. By solving this equation the magnification of particle velocity and displacement can be computed for any easily defined shape of velocity transformer.

In the case of a stepped transformer the problem is so simple that, by looking at the equilibrium of elastic forces in the step of the horn, one can find the magnification factor of the transformer.

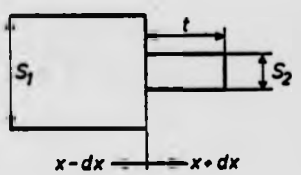

Fig.41

The magnification factor of a transformer is defined as the ratio

$$\frac{\xi_2}{\xi_1} = \frac{\text{Displacement in smaller cylinder}}{\text{Displacement in larger cylinder}}$$

Equilibrium of Force requires:

$$F\ (\ x+dx\ ) = Y\ \frac{\partial \xi_2}{\partial x} S_2$$

$$F\ (\ x-dx\ ) = Y\ \frac{\partial \xi_1}{\partial x}\ S_1$$

Assuming that the two elastic forces are equal we have consequently that

$$\frac{\xi_2}{\xi_1} = M = -\frac{S_1}{S_2}$$

The magnification of displacement in a stepped horn is proportional to the inverse of the cross-sectonal area ratio. In other words, by making the diameter ratio in a stepped transformer $\frac{D_1}{D_2} = \delta$ the magnification of the particle displacement would increase with a factor δ^2. If a 1/2 wavelength resonant bar is considered the node of the soundwave would be located in the centre. In this region there would be intolerable stress if the two cylindrical bars were joined together as illustrated above (Fig. 41). It is necessary to fabricate a stepped transformer with a fillet to reduce the stresses at that point.

Assuming that the soundwave in the stepped horn is sinusoidal we may calculate the maximum stress in the step if the maximum displacement of the tip of the smaller ends is known and the wavemotion is one dimensional.

If the length of the smaller cylinder is t, we may write that the amplitude is:

$$a = \xi_2 \sin \frac{x}{t} \frac{\pi}{2}$$

The strain $\varepsilon = \frac{da}{dx}$, and da derived from the sine wave equation

$$da = \frac{\xi_2 \pi}{2t} \cos \frac{x\pi}{2t}\, dx$$

gives $\varepsilon = \frac{\xi_2 \pi}{2t} \cos \frac{x\pi}{2t}$

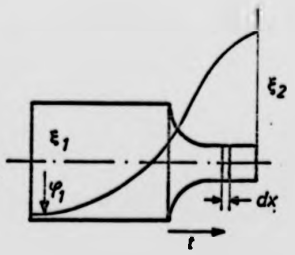

Fig.42

at x = 0, in the high stress area is ε max = $\frac{\xi_2 \pi}{2t}$ and the stress

$$\sigma \text{ max} = \frac{\xi_2 \pi}{2t} Y$$

This expression for maximum stress is only correct at radius/wavelength ratios higher than 2.5 and does not take into account the fillet radius.

There are shapes other than the double cylinder which give the same magnification factor and less concentration of stress. Figure 43 shows some alternative shapes with the curves for stress and velocity (from 25).

For the same magnification the stepped transformer is shorter than other transformers, and allows a larger surface area on the tip.

For the purpose of atomisation the size of the transformer end is of course very important as it is on this vibrating surface that the liquid must be applied for atomisation. There are several technicalities involved too. The stepped horn is easiest to manufacture and, as will be discussed later, the shape allows simple tools to be used during turning in the lathe and when mounting the parts together.

The Fourier horn is perhaps the best alternative to the stepped horn, but it gives a smaller magnification at the same diameter ratio, and is longer. The most effective type of horn, the exponential, is very long and slender with the smallest area on the tip of all the shapes considered.

Figure 44 shows the diametral ratios as functions of magnification for the transformers mentioned.

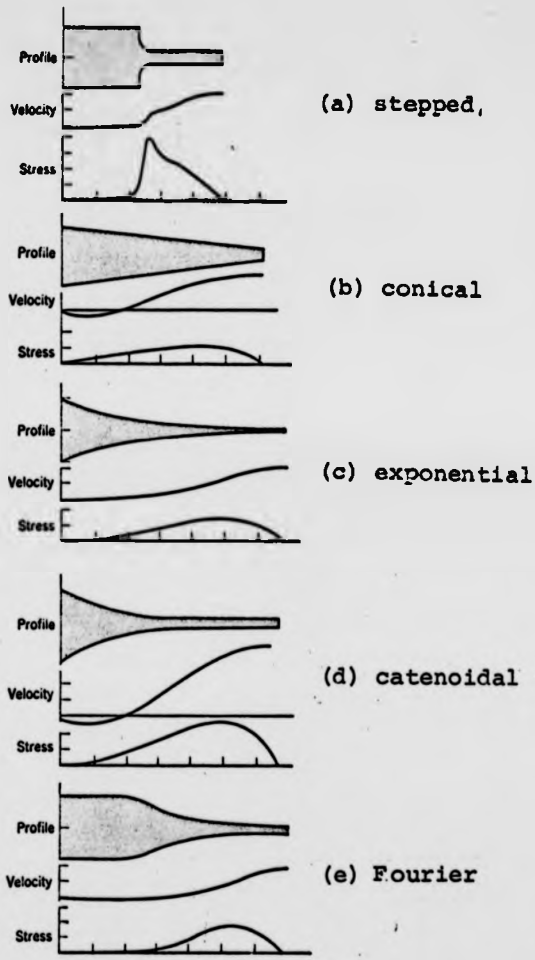
Profile
Velocity
Stress
(a) stepped,
Profile
Velocity
Stress
(b) conical
Profile
Velocity
Stress
(c) exponential
Profile
Velocity
Stress
(d) catenoidal
Profile
Velocity
Stress
(e) Fourier

Fig.43

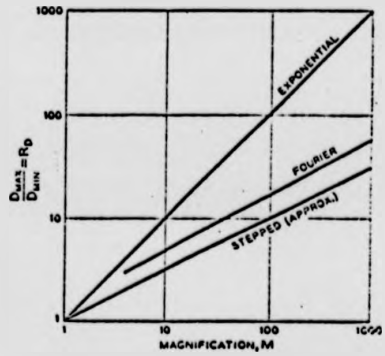
1000
100
10
1
EXPONENTIAL
FOURIER
STEPPED (APPROX.)
1
10
100
1000
MAGNIFICATION, M

Fig.44

4.4 Piezoelectric transducers

A piezoelectric transducer transforms electrical energy into mechanical energy or vice versa.
There are two principal types of piezoelectric transducer, namely those made of material which is naturally piezoelectric and those made of material that is piezoelectric only after special treatment.
Quartz is a material occurring naturally with piezoelectric properties. Certain manmade materials, such as Rochelle salt and lead niobate, are piezoelectric without special treatment. The most widely used piezoelectric transducers are electrostrictive and are made piezoelectric by polarization, involving an intense electric field applied whilst the material is cooled from higher temperature (above the Curie temperature). If an electrical charge is applied to the surfaces of a piezoelectric slab, the material will contract or expand depending upon the polarisation and the direction of current. On the other hand a charge will be produced on the same surfaces if the slab is compressed or expanded mechanically. The electromechanical coupling coefficient k describes the ability of the material to change the energy from one form to the other.

$$k^2 = \frac{\text{electrical energy produced}}{\text{mechanical energy into transducer}}$$

$$k^2 = \frac{\text{mechanical energy produced}}{\text{electrical energy into transducer.}}$$

Another important factor is the dielectric constant K defined, like that for a condenser, as the charge which can be stored on the electrodes on a piezoelectric slab compared with the charge which would be stored if the electrodes were separated by air. There is, however, a change in the dielectric constant K according to whether the slab is clamped or free.
If clamped, neither expansion nor contraction is possible. The relation between the clamped and free values is

$$K_{\text{free}} = \frac{K_{\text{clamped}}}{1 - k^2}$$

In a similar way the elastic properties are changed according to whether the electrodes of the transducer are on open circuit or short circuit.

$$Y_{open} = \frac{Y_{short}}{1 - k^2}$$

Y is Young's Modulus of the material.

More important constants are the piezoelectric coefficients d and g, defined as follows.

$$g = \frac{\text{field produced}}{\text{applied stress}} \qquad \frac{\text{volts/m}}{N/m^2}$$

$$d = \frac{\text{charge}}{\text{force}} \qquad \frac{\text{coul}/m^2}{N/m^2}$$

$$d = g\, k\, \varepsilon_0 \qquad \frac{m/m}{V/m}$$

where ε_0 = permittivity of a vacuum (9×10^{-12} farad/m)
The relationship with the coupling coefficient is

$$k^2 = g\, d\, E$$

In the research carried out lead zirconate titanate was used with $k = 0.70$, $g = 26.1 \times 10^{-3}$ $\frac{V/m}{N/m^2}$, $d = 289 \times 10^{-12}$ m/V

and $E = 8.15 \times 10^{10}$ N/m^2.

This material with the trade name PTZ4 has a high Curie temperature of 328 °C and a dynamic tensile strength of approximately 245 kp/cm² (25MN/m²).
The piezoelectric coefficent $g = 26.1 \times 10^{-3}$ $\frac{V/m}{N/m^2}$ indicates that a stress equal to the max. tensile strength for instance, 25 MN/m², produces potential differences of approx 650 Volts in a crystal 1mm thick. The same material 1cm thick would accordingly produce 6500 volts. The compression of big piezoelectric ceramics must therefore be done with care. Although the current involved is not high, a composite transducer for instance (several crystals in series) can produce a high voltage and cause dangerous electric shocks. When a large ceramic is compressed the electrodes must be insulated or shorted for safety reasons. A very important factor when choosing ceramics is the temperature range of the material. If the ceramic temperature exceeds the Curie temperature the polarisation of the ceramic is neutralized and the ceramic is damaged. Piezoelectric ceramics have a Curie temperature from 50 °C, (Rochell salt) and up to over 600 °C for some electrostrictive ceramics. Quartz has a high Curie temperature too, 575 °C, but is expensive and needs a high driving

voltage (having d = 2.3×10^{-12} m/V compared with 400×10^{-12} m/V for some manmade ceramics).

Unlike artificially made ceramics the natural piezoelectric crystal such as quartz will regain its piezoelectric properties after an accidental overheating of the crystal. This can often be experienced in piezoelectric pressure-transducers used to measure pressure in combustion chambers of IC engines, where the temperatures exeed 1000 °C.

Another limitation in the use of piezoelectric transducers is the tensile strength. If too much power is fed to the transducer the stress created in the material exeeds the tensile strength and the transducer splits. A crack in the transducer most certainly reduces the efficency if the transducer is bound to the transformer with adhesive. A clamped transducer could continue to perform if the crack does not reduce the clamping force or the electrical and mechanical contact to the transformer.

Higher power to the transducer will always create higher temperature. An important thing to remember in the application of piezoelectric transducers is that the heat created must be allowed to be transported from the ceramics to the surroundings. If necessary artificial cooling must be considered. High temperature reduces thetensile strength of the material,therefore the control of heat transfer and of the maximum electric power input is so important. As will be explained later, the piezoelectric transducer used for atomisation of liquid is cooled by the liquid flow. In this case there could be a danger of overheating if the atomiser is working without fuel flow. This must be considered when the application is designed.

The stress created in the velocity transformer by the vibrations dissipates energy that also raises the working temperature of the ceramic.

When an alternating voltage is applied to its electrodes a piezoelectric transducer will be forced to vibrate in a manner which depends on how the piezoelectric material is cut in relation to the axis of the crystals. In manmade ceramics the direction of polarisation will give the direction of vibration related to the voltage applied. If the direction of movement is in the same axis as the polarisation the transducer is X - cut (Figure 45).

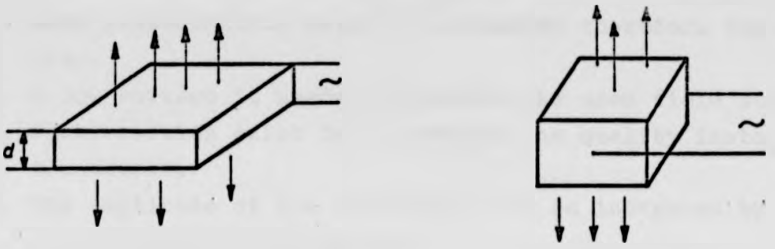

Polarisation parallel to direction of vibration.

Polarisation normal to direction of vibration.

Fig.45

The frequency of a forced vibration of a piezoelectric material is equal to that of the applied voltage.
If the thickness of the transducer material is adjusted to be half the wavelength of the sound waves $d = \frac{\lambda}{2}$, or with $c = \lambda f$, $d = \frac{c}{2f}$, a standing wave is formed in the transducer and the impedance is at minimum. A transducer has a series of resonant frequencies at the same thickness corresponding to the multiple of $\frac{\lambda}{2}$ which forms the standing wave: but the half wavelength resonance (first harmonic) normally has the lowest impedance.
The resonant frequency of a piezoelectric slab will change if a non-piezoelectric material is bonded to it, assuming that the thickness of the second material is different from the value $d_2 = \frac{c_2}{2f}$ where f is the resonance frequency of the piezoelectric slab and c_2 the speed of sound in the new material. A transducer is often built up of a piezoelectric material together with a non-piezoelectric material such as steel or aluminium bonded to it. Transducers made of sections of several materials are called composite transducers.
The transducer consisting of half wave crystal and a half-wave non-piezoelectric material is the simplest form of composite transducer and the load impedance is transformed at a 1:1 ratio. The mechanical load is transformed back to the piezoelectric material and lowers its electrical input impedance. This is a very useful feature because it is easy to tune the mechanical impedance by matching the electrical impedance of the input electric load. This will be discussed later in the chapter concerning the design of horns.
A composite transducer has several advantages, some of which are outlined as follows.

1. Effective heat transfer from the ceramic (crystal).
2. Less piezoelectric material is needed therefore the cost is less.
3. A low voltage is needed to create the same field strength.
4. Possibilities exist for adjusting the quality factor of the transducer.
5. The amplitude of the vibrations can be increased by sandwiching different materials.
6. Increase of inertia forces improves resonant conditions and increases the amplitude where needed.

It was mentioned earlier that the energy dissipated in the crystal due to the vibration strain will cause damage to the piezoelectric effect if heat is not transferred to cooler surroundings. The piezoelectric material has a low thermal conductivity and a close bond to metallic material improves the cooling capacity. PTZ has a thermal conductivity of 2.1 watt/m^{o}C compared with a value of 208 watt/m^{o}C for aluminium.

The quality factor of a transducer is defined as $Q = \frac{fo}{f_2 - f_1}$ where fo is the resonant frequency and f_2 and f_1 the frequencies on each side of the resonance, where the vibration amplitude is 0.707 times the amplitude at fo.

$f_2 - f_1$ is called the bandwidth of the transducer. A broad-bandwidth transducer has a lower amplitude at resonance, but will have a better performance when the frequency is slightly off resonance.

The high Q transducer must have an accurate frequency of AC-voltage to perform well.

The tuning of lengths in a multiple layer transducer allows the Q factor to be changed to the desired value.

When the piezoelectric material is bonded between two different materials as shown in Figure 46 the material with the lower characteristic impedance will vibrate with a larger amplitude, according to the relation $M = \frac{\rho_1 c_1}{\rho_2 c_2}$

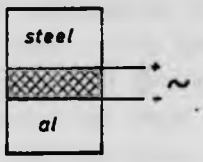

Fig.46

or $M = \sqrt{\frac{E_1 \rho_1}{E_2 \rho_2}}$

When steel and aluminium are used the magnification factor is M = 2.7

The arrangement shown in Figure 46 has a disadvantage in that there is a high voltage between the two metallic parts of the transducer.

This can be avoided if ceramics are used back to back as illustrated in Figure 47

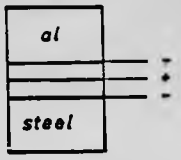

Fig.47

The two thin ceramic slices are bonded together with an electrically conducting cement. An electrode is fitted to the cement layer. In order to improve the contact (electrical as well as mechanical) a thin copper washer can be placed between the ceramics. The polarity of the ceramics must be such that when a current is fed to the electrodes both ceramics contract or expand at the same time.
This increases the amplitude and causes the boundary between the ceramics to be at a node if the length of the metallic slabs on each side is $\frac{\lambda}{4}$ or an odd multiple of $\frac{\lambda}{4}$.
The ceramics can be bonded with special adhesive such as silver Araldite. But the need for adhesive in high stress regions represents a disadvantage of the sandwiched transducer of this design.
Another technique is to assemble the transducer by compressing the ceramics between the metallic slabs by means of a screw arrangement in the center of the transducer or by fixing the two halves together with screws through flanges on the outside of the ceramics.
Static compression improves not only the mechanical-electrical contact but also the axial stress conditions in the ceramic. If the compression is high enough the net axial stress is never tensile and no adhesive is needed. Conductive grease between the elements improves the electrical contact between the interfaces and is recommended.
The contact between the faces is of fundamental importance. Study of different designs of transducers is very difficult mainly because of differences from experiment to experiment in the contact between faces. This leads one to believe that the changes which occur are caused by the change in design. A very strict procedure is necessary for such experiments.
Even if the transducer is of clamped design it is desirable to use epoxy resin because this in any case improves contact. The tests on transducers were carried out using a very simple electronic drive unit which needs a low impedance of the transducer to start oscillation. Therefore in all the atomisers produced the

This can be avoided if ceramics are used back to back as illustrated in Figure 47

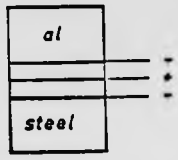

Fig.47

The two thin ceramic slices are bonded together with an electrically conducting cement. An electrode is fitted to the cement layer. In order to improve the contact (electrical as well as mechanical) a thin copper washer can be placed between the ceramics. The polarity of the ceramics must be such that when a current is fed to the electrodes both ceramics contract or expand at the same time.
This increases the amplitude and causes the boundary between the ceramics to be at a node if the length of the metallic slabs on each side is $\frac{\lambda}{4}$ or an odd multiple of $\frac{\lambda}{4}$.
The ceramics can be bonded with special adhesive such as silver Araldite. But the need for adhesive in high stress regions represents a disadvantage of the sandwiched transducer of this design. Another technique is to assemble the transducer by compressing the ceramics between the metallic slabs by means of a screw arrangement in the center of the transducer or by fixing the two halves together with screws through flanges on the outside of the ceramics.
Static compression improves not only the mechanical-electrical contact but also the axial stress conditions in the ceramic. If the compression is high enough the net axial stress is never tensile and no adhesive is needed.Conductive grease between the elements improves the electrical contact between the interfaces and is recommended.
The contact between the faces is of fundamental importance. Study of different designs of transducers is very difficult mainly because of differences from experiment to experiment in the contact between faces. This leads one to believe that the changes which occur are caused by the change in design. A very strict procedure is necessary for such experiments.
Even if the transducer is of clamped design it is desirable to use epoxy resin because this in any case improves contact. The tests on transducers were carried out using a very simple electronic drive unit which needs a low impedance of the transducer to start oscillation. Therefore in all the atomisers produced the

ceramics were not only clamped but also cemented.

Fig.48

The use of cement is essential because of the poor surface finish of some of the ceramics.
Figure 48 shows a 1/2 in and a 1 in ceramic after being mounted without adhesive. It is clear that only half of the surface of each of the ceramics has had contact with the matching material.
The elasticity of the element producing the static compression of transducers of clamped design is not critically important, but it should be more elastic than the piezoelectric elements compressed, especially if a wide bandwidth of the transducer is desired. If the compression element is much less elastic than the ceramics the resonant frequency is more affected by the compressional force and more care has to be taken to achieve the right compression. One way to measure the compression of the ceramics is to connect the electrodes to a charge amplifier. The reading of the instrument while applying the force is a very good indication of the compression involved. The calibration of the ceramics is easily carried out in a hydraulic press having a scale indicating the applied force. It is of course also possible to use weights, but it is very important that the force on the ceramic discs is applied exactly axially and a jig arrangement is necessary to ensure parallel movement.
The ratio of elasticity of the transducer clamping force may be expressed as follows.

$$\frac{\Delta l_t}{\Delta l_c} = \frac{Y_c \, A_c \, 1/l_c}{Y_t \, A_t \, 1/l_t}$$

where Y = Young's Modulus
A = Area
l = length
Δl = compression or elongation
c = compression element
t = transducer

ceramics were not only clamped but also cemented.

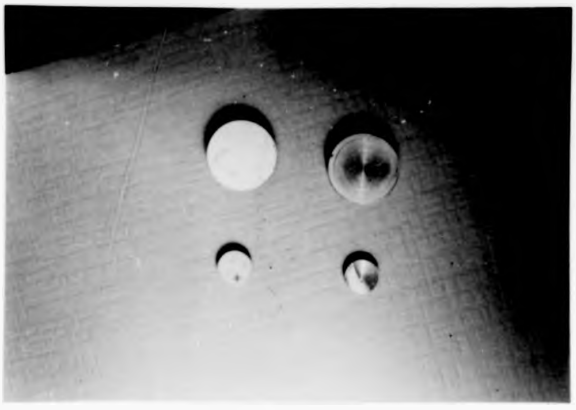

Fig.48

The use of cement is essential because of the poor surface finish of some of the ceramics.
Figure 48 shows a 1/2in and a 1in ceramic after being mounted without adhesive. It is clear that only half of the surface of each of the ceramics has had contact with the matching material.
The elasticity of the element producing the static compression of transducers of clamped design is not critically important, but it should be more elastic than the piezoelectric elements compressed, especially if a wide bandwidth of the transducer is desired. If the compression element is much less elastic than the ceramics the resonant frequency is more affected by the compressional force and more care has to be taken to achieve the right compression. One way to measure the compression of the ceramics is to connect the electrodes to a charge amplifier. The reading of the instrument while applying the force is a very good indication of the compression involved. The calibration of the ceramics is easily carried out in a hydraulic press having a scale indicating the applied force. It is of course also possible to use weights, but it is very important that the force on the ceramic discs is applied exactly axially and a jig arrangement is necessary to ensure parallel movement.
The ratio of elasticity of the transducer clamping force may be expressed as follows.

$$\frac{\Delta l_t}{\Delta l_c} = \frac{Y_c A_c \, l/l_c}{Y_t A_t \, l/l_t}$$

where Y = Young's Modulus
A = Area
l = length
Δl = compression or elongation
c = compression element
t = transducer

ceramics were not only clamped but also cemented.

Fig.48

The use of cement is essential because of the poor surface finish of some of the ceramics.
Figure 48 shows a 1/2in and a 1in ceramic after being mounted without adhesive. It is clear that only half of the surface of each of the ceramics has had contact with the matching material.
The elasticity of the element producing the static compression of transducers of clamped design is not critically important, but it should be more elastic than the piezoelectric elements compressed, especially if a wide bandwidth of the transducer is desired. If the compression element is much less elastic than the ceramics the resonant frequency is more affected by the compressional force and more care has to be taken to achieve the right compression. One way to measure the compression of the ceramics is to connect the electrodes to a charge amplifier. The reading of the instrument while applying the force is a very good indication of the compression involved. The calibration of the ceramics is easily carried out in a hydraulic press having a scale indicating the applied force. It is of course also possible to use weights, but it is very important that the force on the ceramic discs is applied exactly axially and a jig arrangement is necessary to ensure parallel movement.
The ratio of elasticity of the transducer clamping force may be expressed as follows.

$$\frac{\Delta l_t}{\Delta l_c} = \frac{Y_c \; A_c \; l/l_c}{Y_t \; A_t \; l/l_t}$$

where Y = Young's Modulus
A = Area
l = length
Δl = compression or elongation
c = compression element
t = transducer

If the length of compression element and the thickness of the transducer are equal the ratio will be equal to the ratio of the products of Young's Modulus and cross-sectional area.

$$\frac{\Delta l_t}{\Delta l_c} = \frac{Y_c \; A_c}{Y_t \; A_t}$$

The compression of a transducer is illustrated in Figure 49, where the force F on the ceramics causes an elongation of the compression element Δl_c and a compression of the transducer ceramics Δl_t.

The diagram is drawn for the $\frac{\Delta l_t}{\Delta l_c}$ ratio = 1.0 (I)

In this case the force amplitude of the vibrating transducer is equal to the amplitude in the compression element .

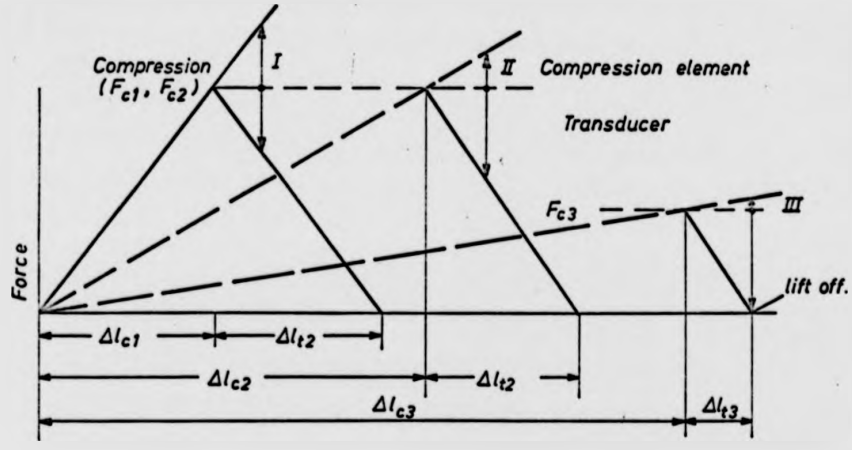

Fig.49

A more elastic compression element reduces its stress amplitude, but increases the stress in the transducer material if force from the vibrating crystal remains the same.

If the clamping force is too small (F III) the contact between transducer and the velocity transformer can be " tensile ". In other words, if the faces were not cemented they would separate when the transducer contracts.

Before the value of the clamping force is chosen the following factors have to be considered.

1. A very stiff mounting causes high stresses in element
2. The compressive force is difficult to apply correctly
3. The frequency depends upon the compression force. It may be

difficult to achieve perfect matching to the tuned transformer.

4. A very elastic mounting can cause the compression elements to stretch and cause loss of tuning between transducer and transformer
5. The impedance of transducer is dependent upon the clamping force. Higher clamping force gives a higher Q-factor.
6. The bandwidth reduces as the force increases.

The atomisers made in this project have a ratio of elasticity of about 1.0, but a higher value would have been better. For the chosen design of velocity transformer however it is difficult to get the necessary length of compression elements to achieve the desired elasticity.

The design must be a compromise between many factors. And the particular difficulty with velocity transformer design is that the design has a direct influence on the efficiency as vibrator. This will be shown in the next paragraph concerned with the development of atomisers for the project.

The use of spring washers or a flange-screw arrangement as flexible members can easily cause parasitic resonances to take place and make the transducer less efficient.

4.5 The development of ultrasonic atomisers

There are a few manufacturers of piezoelectric ceramics who have a range of different shapes and sizes in production. The ceramic suitable for use in powerful vibrators, namely lead zirconate titanate, is used for sonar and underwater depth sounding equipment, ultrasonic cleaning, etc., and is produced in large quantities on a continous basis. Some ceramics are therefore available at much lower prices than ones on special order.

Transducers in the cheaper series are produced as discs or rings of diameter 2 in., 11/2 in., 1 in., 1/2 in., with thicknesses of 1/8 in., or 1/4 in.

The standard size 1 in. ceramic is 1/4 in. thick and the 1/2 in. ceramic is 1/8 thick.

The 1 in. and 1/2 in. sizes were therefore the obvious choice for use in the first experiments.

All transducers are marked on the positive polarised side, but the marks disappear very easily and it was nesessary to make an arrangement for testing the transdusers for polarity. As Figure 50

shows, the transducer test equipment consists of a weight-arm set-up that allows the ceramic disc to be clamped with a known force.

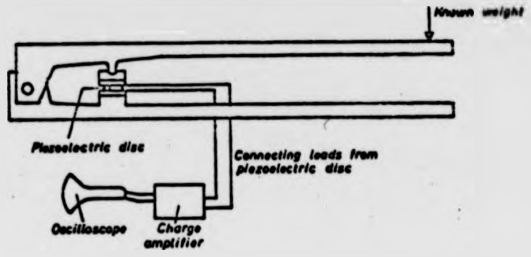

Fig.50

The charge amplifier and oscilloscope show the respective load of the ceramic.
When transducers are to be compared, it is very important to take care that the contact between the trans-ducer and the clamping blocks is good and the same for each test. The use of grease to improve contact is a necessary precaution.

During the research with ultrasonic atomisers, 30 different designs were investigated. Within those 30, the outside geometry was changed using the same bodies. Every shape and change in profile had to be tuned by using a " trial and error " method to get the best possible resonance.
Not all the experiments are described in this report, as most of them were unsuccessful. The failures can be attributed partly to the radius/wavelength ratio. Much time had been lost before it was discovered that publications dealing with ultrasonic concentrators for welding and other applications were only valid for relatively low frequencies at which the sound propagation is more nearly one-dimensional. This lack of basic knowledge of ultrasonics caused the first wrong decision, which was to base the research on 1 in. discs. The use of 1 in. ceramic transducers at frequencies of approximately 100 kHz seems to be unsuccessful although some of the concentrators made did work at approximately 100 kHz. But they also had low impedance resonance at other frequencies and this,as will be discussed later, would complicate the design of the electronic drive unit considerably.
The efficiency of the atomisers based on 1 in. ceramics was not

shows, the transducer test equipment consists of a weight-arm set-up that allows the ceramic disc to be clamped with a known force.

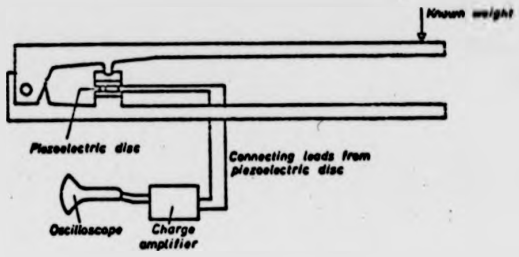

Fig.50

The charge amplifier and oscilloscope show the respective load of the ceramic.
When transducers are to be compared, it is very important to take care that the contact between the trans-ducer and the clamping blocks is good and the same for each test. The use of grease to improve contact is a necessary precaution.

During the research with ultrasonic atomisers, 30 different designs were investigated. Within those 30, the outside geometry was changed using the same bodies. Every shape and change in profile had to be tuned by using a " trial and error " method to get the best possible resonance.
Not all the experiments are described in this report, as most of them were unsuccessful. The failures can be attributed partly to the radius/wavelength ratio. Much time had been lost before it was discovered that publications dealing with ultrasonic concentrators for welding and other applications were only valid for relatively low frequencies at which the sound propagation is more nearly one-dimensional. This lack of basic knowledge of ultrasonics caused the first wrong decision, which was to base the research on 1 in. discs. The use of 1 in. ceramic transducers at frequencies of approximately 100 kHz seems to be unsuccessful although some of the concentrators made did work at approximately 100 kHz. But they also had low impedance resonance at other frequencies and this,as will be discussed later, would complicate the design of the electronic drive unit considerably.
The efficiency of the atomisers based on 1 in. ceramics was not

as good as those based on smaller diameters at the desired frequency of approximately 100 kHz.
In the first experiments only one 1 in diameter transducer was used, mounted as shown in Figure 46 (page 101).
The alternating current was supplied from a 100 W power amplifier driven from an oscillator as shown in Figure 51. In order to study the impedance of the design a 2-trace oscilloscope was connected to the transducer input. One trace was used to measure the voltage across a 10 Ω resistance and the other to show the voltage across the transducer. The two traces also show the resonance clearly due to the phase angle between the two signals (current, voltage).

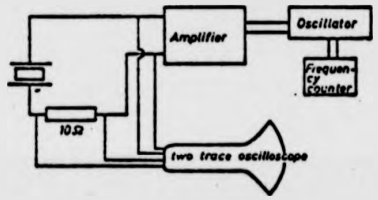

Fig.51

A forced vibration at high impedance of a piezoelectric transducer can create very high voltages. This was experienced during the first hours of the research, as amplitudes of up to 1000 V were traced.
Difficulties with the insulation and the safety of the mounting underlay the decision to change to the two transducer-system shown in Figure 47 . The use of two ceramics allows two exactly equal " halves " to be clamped together as shown in Figure 52.

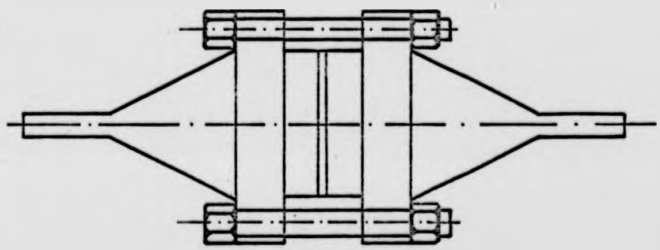

Fig.52

The aluminium horns were clamped together with five 4mm screws. The use of such a symmetrical design ensures that the first node is in the boundary between the ceramics, at 3/4 wavelength resonance. For practical reasons it is not possible to make 1/4

wavelength resonance clamped horns for frequencies as high as 100 kHz.
The approximate length for 1/4 wavelength resonance at 100 kHz is 12 mm and the thickness of a 1 in. crystal represents already 6.3 mm of this length. 6 mm is of course not enough length in which to shape an effective concentrator and to create the necessary clamping force.

The use of symetrical clamped horns is a way to tune the horns to the desired frequency. In order to increase the amplitude one of the halves can be replaced by a " dummy " backing, also tuned to resonate at the same frequency. The stainless steel backings can be tuned separately in the same way by clamping two dummies together and then adjusting the length in the lathe to give the same frequencies as the " active " horns.
Symmetrical tuning seems to be the only safe way to do investigations with clamped concentrators, where the thickness of the ceramic is much less than the resonant thickness.

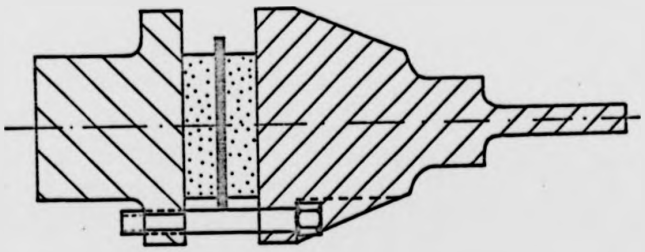

Fig.53

If the resonant frequency is unknown for both active and dummy parts there is very little chance of getting a good match by trial and error. The result is total confusion among all the different resonant peaks.
Figure 53 shows a 1 in. atomiser for approximately 45 kHz. This atomiser is open and the elastisity can be adjusted by using thinner screws which provide the clamping force.
The flange system and the screws absorb much energy and the efficiency as atomiser is not good enough, considering the power source available in a car.

The efficiency was improved by the addition of a vibrating plate on the end of the horn as shown in Figure 54.

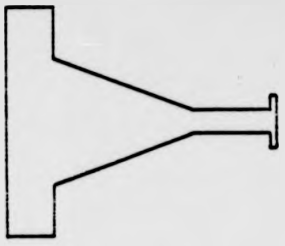

Fig.54

A horn of that shape was brought to resonance at a frequency as high as 95 kHz. The efficiency as an atomiser is quite good because there is a combined effect from the surface waves on the tip and bending vibrations of the plate. However, the endurance of this design is not good enough. The plate on the end broke off after some minutes of running because of fatigue failure. Another weakness of the design is that the ceramics easily crack. The reason for this is the uneven clamping force from the five screws.
For use on an engine, the ceramics need more protection than is provided in such an open structure.
Figure 55 shows an example of a design where a threaded sleeve is used to match symmetrical horns.

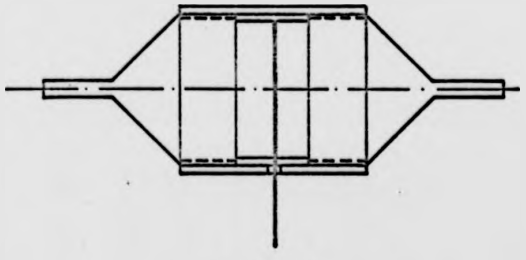

Fig. 55

The threads and contact surfaces of the horns had to be turned accurately, to avoid misalignment which would cause uneven forces on the ceramics. The contact surfaces were polished to give the best possible mechanical contact.
The atomiser shown in Figure 55 could be tuned to extremly low electrical impedance (less then 20 Ω at resonance) but the efficiency of the vibrations on the atomising surface was not good enough.
The reason for this, as explained earlier, is that the sound

waves do not propagate only in the desired direction along the axis, but also in the radial direction and along the surface. These movements are at low radius/wavelength ratios absorb too much energy.
The design shown in Fig. 55 is more successful at lower frequencies where the radius/wavelength ratio is greater than say 1.5 although there is reason to belive that even at that ratio scattering and parasitic resonances can influence the performance considerably.
The diameter of the resonator was kept as small as possible, but using 1 in. ceramics it is not possible to make the diameter less than approximately 33 mm.

The best atomiser using a 1 in. ceramic had a stepped concentrator of lengh 38.1 (including one ceramic). This atomiser worked at 95.5 kHz and needed 3.1 watt to atomise water applied to the surface. The average sound speed was 4.8×10^3m/s and the electrical impedance varied from 150 to 200 Ω depending on the compression. On both sides of the frequency 95.5 kHz there were a range of resonances. At 75 kHz, for instance the impedance was as low as 14 Ω, and it was impossible to get the simple electronic drive unit to pick up the feedback signal from 95.5 kHz when the 75 kHz resonance has such a low impedance. Without very complicated filters, a drive unit would respond to the signal from 75 kHz and continue to work at that frequency. At 75 kHz there were hardly any axial vibrations on the tip of the horn, but there was strong activity on the first step and in the radial directions. Many other designs were tried in an attempt to get rid of strong parasitic resonances close to the desired frequency, but without much success. The experiments with 1 in. ceramics were then stopped and a series of experiments were carried out using 1/2 in. ceramics.
It is necessary to appreciate the performance of an ultrasonic atomiser aimed for in this project in connection with the electronic drive unit and the power source available. It would be possible to get almost any construction of horn to work if the frequency could be " fixed " by using expensive electronic circuits and filter arrangements to exclude the influence of adjacent resonances, and if enough power were available to compensate for the losses in the electronic drive unit and in the vibrator itself.

For use on an engine, where limited electric power is available, an atomiser arrangement has to be efficient and the electronics involved must be simple and inexpensive.
To study vibrators using the smaller ceramics, an arrangement similar to that shown in Figure 55 was made for 1/2 in. diameter ceramics. It became apparent that a number of resonant frequencies disappear and there is less activity of vibrations in the radial direction.
Another basic advantage of using smaller transducers is that it is simpler to get the contact areas flat and parallel. The larger ceramics are easily cracked on the outside if elasticity of the horns causes bending. Such bending can be produced especially when screws are used as compression members, or when a distortion takes place when the transducers are in vibration.
Experiments with the 1/2 in. transducers show that the average sound speed is very unpredictable.
The arrangement in Figure 56, of a total length of 116.5 mm, when exactly tuned to resonance at 60.9 kHz gives the speed of sound as 4.72×10^3 m/s

Fig.56

Shortened to 70 mm the resonance frequency is approximately 90 kHz (giving 4.2×10^3 m/s . The soundspeed drops so that a higher resonant frequency than approximately 95 kHz cannot be achieved. With the drop in sound speed, the impedance at resonance increases. How the geometry affects the sound propagation can be illustrated by turning a step on each side, as shown by the dotted line in Figure 56.
For a tip length of approximately $\lambda/8$, the frequency increases to a maximum and decreases to the frequency for the plain cylin-

drical bar when $t = \lambda/4$.
The frequency is also dependent on the diameter but this influence is hard to predict. In most cases a reduction of the diameter increases the frequency.

Several experiments based on the design shown in Figure 56 finally led to the most successful design (Figure 57), where the stainless steel sleeve and the dummy backing are made of one piece.

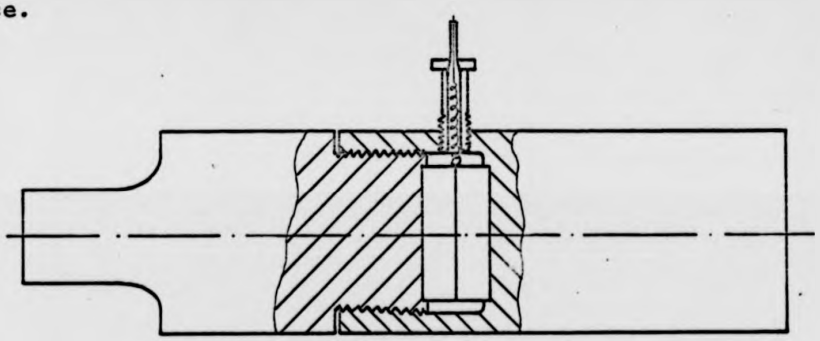

Fig.57

This design was the number 22 in the series of experiments. The vibrator 22 works at 98.5 kHz. The average soundspeed in the aluminium part is 5.2×10^3m/s.
In the dummy the sound speed is 3.9×10^3 m/s, assuming a node for the vibration at the interface between the two ceramics. It is possible to make a vibrator of the same design for frequencies higher than 100 kHz, but the efficiency of the vibrations is not as good. When exactly tuned the impedance of the atomiser is approximately 35 Ω. The impedance is slightly dependent upon the production tolerances and the quality of the contact between the transducers and the metallic material.
In order to maintain such a low impedance, care has to be taken when the components are joined together and especially when Araldite cement is applied to the surfaces.
As mentioned in the chapter 4.4, the elasticity of the compression member is an important factor to consider when designing sandwiched type resonators. For the design the elasticity can be changed by weakening the sleeve or the walls of the chamber containing the transducers.
However, wall thicknesses of 0.5 mm and less caused loss of com-

pression due to the excessive stresses. In order to make a resonator with a more elastic compression member other designs were tried. Figure 58 shows one of the types considered.

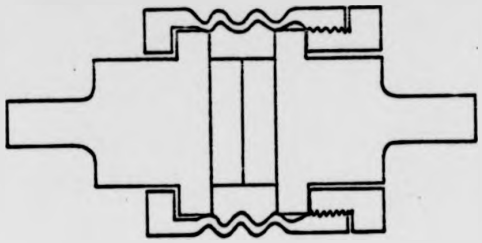

Fig.58

The longer sleeve and the elastic design allowed this atomiser to be made with various stiffnesses.
Another thought behind this design was that when assembling the atomiser the transducer would not be rotated on the surface.
A transducer is easily scratched by the turning motion. This design like so many others, was a failure. The nut and the sleeve absorbed too much energy to make the design efficient.
Other experiments in which the stiffness was adjusted by weakening the flanges on the horns, as shown in Figure 59, were also unsuccessful.

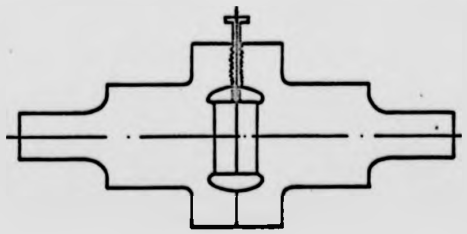

Fig.59

In atomisers of elastic flanged design the transducers easily get damaged owing to the bending motion at the outside.
Appendix IV includes photographs and drawings of some of the types of horn investigated. Type 22 was by far the most success-

ful and was developed further. To overcome some of the difficulties of damage to transducers in assembly the ceramics were stuck to the horns with silver Araldite type ESP49 and to copper washers at the positive polarised side. The washers constitute the electrical contact member but also give protection against the turning motion when the two halves are screwed together. To provide contact with the washers from the electronic drive unit, a special screw was made, as shown in Figure 60.

The spring is wound of brass spring wire and for insulation a 2 mm shrink sleeve can be formed very easily using heat.

Fig.60

There are not many different types of material suitable for ultrasonic concentrators.
Titanium alloy is the best material available, because of its extremely high Q (giving a low dissipation of acoustic energy) and its ability to sustain large amplitudes without failure.
However, titanium alloy is expensive and very difficult to machine.
The next best is probably aluminium alloy, and so for the experiments carried out in this work a special aluminium developed for the Concorde project was used.
Some fatigue damage of atomisers occurred but only in the less effective designs where the diameter ratio of the stepped horn was made very big in order to get sufficient amplitude on the tip.

Atomisers of type 22 with a diameter ratio 18:8 or a magnification factor M ≈ 5.0 have been used for many hours without damage. The fillet radius of 4 mm seems to be big enough to give the necessary strength. According to the one-dimensional theory the stress in the region between the two cylinders can be calculated using the formula i $\sigma_{max} = \frac{\xi_2 \pi Y}{2t}$. See page 9 4.

where : Y = Young's Modulus
t = length of tip
ξ_2 = amplitude at end

ful and was developed further. To overcome some of the difficulties of damage to transducers in assembly the ceramics were stuck to the horns with silver Araldite type ESP49 and to copper washers at the positive polarised side. The washers constitute the electrical contact member but also give protection against the turning motion when the two halves are screwed together. To provide contact with the washers from the electronic drive unit, a special screw was made, as shown in Figure 60.

The spring is wound of brass spring wire and for insulation a 2 mm shrink sleeve can be formed very easily using heat.

Fig.60

There are not many different types of material suitable for ultrasonic concentrators.
Titanium alloy is the best material available, because of its extremely high Q (giving a low dissipation of acoustic energy) and its ability to sustain large amplitudes without failure.
However, titanium alloy is expensive and very difficult to machine.
The next best is probably aluminium alloy, and so for the experiments carried out in this work a special aluminium developed for the Concorde project was used.
Some fatigue damage of atomisers occurred but only in the less effective designs where the diameter ratio of the stepped horn was made very big in order to get sufficient amplitude on the tip.

Atomisers of type 22 with a diameter ratio 18:8 or a magnification factor M ≈ 5.0 have been used for many hours without damage. The fillet radius of 4 mm seems to be big enough to give the necessary strength. According to the one-dimensional theory the stress in the region between the two cylinders can be calculated using the formula i $\sigma_{max} = \frac{\xi_2 \pi Y}{2t}$. See page 9 4.

where : Y = Young's Modulus
t = length of tip
ξ_2 = amplitude at end

As stated in Chapter 5.1, amplitudes ξ_2 of up to 15μ have been measured in type 22 horns. This would mean a theoreticel stress of $\sigma = 13.5 \times 10^8$ N/m². The fillet is not taken into account in this calculation but it seems that the material is very much on the limit of its fatique strength and that the fillet radius gives the necessary safety factor to the design. For the aluminium alloy used the maximum is approximately 15 bars . At the high frequency of 98.5 kHz only a short period of time at load in excess of the fatique strength of the material is necessary to cause failure. In a period of 1 minute 5.9 million load changes occur.
As mentioned above, the fatique failure occurs at the maximum stress region, which for stepped horns is situated in the fillet between the two cylinders.
Often the crack is not visible. The vibration simply stops. The explanation is that a small crack in the horn causes a change in the resonant frequency, after which the horn does not vibrate efficiently enough for complete damage to occur. Fatigue failures can therefore be very difficult to discover.

The circular shape of the type 22 vibrator makes assembly easy. Two specialy made clamps are handy tools for the compression of the transducers. In the early work the compression was correctly adjusted by measuring the gap between the two halves: later, with experience, the compression was simply regulated by counting the number of sparks between the copper washers and the atomiser body. Four sparks is a measure for 0.075 mm compression of transducers. As the stiffness ratio is approximately 1.0, the compression of the transducers is 0.038 mm. With a Young's Modulus of 11.5×10^{10} N/m², the stress in the transducer after compression would be approximately 6.65×10^8 N/m².
The maximum compressive strength of the transducer material is given by the producer as greater than 5.00×10^8 N/m²
After a short period the material seems to settle and the compression will be somewhat lower than 6.65×10^8 N/m².
A more accurate way to measure the compression is to use a charge amplifier to register the charge from the transducers during compression. This charge is directly related to the strain through the piezoelectric pressure constant d.(PTZ 4, $d_{33} = 289 \times 10^{-12}$ m/V).

The transducer testing equipment (see Figure 50) gives the relation between compression and voltage, and the same electronic equipment can be used when compressing the transducers in the atomiser body. However, there is no need for such a complicated procedure when atomisers are produced with small tolerances. To investigate how the atomiser could be produced five bodies were made all within the close tolerances shown in drawing (Appendix IV).
In cold condition the resonant frequencies for the five were 89.5, 98.8, 98.85, 98.4, 98.38 kHz.
The impedances were 60, 30, 36, 40, 44 Ω.
All these five atomisers are capable of atomising at least 5 l/min. but, as will be explained in a later chapter, the average droplet size increases with the flowrate.

4.6 Electronic drive unit

The atomiser has a very high Q-factor and has to be driven at an almost exact frequency. The resonant frequency is not constant, but changes with the temperature and when liquid is applied to the tip. Therefore an electronic oscillator to drive the atomiser must be able to drift with those changes for the best possible efficency. As is the case with every acoustic resonator, there are many resonant frequencies to consider, namely the " basic " 1/2 wavelength resonance and the higher harmonics. Additionally there can be various parasitic resonances dependent on the geometry. Normally the basic 1/2 wavelength resonance corresponds to lowest impedance and is easiest to tune in. In our case we are using the third harmonic and all lower and higher harmonics must be avoided.
To meet the requirements, the electronic drive unit has to be a feedback oscillator, but it is not possible to filter a feedback signal effectivly from a low impedance resonance as close as say 20 kHz without using complicated circuits. If the aim is to keep the cost down, the atomiser must have only high impedance resonances adjacent the important working frequency. If this is achieved the drive unit can be made very simple.
The atomiser type 22 works at 98.5 kHz and has a high impedance at the second harmonic but a low impedance at the first. The difference between the first and the third is nearly 50 kHz. The first

harmonic can therefore be separated by a oscillator circuit.
The problem was to eliminate the influence of the second and the fourth harmonic resonances which are approximately 74 kHz and 123 kHz respectively. If the atomiser is properly assembled the second harmonic will be of higher impedance than the third: this could be achieved due to the design and the tuning of the geometry.
With increasing number of harmonics the impedance increases even if the resonator is especially tuned to the higher frequency. The fifth or higher harmonics are therefore usually not so difficult to avoid as the lower ones. If however the atomiser is supported in a way that gives increasing stiffness, the higher harmonics could be more dominant, and cause a feedback oscillator to jump to another resonance.
Several known oscillator circuits were tried but most crystal feedback oscillators have been developed to create constant frequency oscillations with very little power to the crystal and are therefore not suitable as drives for power applications without an amplifier. Such drive units exist and are necessary for operating high power ultrasonic drills or cleaning tanks.
To drive a type 22 atomiser requires only approximately 5 watts, therefore is a two stage drive unit consisting of an oscillator and an amplifier is not neccessary.
The development of the electronic drive unit had to be done in parallel with the investigation of different types of transformers.

A drive unit with more oscillator circuits tuned to approximately the correct frequency was necessary for driving the less sucessful designs, where a number of resonances had approximately the same impedance. It was especially difficult to get the oscillation started at the correct frequency. Feeding fuel to the atomiser could also cause a jump to another undesired resonance.

Figure 61 shows how the drive unit for the type 22 atomiser was finally made.

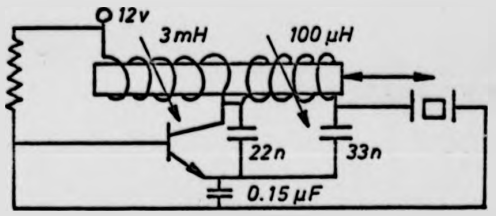

Fig.61

A ferrite rod can be moved in a double coil for tuning to exactly the correct frequency: that is when the phase angle between voltage and current is zero.
The AC signal for voltage and current fed to the atomiser can be used for calculating the efficency of the drive unit

$$\eta = \frac{\text{Power to the atomiser}}{\text{Power to the drive unit}}$$

The efficency of the designed drive unit is measured to be better than 65%.
The D.C. current needed from a 12 V battery is 0.6A. The total consumption for each atomiser is consequently 7.2 W.
Almost any power transistor of pnp type can be used. Cheap transistors such as 2 N 3054 and 2 N 3055 have both been used successfully.
Since the transducers are a part of the oscillating circuit there must be a drive unit for each atomiser.
For the work with 4 atomisers on the engine, the drive units were assembled in small aluminium casings, but a better solution would be to mount all the units in one box.
If transistors in the cheaper range are used a current limitation would be of advantage.
In case of failure, when the atomiser stops vibrating the current through the transistor is about 2 A. For a 2 N 3055 this current does no harm, but the smaller 2 N 3054 can be damaged after some time by overheating.
In order to keep the transistor cool, it is mounted on one side of the aluminium casing. (See the photograph in Appendix IV).
A printed circuit version of the drive unit would make it a very small device which could easily be mounted on the engine close to the atomiser.

4.7 Fuel feed to atomiser

As was seen earlier, the average droplet diameter of the atomised fuel is frequency dependent, but the fuel flow rate and the way in which the liquid is applied to the atomiser surface are also of importance. The most successful atomisers have 8 mm diameter of the smaller end. This means that more than 50 mm^2 is available for atomisation. The difficulty, however, is to apply liquid to this area in such a way that the whole area is effective. A

single jet of fuel to the surface allows only a small part of the area to be used and gives good conditions for atomisation at low flow rates. When the flow rate increases the liquid is thrown off in droplets which collide and build up larger drops on the way from the surface.
Several methods have been tried to achieve the best possible distribution.

a. Hole in the centre of small cylinder
b. Feed from the front
c. Feed from the side on to the atomising surface
d. Feed on to the side of the atomiser tip

The experiments with fuel distribution were carried out in a steady state flow rig, where the atomiser could operate in an airstream of variable speed, comparable to that in an engine manifold. For these experiments water or alcohol was used. Water is not very suitable because of corrosion of the aluminium. After some hours the aluminium becomes a black colour in places with strong vibration. Petrol or alcohol do not affect the aluminium.

a. Fuel feed through a central hole represents the simplest way, but has some disadvantages. Even if the feed into the atomiser is done at a node on the step, as shown in Figure 62 (a)

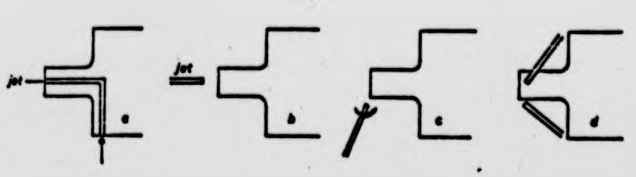

Fig.62

it will affect the impedance of the horn considerably. Additionally a single bore on the tip does not ultilize the area very fully as the liquid is thrown off in the centre region and the larger outside area remains dry.

b. The feed from the front can be via one jet or more. It is posible to direct the jets at different parts of the surface. However, with this setup it is necessary to have access to the

atomiser from the front side, as would be the case for instance when the atomiser is mounted in a tube. Impaction of droplets on the feed tubes has also to be considered (Figure 62 b)

c. To avoid impaction the feed jets were mounted upstream of the atomiser. There is a danger that the liquid fuel is blown off by the high speed air before it hits the atomising surface. Various methods of shielding the atomiser were tried. It was later discovered that the " blow off " effect is easier to avoid in the pulsating flow in the engine than in the steady state flow. This difficulty only arises when the fuel feed pressure is low (Figure 62 c).

d. When the atomiser is arranged with the tip directed down-wards it is possible to feed the fuel at low pressure on to the side of the atomiser tip. The vibrations, the airspeed and gravity cause the fuel to flow around the atomiser tip and on to the surface. This method has many advantages but it is more difficult to arrange the pipes supplying the fuel. It can be argued that in the case where the fuel is fed from the outside rim, the fuel is thrown off before it can get to the centre. A combination of a central jet and gravity feed is possibly needed to achieve the best utilization of the surface.
For instance,the central jet could be a high load jet operating in conjunction with a low load jet feeding on to the side. The question of fuel feed has to be seen in relation to the mounting of the atomiser in the inlet system, and the means of support of the atomiser.

The atomisers used in this research have all been used at constant power input. At a low fuel flow rate, suitable for an engine at idle, the droplets formed would be smaller at lower power input to the atomiser. A high power atomiser throws off the low fuel feed instantly, and the droplets so formed are larger than if the atomiser input power is less and the fuel has time to spread over a larger area of the atomiser surface.
It would not present any difficulty to regulate the atomiser power in proportion to the fuel flow rate. The electronic drive unit could be regulated via the base current or by simply altering the level of the input DC voltage.

4.8 Support of atomiser

According to the number of nodes of the standing wave in the type 22 atomiser there should be three places on the body with no axial vibration. Because of the arrangement of the sleeve with strong radial movement there are only two nodes which can be used for supporting the atomiser body. One node is situated on the step, and the other at the stainless steel backing piece 12 mm from the end. At all other places the atomiser is in vibration and a support would damp the movement and result in an increase of the mechanical-electrical impedance.

In the first experiments the support of the atomiser was considered together with the arrangement of the fuel feed. The atomiser body was mounted on three nylon screws clamped to the node in the backing piece, a number of pipes were bent and provided the fuel feed to the atomiser (Fig.63). Later instead of screws a Teflon ring was made to fit in a slot in the atomiser body.

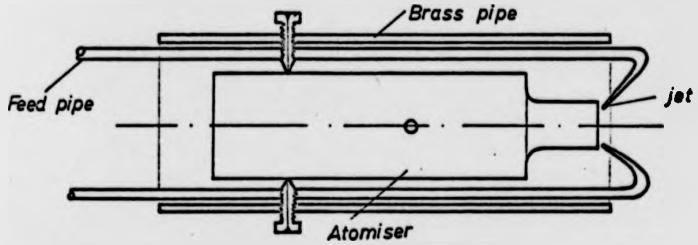

Fig. 63

The arrangement of the feed tubes was also made somewhat neater. As Figure 64 shows, a seal was made at the front end to avoid air leakage through the atomiserarrangement when mounted on the engine.

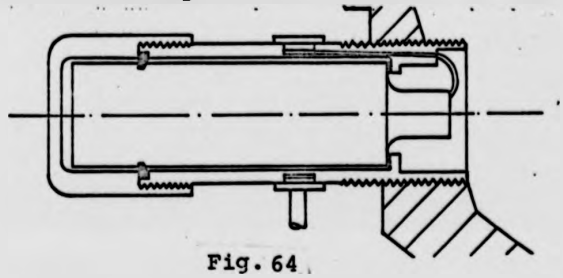
Fig. 64

The front part of the support body was meant to be a shield against the force of the air. Threads on the end allowed the unit to be mounted in the manifold. Figure 65 shows the more successful assembly which was used in experiments on the engine manifold where fuel was atomised close to the inlet valves.

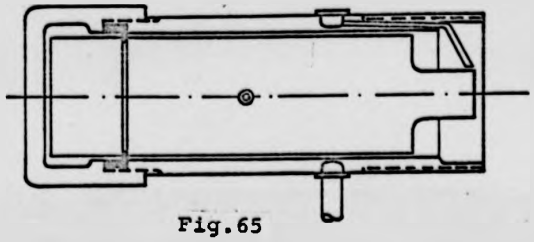
Fig.65

The atomiser was supported by teflon rings of a shape designed to avoid fixing the atomiser body over a significant length. If the mounting is to be almost loss - less the atomiser must be held only in a very narrow slot. Also since exact location in the radial direction must be avoided a gap between the atomiser body and the teflon ring is necessary.

In the arrangement shown in Figure 65 the atomiser is open at the front.

Atomisers of this design must be mounted with the tip downwards. Fuel between the atomiser and the support body, would influence the performance of the atomiser considerably. Another disadvantage with arrangements like Figure 65 is the size.It is more difficult to find space on the induction system for atomiser units as big as that in Figure 65. The diameter of the threaded end is 27 mm.

During the investigations on the engine it was discovered that the volume of the fuel feed was too great. The unsteady fuel feed caused by the pressure variation in the feed line caused maldistribution to the cylinders and therefore increased the hydrocarbon level in the exhaust.

Fuel feed on to the side of the horn has to be from a low pressure supply. This causes the fuel to be sucked out of the system, especially at idle when the pressure in the manifold is low.

For individual atomisers on each cylinder it is necessary to have a higher pressure fuel supply and to arrange for the pressure drop to occur as close to the outlet as possible.

At low pressure feed the regulating valve must be situated as close to the outlet as possible. With designs like that in Figure 65 it is not easy to fit adjustment needles at the ends of the feed tubes. A new atomiser was made with a small flange at the step of the horn. If the flange is small enough it does not influence the impedance significantly. Additionally, as the atomiser must be electrically insulated from the engine a rubber seal makes the mounting somewhat flexible.

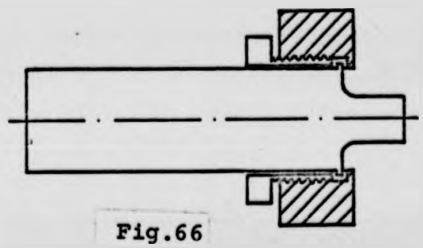

Fig.66

Figure 66 shows this arrangement. Using the flange system, the atomiser set up is only 18.5 mm in diameter, is sealed

in the front and can be mounted in any direction. However, it is not protected and has no fuel feed arrangement. The fuel has to be led to the atomiser from " outside ". This makes experiments more flexible but the atomiser is not a complete unit and the feed tubes must be arranged in the manifold independently.
Further discussion of the application of the atomisers will be found in chapter 6.
Photographs of some of the arrangements used can be found in Appendix IV.

5 Measurement on the vibrators

5.1 Amplitude and stess

Vibrative atomisation can only take place if a certain minimum amplitude is exceeded. For a type 22 horn of frequency 98.5 kHz this minimum amplitude is approximately 1.5 µm. At such small amplitudes only a very thin film of liquid can be applied to the surface. Flooding of the tip is to be avoided. Figure 67 shows the relations between power and flowrate.

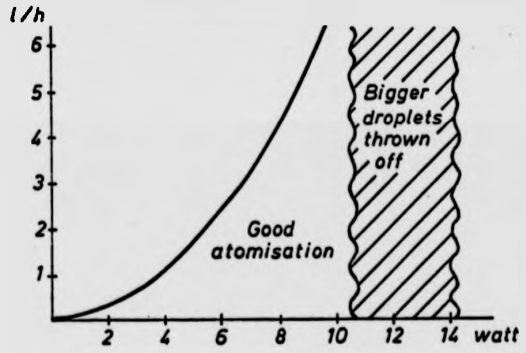

Fig.67

It is difficult to draw such a diagram accurately. The limits for atomisation are dependent upon subjective judgement and upon how the fuel is fed to the atomiser. For the type 22 atomiser amplitudes of 10 to 12 µm give reliable atomisation at flow rates of more than 5 l/h. If the flow rate increases, bigger drops are thrown off. An increased amplitude permits atomisation of higher flow rates too but the droplets seem to increase in diameter, possibly owing to a cavitation effect. Figure 68 shows the measured amplitude at the vibrating end in relation to the power fed to the transducer. Less than 1/2 watt input power is necessary to achieve amplitudes of 1 to 2 µm, but at higher power there is little or no increase of amplitude. For transducers which rely on clamping without adhesive, the curves fall off with increasing power. This suggests that an increase in power causes a worsening of the contact between the transducers and the metallic material.

As the Figure 68 shows, the clamped and cemented version is more reliable at higher power than the clamped only type. If the clamping force is not sufficently high an increase in power causes the amplitude to fall for reason stated above. The atomisers used in the research were adjusted to approximately 5 W on the transducer or 8.5 watts on the DC. side of the drive unit (12 V, 0.7A).
The vibration amplitude were measured by means of a special micros-

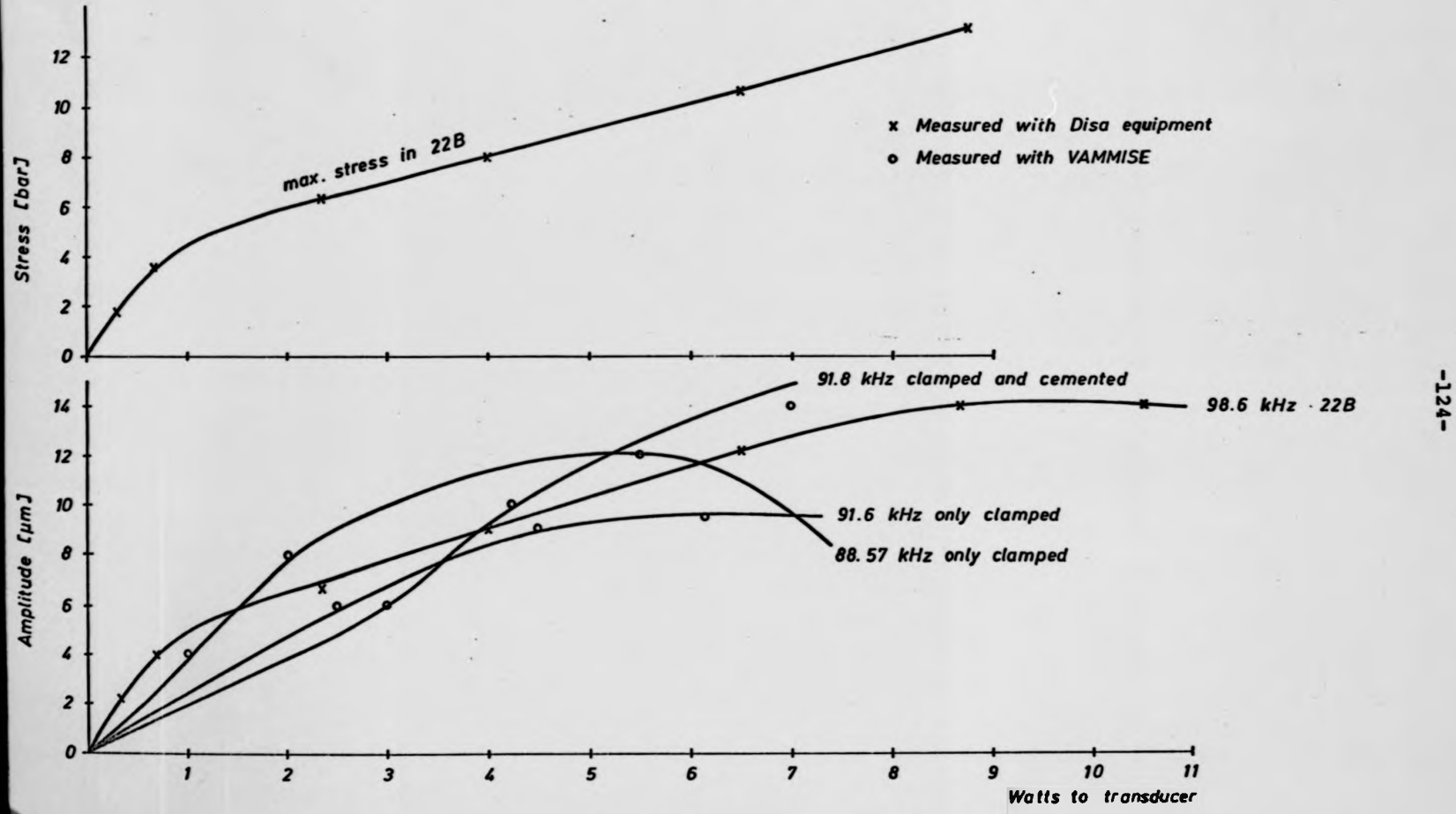
Stress [bar]
max. stress in 22B
x Measured with Disa equipment
o Measured with VAMMISE
Amplitude [µm]
91.8 kHz clamped and cemented
98.6 kHz · 22B
91.6 kHz only clamped
88.57 kHz only clamped
Watts to transducer

Fig.68

cope based on the image shearing method. The instrument VAMMISE has the advantage that it is not necessary to fix anything to the tip which might change the performance of the atomisers. The light reflected from the polished edge of the tip was sufficent to measure the amplitudes. At small amplitudes the accuracy is not very good, but amplitudes bigger than 3 µm could be distinguished quite well. In order to confirm the results from the measurements with VAMMISE the latest version of the type 22 atomiser was measured by means of a DISA universal indicator which is able to register signals from capacitive or inductive transducers. An amplitude can be detected from the change in capacitance when a metallic plate is hold close to the vibrating surface. The result of these measurements corresponded reasonably well with those of the VAMMISE (on Figure 68 see the curve for 22 B).

The calibration of the signal from the frequency-modulated reactance converter was carried out using a micrometer screw for controlling the distance between the plate and the vibrating surface and an electronic sensor based on a differential transformer pickup for exact measurement and calibration of the movement.

The Photograph Figure 69 shows the instrumentation.

Fig.69

As we have seen, the maximum stress in the concentrator is given by $\sigma \text{ max} = \frac{\xi_2 \pi Y}{2t}$, where ξ_2 is the amplitude at the end, Y is Young's Modulus and t the length of the smaller cylinder. Figure 68 shows the maximum stress, calculated from this equation at different power. The curve is drawn for the atomiser 22 B.

From the equation $v = \frac{\sigma}{\rho c_o}$ (obtained from the solution of the wave equation (25)) where v is the velocity of the particles at the small end and ρc_o is the characteristic impedance, it follows that at 8 watts input the particle velocity would be given appro-

cope based on the image shearing method. The instrument VAMMISE has the advantage that it is not necessary to fix anything to the tip which might change the performance of the atomisers. The light reflected from the polished edge of the tip was sufficent to measure the amplitudes. At small amplitudes the accuracy is not very good, but amplitudes bigger than 3 µm could be distinguished quite well. In order to confirm the results from the measurements with VAMMISE the latest version of the type 22 atomiser was measured by means of a DISA universal indicator which is able to register signals from capacitive or inductive transducers. An amplitude can be detected from the change in capacitance when a metallic plate is hold close to the vibrating surface. The result of these measurements corresponded reasonably well with those of the VAMMISE (on Figure 68 see the curve for 22 B).

The calibration of the signal from the frequency-modulated reactance converter was carried out using a micrometer screw for controlling the distance between the plate and the vibrating surface and an electronic sensor based on a differential transformer pickup for exact measurement and calibration of the movement.

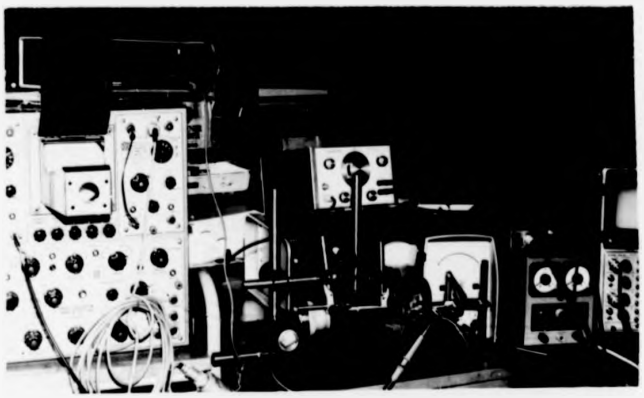

The Photograph Figure 69 shows the instrumentation.

Fig.69

As we have seen, the maximum stress in the concentrator is given by $\sigma_{max} = \frac{\xi_2 \pi Y}{2t}$, where ξ_2 is the amplitude at the end, Y is Young's Modulus and t the length of the smaller cylinder. Figure 68 shows the maximum stress, calculated from this equation at different power. The curve is drawn for the atomiser 22 B.

From the equation $v = \frac{\sigma}{\rho c_o}$ (obtained from the solution of the wave equation (25)) where v is the velocity of the particles at the small end and ρc_o is the characteristic impedance, it follows that at 8 watts input the particle velocity would be given appro-

ximately by

$$v = \frac{1.17.10^{9}}{13.9.10^{5}} = 8.41 \ ^{m}/s$$

This is to be compared with the maximum velocity obtainable in a rod, which is given by

$$v_{max} = \frac{F}{\rho.c_o} = \frac{1.9.10^{9}}{13.9.10^{5}} = 13.20 \ ^{m}/s$$

F represents the fatigue stress of the material, here taken to be 1900 bar.
According to this investigation there seems to be little chance of fatigue failure of the type 22 atomiser, because even at very high power the amplitude does not exeed about 14 µm. It must be remembered, however, that at idle the temperature may rise, causing the material to weaken considerably.

5.2 Impedance and Q-factor

The impedance of the concentrator is a very important parameter in the tuning procedure. The impedance and phase angle were measured with a vector impedance meter.
Figure 70 shows the impedance of the unfinished atomiser, consisting of an aluminium and a stainless steel symmetrical tuned bar, at frequencies around resonance and the impedance of the finished atomiser with the tuned tip. The resonance curve is extremely sharp for both the finished and the unfinished resonators but, as can be seen, the curve for the finished atomiser is somewhat sharper especially at frequencies lower than resonance. For the tuned atomiser a decrease of 250 Hz causes an increase in the impedance of approximately 450 Ω (for an atomiser working at 92 kHz).

The sharpness of the resonance is as mentioned before expressed in terms of the Quality factor $Q = \frac{f_o}{f_1 - f_2}$

where $(f_1 - f_2)$ is the band-width of the resonator (see page 100).
The Q factor is a measure of the damping of the vibrating system and depends not only on the geometrical match but also on the material used.

In order to calculate the quality factor for the type 22 atomiser it is necessary to measure the change of the amplitude on each side of the resonance keeping the power constant. This is a difficult thing to do with a resonator having a narrow band-width but could be done by tuning the feedback oscillator slightly out of resonance so that the feedback signal altered the frequency slightly.

Figure 71 shows the decrease of amplitude on each side of the resonant frequency. As can be seen, the band with of the atomiser is approximately 30 Hz. The Q-factor according to the definition is about 3290.

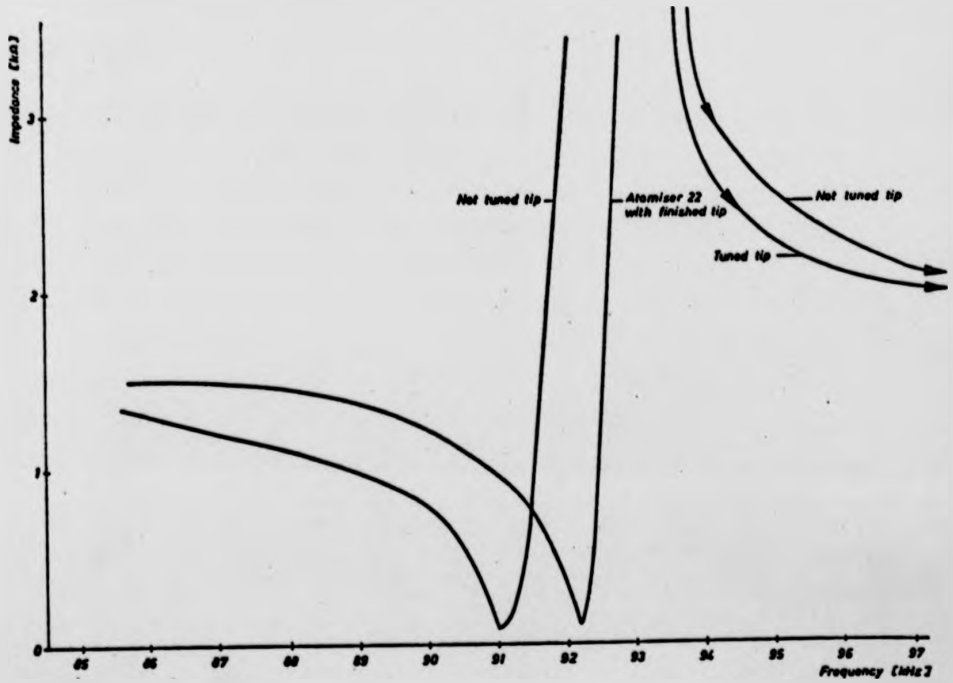

Fig.70

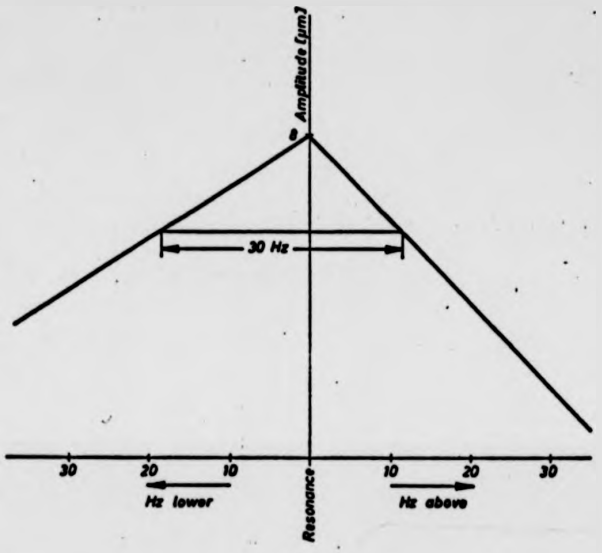

Fig.71

As Figure 71 shows, a frequency change of 12 Hz above the resonant frequency causes a 30% decrease of amplitude. This explains the importance of having an electronic drive unit which runs at the correct frequency all the time both on load and when temperature changes cause the resonant frequency to drift.

5.3 Temperature effects

As we have seen the damping of the vibration system is relatively small. The heating up of the atomiser is not expected to be a problem under normal conditions.
During atomisation the cooling capacity of the liquid which is applied to the atomising surface is always sufficient to cool the atomiser body. Even at idle, when the atomiser is vibrating without fuel, the temperature level is low and there is no danger of overheating if the heat can be transferred to cooler surroundings.
The problem with overheating can occur if the surroundings are at high temperature.
A high engine temperature together with operation of the atomiser at idle may give rise to temperatures high enough to affect the impedance of the atomiser considerably.

Above about 270 °C the transducers slowly lose their polarization, but the efficiency decreases at far lower temperatures than the Curie temperature. Furtheremore, a temperature rise causes changes of the clamping force. For the best possible performance it is necessary to keep the temperature at the lowest possible level. As mentioned earlier, the temperature increase causes the resonant frequency to drop until an equilibrium is established. Figure 72 shows the frequency change in the heating up period when an atomiser is switched on and driven at idle (without atomisation) with an ambient temperature of 20 °C.

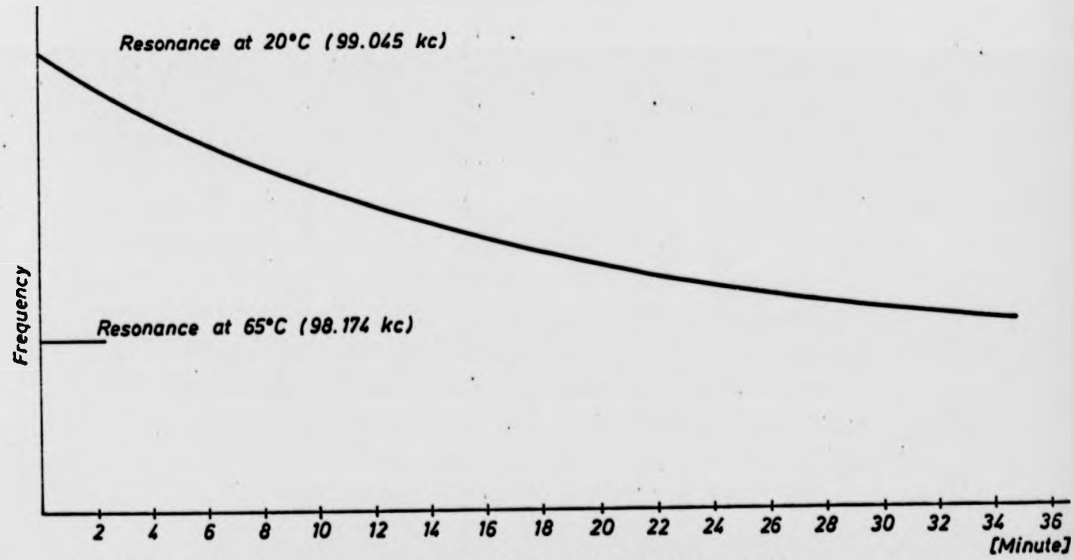

Frequency drop with temperature (heating up period of atomiser).

Fig.72

Atomisers which are supported by a flange on the step are better cooled than those supported on the dummy, at distance $\lambda/4$ from the end, and kept in a closed cylinder.

5.4 Droplet Formation

The atomisation of liquid by ultrasound was first discovered as early as 1925, but the first studies of the mechanism of atomisation were carried out many years later by K. Sollner (26). Sollner proposed the so-called cavitation hypothesis which suggests that atomisation by acoustic vibrations is due to hydraulic shocks generated by the implosion of cavitation bubbles close to the vibrating surface.

In 1954 some scientists (27) proposed the capillary-wave hypothesis. According to this hypothesis the droplets are formed at the crests of a standing capillary wave on the surface of the liquid applied to the vibrating surface.

The photographs in Figure 73 show the standing wave formation in a layer of alcohol at 0.25 kHz (a), 1.0 kHz (b), and 1.5 kHz (c).

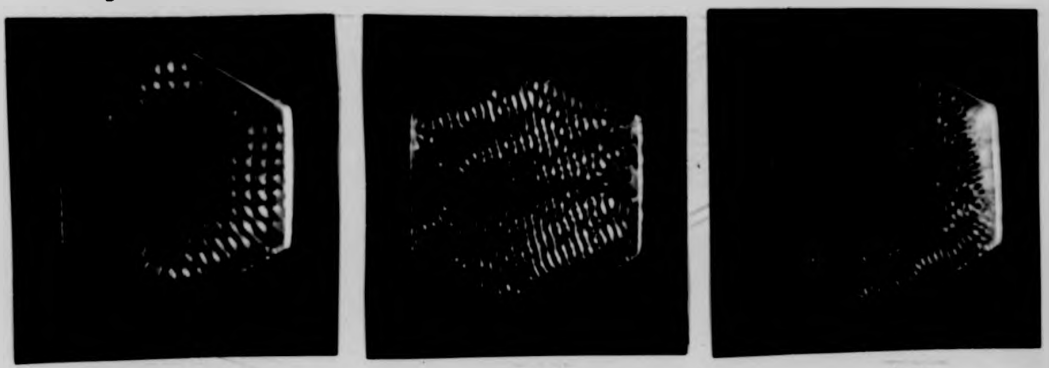

(a) (b) (c)

Fig.73

The decrease of the capillary wavelength with increasing frequency is illustrated in Figure 72.

Fig.74

5.4 Droplet Formation

The atomisation of liquid by ultrasound was first discovered as early as 1925, but the first studies of the mechanism of atomisation were carried out many years later by K. Sollner (26). Sollner proposed the so-called cavitation hypothesis which suggests that atomisation by acoustic vibrations is due to hydraulic shocks generated by the implosion of cavitation bubbles close to the vibrating surface.

In 1954 some scientists (27) proposed the capillary-wave hypothesis. According to this hypothesis the droplets are formed at the crests of a standing capillary wave on the surface of the liquid applied to the vibrating surface.

The photographs in Figure 73 show the standing wave formation in a layer of alcohol at 0.25 kHz (a), 1.0 kHz (b), and 1.5 kHz (c).

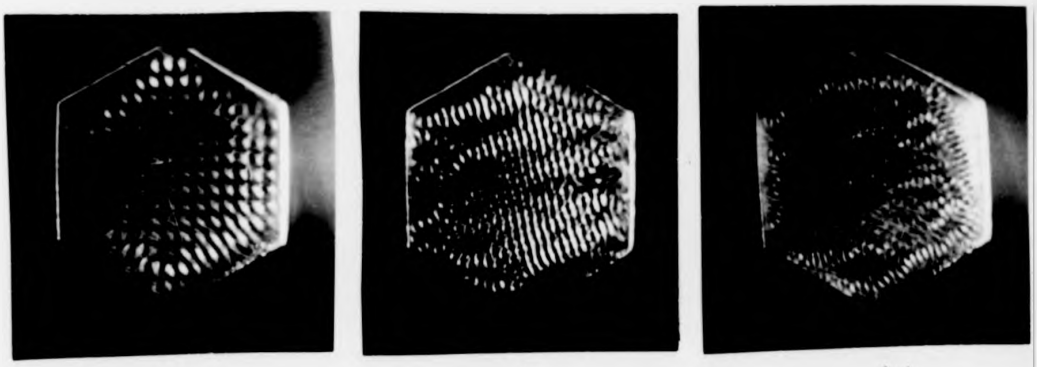

(a) (b) (c)

Fig.73

The decrease of the capillary wavelength with increasing frequency is illustrated in Figure 72.

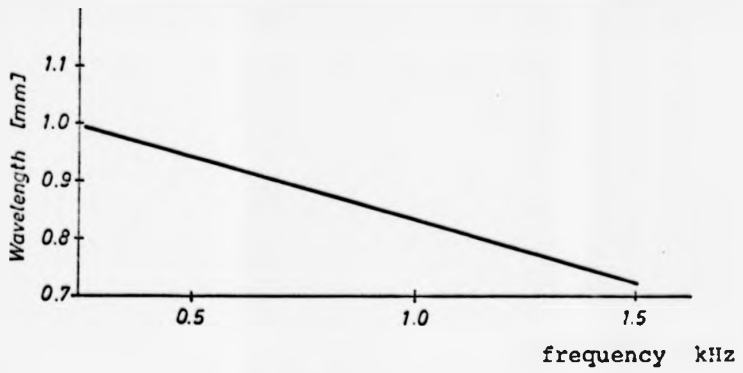

Fig.74

The photographs were taken with an ordinary camera equipped with a macrolens . At higher frequencies than 1.5 kHz the wavepattern is too small to be seen without a microscope. As can be seen from the photographs, the capillary waves are not uniform. This is possibly due to non-uniform amplitude of vibration over the surface and the variation in the thickness of the liquid layer. If the wavelength λ_c of the capillary wave is related to the droplet diameter by the expression $D = \alpha \lambda_c$, it is found that α is a constant almost exactly equal to 0.3 for all frequencies.

The formula(28) $\lambda_c = \frac{8\pi\sigma}{\rho f^2}$ gives the connection between the capillary wavelength and the exciting frequency. Using this formula to calculate λ_c for 1.5 kHz we find the value 0.709 mm, compared with the measured value of 0.71 mm from the photographs. Considering the simplicity of the experiment the agreement is very good. The formula for the capillary wavelength, multiplied by the factor 0.3, gives an expression for the droplet diameter.

$$D = 0.3 \frac{8 \pi \sigma}{\rho f^2}$$

σ = surface tension
ρ = density
f = exciting frequency.

This formula gives (Figure 75 for Gasoline) the theoretical droplet diameter as a function of frequency.

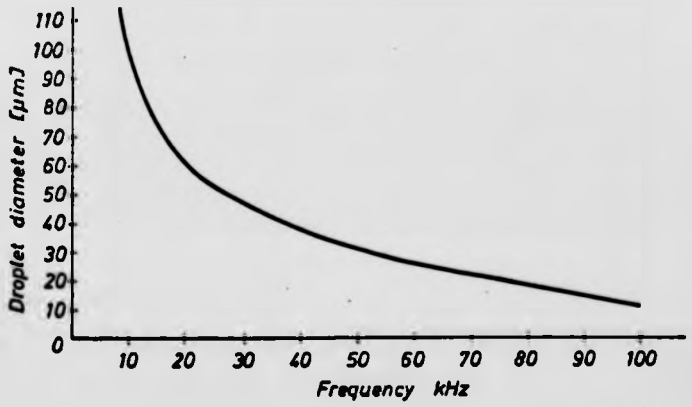

Fig.75

Experiments show clearly that in an ultrasonic atomised spray there are a large number of droplets both bigger and smaller than this theoretical value. At the frequency of the type 22 atomiser,

98.7 kHz, the theoretical value for the droplet diameter of petrol is 12.5 μm .

However, investigations show clearly that only at very low flow rates are such small droplets obtained.

As was mentioned in a chapter 4.8 there are a number of parameters which influence the quality of the spray.

It is interesting to notice that the droplet size increases rapidly at high flow rates.

Also an increase in power (bigger amplitude) at constant flow-rate causes an increase in the droplet size.

An atomiser adjusted to take high flow rates needs more power and the large droplets formed at high flow rate might be a result of both these effects.

For a certain amplitude of vibration there is an optimum liquid layer thickness. This optimum is difficult to obtain without accurate control both of the liquid feed to the atomiser and of the power. Obviously an ultrasonic atomiser, like a pressure atomiser, is best suited to a certain flow rate, but whereas the pressure atomiser performs better at high flow rates the ultrasonic atomiser gives the smaller droplets at lower flow rates. In the context of the engine manifold system the ultrasonic atomiser is of most advantage when the engine is idling: the two phase flow atomisation of a normal carburettor is then not satisfactory.

At higher flow rates the air speed is higher and the atomisation better. As was shown in chapter 2.3 a high temperature level accelerates the evaporation, but the shorter residence time in the manifold does not ease the demand for small, evaporating droplets. Even at high flow rate the droplets produced by an ultrasonic atomiser at about 99 kHz will of course be far smaller than those produced in a carburettor.

There is no certain explanation of why some bigger droplets are formed in the spray from an ultrasonic atomiser, but studies of the spray give the impression that some sort of cavitation takes place. The occurrence of collision may explain why larger droplets are found, particularly at high flow rate and with big amplitudes.

If the atomisation were as described by the capillary wave theory, the number of droplets produced could be expressed as

$N = \frac{4}{T_c \lambda_c^2}$ on the area $\lambda_c^2 \cdot T_c$ is the period of vibration.

According to the relation $D = a\,\lambda_c$ given earlier and the equation

$$\lambda_c = \sqrt[3]{8\pi\sigma/\rho f^2} \quad , \text{ we have} \quad N = \tfrac{1}{2}\sqrt[3]{(\rho/\pi\,\sigma)^2}\; f^{7}/_{3}$$

where N = number of droplets /cm^2s.
It is not easy to prove this relation experimentally. All experiments give far lower values for the flow rate. As mentioned in an earlier chapter, one reason for this could be the difficulty of distributing the liquid in such an way that the vibrating surface of the atomiser is properly used. Usually the ratio

$$\frac{Q\ \text{calculated}}{Q\ \text{measured}}$$

is as low as about 0.3. It is therefore reasonable to believe that the whole truth about the physics of droplet formation is not yet known.

5.5 Capillary waves on atomiser surface

In order to try to clarify further how droplets are formed in the liquid layer applied to a vibrating surface, an atomiser working at 98.5 kHz was studied under a microscope giving a magnification of up to several hundred times. A camera was fixed to the microscope to enable photographs to be taken.
The capillary waves created can have different patterns, but in most cases the one directional type of waves shown in Figure 76 represents the start of the process. The next stage is the formation of two directional wave pattern shown in Figure 77

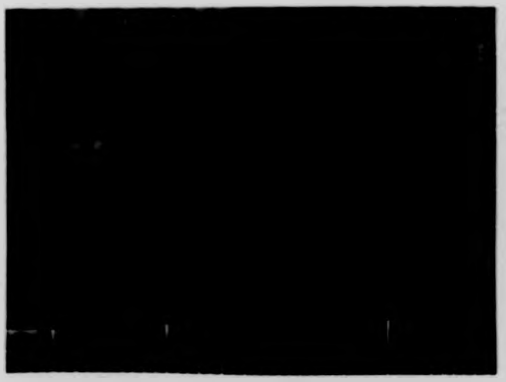

Fig.76

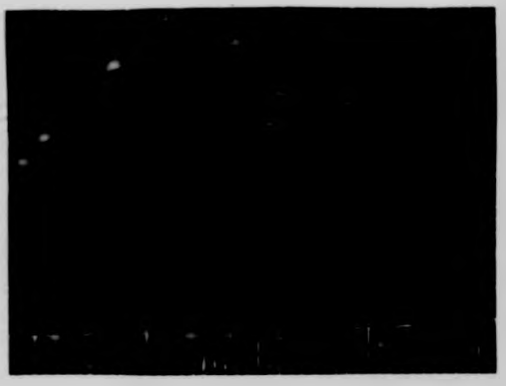

Fig.77

According to the relation $D = a\,\lambda_c$ given earlier and the equation

$$\lambda_c = \sqrt[3]{8\pi\sigma/\rho f^2} \quad , \text{ we have} \quad N = \tfrac{1}{2}\sqrt[3]{(\rho/\pi\,\sigma)^2}\; f^{7/3}$$

where N = number of droplets /cm^{2}s.
It is not easy to prove this relation experimentally. All experiments give far lower values for the flow rate. As mentioned in an earlier chapter, one reason for this could be the difficulty of distributing the liquid in such an way that the vibrating surface of the atomiser is properly used. Usually the ratio

$$\frac{Q \text{ calculated}}{Q \text{ measured}}$$

is as low as about 0.3. It is therefore reasonable to believe that the whole truth about the physics of droplet formation is not yet known.

5.5 Capillary waves on atomiser surface

In order to try to clarify further how droplets are formed in the liquid layer applied to a vibrating surface, an atomiser working at 98.5 kHz was studied under a microscope giving a magnification of up to several hundred times. A camera was fixed to the microscope to enable photographs to be taken.
The capillary waves created can have different patterns, but in most cases the one directional type of waves shown in Figure 76 represents the start of the process. The next stage is the formation of two directional wave pattern shown in Figure 77

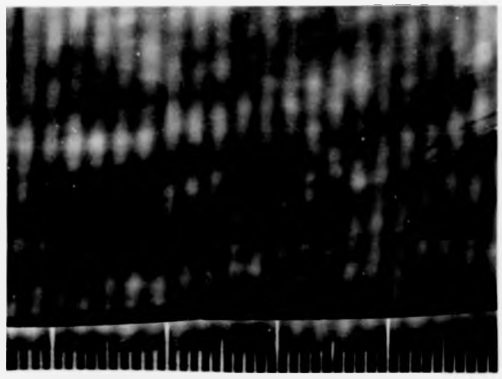

Fig.76

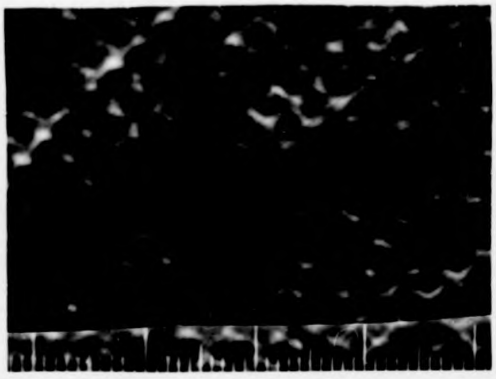

Fig.77

Further development of the two directional wave pattern creates the droplets. In Figure 78 it can be seen that some of the droplets are already formed and are about to be thrown off the surface.

In the experiment 96% alcohol was used. According to the theory the capillary wavelength at 98.5 kHz should be 43 µm. This corresponds very well with the measured values from the photographs shown. The distance between two lines in the scale imposed in the photographs is 10 µm.

The droplets which can be seen on the photographs seem to be of the size 10 to 15 µm. Theoretically the droplet size is 12.9 µm (43 µm × 0.3).

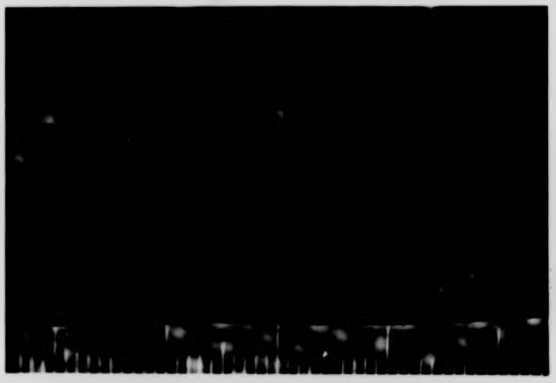

Fig.78

The time needed for the creation of droplets is dependent upon the vibration amplitude and the thickness of the liquid layer.

The studies of the capillary waves through the microscope revealed that at large vibration amplitudes and with a thick liquid layer the two directional wave pattern is not formed properly and droplets are thrown off from the one directional waves, giving droplets of various sizes, always bigger than those formed from the regular pattern shown in Figure 78. This is certainly the explanation of the formation of larger droplets at higher flow rates.

Early in the work it was found that if the power supply to the atomiser transducer is increased the droplets increase in size. The reason for this is that less of the vibrating surface is utilized as there is insufficient time for the liquid to spread onto a larger area. The droplets formed are then similar to those formed in a thick layer. It is very difficult to tell where the cavitation effect comes in. Studies of that effect could not be carried out using the microscope.

It is uncertain under what conditions the cavitation effect creates droplets, but with very thick liquid layers and large amplitudes no surface wave could be seen although droplets and drops

Further development of the two directional wave pattern creates the droplets. In Figure 78 it can be seen that some of the droplets are already formed and are about to be thrown off the surface.

In the experiment 96% alcohol was used. According to the theory the capillary wavelength at 98.5 kHz should be 43 µm. This corresponds very well with the measured values from the photographs shown. The distance between two lines in the scale imposed in the photographs is 10 µm.

The droplets which can be seen on the photographs seem to be of the size 10 to 15 µm. Theoretically the droplet size is 12.9 µm (43 µm × 0.3).

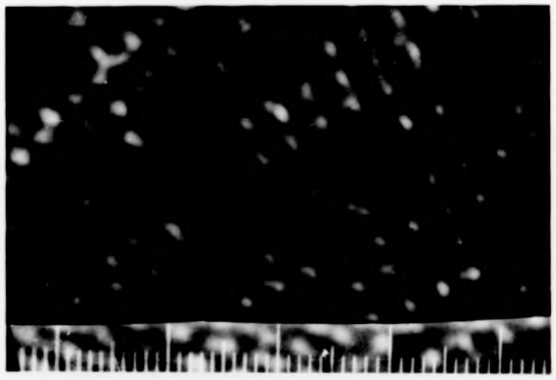

Fig.78

The time needed for the creation of droplets is dependent upon the vibration amplitude and the thicknes of the liquid layer.

The studies of the capillary waves through the microscope revealed that at large vibration amplitudes and with a thick liquid layer the two directional wave pattern is not formed properly and droplets are thrown off from the one directional waves, giving droplets of various sizes, always bigger than those formed from the regular pattern shown in Figure 78. This is certainly the explanation of the formation of larger droplets at higher flow rates.

Early in the work it was found that if the power supply to the atomiser transducer is increased the droplets increase in size. The reason for this is that less of the vibrating surface is utilized as there is insufficient time for the liquid to spread onto a larger area. The droplets formed are then similar to those formed in a thick layer. It is very difficult to tell where the cavitation effect comes in. Studies of that effect could not be carried out using the microscope.

It is uncertain under what conditions the cavitation effect creates droplets, but with very thick liquid layers and large amplitudes no surface wave could be seen although droplets and drops

were splashing from the layer.
Obviously the changes in wave pattern occur in a very short time. As soon as a droplet has left the surface a new crest is formed in its place by means of continuous movement of the liquid layer.
In order to take the photographs and study the wave-formation under the microscope the power to the transducers was controlled. With the atomiser working at normal power there is no chance of seeing the creation of droplets at all as it is only a matter of milliseconds between the creation of successive droplets at the same spot.

5.6 Droplet size measurement

There are several publications dealing with spray quality investigations (29,30). In (31) many methods of measurement are listed and described.
The investigation of droplets in this project had to be carried out by simple means.
Some of the methods for droplet diameter measurement can be done without expensive special equipment. One of these is the absolute slide method where droplets are collected on slides coated with a suitable material. However, using this method it is difficult to discover anything about the average droplet size, because droplets will collide and build up heavy concentrations on the slide.
For studying many droplets in a spray, in order to determine the sizes, the Frozen-Drop or the Wax method seems to be the easiest and most accurate way. A spray of paraffin wax behaves very much like a gasoline spray, because important properties such as viscosity and surface tension are similar for the two liquids. Wax alloys can be made to give almost exactly the same values, but in the investigation carried out an ordinary acid-free paraffin wax with melting point of 54 to 58 ^{o}C was used.
At 140 ^{o}C the viscosity was found to be 29.5 s. Redwood, compared with 26 s. Redwood for Petrol at 18 ^{o}C.
It was very difficult to obtain a higher temperature than 140 ^{o}C in the arrangement used because of dangerous fumes from the heating pot. The heated wax was applied to the vibrating surface of the atomiser by means of a preheated syringe.
To ensure quick solidification of the wax droplets a steel plate cooled by means of liquid nitrogen was situated underneath the atomiser and the spray. The solid wax drops can easily be collected

on microscopic slides for observation and measurement under the microscope. The only problem about this arrangement is to get a representative sample. Smaller droplets do not settle as quickly as the bigger ones. In fact, the smaller droplets were difficult to catch. The draught in the room caused the smallest droplets to drift away. Some were found at the collecting plate, but it is believed that too many of the smaller droplets had drifted away for the sample from the collecting plate to give the correct assortment. However, the arrangement used should give reasonably correct information about the sizes of the smallest and the biggest droplets in the spray, if enough samples are taken.
It is probably not possible to obtain a correct average droplet size by this method, but change of droplet sizes with flowrate or method of distribution is noticeable.

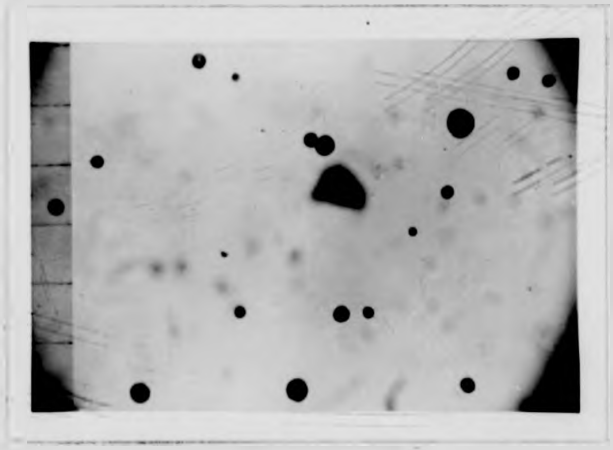

Fig.79 (a)

Fig.79 (b)

on microscopic slides for observation and measurement under the microscope. The only problem about this arrangement is to get a representative sample. Smaller droplets do not settle as quickly as the bigger ones. In fact, the smaller droplets were difficult to catch. The draught in the room caused the smallest droplets to drift away. Some were found at the collecting plate, but it is believed that too many of the smaller droplets had drifted away for the sample from the collecting plate to give the correct assortment. However, the arrangement used should give reasonably correct information about the sizes of the smallest and the biggest droplets in the spray, if enough samples are taken.
It is probably not possible to obtain a correct average droplet size by this method, but change of droplet sizes with flowrate or method of distribution is noticeable.

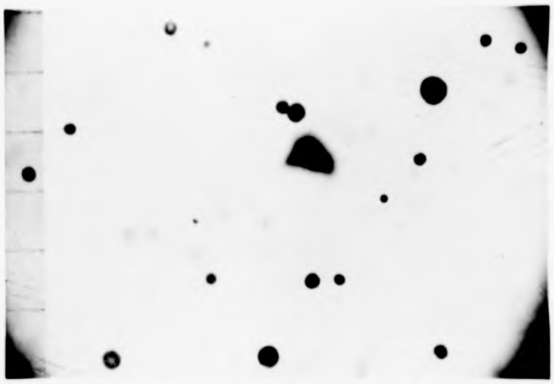

Fig.79 (a)

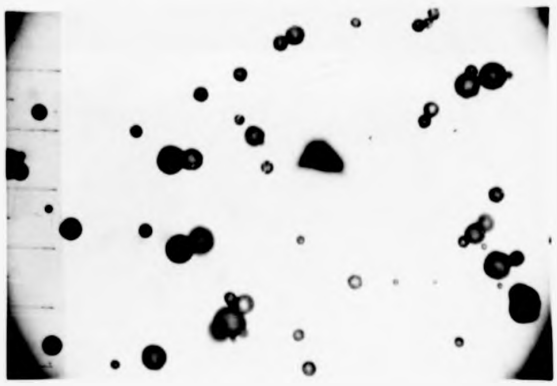

Fig.79 (b)

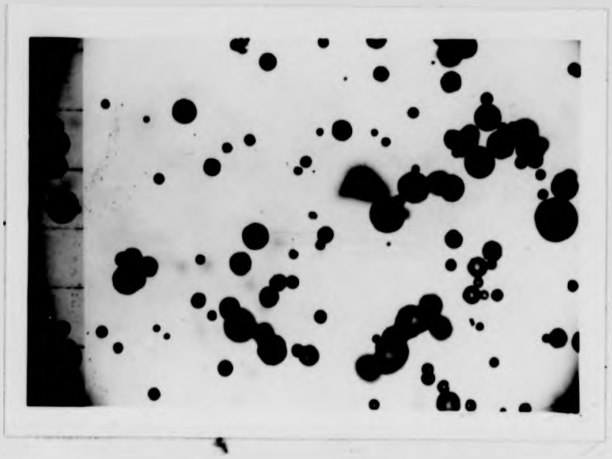

Fig.79 (c)

The investigation was carried out with an atomiser working at 92 kHz. According to the theory this frequency should give droplets of average diameter 13 µm (according to Figure 75).
Figure 79 shows photographs of wax droplets at different flowrates. Imposed in the photographs is a scale giving 50 µm distance between the lines.
Photograph (a) shows droplets collected at low flow rate. The smallest droplet is found to be smaller than 10 µm, but these droplets are difficult to detect on the photograph because of the light conditions of the microscope. The biggest droplet on the photograph a is approximately 45 µm, but the average dropletsize taken from a number of samples gives a value at very small flow rate of 18 to 20 µm. With increasing flow rate the average droplet size increases because the number of bigger droplets gradually rises. Photograph (c) is taken at almost maximum flow rate and it is easy to see that the drops are very much larger. The biggest droplet measured is almost 100 µm. It must be remembered, however, that at high flow rate the density of the spray causes collisions between droplets close to the vibrating surface and that the speed of the droplets is higher owing to the demand for more power to the transducers to give increased amplitude.As was explained earlier, the increase of amplitude will itself cause a number of bigger droplets to be thrown off owing to unknown effects (possibly cavitation).

Fig.79 (c)

The investigation was carried out with an atomiser working at 92 kHz. According to the theory this frequency should give droplets of average diameter 13 µm (according to Figure 75).
Figure 79 shows photographs of wax droplets at different flowrates. Imposed in the photographs is a scale giving 50 µm distance between the lines.
Photograph (a) shows droplets collected at low flow rate. The smallest droplet is found to be smaller than 10 µm, but these droplets are difficult to detect on the photograph because of the light conditions of the microscope. The biggest droplet on the photograph a is approximately 45 µm, but the average dropletsize taken from a number of samples gives a value at very small flow rate of 18 to 20 µm. With increasing flow rate the average droplet size increases because the number of bigger droplets gradually rises. Photograph (c) is taken at almost maximum flow rate and it is easy to see that the drops are very much larger. The biggest droplet measured is almost 100 µm. It must be remembered, however, that at high flow rate the density of the spray causes collisions between droplets close to the vibrating surface and that the speed of the droplets is higher owing to the demand for more power to the transducers to give increased amplitude.As was explained earlier, the increase of amplitude will itself cause a number of bigger droplets to be thrown off owing to unknown effects (possibly cavitation).

Sampling is more difficult at high flow rates. The intensity of the spray causes the smaller droplets to be kept in the air whereas the weight of the bigger droplets causes the bigger droplets to settle down quickly. The result therefore depends very much on how and where the sample is collected. In a heap of wax droplets the average droplet size will vary depending on where the atomiser was situated. The only way to measure average droplet size seems to be to sort the droplets into several sizes and work out the average size by counting. The sorting can be done using graded gauge sieves for bigger droplets, but smaller droplets must be examined microscopically. The wax-method is probably not suitable for very small droplets.

The holographic method might be useful in this work, but for very small droplets it will be difficult to make the droplets visible on the photographic plate. Holographic methods have the same disadvantage as the photographic method; it is difficult to measure droplets in the middle of the spray where the drop concentration is high. Figure 80 shows photographs of an alcohol spray taken with a normal camera and a macrolens, giving approximately 14 times magnification. The distance between two lines in the scale on the side of the photograph represents a true distance of 0.5 mm.

Fig.80 (a)

Fig.80 (b)

Sampling is more difficult at high flow rates. The intensity of the spray causes the smaller droplets to be kept in the air whereas the weight of the bigger droplets causes the bigger droplets to settle down quickly. The result therefore depends very much on how and where the sample is collected. In a heap of wax droplets the average droplet size will vary depending on where the atomiser was situated. The only way to measure average droplet size seems to be to sort the droplets into several sizes and work out the average size by counting. The sorting can be done using graded gauge sieves for bigger droplets, but smaller droplets must be examined microscopically. The wax-method is probably not suitable for very small droplets.

The holographic method might be useful in this work, but for very small droplets it will be difficult to make the droplets visible on the photographic plate. Holographic methods have the same disadvantage as the photographic method; it is difficult to measure droplets in the middle of the spray where the drop concentration is high. Figure 80 shows photographs of an alcohol spray taken with a normal camera and a macrolens, giving approximately 14 times magnification. The distance between two lines in the scale on the side of the photograph represents a true distance of 0.5 mm.

Fig.80 (a)

Fig.80 (b)

The photographs were taken with two electronic flashes giving a time of exposure of 1/1000 s. The depth of focus is only ± 5 mm at a shutter opening of 4.0. Most of the droplets are therefore not sharp.

Several photographs show that the droplets are more uniform in size when using petrol or alcohol than when using liquid wax, but it is difficult to measure an exact size because of the vapour tail and the vapour cloud surrounding the droplets.

In that respect it would have been an improvment to work in a low temperature room or to use a liquid with a higher boiling point.

The average droplet sizes determined from the photographs at a medium flowrate of alcohol using the atomiser 22 is nearly 40 µm.

It can be argued that immediate evaporation causes a reduction of the droplet diameter and that the photograph shows too small a droplet size. At higher temperatures at which the evaporation rate is big this would certainly be the case.

During the experiments the air temperature was kept at 15 ^{o}C and the photographs were taken close to the atomiser. Figure 80 (b) shows droplets standing still in the air about 0.5 meter from the atomiser. As can be seen, some of the droplets appear to be even bigger than those close to the vibrating surface. The reason is obviously that a slow moving droplet will be surrounded by a vapour shell which reflects light to the film and gives the image of a big drop.

The measurement of droplet size is difficult. The measurement of droplets produced due to ultrasonic vibration could however be done using a special feature of ultrasonics.

If droplets are sprayed in a strong ultrasonic field the droplets can be made to coalesce on ultrasonic pressure planes and to remain in field long enough to be measured optically.

Figure 81 shows a photograph of droplets in such an ultrasonic field.

At low temperatures a stationary droplet appears very sharp.

In an ultrasonic carburettor made for the project, the standing wave kept a cloud of spray in place for some tenths of seconds. After that time the droplets slowly join together in-to large drops resting exactly at the nodes of the standing wave, where they remain until they evaporate.

Fig.81

Photographs of droplets and the measurement of droplet size using liquid wax gives the impression that only at very low flow rate is the theoretical value of droplet size obtained. At medium flow rates, at which the atomiser is mostly used, the droplets are more likely to be about 40 µm. At flow rate too big for the capacity of the atomiser the droplets increase rapidly in size. This observation corresponds well with what could be seen looking at the liquid layer under the microscope.

6 The application of atomiser in an inlet system

6.1 Steady state flow rig tests

The first experiments with atomisers working in an airstream were carried out using a blower with a maximum capacity of approximately 160 m^3/h. The blower speed could be regulated to simulate the airflow at different engine speed and power.
Preliminary studies under steady conditions are much easier to arrange than those involving pulsating flow like that in the real inlet system of an engine. Transparent perspex tubes of various shapes were used to look at the performance of the spray in various arrangements for a range of air and "fuel" flow rates. In the steady state rig the impaction of droplets could be studied. Another important task was to find the arrangement giving the best possible fuel feed to the atomiser end.
There are two main ways of arranging the atomisers in a pipe.

The atomiser body can either be mounted inside at the middle of the tube, with the atomiser pointing downstream, or be mounted from the outside fixed to the wall of the tube and pointing inwards.
The atomiser situated in the middle of the airstream is the best solution and gives little impaction, assuming that the tube is wide enough and has no downstream restrictions.
The last condition is difficult to realise in the real system because of the relatively small inlet diameter of the engine port and the inevitable bends. At simulated maximum load the atomiser fixed at the wall pointing at right angled (90^o) into the pipe normally gave impaction at the opposite wall. If the atomiser is pointing downstream the impaction in the tube is less than if the atomiser is fixed at 90^o to the axis.
Narrow tubes giving high air velocities cause the droplets to be forced in the direction of the air flow, but there is reason to believe that the droplets then collide and form bigger droplets because of increased spray density.One of the main advantages of ultrasonic atomisers is the fact that no venturi that gives significant restriction to the system is needed. A narrow inlet manifold would reduce this advantage. A high airspeed is undesirable also because of the danger of build up of fuel drops at places such as on feedtubes or in bends and at edges which create vortex motion.

Feed tubes are better mounted upstream, (Figure 86) although downstream arrangements have been very sucessful in some experiments where the atomiser was angled approximately 30 ^{o} to the axis (Figure 85). At some flowrates the vortex created by the angled atomiser end gave a very fine distribution of fuel to the vibrating surface. At low flowrates however, fuel drips from the feed tubes without reaching the surface of the atomiser. This is obviously caused by the use of too low a fuel pressure to form a jet.

Later investigations on the engine revealed that under all conditions the fuel feed is the most difficult part of the experiments. This is discussed later in chapters concerned with actual experiments on the engines. Fuel feed via small pipes pointing at the vibrating surface upstream or downstream (see Figure 85 and 86) was later abondoned because it was discovered that the atomising area was better utilized by pointing the feed pipes at the side of the tip as illustrated in Figure 62 d.

The atomiser must then be pointing in direction of the air flow in order to get the fuel forced around the circumference. In straight pipes of the sizes used in inlet systems, it is difficult to avoid impaction at the opposite wall when the atomiser is flanged to the induction pipe.

For technical reasons it is not possible to angle the atomiser in a pipe sufficiently to direct the spray parallel to the axis of the pipe. The mounting of the atomiser in a bend makes it possible to direct the fuel spray more into the middle of the air stream. In the situation in which one atomiser is connected to each cylinder the atomisers can be arranged rather like the injectors in a manifold of an engine with fuel injection.

All experiments involving the steady state flow rig were aimed at solving some of the problems involved in carrying out comparative tests on a two-stroke and four stroke test engine.

As is often the case in research, most of the experiments were not sucessful and are not discussed in detail.

One of the experiments with an ultrasonic carburettor is worth mentioning because it raised many of the difficulties in the application of ultrasonic atomisers.

Figure 82 shows the arrangement. The atomisers are mounted in separate cylinders as shown in Figure 64 (paragraph 4.8).

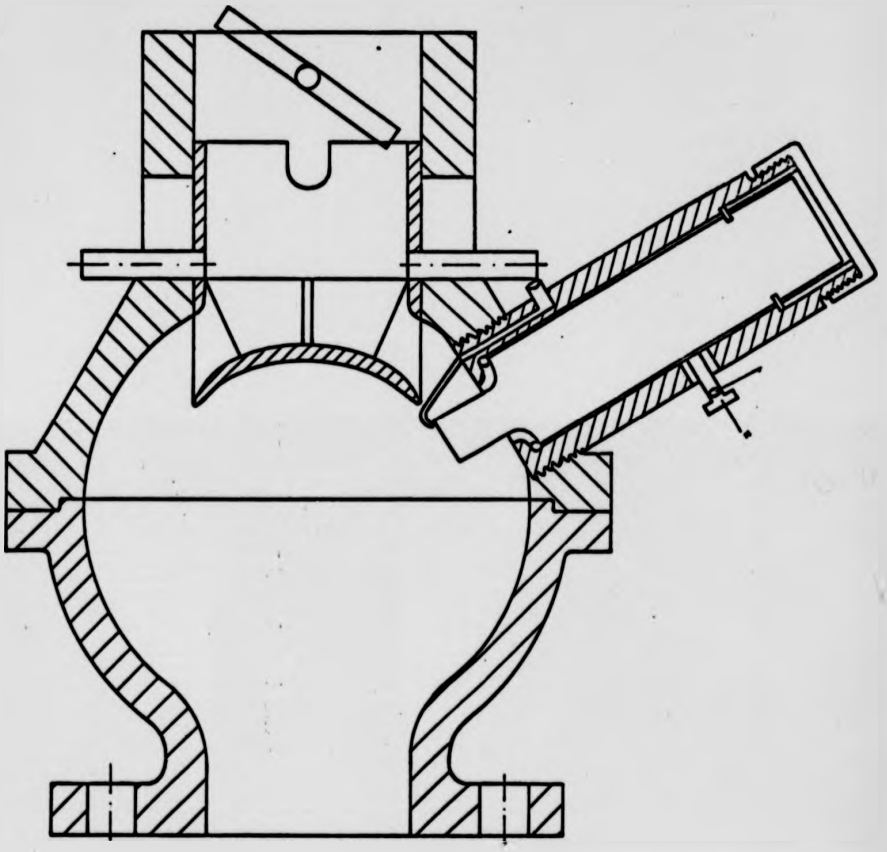

Fig.82

The flange at the bottom of the carburettor was made to fit the original manifold of the Ford test engine. In the upper half there is a moving shield, forced down gradually with increasing air consumption.

The shield was meant to have two functions: firstly it was intended to direct the air along the walls of the bowl to cause better mixing and to prevent the impaction of droplets. Secondly, the movement of the shield could eventually be used as a part of a system for metering the fuelsupply to the atomisers.

Perspex windows made it possible to watch the four atomiser vibrating surfaces and the impaction in the " bowl ".

This ultrasonic " carburettor " was made exactly the same length as

the original carburettor with the same inside diameter at the flange. The experience in the flow-rig with this design was not very promising. A vortex in the bowl caused impaction at the walls and at high air flow rates a wave of liquid moved up the walls and big drops of liquid were thrown off as the liquid reached the shield in the upper half of the spherical chamber. The main reason for the failure is obviously the narrow outlet of the bowl and the failure to direct the air along the walls to prevent impaction of droplets.

Figure 83 shows photographs of a two-dimensional model which was used for studies of various arrangements in a wind tunnel. The arrangement (b) had small fixed shields mounted through an extended " moving " shield and represented the best solution using the " bowl " and four atomisers mounted from the outside.

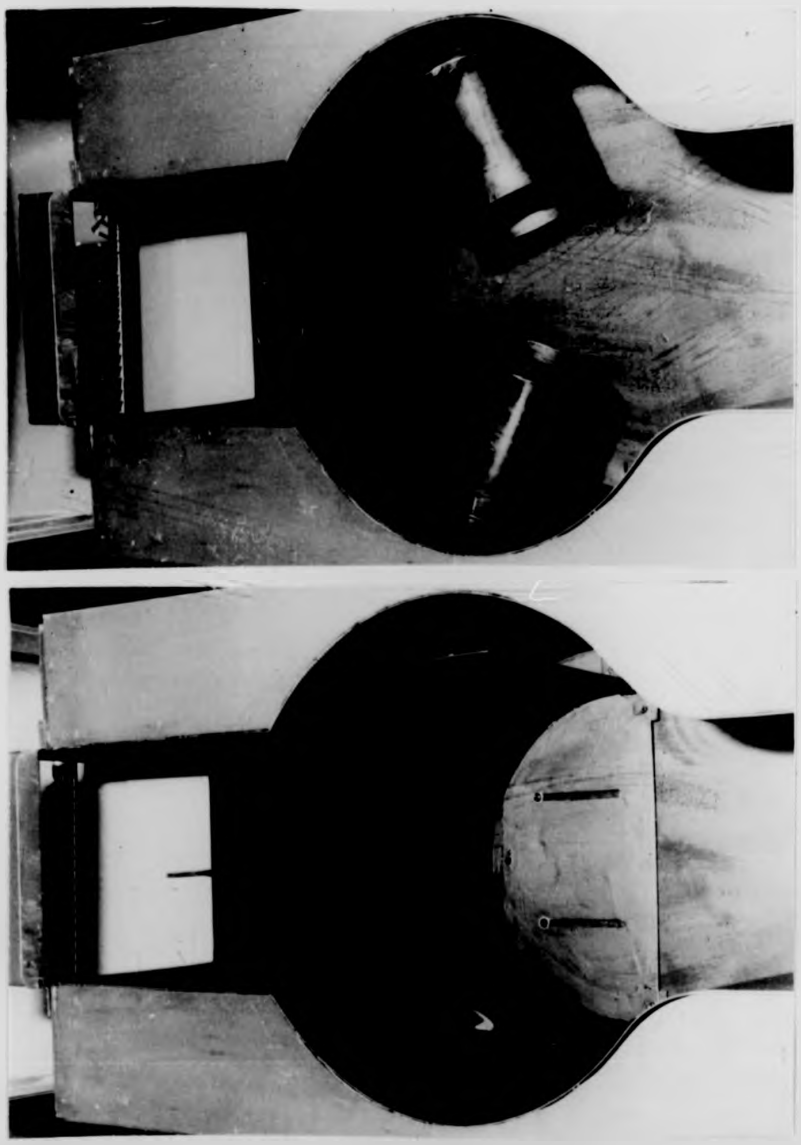

Fig.83
(a)
(b)

the original carburettor with the same inside diameter at the flange. The experience in the flow-rig with this design was not very promising. A vortex in the bowl caused impaction at the walls and at high air flow rates a wave of liquid moved up the walls and big drops of liquid were thrown off as the liquid reached the shield in the upper half of the spherical chamber. The main reason for the failure is obviously the narrow outlet of the bowl and the failure to direct the air along the walls to prevent impaction of droplets.

Figure 83 shows photographs of a two-dimensional model which was used for studies of various arrangements in a wind tunnel. The arrangement (b) had small fixed shields mounted through an extended " moving " shield and represented the best solution using the " bowl " and four atomisers mounted from the outside.

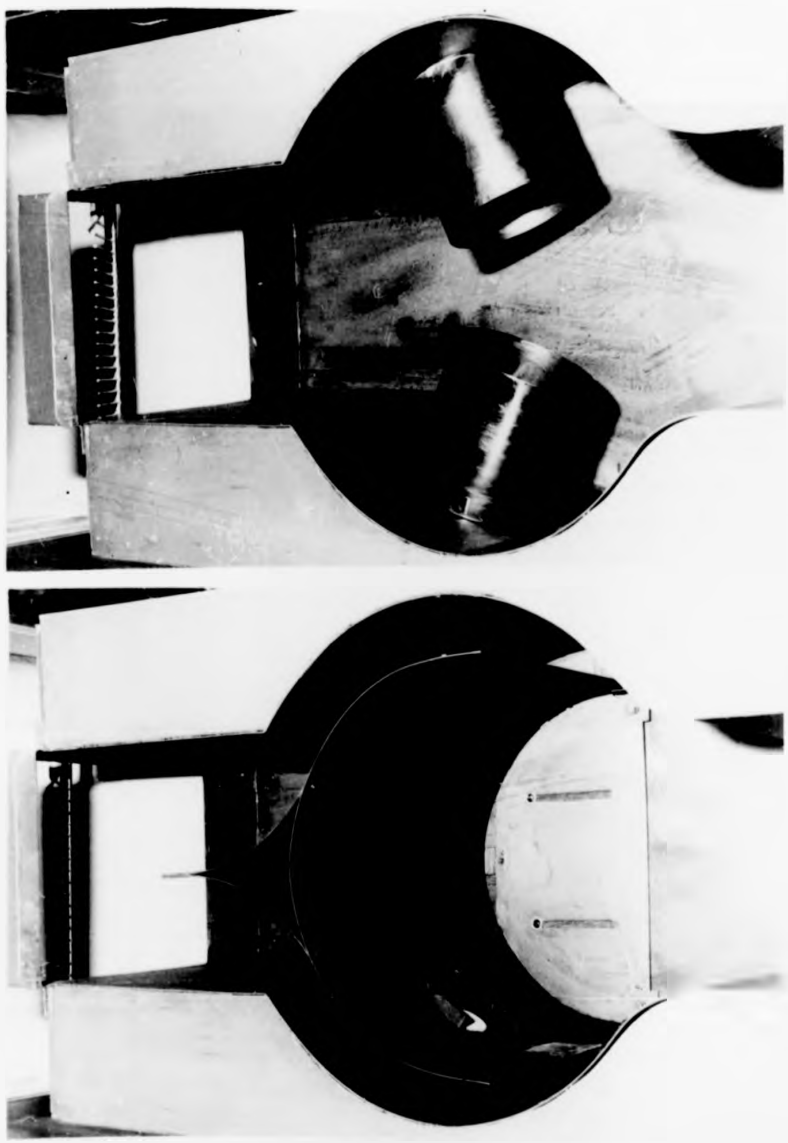

Fig.83
(a)
(b)

Additional difficulties with the individual fuel feed to the atomisers finally led to another design where the four atomisers were mounted in the middle of the bowl, pointing downstream (Figure 89). In this case it is simpler to direct the air around the droplet spray. However, this arrangement needed somewhat more length.

As was mentioned in the chapter 3 , the testbed for the four stroke engine is equipped with a dynamometer that is able to run as a motor. An obvious feature of this testbed is that it is possible to motor the engine for studying conditions in the inlet system without combustion. This feature was used to compare the results from the steady state tests with those in a pulsating flow.
Experiments with individual atomisers close to the inlet ports was not studied only in the steady state air stream because the pulsation from the opening and closing inlet valve can cause quite different conditions for the atomiser. A part of the work on atomisers situated in the manifold was therefore carried out on the engine itself, using methylated spirits instead of petrol to avoid dangerous gas concentrations in the exhaust system of the engine.
Studies of droplet behaviour in the pulsating air shows clearly that impaction is more difficult to control with pulsating flow than with steady air flow. The droplets from the atomiser seem to reach the opposite wall more easily as a result of the variation of the air speed.
The only way to avoid impaction in the manifold branch without adding heat seems to be to situate the atomiser as close to the cylinder as possible and to direct the spray straight at the inlet valve.
This knowledge was used in the last experiment on the engine with a manifold specially produced to fit four atomisers, each pointing directly into the inlet port. See Figure 84.

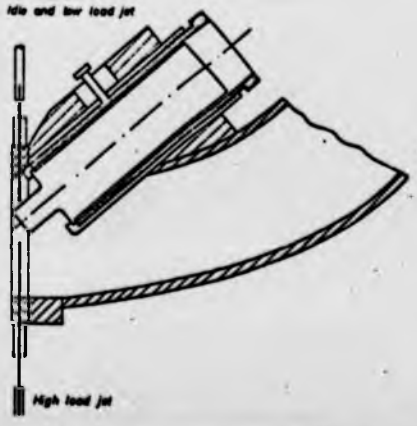

Fig.84

At the end of the development period of the atomisers a simple test-rig was built for endurance tests. A gravity feed system supplied the atomisers with water for atomisation, and the atomisers could be run for several hours.
The endurance of the atomiser 22 is very good. No failure has been discovered during the many hours of use.
The most difficult features have been the feed arrangement and the contact screw to the transducer.

6.2 Preliminary studies on 2-stroke engine

During the development period of the atomisers their performance was studied by applying water or methylated spirits to the vibrating surface.
Petrol was only very seldom used because of the danger of explosion and the toxic fumes. For preliminary studies using petrol, the small two stroke test unit described in chapter 3 was found to be very suitable.
The inlet system of this engine is very simple and the original carburettor could be replaced with a simple arrangement made of transparent perspex, as shown in Figure 85.

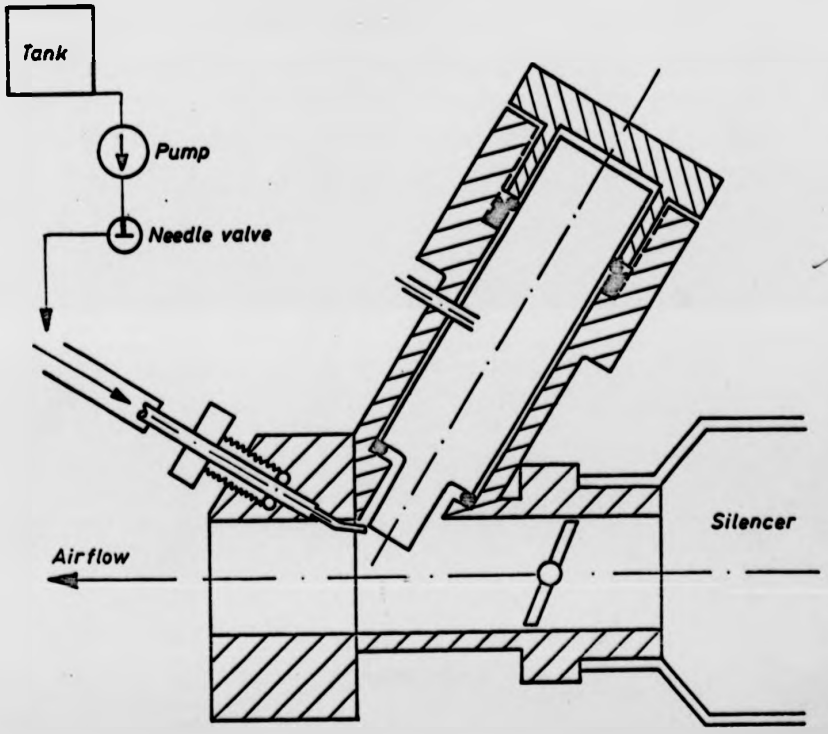

Fig.85

The atomiser was angled at approximately 60 ^{o} to the pipe axis and the fuel was supplied downstream.
A butterfly valve to regulate the air flow was situated between the silencer and the atomiser. To control the fuel a needlevalve was used.
Because there is no need for high fuel pressure to the atomiser, the only pump on the fuel side was the original diaphragm pump situated on the engine, working with the pulsating pressure in the crankcase, normally used for transport of fuel from the fuel tank to the carburettor.
The first experiments with this arrangement were very encouraging. Although some of the fuel atomised did impact in the tube the engine ran satisfactorily. Compared with the carburettor, the idling conditions could be improved significantly and the maximum power was increased by about 30%.
Only a few measurements could be carried out before the perspex carburettor split. The cause of the cracking of the perspex was thought to be the engine vibrations, and so the " carburettor " was fitted with an elastic rubber hose after repair.
However, after only a few minutes run the mended " carburettor " fell apart again and the experiment had to stop.
Later experiments revealed clearly that perspex is not a suitable material for use in connection with ultrasonic vibrations, especially if different perspex parts are joined together with cement, or if perspex tubes are bent in warm air to give a certain shape. " Frozen-in stress " in the material causes the material to crack when exposed to ultrasonic vibrations. Even if the atomiser is mounted at a " node " the vibrations transferred seem to affect the material. None the less, most of the studies of impaction involve the use of perspex, because it is the only cheap material that is transparent and easy to work with, but only straight pipes where the atomiser was mounted in rubber survived without cracks.

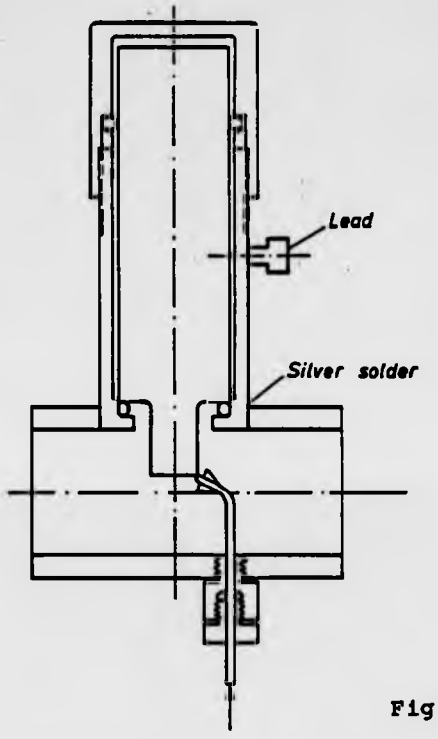

Fig.86

Figure 86 shows an ultrasonic " carburettor " for the two-stroke engine made in brass with upstream fuel feed. The atomiser was mounted directly to the air inlet pipe. A 90° mounting of the atomiser makes the arrangement much simpler. To lead the fuel to the atomiser, a 0.5 mm ID. stainless steel tube was mounted from the opposite side.
As was stated in a previous chapter, having the atomiser pointing in the direction of the air-flow provides a better solution and prevents impaction in the tube to some extent. An angle of 60 °, as used in the first experiment on the two-stroke unit, is enough. An even smaller angle between the atomiser body and the tube axis would inevitably cause restriction of the inlet tube and this would again affect the charge to the engine. The experiments on the two-stroke unit were also intended to be a preliminary study only and could not be allowed to involve too much work and time.

Because of the short distance from the air inlet of the carburettor (Figure 86)to the atomiser it was possible to see the droplet behaviour without having a transparent tube. As the fuel feed was upstream there was no impaction of droplets on the feed pipes.
To avoid " lift off " of the low pressure fuel jet at high air velocity, a small shield was fixed to the feed tube. Without this shield the end of the feed tube had to be situated very close to the edge of the atomiser tip. Later experiments showed that the obvious arrangement, when mounting an atomisers in a pipe and using low pressure feed, is to feed the fuel on to the side of the atomiser tip. The atomiser must then be angled in such a way that the speed of the air forces the petrol down to the end.
Experiments show that such an arrangement can utilize the vibrating

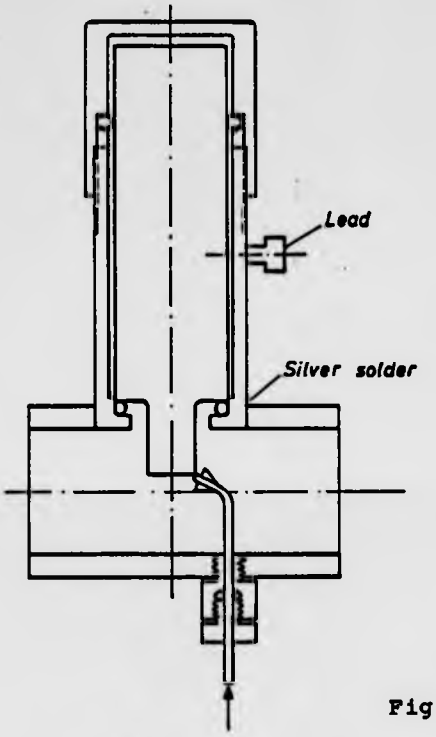

Fig.86

Figure 86 shows an ultrasonic " carburettor " for the two-stroke engine made in brass with upstream fuel feed. The atomiser was mounted directly to the air inlet pipe. A 90° mounting of the atomiser makes the arrangement much simpler. To lead the fuel to the atomiser, a 0.5 mm ID. stainless steel tube was mounted from the opposite side.
As was stated in a previous chapter, having the atomiser pointing in the direction of the air-flow provides a better solution and prevents impaction in the tube to some extent. An angle of 60 °, as used in the first experiment on the two-stroke unit, is enough. An even smaller angle between the atomiser body and the tube axis would inevitably cause restriction of the inlet tube and this would again affect the charge to the engine. The experiments on the two-stroke unit were also intended to be a preliminary study only and could not be allowed to involve too much work and time.

Because of the short distance from the air inlet of the carburettor (Figure 86)to the atomiser it was possible to see the droplet behaviour without having a transparent tube. As the fuel feed was upstream there was no impaction of droplets on the feed pipes.
To avoid " lift off " of the low pressure fuel jet at high air velocity, a small shield was fixed to the feed tube. Without this shield the end of the feed tube had to be situated very close to the edge of the atomiser tip. Later experiments showed that the obvious arrangement, when mounting an atomisers in a pipe and using low pressure feed, is to feed the fuel on to the side of the atomiser tip. The atomiser must then be angled in such a way that the speed of the air forces the petrol down to the end.
Experiments show that such an arrangement can utilize the vibrating

surface very well because petrol reaches the surface from the whole circumference. Using the ultrasonic " carburettor " shown in Fig.86 the performance curves shown in Figure 87 and 88 were made.
Curves marked o relate to results obtained using the original carburettor and those marked □ relate to the experiment with the ultrasonic carburettor at the same power rating and approximately the same air fuel ratio. It was very difficult to obtain exactly the same air fuel ratio; differences of up to 1.0 had to be accepted. The reason for this difficulty is, firstly, the different restriction in the two systems and secondly, the method of measurement of the airflow. As is well known, only very small discrepancies in the flow metering cause large differences in the air fuel ratio. As the curves show, the air consumption and fuel consumption are almost the same for the two experiments, although the variation in the air fuel ratio is significant. The inaccuracy of the air fuel ratio must be taken into account when conclusions from the experiment are drawn.

TWO-STROKE ENGINE EXPERIMENTS

o original carburettor, max. power output
□ ultrasonic carburettor, same power as o
× ultrasonic carburettor, max. power output.

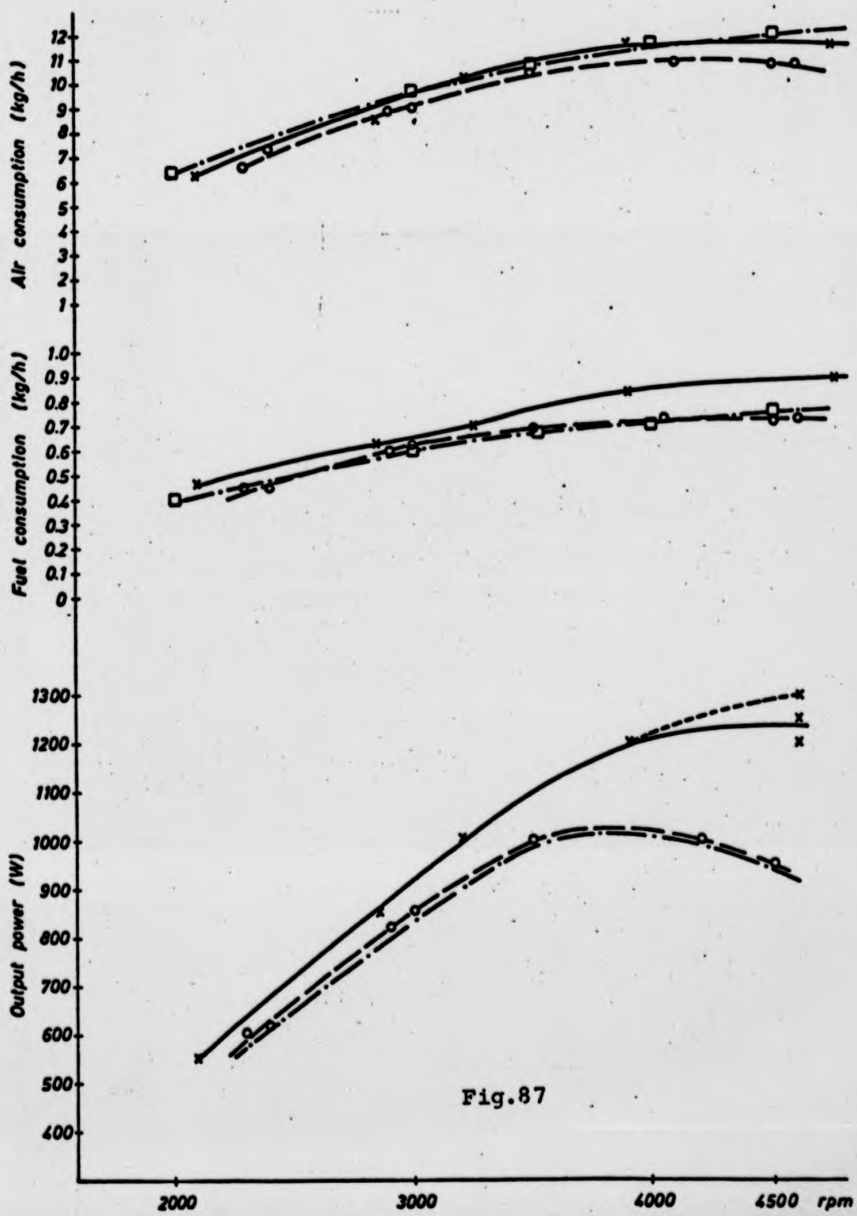

Fig.87

TWO-STROKE ENGINE EXPERIMENTS

o original carburettor, max. power output
□ ultrasonic carburettor, same power as o
× ultrasonic carburettor, max. power output.

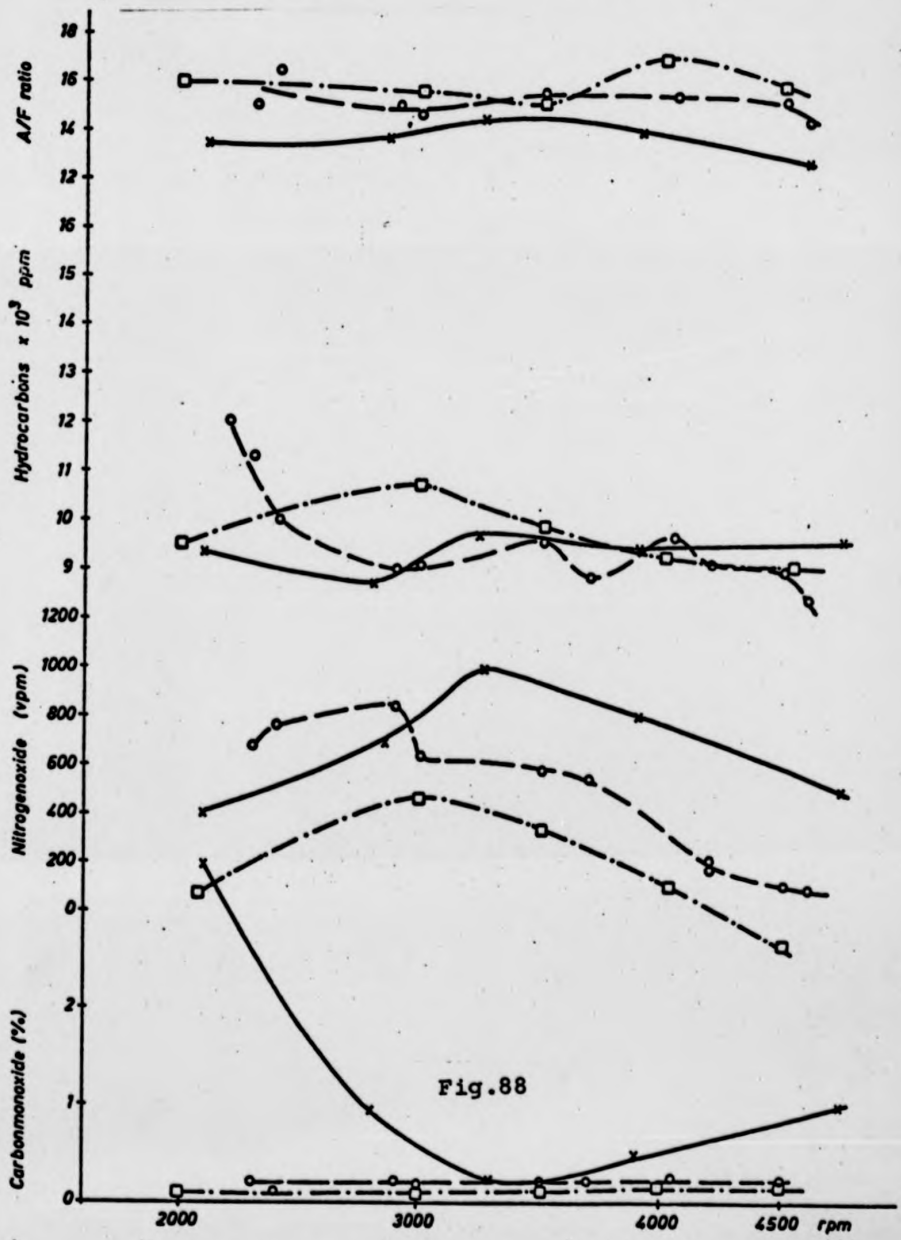

Fig.88

The performance curvers are measured at maximum power of engine. The maximum power (in watts) versus engine speed is shown in Figure 87. Using the ultrasonic arrangement the power could be increased by 30% at an engine speed of 4500 rpm.
The maximum power could be increased at all speeds, but not so much. Obviously, the improvement is partly caused by the reduction in losses in the inlet system, resulting in a better charge-induction the engine cylinder.
What is of particular interest is to notice the improvement of the idling conditions of the engine.
A two stroke engine, especially one without reed valves (one-way valves) in the inlet, is unsteady at low speed because of big differences of the cylinder charge from stroke to stroke.
With the ultrasonic carburettor the engine could idle at 400 rpm compared with a minimum speed of 800 rpm with the original carburettor. The airflow was not easy to measure at that low speed, but efforts were made to give the engine the same air fuel ratio. It is well known that the venturi-carburettor is not a very good atomiser especially at low flowrates, and so the improvement noticed is not surprising. The better low speed characteristics of the engine with the ultrasonic device gave a lower hydrocarbon level in the exhaust gas.
Figure 88 shows the content of HC, NO on CO corresponding to the engine power shown in Figure 87. As expected for the two stroke engine the hydrocarbon level is very high. When idling, the engine equipped with the original carburettor gave values up to 16000 ppm (as propane). With the ultrasonic carburettor the level was down to 10 000 ppm, but a comparison is not fair without knowing the air fuel ratio more exactly. It is more correct to compare the results under load, as represented in Figure 88.
As can be seen, the hydrocarbon content in the exhaust at higher power and speed is almost the same with the original carburettor as with the ultrasonic device. At maximum power the engine with original carburettor could hardly be run at 2200 rpm. The ultrasonic device gave good engine stability at far lower speed, and the hydrocarbon level was lower.
The nitrogen oxide content is lower with the ultrasonic carburettor, when the engine power is equal to the maximum power with original carburettor. If the engine equipped with the ultrasonic device is run at maximum output the NO level is higher than at maximum power

with the carburettor. As the NO-level is dependent upon the temperature in the cylinder this result is as expected.
The reason why the NO- concentration is lower at the same power is more difficult to understand, because the air and fuel consumption were almost unchanged. A more efficent combustion would theoretically give a higher cylinder peak temperature and therefore a higher NO-level. The CO concentration is surprisingly low at all load conditions.
Even at maximum load with the ultrasonic device the CO level did not exceed 4%. Measurements carried out in the laboratory for Internal Combustion Engines in Trondheim and also reports from Volvo-Penta, the producer of the engine, show that the CO level for two-stroke engines can be far lower than the average for four-stroke engine. This might be due to the temperature level, which is relatively high for two-stroke engines at high output.

It is difficult to draw any conclusion from the experiments with the two-stroke unit. The experiments were meant as an aid in the development and application of ultrasonic atomisers, but obviously improvments in two-stroke engines must be possible if such a simple experiment as that described above gave such promising results.

6.3 Investigations on four-stroke engine

The experiments on the four-stroke Ford Pinto engine consisted of three different tests.

A. Tests on the engine with original carburettor
B. Tests with the ultrasonic carburettor replacement.
C. Tests with four independent atomisers in the inlet system for best possible utilisation.

The importance of keeping some of the engine parameters constant is particularly vital if the exhaust gas emissions under varions operating conditions are to be compared. In chapter 1.1 some of the effects on emissions of engine parameters are explained in detail.
The tests on the engine with the original carburettor had to be carried out carefully in order to establish the performance of the engine as it leaves the factory.
As was stated before it is essential to control the following engine parameters if a comparison is to have any value.

1. Air-fuel ratio
2. Ignition timing
3. Engine power and speed

The air fuel ratio is by far the most difficult parameter to measure accurately. Although the method used is considered to be the most accurate way to measure air fuel ratio, pulsations and inaccurate readings cause differences and faults which can influence the results. As will be explained later, when using this indirect method it is difficult to adjust to exactly the same air fuel ratio while running comparative experiments. It is necessary to repeat measurements more often than would be the case if a more direct A/F measuring method were used, also the manifold vacuum and the exhaust temperature were measured. At constant speed and load these measurements are directly related to the air-fuel ratio.

The experimental engine has its ignition retarded at low speed or when the butterfly is almost closed, by means of a connection from the venturi to the back side of the diaphragm of the vacuum regulator.

It is impossible to get this system to work correctly when using ultrasonic devices which give a quite different depression in the manifold. Therefore a manual adjustment of the ignition timing was built in. For every measurement the timing had to be adjusted to correspond to the value measured on the tests with the original carburettor, at same speed and power.

The timing was measured with a timing stroboscope triggered from the high tension lead of No 1 cylinder.

It was not considered to be important to solve the problem of the fuel and air metering at this stage of the research. The metering was therefore done by hand by means of a butterfly valve in the air inlet to get the correct amount of air to the cylinders, and a fine adjustment needle valve to adjust the petrol flow to the atomisers. Efforts were made to design the ultrasonic devices so that a fuel metering system easily could be incorporated. For example, a " shield " arrangement for reducing impaction, might be used as a part of an air-metering system. (See Figure 82 page 143).

During the last two years mechanical metering systems seem to be gaining favour compared with electronic, manifold pressure controlled systems for use in petrol injection equipment for car engines.

The reason for this is that the pulsating pressure in the induction system is not good enough, even as one of several input values in the electronic metering system, to cover all engine operating conditions.

The use of hotwire or other more sophisticated air speed metering methods is still too expensive and the devices too vulnerable.
Fuel metering for a system using ultrasonic atomisers is not expected to be difficult to arrange. Air/Fuel metering similar to the Bosch K-Jetronic could easily be adopted, but the ability of the atomisers to operate with a low pressure fuel feed should make the arrangement even simpler and cheaper.

6.3.1 Carburettor replacement

The ultrasonic carburettor that was finally mounted on the engine is shown in Figure 89.
The main difference between this carburettor and that shown in Figure 82 page 143, is that the four atomisers are situated inside the " bowl " shaped chamber in a cage made of aluminium.
The atomisers were supported in a slot at the nodal point in the dummy. Teflon rings, made to fit the slot exactly keep the atomisers rigidly in place without loss of efficency. A dome was made at the top of the atomiser cage to give an aerodynamic shape. The atomiser cage was supported by four brass tubes through one of which the fuel to the atomiser feedpipe was run. The other pipes were used for the leads to the transducers. Because of the design of the feedback oscillator used, it was necessary to insulate the atomisers from each other and to connect + and - leads to each atomiser from the drive unit.
In the middle of the four atomisers a feedpipe was connected, at the end of which was fixed a distributor to feed fuel to each atomiser.
In order to ventilate the " cage " slots were cut at the side of the aluminium casing. The protruding fins directed a small part of the airstream along the atomiser bodies.

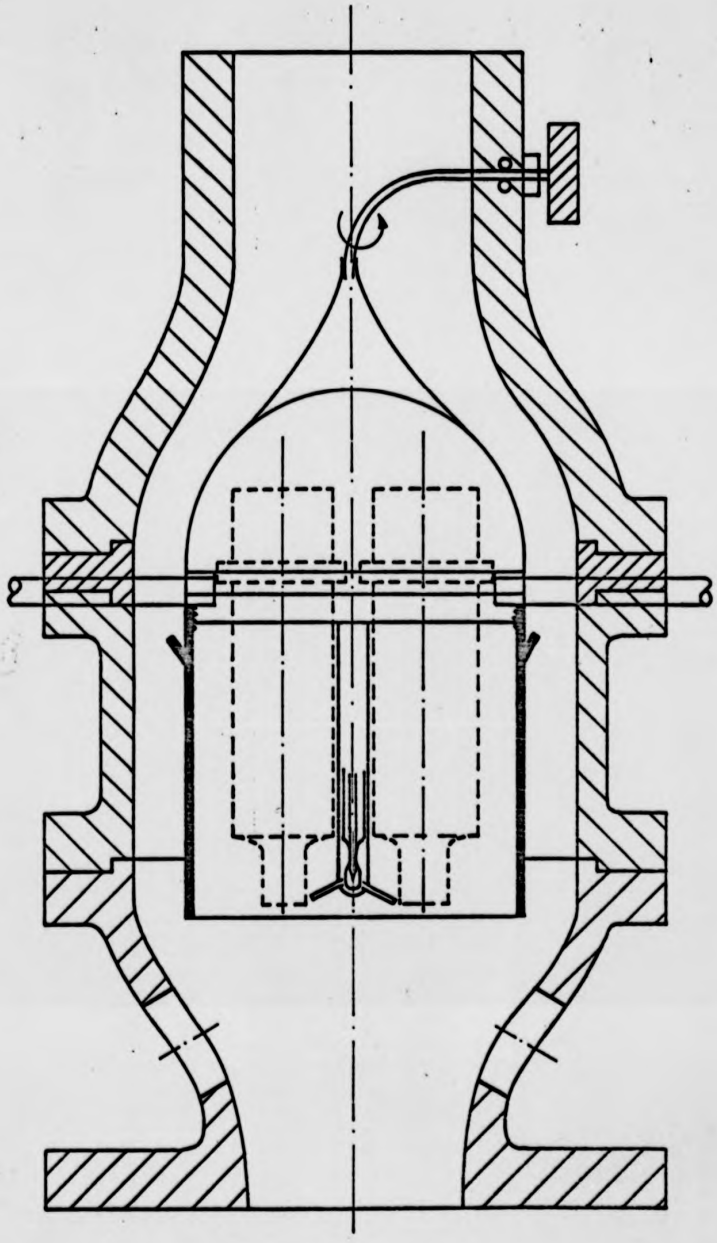

Fig.89

Fig.90

For ease of comparison all the performance curves are put at the end of this chapter. In the discussion of the results some of the possible errors are discussed and the results are analysed taking into account the changes in air fuel ratio from experiment to experiment. Appendix IV includes a photograph that shows details of the ultrasonic carburettor unit.

Fig.90

For ease of comparison all the performance curves are put at the end of this chapter. In the discussion of the results some of the possible errors are discussed and the results are analysed taking into account the changes in air fuel ratio from experiment to experiment. Appendix IV includes a photograph that shows details of the ultrasonic carburettor unit.

Fig.90

For ease of comparison all the performance curves are put at the end of this chapter. In the discussion of the results some of the possible errors are discussed and the results are analysed taking into account the changes in air fuel ratio from experiment to experiment. Appendix IV includes a photograph that shows details of the ultrasonic carburettor unit.

The advantage of this system compared with the setup described on page 142 is that there is a common feed of fuel and the fuel valve can be situated close to the fuel distributor. With low pressure fuel feed it is very important to have the shortest possible distance between the fuel valve and the outlet. As explained earlier, the air flow is regulated by a butterfly valve at the inlet, before the atomisers. This is done to avoid impaction of droplets. In the ordinary carburettor system, in which the butterfly valve is situated after the venturi, heavy impaction takes place at the butterfly valve.

In the ultrasonic carburettor, Figure 89, the pressure drop is at the top of the system and the carburettor is at the same low pressure as the manifold.

This causes a bigger pressure drop at the fuel valve and vapour bubbles are created in the fuel line to such an extent that the fuel flow is difficult to control, if the volume of the fuel line in the low pressure area is too great. A constant stream of fuel is necessary if a constant air fuel ratio is to be maintained. Especially at idle, vapour bubbles cause unstable running conditions.

A higher fuel pressure would solve the problem of the vaporisation in the fuel lines. At a minimum manifold pressure of 0.5 bar (at idle) the creation of bubbles would be avoided. It would then be necessary to have a pressure pump to deliver enough fuel at higher engine loads. Pressures of 6 bar or more would be required assuming a constant restriction of the jet close to the outlet.

For the experiments with the ultrasonic carburettor the need for a high pressure pump was avoided by having the regulating valve at the end of the feed system. The original fuel pump, giving an almost constant pressure of apprximately 0.4 bar, was sufficient.

The fuel valve was made with a needle. Threads at the end of the needle permitted adjustment of the gap between the needle and the seat in the distributor piece. Figure 89 page 156 shows the final arrangement. A Bowden cable transferred the needle movement to the out side of the carburettor for regulation.

Figure 90 is a photograph of the atomiser section in operation at a medium fuel flow rate.

6.3.2 Atomisers on an engine manifold

In chapter 2 it was shown that there is little chance of getting homogeneous mixture and uniform distribution to all cylinders in a multi-cylinder engine without having evaporation of the fuel droplets early in the inlet manifold, so early that only air and evaporated fuel enter the branches.
In a single carburettor system early evaporation is probably the only way to prevent droplet impaction under all engine load conditions. In petrol injection systems the injectors are situated close to the inlet valves. Maldistribution of fuel is then eliminated if the injectors work equally. In all systems, however, there is a possible maldistribution of air, depending of course how well the inlet manifold succeeds in delivering equal amounts of air to the cylinders. The experiments carried out with four ultrasonic atomisers mounted on an original carburettor manifold clearly show the nature of the maldistribution of both air and fuel and its effects on engine performance.
Figure 91 shows the arrangement. In the steady state test rig it was found that impaction shortly after the atomisers could be partly avoided by diverting air from the intake, close to the butterfly valve, to the front of the atomisers, as illustrated on the Figure 91.
Experiments on the engine showed that there was no impaction of fuel in the manifold. The results of the exhaust gas measurements were less promising however. At nearly all loads the CO content in the exhaust was higher than with the carburettor. The hydrocarbon level at idle was higher than in the original situation. Detailed results of this experiment are not considered to be of great interest and are not given in this report. However, it is very interesting to notice the reason for the poor results. At idle maldis-

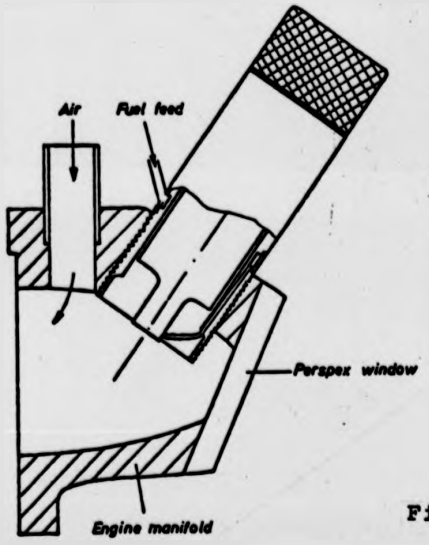

Fig.91

tribution of the fuel arose, principally because of problems with vapour bubbles in the feed tubes. At higher load there was also maldistribution of air, caused mainly by differences in the flow rates of air by-passed from the air inlet to the fronts of the atomisers.
A higher pressure feed and restricted outlet of the fuel would definitely improve the performance of the design, but the maldistribution of air would still give different charges to the cylinders.
Although the time available for the research was running out, it was decided to make a completely new manifold and a fuel system working at higher pressure.
The difficulty with one atomiser on each cylinder is that a common fuel valve is too far away from the fuel outlet. With individual regulation on each atomiser it is difficult to get equal fuel-supply to all the atomisers.
An attempt was made to produce spring-loaded valves to open at 0.5 bar, but with the equipment available they were all too inaccurate to give the same opening pressure.

6.3.3 New manifold design for better distribution of air and fuel to the cylinders

The engine manufacturer has many different factors to consider when designing an engine inlet system, one of which is the limited space available to give the manifold branches to the cylinders the best possible shape.
In an inlet system with carburettor it is desired to place the carburettor fairly close to the valve port to keep the volume between the venturi and the inlet valve as short as possible.
In injection systems more care can be taken to give the branches the geometry required for best possible air distribution.
The manifold especially manufactured for the use of atomisers close to the inlet valve could be designed without thinking of the restriction of space under the bonnet of a car as only laboratory tests were in question.
In the case of the four-cylinder research engine each pair of adjacent cylinders have the inlet ports close together. In order to avoid disturbance between the two cylinders the branches were made separate. A siamesed system which is often used, causes unequal filling of the cylin-

ders because of robbing effects.
The shape and dimensions are identical for each pair of cylinders, and each the branch are joined together as smoothly as possible. Fig.92 shows a photograph of the manifold. The atomisers are fitted in the same way as shown on the experimental manifold Fig. 84. The feed system operating with pressure from approximately 0.5 to 8 bar is different from previous experiments. The pressure of the fuel feed necessary to avoid depression in the feed line had to be approximately 0.5 bar at idle. At this pressure the fuel flow through each jet, corresponding to the fuel consumption at idle is only 4 to 5 cm^3/min. On the other hand if the same jet is used for maximum power of the engine, the fuel flow through each jet must be approximately 85 cm^3/min. Besides the difficulty of manufacture the four jets to give exactly the same amount of fuel, it was not possible to reach the amount of 85 cm^3/min. using the electric fuel pump available, with a maximum pressure of approximately 8 bar. The investigation on the engine with the new manifold could not cover the performance at higher power, but for reasons stated previously the low load conditions are more interesting to study, because it is especially at lower flow rates that an improvment using the ultrasonic atomisers is expected. If further experiments were to be carried out, the use of two-jet feed seems necessary with an idle and low load jet feeding on to the side of the atomiser tip, and a high load jet feeding directly to the middle of the vibrating surface. This double jet system represents a good utilisation of the atomiser, but makes the feed control system slightly more complicated than the one jet system used. The fuel flow to the jets was regulated with a valve controlling the fuel pressure of the pump. The arrangement is shown at Fig. 93.

Fig.92

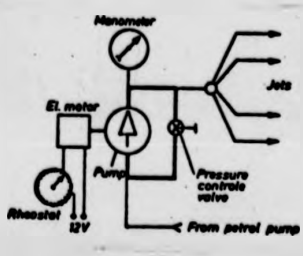

Fig.93

ders because of robbing effects.
The shape and dimensions are identical for each pair of cylinders, and each the branch are joined together as smoothly as possible. Fig.92 shows a photograph of the manifold. The atomisers are fitted in the same way as shown on the experimental manifold Fig. 84. The feed system operating with pressure from approximately 0.5 to 8 bar is different from previous experiments. The pressure of the fuel feed necessary to avoid depression in the feed line had to be approximately 0.5 bar at idle. At this pressure the fuel flow through each jet, corresponding to the fuel consumption at idle is only 4 to 5 cm^3/min. On the other hand if the same jet is used for maximum power of the engine, the fuel flow through each jet must be approximately 85 cm^3/min. Besides the difficulty of manufacture the four jets to give exactly the same amount of fuel, it was not possible to reach the amount of 85 cm^3/min. using the electric fuel pump available, with a maximum pressure of approximately 8 bar. The investigation on the engine with the new manifold could not cover the performance at higher power, but for reasons stated previously the low load conditions are more interesting to study, because it is especially at lower flow rates that an improvment using the ultrasonic atomisers is expected. If further experiments were to be carried out, the use of two-jet feed seems necessary with an idle and low load jet feeding on to the side of the atomiser tip, and a high load jet feeding directly to the middle of the vibrating surface. This double jet system represents a good utilisation of the atomiser, but makes the feed control system slightly more complicated than the one jet system used. The fuel flow to the jets was regulated with a valve controlling the fuel pressure of the pump. The arrangement is shown at Fig. 93.

Fig.92

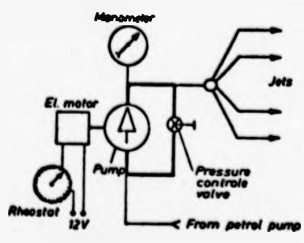

Fig.93

In order to have the possibility of a fine adjustment a rheostat could be operated to vary the pump speed. A manometer indicated the pressure of the fuel and was concequently a measure of the fuel flow. The air flow was adjusted with a butterfly valve in the manifold. A butterfly valve like those used in inlet systems of engines tends to split the air stream and may cause maldistribution to the different branches. In the manifold produced for the experiment the butterfly was situated approximately 100 mm from the diversion to the branches. The first junction diverts the air to two equal pipes which are again divided in two equal bends where the atomisers are fixed. The atomiser spray is directed into the inlet-opening of the cylinderhead of the engine. There was no window for the purpose of studying inpaction in the manifold. Earlier experiments where inlet bends were made of perspex tubes as described in paragraph 6.1 could show that the system works satisfactorily as to droplet formation and impaction. The performance of the atomisers and the fuel feed could be checked before fitting the manifold to the engine (see photograph Figure 94). The performance of the atomisers can easily be checked during the experiment by reading the DC-current to the drive units. The jets used for the experiment were made 0.1 mm diameter bore. In order to get the same flow rate at all 4 jets the bores were polished using grinding paste on a thin wire.

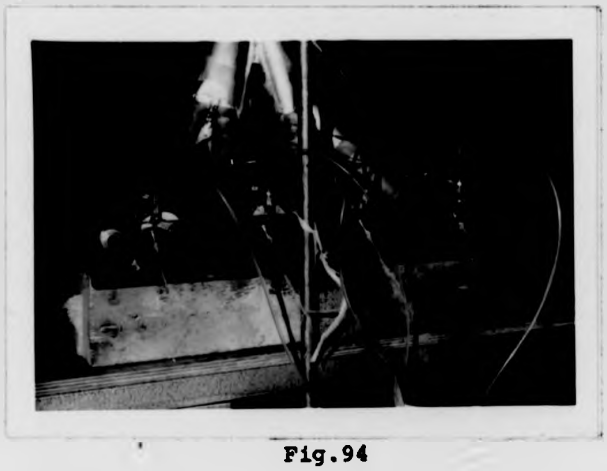

Fig.94

The jets finally gave very near to the same flow rate in the range possible using the pressure from 0.5 to 8 bar. Within this pressure-range the engine could not be run at maximum power at speeds higher than 3000 rpm. An increased flow rate achieved by means of the second set of jets pointing to the middle of the atomiser surface from underneath was not used for emission experiments. The problem with a double jet system is that the second jet has to start performing at higher load, and the arrangement of the control valves would have taken too much time to manufacture.

In order to have the possibility of a fine adjustment a rheostat could be operated to vary the pump speed. A manometer indicated the pressure of the fuel and was concequently a measure of the fuel flow. The air flow was adjusted with a butterfly valve in the manifold. A butterfly valve like those used in inlet systems of engines tends to split the air stream and may cause maldistribution to the different branches. In the manifold produced for the experiment the butterfly was situated approximately 100 mm from the diversion to the branches. The first junction diverts the air to two equal pipes which are again divided in two equal bends where the atomisers are fixed. The atomiser spray is directed into the inlet-opening of the cylinderhead of the engine. There was no window for the purpose of studying inpaction in the manifold. Earlier experiments where inlet bends were made of perspex tubes as described in paragraph 6.1 could show that the system works satisfactorily as to droplet formation and impaction. The performance of the atomisers and the fuel feed could be checked before fitting the manifold to the engine (see photograph Figure 94). The performance of the atomisers can easily be checked during the experiment by reading the DC-current to the drive units. The jets used for the experiment were made 0.1 mm diameter bore. In order to get the same flow rate at all 4 jets the bores were polished using grinding paste on a thin wire.

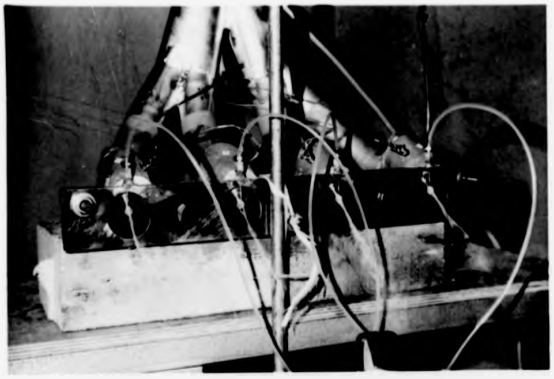

Fig.94

The jets finally gave very near to the same flow rate in the range possible using the pressure from 0.5 to 8 bar. Within this pressure-range the engine could not be run at maximum power at speeds higher than 3000 rpm. An increased flow rate achieved by means of the second set of jets pointing to the middle of the atomiser surface from underneath was not used for emission experiments. The problem with a double jet system is that the second jet has to start performing at higher load, and the arrangement of the control valves would have taken too much time to manufacture.

6.3.3 Discussion of results

The results from the experiments carried out on the Ford test engine are shown on the following pages 165 to 170. Curves a to h show " under load " conditions of the engine, where interesting parameters and emissions of CO, NO and HC are plotted versus engine output power at constant speeds.
Curves marked x represent the results obtained with the original carburettor and the standard ignition setting of the engine. It is of little interest that different timing of the engine may cause lower emissions. The results are here only important for a comparison with results achieved with ultrasonic devices used under as close to the same conditions as possible. However it is not possible to achieve exactly the same conditions from measurement to measurement. In order to be able to take different running conditions into consideration the curves for A/F ratio and exhaust temperature are shown on the same diagram.
Curves marked o are related to the ultrasonic device replacing the carburettor and results from the experiments carried out with the manifold designed for the use of ultrasonic atomisers close to the inlet port are marked Δ.
The ignition timing and the A/F ratio were considered to be the most important parameters to control. Because of the possibility of setting the ignition timing by hand each time this parameter is easier to set to a certain value than the A/F ratio.
It was not possible at all points to get exactly corresponding values for the A/F ratio and the exhaust temperature. The adjustment of the A/F ratio to the same value as with the carburettor was, as explained earlier, not straight forward, because the air flow and the fuel flow were adjusted independantly. Often an exhaust temperature and a ignition timing corresponding to values measured with the carburettor gave different values for the A/F ratio with the ultrasonic devices. The reason for this can be differences in the fuel flow rate and consequently changes in heat release. It is well known that air-flow meters of the type used may give inaccurate readings in pulsating flow and discrepancies may occur due to that effect. During the last experiment, involving the new manifold, the exhaust temperature and the ignition timing were regarded as more important parameters than the measured A/F ratio. According to the theory a higher air-fuel ratio gives at the same speed and power of the engine a lower exhaust temperature if the

ignition timing is the same and the air-fuel ratio is on the lean side. It is important to consider the exhaust temperature and the variation of the measured A/F ratio before conclusions of the results are drawn.

At medium power the CO level is low for all speeds measured. The ultrasonic carburettor seems however to be able to keep the low CO level even at higher power. This could be caused by less restricted inlet, but at 2000 rpm (Figure 96 c) the A/F ratio measured is closely the same with carburettor as with the ultrasonic carburettor and even here the CO level is significantly lower with the ultrasonic device. It is possible that the engine equipped with the original carburettor has disturbing resonance in the inlet system at 2000 rpm. The curve for NO shows an inexplicable increase at approximately 6 KW.
The curves for NO show some reductions in concentrations for the engine with ultrasonic atomisers, but in most cases the different charge to the cylinders and also the change in A/F ratio explain this effect. A reduction in NO emissions is expected if the A/F ratio is much leaner than stochiometric. If a rich mixture cause reduction in NO the CO level will increase. The small all over reduction of NO is therefore thought to be caused by a small discrepancy in A/F ratio and should not be credited to ultrasonic atomisation. It is more interesting to study the hydrocarbon emissions. The level of HC emissions seems to be lower with the use of ultrasonics- especially at low speed: At for instance 1100 rpm the HC level did not increase significantly at A/F ratios above 17 using the ultrasonic carburettor. With the venturi carburettor the HC level was increasing rapidly at A/F ratios above 15 at this speed. This tendency can be noticed also in Figure 99 i which shows the comparison between standard carburettor and ultrasonic carburettor at idle. The tendency to misfire is far more noticeable when the engine is run with the ordinary carburettor, at the same A/F ratio higher than 15.
Even more convincing are the results from the experiments with the specially produced manifold. With this arrangement the level of HC at idle could be reduced to 50 ppm (as propane). Those results are shown in Figure 99 j.
When atomisers are situated close to the inlet ports no impaction occurs in the manifold.

The adjustment of air and fuel flow can be done accurately with hand operated valves, to achieve the lowest possible level of emitted CO and HC. Such an accurate adjustment is normally not possible with the carburettor. In order to see how low an emission level of CO and HC can be obtained, the carburettor was adjusted with the air bleed screw at each point.
The ignition timing and the exhaust temperature was kept the same in both experiments but it was not intended to get the same A/F ratio.
The lowest level of CO and HC is with the manifold arrangement obtained at lower A/F ratios than with the carburettor. Considering the very low CO level it seems strange that the A/F ratio is only approximately 14 . There is therefore reason to believe that the A/F ratio-curve concerning measurements with the manifold is too low. Different pulsations in the inlet system may cause a change of the air flow meter reading.

In Figure 96 some results from the experiments with the manifold are shown for under load conditions.
The A/F ratio is also on load lower than is expected according to CO emissions. The emission of CO for the test with the manifold was lower than 0.8 % for all loads.
Tables of the results can be found in Appendix VI.
Figure 98 h shows that the fuel consumption is almost unchanged for the engine equipped with the ultrasonic carburettor. There is therefore little evidence that the better atomised fuel improves the thermal efficiency of the engine.
According to some measurements the fuel consumption is even higher than with the carburettor.

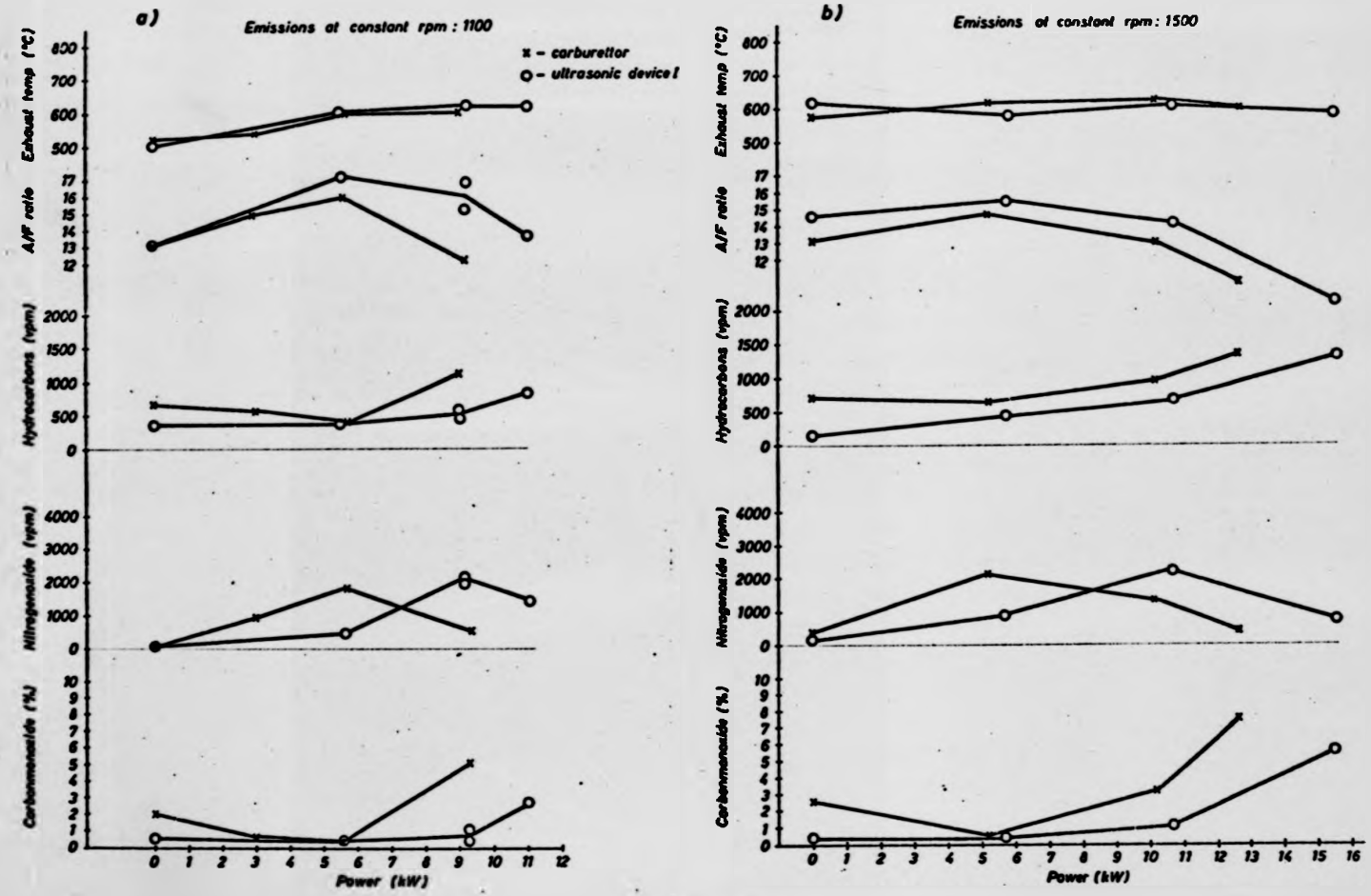
a)
Emissions at constant rpm : 1100
x - carburettor
o - ultrasonic device
Exhaust temp (°C)
A/F ratio
Hydrocarbons (rpm)
Nitrogenoxide (rpm)
Carbonmonoxide (%)
Power (kW)
b)
Emissions at constant rpm: 1500
Exhaust temp (°C)
A/F ratio
Hydrocarbons (rpm)
Nitrogenoxide (rpm)
Carbonmonoxide (%)
Power (kW)

Fig.95

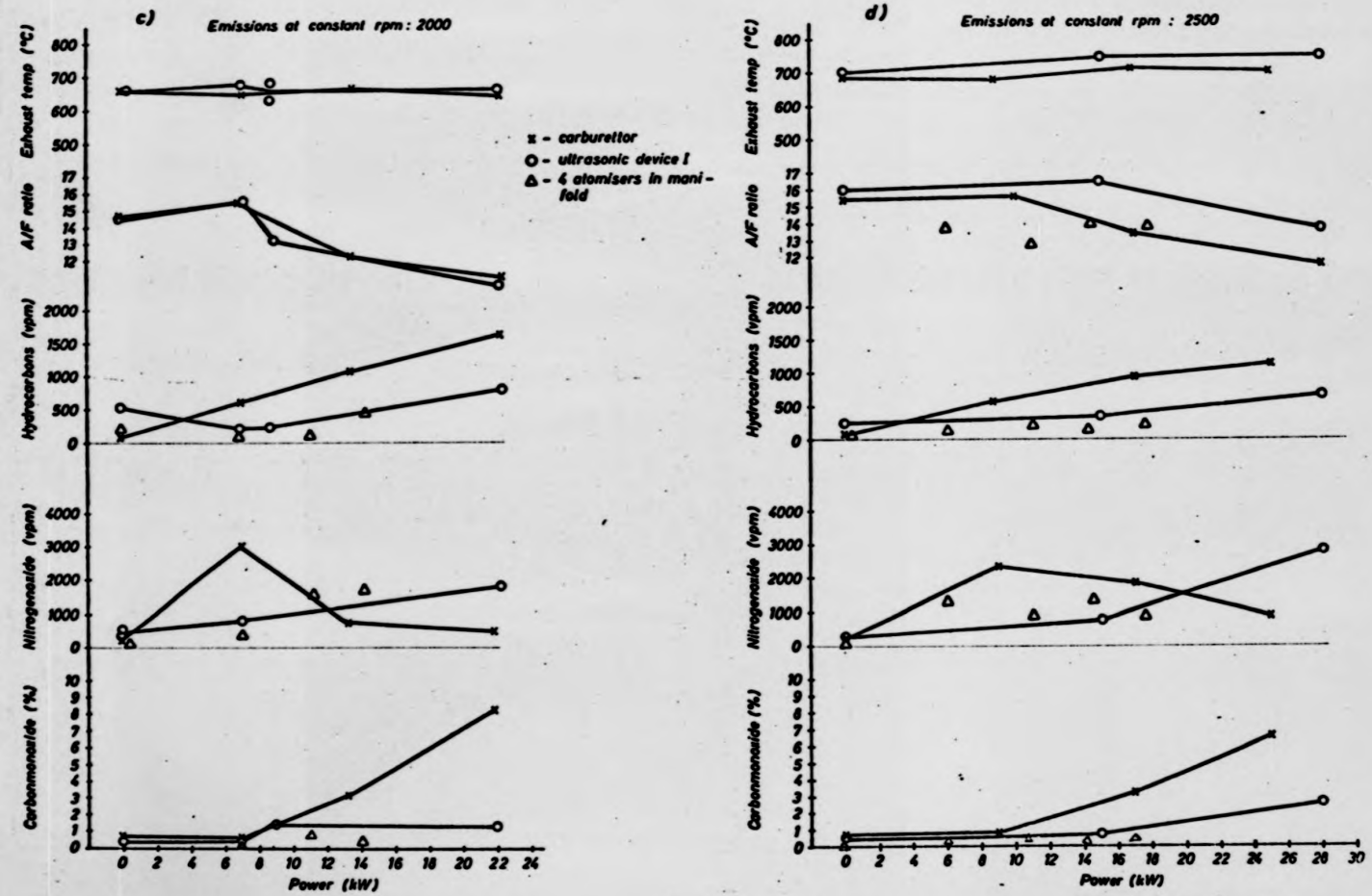
c)
Emissions at constant rpm : 2000
d)
Emissions at constant rpm : 2500
x - carburettor
O - ultrasonic device I
Δ - 4 atomisers in manifold
Exhaust temp (°C)
A/F ratio
Hydrocarbons (vpm)
Nitrogenoxide (vpm)
Carbonmonoxide (%)
Power (kW)

Fig.96

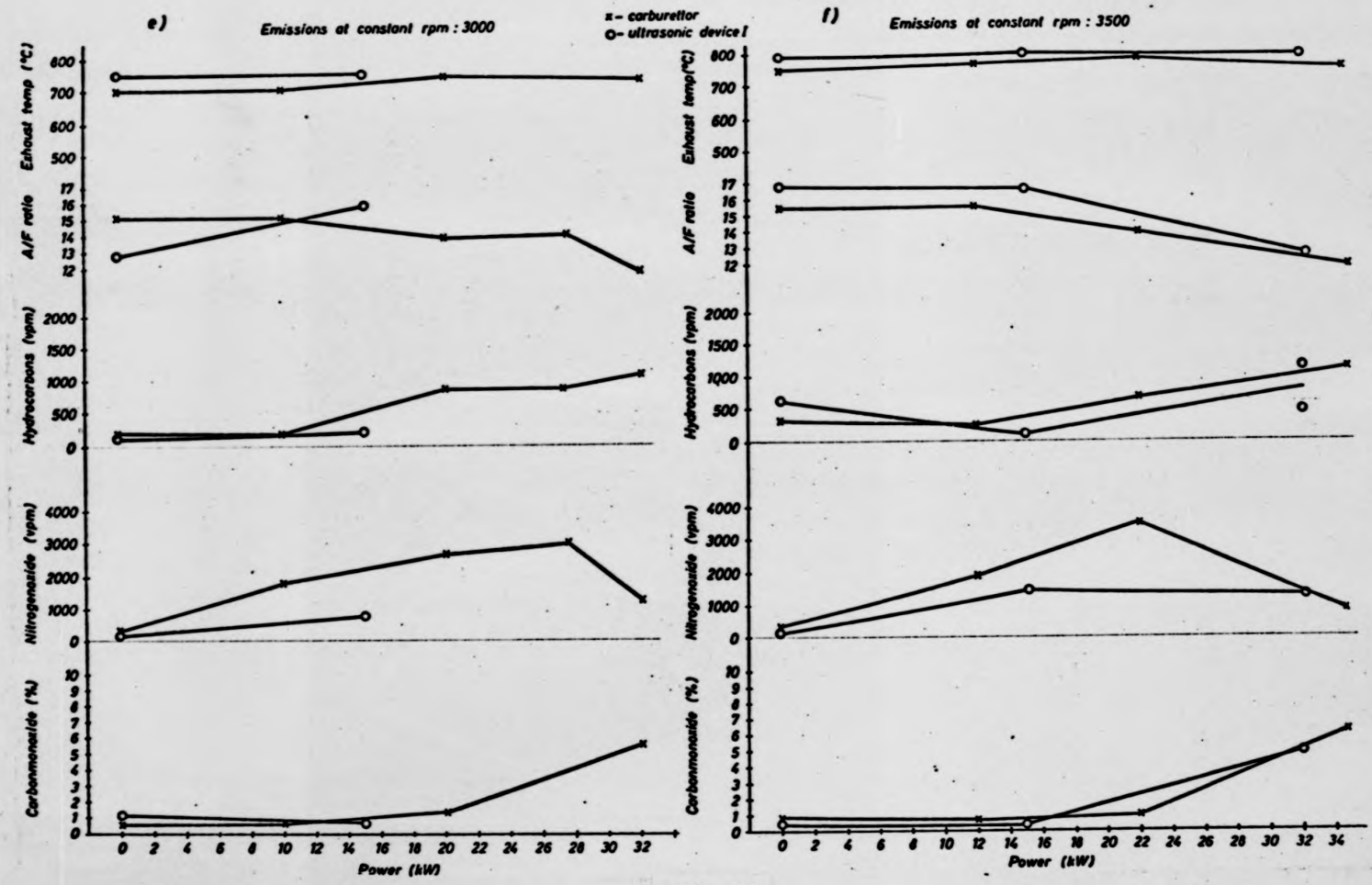
e)
Emissions at constant rpm : 3000
x- carburettor
o- ultrasonic device I
f)
Emissions at constant rpm : 3500
Exhaust temp (°C)
A/F ratio
Hydrocarbons (vpm)
Nitrogenoxide (vpm)
Carbonmonoxide (%)
Power (kW)

Fig.97

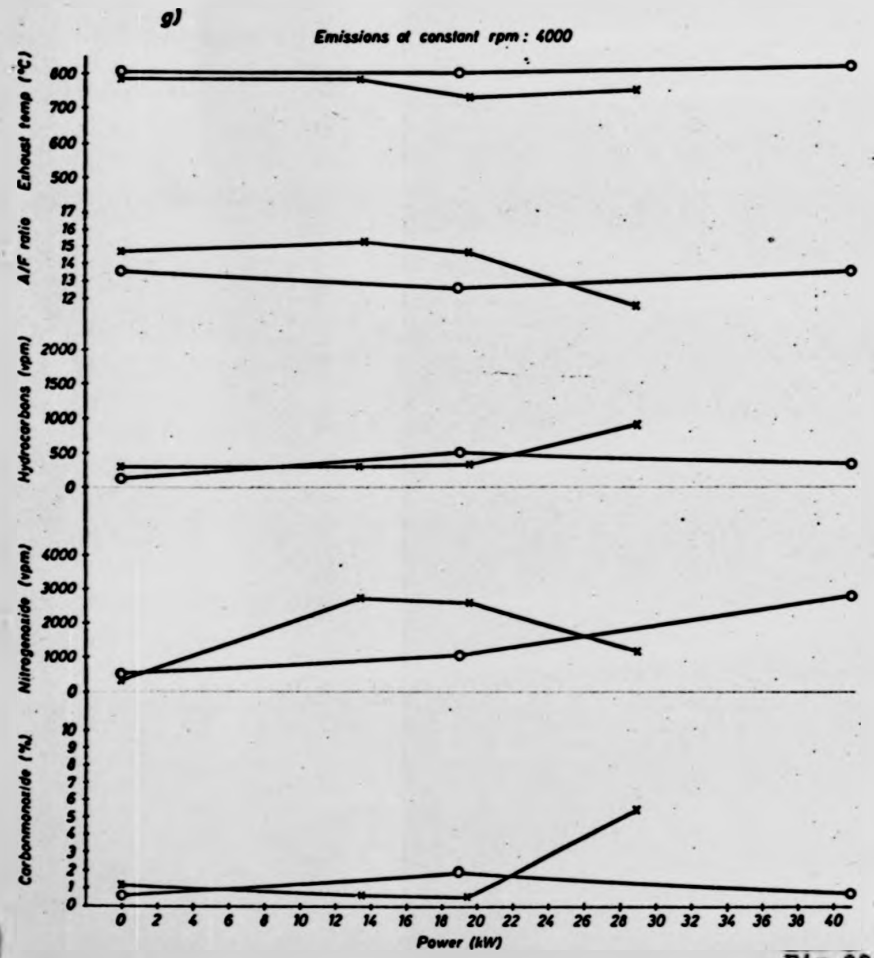
g)
Emissions at constant rpm : 4000
Exhaust temp (°C)
A/F ratio
Hydrocarbons (vpm)
Nitrogenoxide (vpm)
Carbonmonoxide (%)
Power (kW)

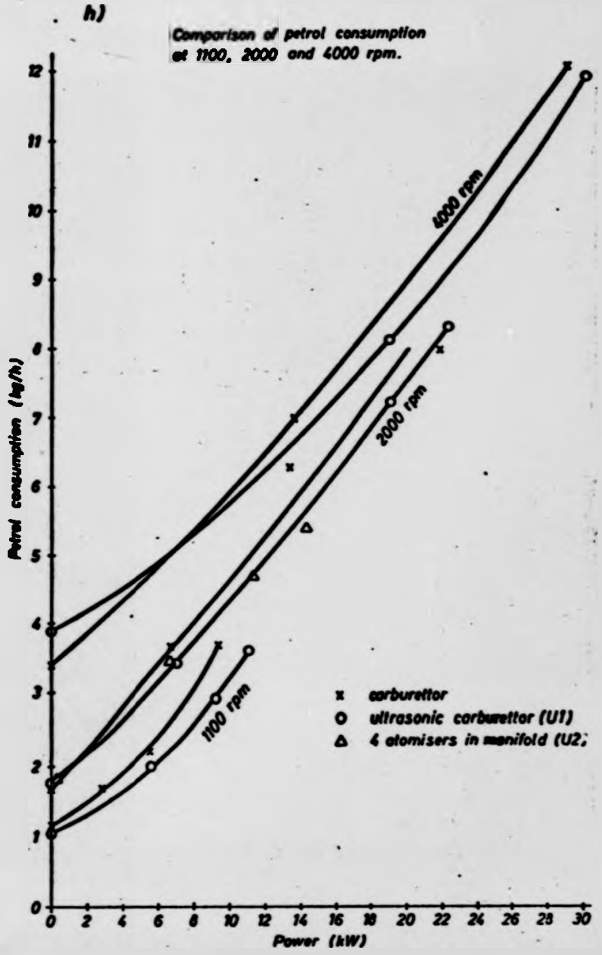
h)
Comparison of petrol consumption at 1100, 2000 and 4000 rpm.
Petrol consumption (kg/h)
4000 rpm
2000 rpm
1100 rpm
carburettor
ultrasonic carburettor (U1)
4 atomisers in manifold (U2)
Power (kW)

Fig.98

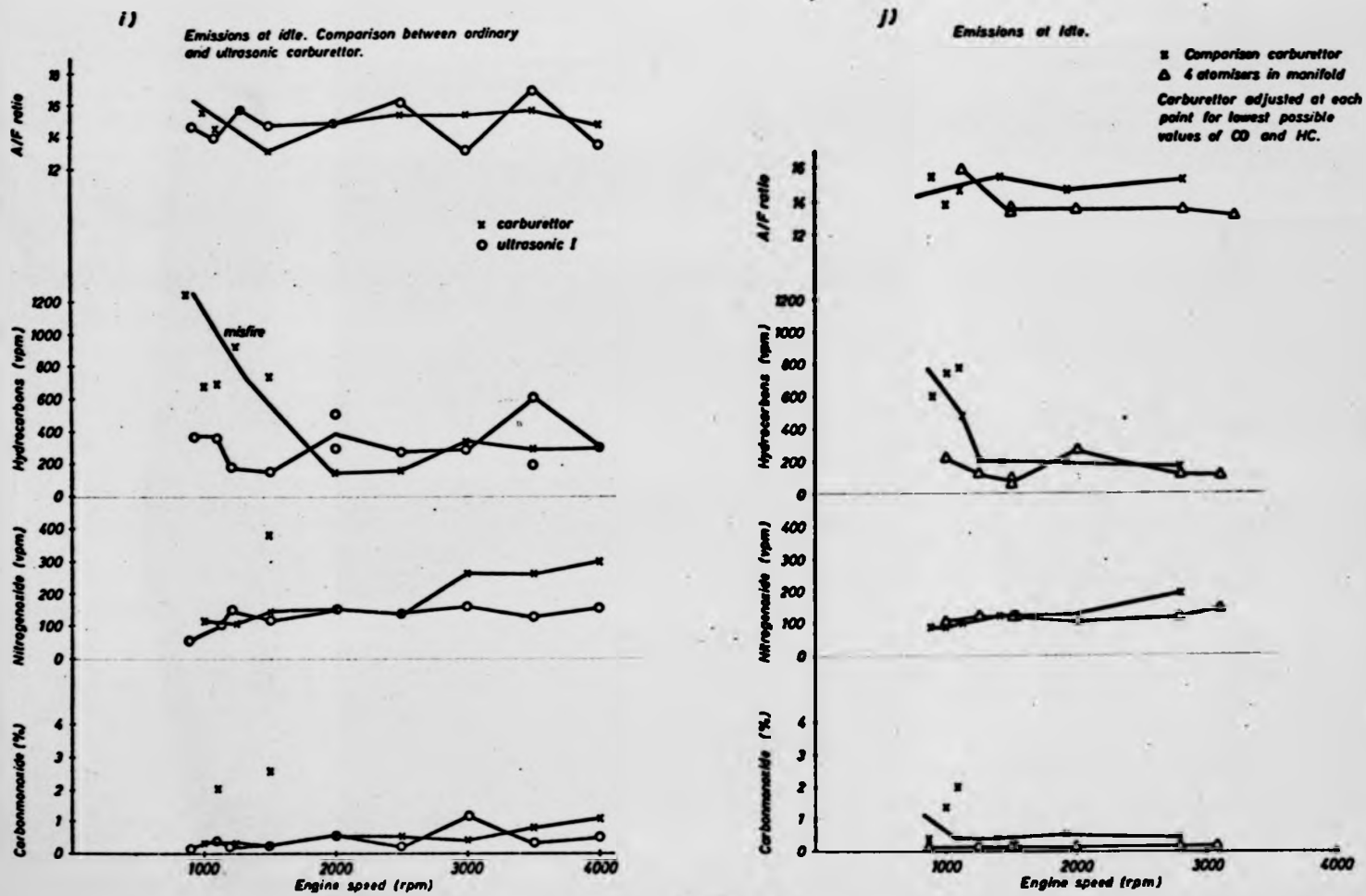
i)
Emissions at idle. Comparison between ordinary and ultrasonic carburettor.
A/F ratio
Hydrocarbons (rpm.)
Nitrogenoxide (rpm.)
Carbonmonoxide (%)
x carburettor
o ultrasonic I
misfire
Engine speed (rpm)
j)
Emissions at idle.
x Comparison carburettor
Δ 4 atomisers in manifold
Carburettor adjusted at each point for lowest possible values of CO and HC.
Engine speed (rpm)

Fig.99

7. Conclusions and recommendations

An atomising device for petrol engines can only be as good as the metering system permits.
The experiments carried out on the two engines show this clearly.
If the mixture is correct the use of ultrasonic atomisers in the inlet system can reduce the exhaust emissions of carbonmonoxide and hydrocarbons especially at low load and idle.
The use of ultrasonic atomisation enable one to design the inlet system of an engine to give less resistance and consequently it is possible to increase the cylinder charge for a higher b.m.e.p. and maximum power.
During the period of research there has been very little failure of the atomisers or the electronics involved. The first atomisers made did not change impedance significantly during the period of research, and performed just as well after 2 years time.
Atomisers mounted in a " carburettor unit " can not prevent impaction in the inlet manifold without addition of heat to evaporate the fuel quickly after the droplets are produced. Only with evaporated fuel-air mixture it is possible to avoid maldistribution and inhomogeneous charge to the cylinders.
The atomisers produced need more space and are more difficult to mount in the manifold near the inlet port of an engine than injectors made for petrol injection systems. However ultrasonic atomisers can surely be made smaller and more effective than those used in the experiments described in this report.
Ultrasonic atomisers could be incorporated in conventional carburettors to improve the performance especially at low venturi air speeds.
The experiments carried out on the two stroke engine improved the engine performance by relatively simple means using an ultrasonic arrangement.
If further research is to be carried out to develop ultrasonic atomisers similar to the atomiser type 22, a computer programme based on an axi-symmetrical solution would be very useful in the optimisation process.
The experiments carried out on atomisers did not involve other materials than aluminium and steel. The use of titanium seems to be an easy way to improve the efficiency of the atomiser developed in this project: although the difficulty associated with the application of ultrasonic atomisers in petrol engines seems not to be the atomiser itself but the fuel feed and the closely related fuel-air metering.

REFERENCES AND NOTES

(1) Moller, F. 'On the Influence of Changes in CO_2 concentration in Air on the Radiation Balance of the Earth's Surface and the Climate. J. Geophys. Res., 68, 3877 (1963)

(2) Williamson, S. J. Fundamentals of Air pollution Addison-Wesley N.Y. 1973

(3) Levy, H. Normal Atmosphere: Large Radical and Formaldehyde concentrations predicted. Science 173, 290 (1972)

(4) Wenestock, R and Niki, H Carbon Monoxide Balance in Nature Science 176, 290 (1972)

(5) Agnew, W. Automotive Air pollution Research Proc. Roy. Soc. 307A, 153 (1968)

(6) Warner, F. Possibilities in Pollution controle Proc. Instn. Mech. Engrs. 187, 115 (1973)

(7) Heywood, J. B. Formation of Hydrocarbons and Oxides of Nitrogen in Automobile Engines. Environmental Sc. and Techn. 7, 216 (1973)

(8) Wentworth, J. T., and Daniel, W. A. Flame photographs of light load combustion point the way to reduction of hydrocarbon in exhaust gas. SAE Technical Progress Series Vol. 6 Vehicle Emissions, SAE N.Y.

(9) Wentworth, J. T. Effect of combustion chamber surface temperature on exhaust hydrocarbon concentration SAE 710587 (1971)

(10) Sheffler, C. E. Combustion Chamber surface area; A key to Exhaust Hydrocarbons SAE PT-12, 60 (1963 - 1966)

(11) Blackmore, D. R. The Measurement of Gasoline engine Air/Fuel ratios Shell Mor. 641 F

(12) Ranz, W. E. and Marshall, W. R. Evaporation from Drops Chem. Eng. Prog. 48, (3), 141 and 173 (1952)

Ranz, W. E. Survey of principles of Inertial Impaction. Dept. of Eng. Research Penn. State Univ. Bulletin No. 66 (1956)

(13) Lindsay First symposium on low pollution power system development. Shell report Oct. 1973

(14) McAdams, W. H. Heat Transmission. McGraw-Hill N.Y. 1954 3rd Ed.

(15) Zapf, H. Untersuchung des Warmeüberganges. MAN Forschungsheft Augsburg 1968/69

(16) Kutateladze, S. and Borishanskij, V. M. A concise encyclopedia of heat transfer Pergamon Press 1966

(17) Patterson, D. J. and Henein N. A. Emission from Combustion Engines and their control. Ann Arbor Science 1972

(18) Almas, T. Pollution from outboard Engines. Institute for int. comb. eng. Techn. Univ. Trondheim IR/R11 Norway. 1972

(19) Joyce, J. R. Atomisation of liquid fuel. J. Inst. Fuel 22, 150, (1949) and 26, 200 (1953).

(20) Norster, E. R. Improvement in Petrol engine performance with ultrasonic fuel atomisation. College of Aeronautics, Cranfield. Internal Report 1967.

(21) Tu, L. Y., Brennan, I. N. and Sauer, J. A. Dispersion of Ultrasonic Pulse Velocity in Cylindrical Rods Journal Ac. Soc. Am. Vol 27 No 3.

(22) Merkulov, L. G. Design of Ultrasonic concentrators Acoustics journal (USSR) 3, 230 (1957) and Acoustics journal (USSR) 3, 246 (1956)

Part 2

Merkulov, L. G. and Kharnitonov, A. V: Theory and Analysis of sectional Concentrators.
Acoustics Journal (USSR) 5, 138 (1958)

(23) - Testran II Users manual Inst. of int. comb. engines Techn. Univ. Trondheim (1973)

(24) - Sesam 69 Users manual NV333 Analysis of Solids (1974)

(25) Frederick, J. R. Ultrasonic Engineering
Wiley & Sons. N.Y. (1965)

(26) Sollner, K. The mechanism of formation of fog by ultrasonic waves. Trans. Faraday sec. 32 (1936)

(27) Bisa, K., Dirnagl, K. and Esche, R. Serstäubung von Flüssigkeiten mit Ultraschall. Siemens Zeitz. 28 (1954)

(28) Rosenberg, L. D. Physical Principles of Ultrasonic Technology. Plenum Press (1975)

(29) Browning, F. A. Production and measurement of single drops, sprays and solid suspension. Advance in Chemistry series 20 (1958)

(30) York, F. L., and Stubbs, H. E. Photographic Analysis of sprays. Trans. Am. Mech. Engrs. 74, 1157 (1952)

(31) Sinclair, D. Handbook of Aerosols.
U. S. Atomic Energy Com. (1950)

(32) Smith, P. H. and Morrison, J. C. The Scientific Design of Exhaust and Intake Systems 3rd. Ed. G. T. Foulis (1971)

FORD-ENGINE TESTBED USERS MANUAL

Appendix I

Description and Operating Procedure

The installation is a motoring testbed with unconventional characteristics. It must not be operated by anyone who is not conversant with its characteristics and with the correct operating procedure.

General Description of the Testbed

The engine can be motored or loaded with a d.c. dynamometer (motor/generator), for which the d.c. supply/load is provided by a Ward-Leonard set.

Basically, the "load" control on the engine control panel determines the speed of the dynamometer. The dynamometer will automatically act as a motor or generator according to the power delivered or required by the engine at that speed. In particular when the dynamometer control demands zero speed, the engine will stop (very rapidly if the load control is adjusted very rapidly). Equally the engine cannot accelerate the dynamometer at a given load setting. Consequently this testbed is particularly suited to carrying out tests at constant speed.

Electrical Connections

The Ward-Leonard set can also be connected to another testbed referred to as Testbed No. 1, the Ford testbed being Testbed No. 2. Before the Ward-Leonard set or either engine dynamometer is operated, the correct armature and field connections must be made between the W.L. set and the appropriate test cell. This requires using a large changeover switch (adjacent to the W.L. set) for the armature circuit, and a small changeover switch for the W.L. d.c. machine field circuit and for control of a relay controlled switch in the d.c. armature circuit.

When Testbed No. 2 is in use, a notice to that effect should be displayed on the control panel for Testbed No. 1.

Controls

The normal mode of operation is with constant dynamometer field strength (although adjustment is possible using the rheostat inside the control panel). Load variations are then achieved by varying the W.L. generator field strength (using the rheostat which is controlled from the front of the testbed control panel).

Protection Circuits

The Ward-Leonard set has overspeed and overload trips and corresponding reset facilities.

In addition the supply to the dynamometer and generator field circuits is available only if

(a) The d.c. armature circuit is closed (Key switch).

(b) The "start" button is closed.

(C) No overspeed or overload conditions have occurred on the testbed.

(d) For starting the dynamometer, the generator field is initially zero.

Operation of the overspeed or overload relay also breaks the engine ignition circuit. (The ignition cut-out can be bypassed, if the engine is to run with no electrical power connected to the dynamometer).

Emergency Stop

The testbed can be rapidly decelerated by using the generator field control rheostat. Operation of the "stop" button deenergises the field circuits and is followed by gradual deceleration (in some circumstances preceded by a short period of acceleration).

Starting Procedure for the Testbed

In outline

1. The Ward-Leonard set must be started to provide a d.c. supply to the dynamometer (see operation of W.L. set).
2. The normal engine checks must be carried out (fuel, lubricant, engine coolant, laboratory cooling water, cell ventilation etc.)
3. The dynamometer must be started with the gearbox in "neutral" and accelerated to approximately 2000 r.p.m.
4. The engine can then be started (using the starter motor) and the speed synchronised with that of the dynamometer. (Normal operation is with top gear. Allowance for the gear ratio must be made if another gear is to be selected). The clutch and gearbox can then be used to connect the engine and dynamometer, and tests carried out as required.

Stopping Procedure

1. At a part throttle condition, and low engine speed, disengage the engine and dynamometer.
2. Stop the engine (or use the ignition cut-out by-pass switch to maintain ignition when the dynamometer is stopped).
3. Decelerate the dynamometer using the generator field control and press the "stop" button. Open key switch.
4. Stop the Ward-Leonard set (see operation of W.L. set).
5. If necessary, restore connection of the armature and field for testbed No 1.
6. Isolate fuel and coolant supplies to the testbed in the normal way.

Operation of Ward-Leonard Set

Starting Procedure

1. Set rotor resistance to maximum (large floor mounted control

near to the W.L. set).

2. Close 3-Phase supply isolator (wall mounted switch behind W.L. set).

3. Press "Start" button.

4. Decrease rotor resistance to zero.

Shut Down Procedure

1. Press "Stop" button.

2. Open 3-phase supply isolator.

Starting Dynamometer No. 2

1. An indicator on the dynamometer control panel shows when the Ward-Leonard Set is running (Switch S1).

2. Operation of the panel key switch then closes the main d.c. armature circuit (Switch L1).

3. Set the generator field supply to minimum.

4. Press the "start" button.

5. Raise dynamometer speed to desired value.

Stopping Dynamometer No. 2

See the testbed "stopping procedure".

Electric circuit diagram of dynamometer arrangement

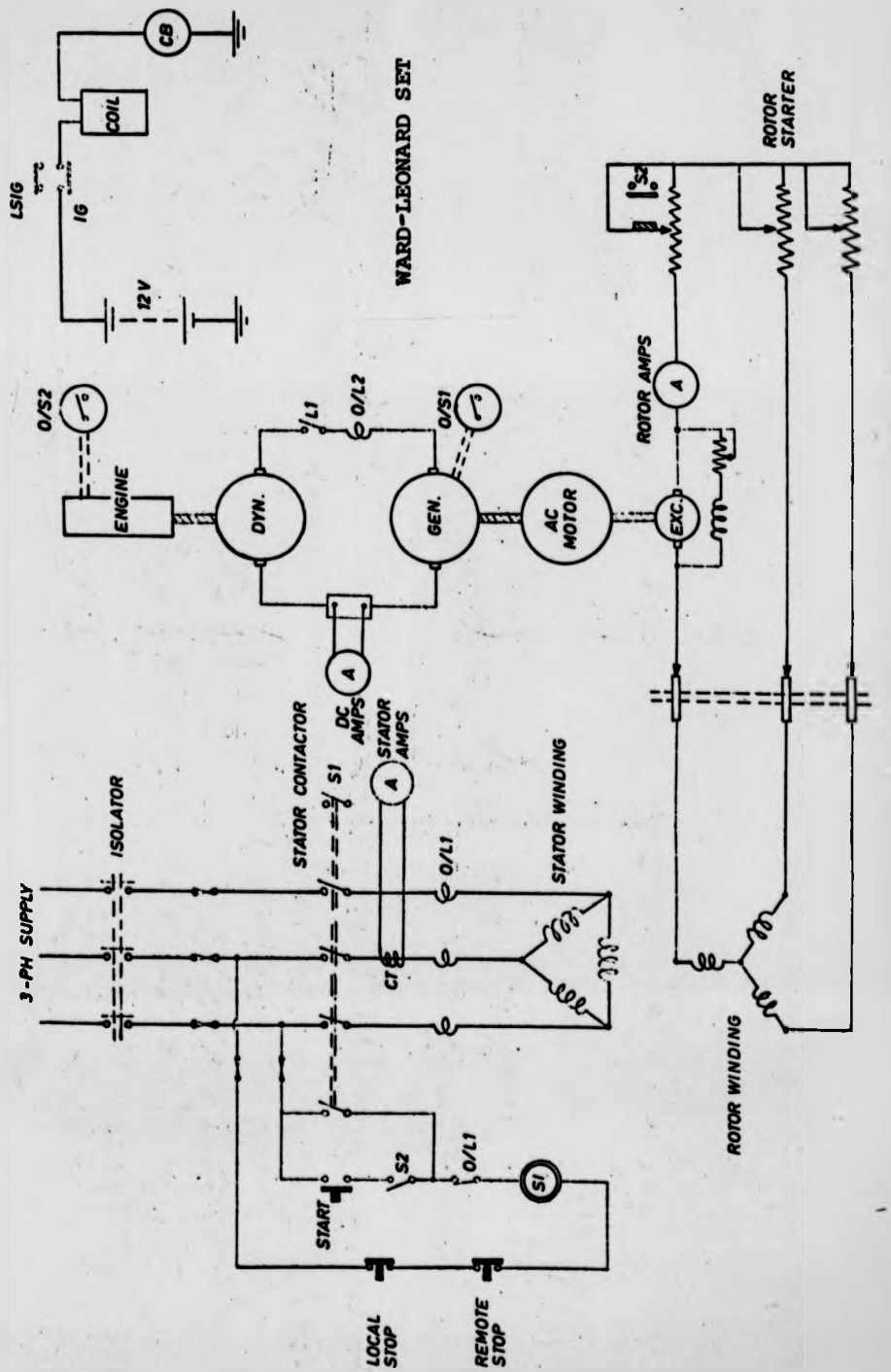

Test cell and 4-stroke engine testbed

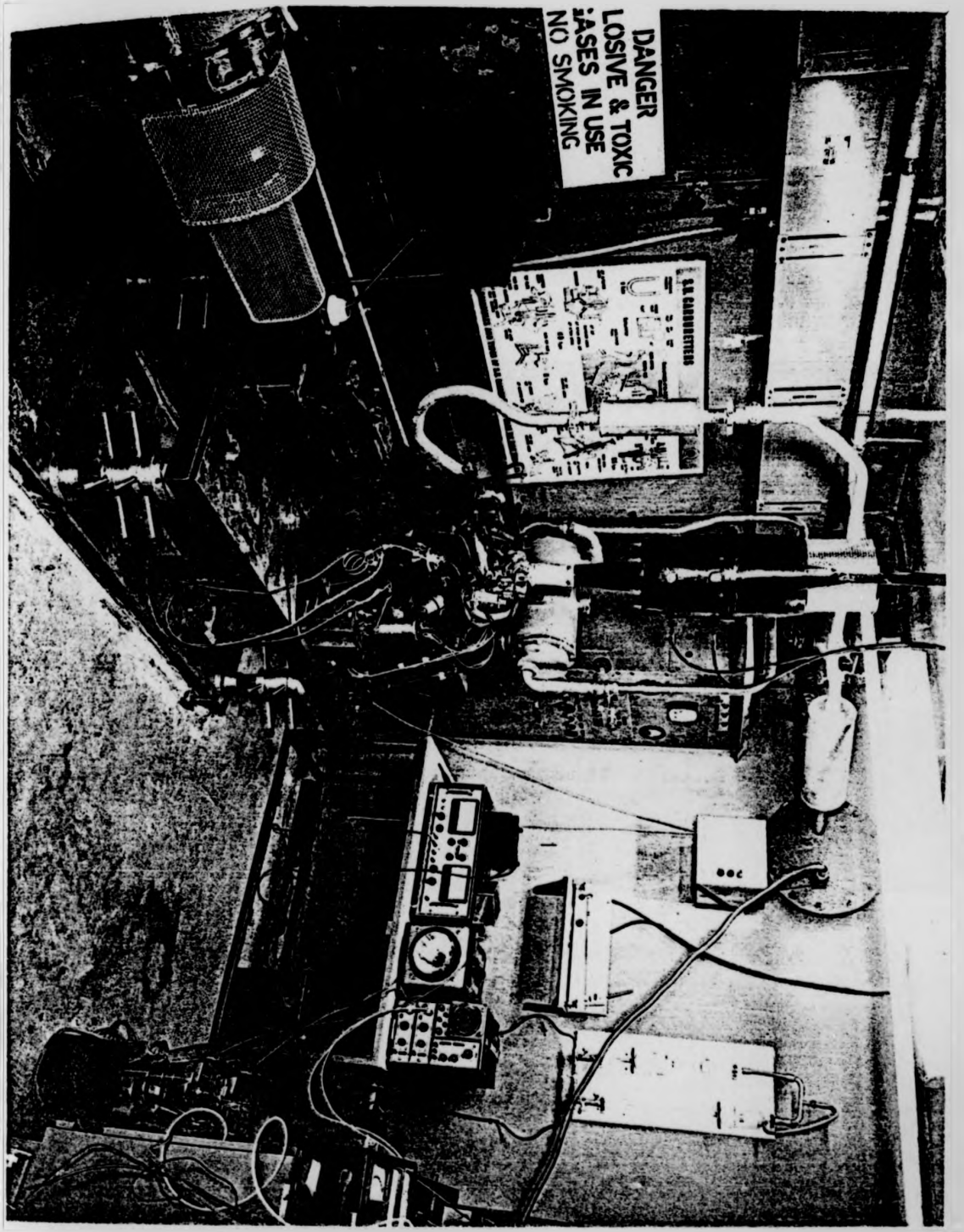

Test cell and 4-stroke engine testbed

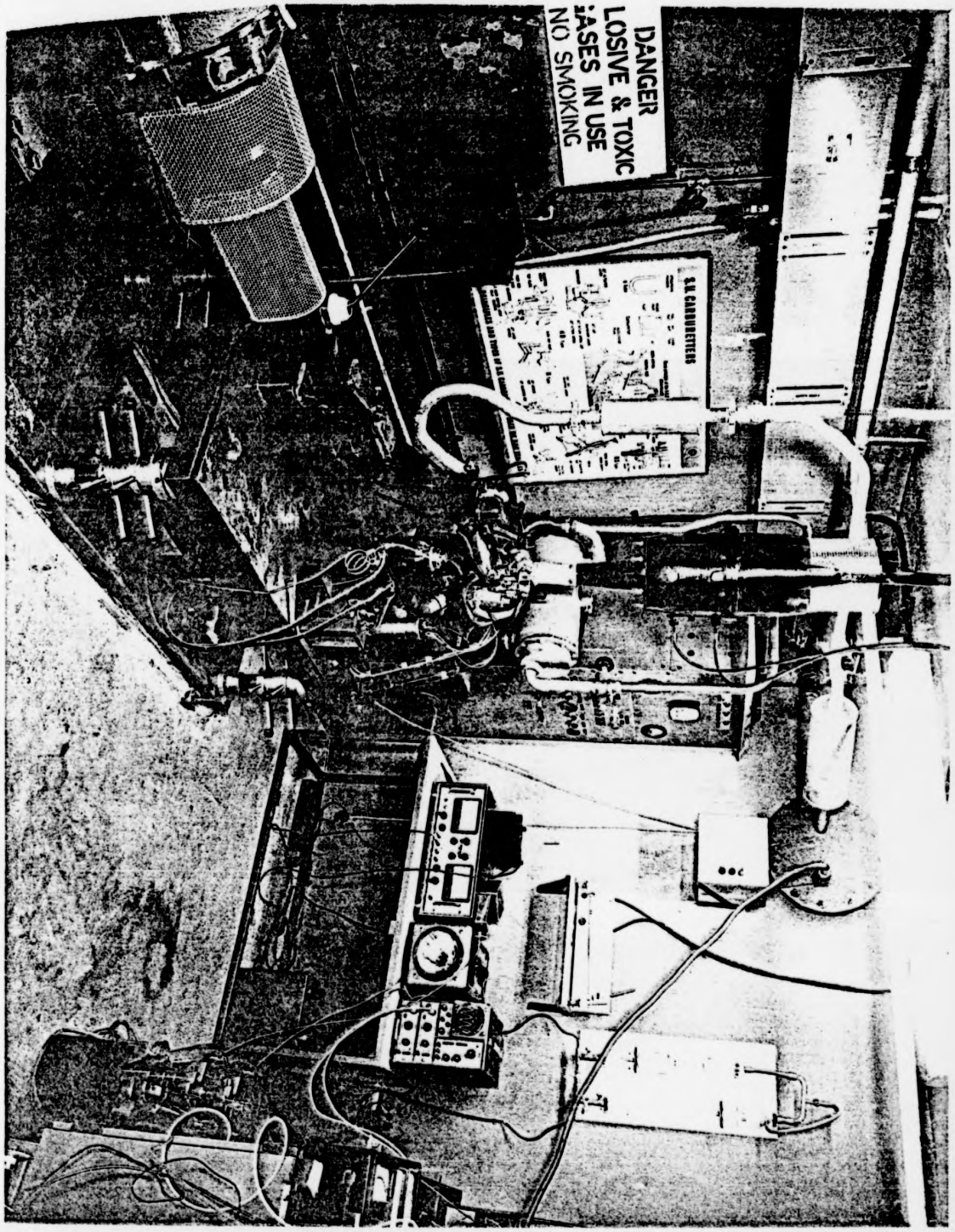

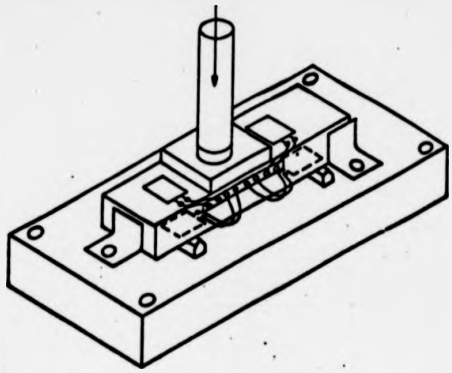

Strain gauge load cell for torque measurement

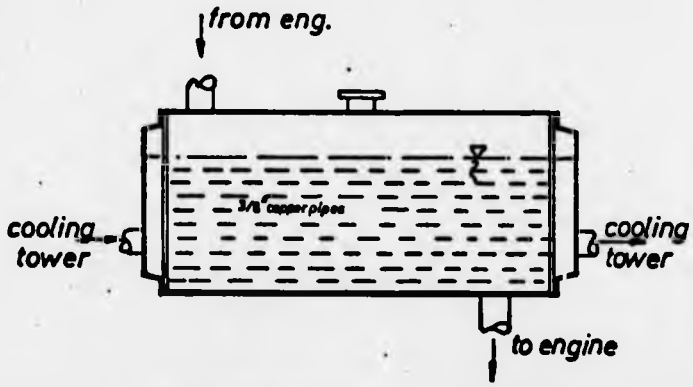

Engine cooler

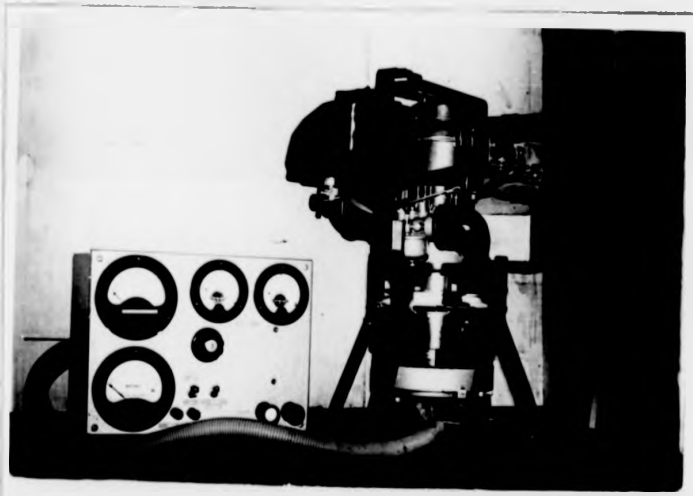

Two-stroke test engine

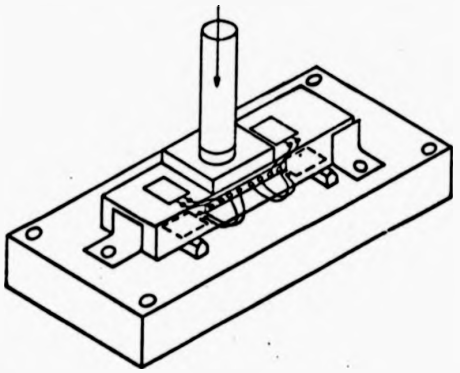

Strain gauge load cell for torque measurement

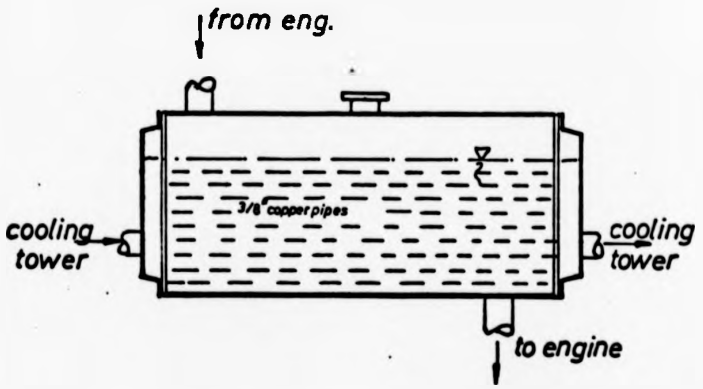

Engine cooler

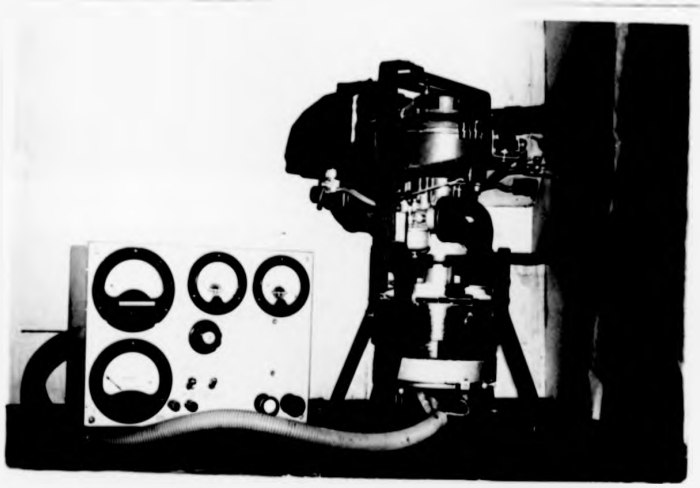

Two-stroke test engine

Appendix II

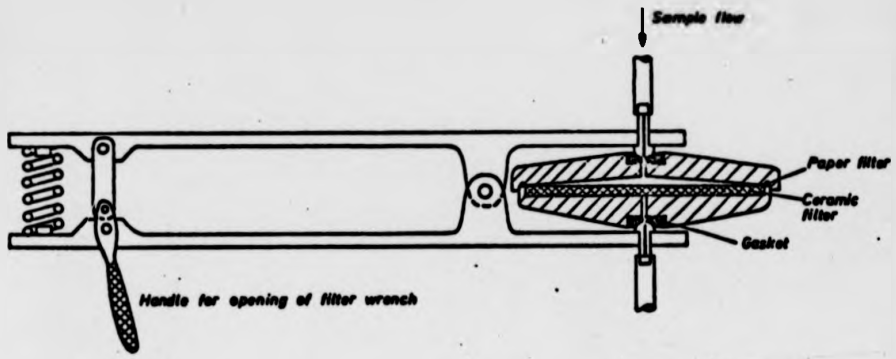

Filter arrangement for the sample gas to the analysers

Plunger regulator for sample pressure control to FID analyser

Starting procedure of FID Ananlyser

1. Switch on recorder and FID-amplifier, allow a warm up period of approximately 1/2 h before measuring.

2. Connect the flow meter to the exhaust pipe of the hydrocarbon detector.

3. Adjust the air-flow to approximately 230 ml/min. and the hydrogen flow to richer than 15 ml/min. Adjust the sample pump pressure to the correct pressure marked on the manometer. Ignite the burner by pressing the ignition switch. When the burner has ignited the float in the flowmeter drops significantly.

4. Disconnect the flowmeter and operate the air regulator to give leaner mixture. The mixture strength is regulated accurately by means of the calibration gas and the sensitivity of the analyser. At max. sensitivity measured with the same flowmeter the A/F ratio is 14.4. During measuring the sample pressure must be checked. The sample pressure can be changed by altering the weight of the regulator plunger and by adjusting the level in the petroleum bubbler.
   When the front panel valves are operated to change over to calibration gas, the sample flow to the FID analyser must not be interrupted by closing the sample flow valve first.
   The calibration gas valve must be open before shutting the sample gas valve, otherwise the FID burner flame may extinguish.

5. Change filter paper before every series of measurement.

6. Details of the FID amplifier can be found in the maintenance manual.

Appendix III

Macro flow of program used in the vibration analysis

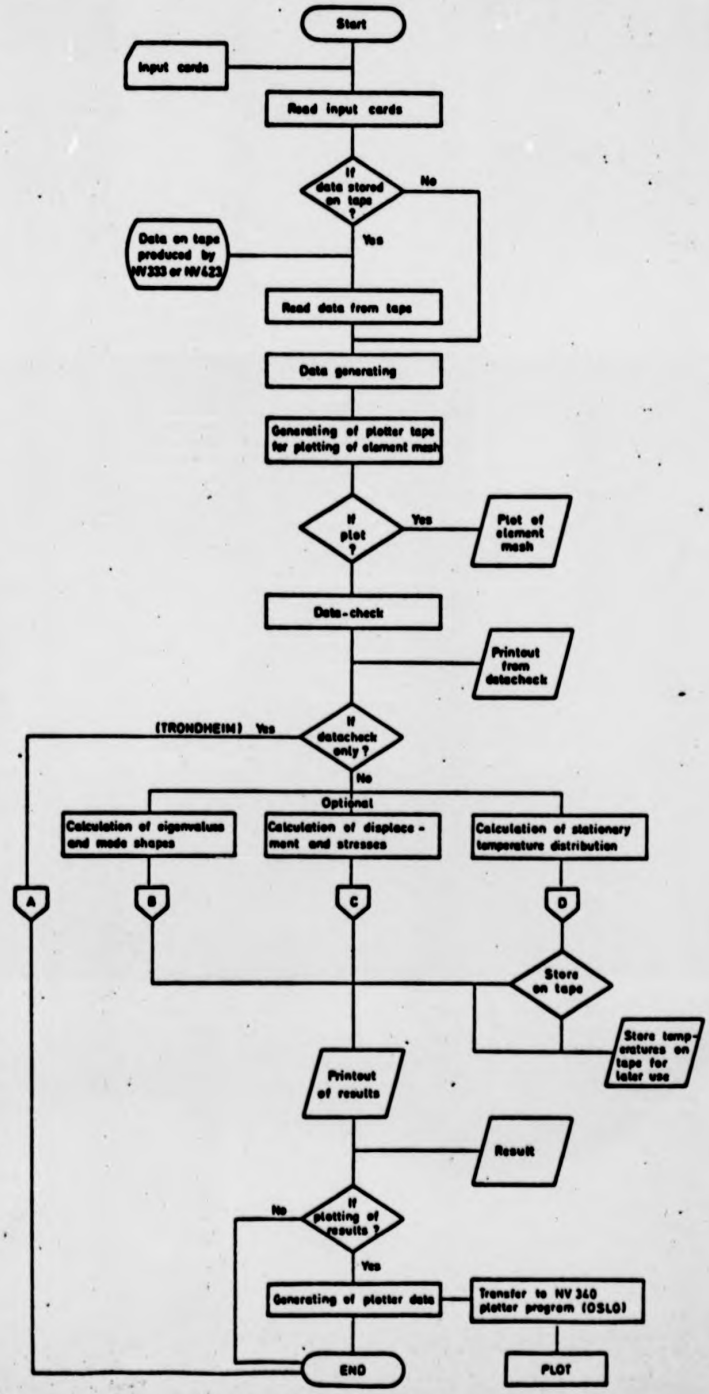

APPENDIX III

MODE NO 4 LINEAR DISPLACEMENTS

NODE	DX	DY	DZ
1	•449-02	•000	•135+01•
2	•000	•000	•000
3	•000	•000	•000
4	•406-02	•000	•961+00
5	•000	•000	•000
6	•756-02	•000	•924+00
7	•000	•000	•000
8	•000	•000	•000
9	-•163-02	•000	•754+00
10	•000	•000	•000
11	•915-01	•000	•744+00
12	•000	•000	•000
13	•587-03	•000	•379+00
14	•000	•000	•000
15	•000	•000	•000
16	•349-01	•000	•369+00
17	•000	•000	•000
18	•101+00	•000	•277+00
19	•000	•000	•000
20	•000	•000	•000
21	•903-01	•000	•124+00
22	•000	•000	•000
23	•717-01	•000	-•941-01
24	•000	•000	•000
25	•000	•000	•000
26	•668-01	•000	-•198+00
27	•000	•000	•000
28	•622-01	•000	-•174+00
29	•000	•000	•000
30	•000	•000	•000
31	•205-02	•000	•223-01
32	•000	•000	•000
33	•755-01	•000	-•586-01
34	•000	•000	•000
35	•104+00	•000	-•151+00
36	•000	•000	•000

MODE NO 4 LINEAR DISPLACEMENTS

NODE	DX	DY	DZ
37	•964-01	•000	-•180+00
38	•000	•000	•000
39	-•233-02	•000	-•191+00
40	•000	•000	•000
41	•000	•000	•000
42	•188-01	•000	-•191+00
43	•000	•000	•000
44	•289-01	•000	-•195+00
45	•000	•000	•000
46	•000	•000	•000
47	•345-01	•000	-•218+00
48	•000	•000	•000
49	•418-01	•000	-•220+00
50	•000	•000	•000
51	•000	•000	•000
52	•469-01	•000	-•211+00
53	•000	•000	•000
54	•486-01	•000	-•195+00
55	•000	•000	•000
56	•000	•000	•000
57	-•120-02	•000	-•218+00
58	•000	•000	•000
59	-•157-02	•000	-•208+00
60	•000	•000	•000
61	-•187-01	•000	-•219+00
62	•000	•000	•000
63	-•219-01	•000	-•204+00
64	•000	•000	•000
65	•636-03	•000	-•168+00
66	•000	•000	•000
67	•000	•000	•000
68	-•714-02	•000	-•168+00
69	•000	•000	•000
70	-•112-01	•000	-•162+00
71	•000	•000	•000
72	•000	•000	•000
73	-•141-01	•000	-•159+00

MODE NO 4 LINEAR DISPLACEMENTS

NODE	DX	DY	DZ
74	.000	.000	.000
75	-.186-01	.000	-.131+00
76	.000	.000	.000
77	.000	.000	.000
78	-.257-01	.000	-.191+00
79	.000	.000	.000
80	-.218-01	.000	-.222+00
81	.000	.000	.000
82	.000	.000	.000
83	-.227-01	.000	-.729-01
84	.000	.000	.000
85	-.217-01	.000	-.321-01
86	.000	.000	.000
87	.000	.000	.000
88	.539-03	.000	-.619-01
89	.000	.000	.000
90	-.427-01	.000	-.638-01
91	.000	.000	.000
92	-.784-01	.000	-.452-01
93	.000	.000	.000
94	-.816-01	.000	-.268-01
95	.000	.000	.000
96	-.189-03	.000	.682-01
97	.000	.000	.000
98	.000	.000	.000
99	-.153-01	.000	.679-01
100	.000	.000	.000
101	-.312-01	.000	.653-01
102	.000	.000	.000
103	.000	.000	.000
104	-.468-01	.000	.549-01
105	.000	.000	.000
106	-.581-01	.000	.350-01
107	.000	.000	.000
108	.000	.000	.000
109	-.637-01	.000	.203-01
110	.000	.000	.000

MODE NO 4 LINEAR DISPLACEMENTS

NODE	DX	DY	DZ
111	-.672-01	.000	.120-01
112	.000	.000	.000
113	.000	.000	.000
114	-.230-03	.000	.933-01
115	.000	.000	.000
116	-.187-01	.000	.879-01
117	.000	.000	.000
118	-.309-01	.000	.686-01
119	.000	.000	.000
120	-.499-01	.000	.529-01
121	.000	.000	.000
122	-.559-01	.000	.319-01
123	.000	.000	.000
124	.233-03	.000	.109+00
125	.000	.000	.000
126	.000	.000	.000
127	-.567-02	.000	.107+00
128	.000	.000	.000
129	-.988-02	.000	.102+00
130	.000	.000	.000
131	.000	.000	.000
132	-.140-01	.000	.906-01
133	.000	.000	.000
134	-.187-01	.000	.801-01
135	.000	.000	.000
136	.000	.000	.000
137	-.383-01	.000	.696-01
138	.000	.000	.000
139	.000	.000	.000
140	-.409-01	.000	.591-01
141	.000	.000	.000
142	-.433-01	.000	.468-01
143	.000	.000	.000
144	.000	.000	.000
145	.182-03	.000	.118+00
146	.000	.000	.000
147	-.601-02	.000	.109+00

MODE NO 4 LINEAR DISPLACEMENTS

NODE	DX	DY	DZ
148	.000	.000	.000
149	-.111-01	.000	.915-01
150	.000	.000	.000
151	-.236-01	.000	.858-01
152	.000	.000	.000
153	-.277-01	.000	.810-01
154	.000	.000	.000
155	-.296-04	.000	.122+00
156	.000	.000	.000
157	.000	.000	.000
158	-.138-02	.000	.120+00
159	.000	.000	.000
160	-.311-02	.000	.114+00
161	.000	.000	.000
162	.000	.000	.000
163	-.516-02	.000	.106+00
164	.000	.000	.000
165	-.748-02	.000	.951-01
166	.000	.000	.000
167	.000	.000	.000
168	-.915-02	.000	.834-01
169	.000	.000	.000
170	-.109-01	.000	.727-01
171	.000	.000	.000
172	.000	.000	.000
173	-.535-04	.000	.917-01
174	.000	.000	.000
175	.109-01	.000	.878-01
176	.000	.000	.000
177	.197-01	.000	.774-01
178	.000	.000	.000
179	.238-01	.000	.668-01
180	.000	.000	.000
181	-.450-05	.000	.993-02
182	.000	.000	.000
183	.000	.000	.000
184	.848-02	.000	.967-02

MODE NO 4 LINEAR DISPLACEMENTS

NODE	DX	DY	DZ
185	.000	.000	.000
186	.166-01	.000	.935-02
187	.000	.000	.000
188	.000	.000	.000
189	.243-01	.000	.888-02
190	.000	.000	.000
191	.309-01	.000	.859-02
192	.000	.000	.000
193	.000	.000	.000
194	.362-01	.000	.822-02
195	.000	.000	.000
196	.404-01	.000	.781-02
197	.000	.000	.000
198	.000	.000	.000
199	-.933-05	.000	-.739-01
200	.000	.000	.000
201	.112-01	.000	-.716-01
202	.000	.000	.000
203	.206-01	.000	-.652-01
204	.000	.000	.000
205	.262-01	.000	-.574-01
206	.000	.000	.000
207	-.201-04	.000	-.109+00
208	.000	.000	.000
209	.000	.000	.000
210	.139-03	.000	-.108+00
211	.000	.000	.000
212	.252-03	.000	-.104+00
213	.000	.000	.000
214	.000	.000	.000
215	.564-03	.000	-.102+00
216	.000	.000	.000
217	.840-03	.000	-.965-01
218	.000	.000	.000
219	.000	.000	.000
220	.137-02	.000	-.917-01
221	.000	.000	.000
222	.186-02	.000	-.863-01
223	.000	.000	.000
224	.000	.000	.000

Appendix IV

Atomiser type 22

Aluminium *Stainless steel*

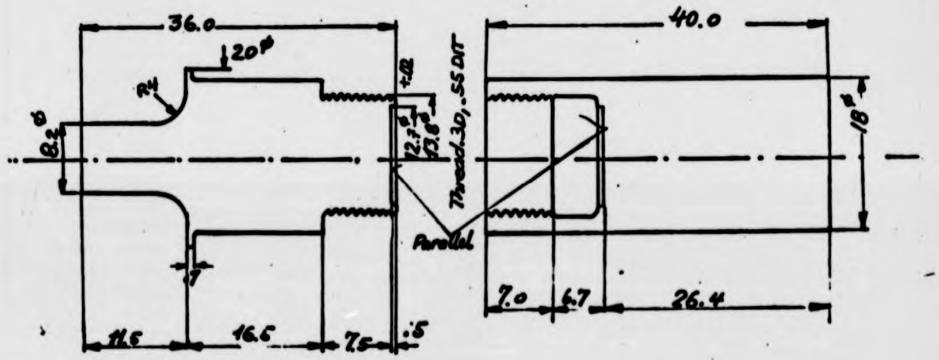

M 2:1
±.05 (±.02)

Some of the transformers investigated

Appendix IV

Atomiser type 22

Aluminium *Stainless steel*

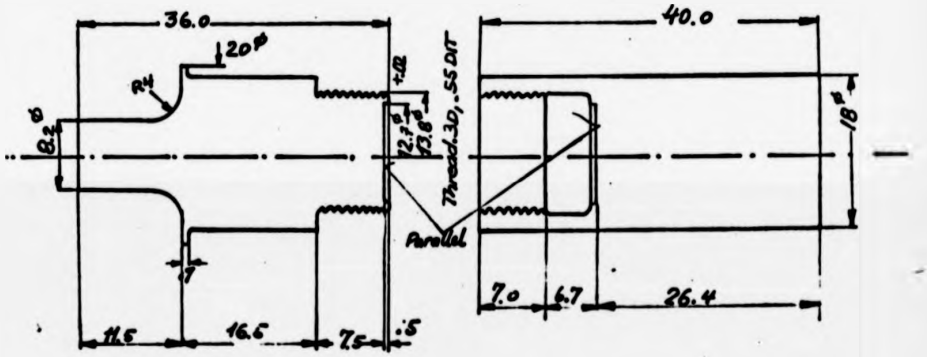

M 2:1
±.05 (±.02)

Some of the transformers investigated

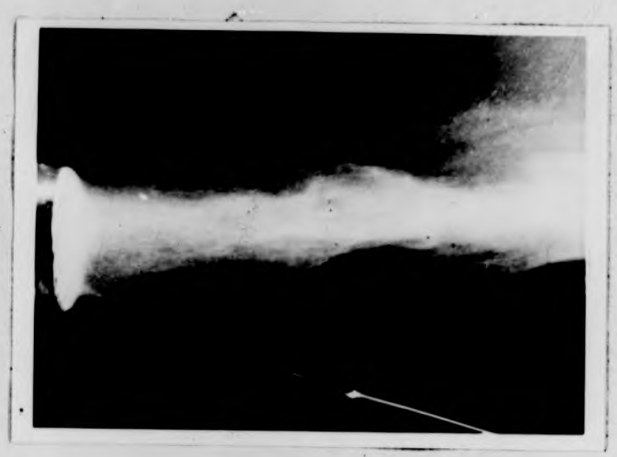

Atomiser working at low power (input approx. 2 W)

Atomiser working with large amplitude (input approx. 6 W)

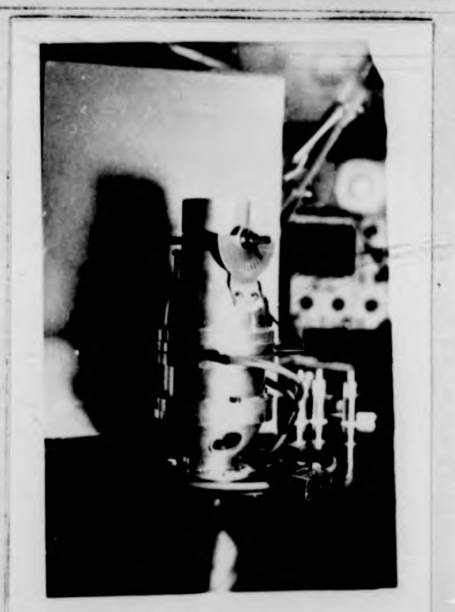

Ultrasonic Carburettor

Atomiser working at low power (input approx.2 W)

Atomiser working with large amplitude (input approx.6 W)

Ultrasonic Carburettor

Appendix V

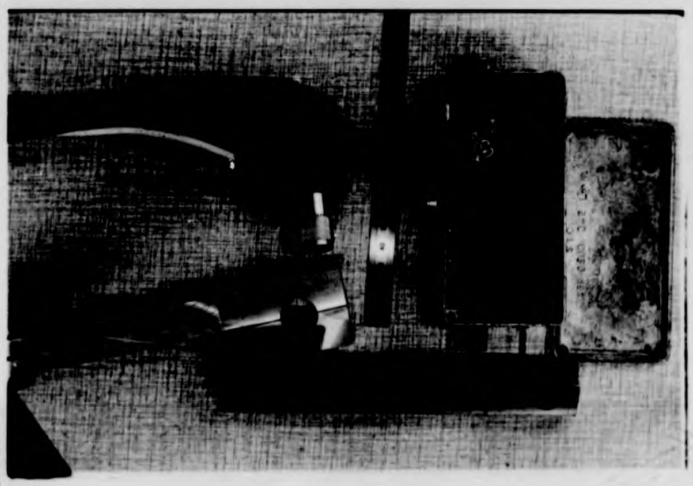

Drive unit and tool used for the assembly of atomisers. Left: adaptor to measure current/voltage to transducer

Instruments used for development of ultrasonic atomisers

1) Power amplifier
2) VAMMISE
3) Video oscillator
4) Impedance meter
5) Oscilloscope
6) Frequency counter
7) power supply
8) R-L-C meter
9) Calculator
10) Experimental manifold

Appendix V

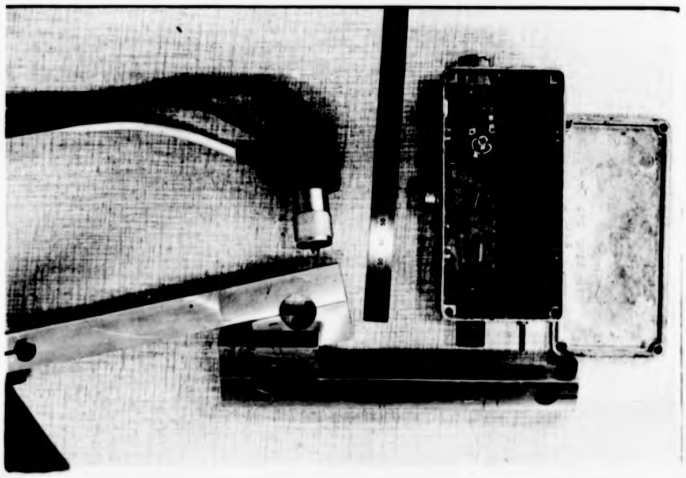

Drive unit and tool used for the assembly of atomisers. Left: adaptor to measure current/voltage to transducer

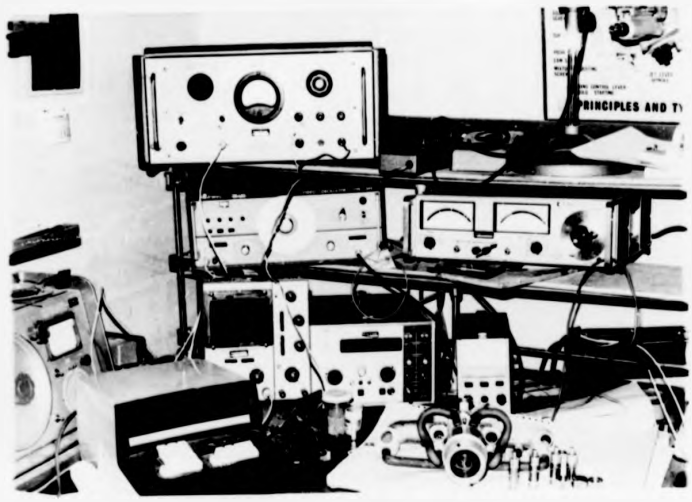

Instruments used for development of ultrasonic atomisers

1) Power amplifier
2) VAMMISE
3) Video oscillator
4) Impedance meter
5) Oscilloscope
6) Frequency counter
7) power supply
8) R-L-C meter
9) Calculator
10) Experimental manifold

Appendix VI

TEST WITH CARBURETTOR — Table 1

	POWER				TEMP					CONSUMPTION				A/F	EMISSIONS						
NO	Rev	mV	Nm	kW	INL	Ex	p_m	IGN	γ_A	Fuel/time	kg/h	Air cm	kg/h		CO	%	CO_2	%	NO	HC	Rema.
1	1100	0	0	0	25	520	14	2	1.17	93/227	1.11	3.2	14.5	13.0	13	2	39.5	11.5	100	690	
2	1100	30	25	2.9	29	540	9	12	1.15	93/151	1.66	5.5	25.0	15.0	2.5	0.5	40.0	12	900	580	
3	1100	60	48.5	5.6	31	600	0	16	1.14	93/109	2.3	8.5	36.7	15.9	1.0	0.25	39.5	11.7	1800	490	
4	1100	100	80	9.25	33	600	0	17	1.13	93/68	3.7	10.4	44.7	12.1	28.0	5	38	10.2	500	1140	
5	1500	0	0	0	34	580	14	10	1.13	93/170	1.48	4.6	19.4	13.1	18.0	2.5	39	11.0	380	710	
6	1500	40	32	5.12	34	610	8	30	1.13	93/97	2.58	9.0	38.17	14.8	2.3	0.4	40.5	12.5	2100	675	
7	1500	80	64	10.1	35	620	0	25	1.13	93/63	3.98	12.2	51.7	13.0	19	3.2	40	12	1300	980	
8	1500	100	80	12.6	33	600	0	20	1.13	93/44	5.71	14.5	61.5	10.8	38	7.5	36.5	9.3	420	1370	
9	2000	0	0	0	34	660	14	22	1.13	93/151	1.66	5.8	24.6	14.8	3.2	0.55	40	12	150	156	
10	2000	40	32.5	6.83	34	650	6	36	1.13	93/68	3.69	13.4	56.8	15.4	2.5	0.5	40	12	1000	660	
11	2000	80	64	13.4	34	660	0	28	1.13	93/40	6.28	17.8	75.5	12.0	30	3	38.5	10.6	660	1170	
12	2000	130	104	21.8	35	650	0	26	1.13	93/31.5	7.97	20.6	87.6	11.0	40	8.2	36.5	9.3	420	1630	
13	2500	0	0	0	36	690	14	28	1.13	93/133	1.89	6.7	28.7	15.2	3.0	0.5	40	12	125	140	
14	2500	40	32.5	8.53	36	680	9	40	1.13	93/65	3.85	14.1	59.8	15.5	3.5	0.6	40.5	12.5	1300	590	
15	2500	80	64	16.8	36	710	2	37	1.13	93/39	6.44	20.2	84.9	13.1	19	3.2	40.5	12.5	1700	950	
16	2500	120	95	25.0	38	700	0	30	1.10	93/27	9.3	26	107.1	11.5	33	6.5	38	10.2	900	1290	
17	3000	0	0	0	38	700	14	43	1.10	93/106	2.37	8.73	36.0	15.2	2.2	0.4	40	12	260	328	
18	3000	40	32.5	10.2	37	700	9	45	1.10	93/56	4.48	16.6	67.8	15.1	30	0.5	40	12	800	355	
19	3000	80	64	20.1	37	750	2	40	1.10	93/37	6.8	22.9	93.5	13.8	8.5	1.2	41.5	13.2	1700	330	
20	3500	0	0	0	40	750	14	45	1.11	93/94	2.67	10.1	41.5	15.5	4.5	0.75	40.5	12.7	250	232	
21	3500	40	32.5	11.95	40	765	9	46	1.11	93/49	5.12	19.1	78.3	15.3	3.0	0.5	41	12.7	850	250	
22	3500	75	60	22.0	40	790	2	43	1.11	93/32	7.85	26.6	109.1	13.9	6.5	1.0	41	12.7	3500	690	
23	3000	86	68.5	17.6	37	720	2	40	1.12	93/31	8.10	4.58	95.0	11.8	5.5	0.8	41.	13	3000	740	
24	3000	140	120	32.1	39	730	0	34	1.11	93/24	10.5	6.10	124.1	11.8	30	5.6	38.5	10.7	1100	1070	
25	3500	120	95	34.9	41	760	0	35	1.1	93/20	12.56	7.46	149.6	11.9	32	6.0	39	11	900	1030	
26	4000	0	0	0	42	790	0	50	1.10	93/73	3.44	2.56	51.3	14.9	6.5	1.0	39.5	11.5	300	280	
27	4000	40	32.5	13.7	43	780	8	50	1.10	93/36	6.97	5.3	106.2	15.2	3.5	0.6	405	12.5	2750	290	
28	4000	87	69	29	37	750	0	50	1.12	93/20.5	12.1	7.67	156.3	13.0	30	5.5	39	11	1100	1030	
29	4000	58	46.5	19.5	39	720	8	50	1.10	93/37	6.79	5.0	100.9	14.9	3	0.5	41	12.7	2600	270	

ULTRASONIC CARBURETTOR

	POWER				TEMP					CONSUMPTION				A/F	EMISSIONS						
NO	Rev	mV	Nm	kW	INL	Ex	p_m	IGN	γ_A	Fuel/time	kg/h	Air cm	kg/h		CO	%	CO_2	%	NO	HC	Rema
30	1100	60	48	5.5	32	600	2	16	1.13	93/130	1.93	7.8	33.2	17.2	1.0	0.25	38	10.5	450	425	
31	1100	100	80	9.2	33	620	0	17	1.13	93/ 89	2.82	10.0	42.6	15.1	6	1.0	40	12.5	2100	590	
32	1100	100	80	9.2	33	620	0	17	1.13	93/ 92	2.73	10.8	46.0	16.8	1.0	0.25	39	11.0	1900	490	
33	1100	120	95	11.0	36	610	0	12	1.12	93/ 70	3.59	11.7	48.5	13.5	17	2.4	39	11	1300	850	
34	1100	0	0	0	38	500	14	4	1.1	93/250	1.0	3.2	13.2	13.2	1.0	0.25	38	10.5	50	390	
35	1100	0	0	0	38	500	14	4	1.1	93/262	0.96	3.2	13.2	13.7	2.0	0.4	38	10.5	100	355	
36	1500	45	36	5.7	35	575	8	30	1.14	93/118	2.13	7.77	32.9	15.5	1.0	0.25	39	11	900	460	
37	1500	85	67.5	10.7	34	610	1.0	25	1.13	93/ 75	3.35	11.2	47.5	14.2	7.0	1.0	40	12	2200	670	
38	1500	120	95	15.6	34	580	0	25	1.13	93/ 37	6.8	1544	65.5	9.6	30	5.5	35	8.2	600	1350	
39	2000	50	40	8.4	35	680	7	25	1.13	93/ 73	3.44	12.8	53.6	15.6	4	0.6	38.5	10.7	880	310	
40	2000	0	0	0	36	650	14	19	1.12	93/145	1.73	5.43	22.9	13.2	5.5	0.8	38	10.4	120	390	
41	2000	0	0	0	23	640	14	22	1.17	93/115	2.18	3.51	31.7	14.5	30	0.5	37	97	150	500	
42	2000	40	33	6.95	28	670	8	36	1.15	93/ 74	3.4	5.8	51.5	17.0	1.0	0.2	35.5	8.2	700	350	
43	2000	130	105	22.1	33	660	0	35	1.13	93/ 30	8.3	10.2	87.5	10.5	8	1.1	35.5	8.2	1800	770	
44	2500	70	57	15	35	750	6	28	1.13	93/ 58	4.33	8.3	71.1	16.4	3.5	0.6	36	9.0	700	280	
45	3000	60	48	15.1	37	750	0	40	1.12	93/ 40	6.28	12.0	100.3	15.9	5.0	0.75	38	10.4	700	225	
46	3000	0	0	0	34	750	14	40	1.13	93/ 82	3.06	4.6	39.2	12.8	8	1.2	40	12	150	300	
47	3500	40	33	12.2	32	800	0	35	1.14	missing	-	-	-	-	15	0.25	37	9.7	200	705	
48	3500	0	0	0	37	800	14	40	1.12	93/ 80	3.14	6.3	53.1	16.9	1.0	0.25	38	10.5	120	600	
49	3500	50	40	14.7	37	800	8	45	1.12	93/ 47	5.34	10.5	89.0	16.6	1.0	0.25	38	10.5	500	195	
50	1500	110	17.5	32.5	41	820	0	35	-	missing	-	-	-	-	30	5.0	35	8.2	1200	415	
51	3500	110	17.5	32.2	42	800	0	35	1.1	93/ 20	12.5	18.8	155	12.4	7.5	1.1	40	12	1600	1200	
52	1000	56	45	19	43	800	6	50	1.1	93/30.5	8.2	12.7	103.2	12.5	13	2.0	40	12	1000	500	
53	1500	0	0	0	24	620	14	20	1.17	93/145	1.73	2.8	25.5	14.7	1.0	0.25	37	9.7	110	170	
54	2500	0	0	0	29	700	26	30	1.15	93/120	2.1	3.8	33.7	16.0	1.0	0.25	37.5	10	140	280 350	
55	2500	134	107.5	28.0	32	750	0		1.14	93/ 30	8.37	13.3	114.9	13.7	15	2.5	38.5	11	2500	580	
56	4000	0	0	0	31	800		-	1.14	93/ 65	3.86	5.86	51.1	13.2	3	0.5	40	12	150	280	
57	2500	0	0	0	30	-	-	-	1.14	93/140	1.79	3.5	30.6	17.1	1.0	0.25	37	9.7	110	705	
58	4000	90	71.5	30	35	820	-	-	1.13	93/ 21	11.9	19.5	162	13.6	50	0.75	-	-	3000	355	
59	4000	124	97.5	41	35	-	-	-	-	missing	-	-	-	-	-	-	-	-	2800	460	

IDLE, ORIGINAL ADJUSTMENT OF CARBURETTOR

	POWER				TEMP					CONSUMPTION				A/F	EMISSIONS						
NO	Rev	mV	Nm	kW	INL	Ex	p_m	IGN	γ_A	Fuel/time	kg/h	Air cm	kg/h		CO	%	CO_2	%	NO	HC	Remark
60	1100	0	0	0	25	520	14	2	1.17	93/227	1.1	3.2	14.5	14.5	13	2	39.5	11.5	100	690	
61	1000	0	0	0	33	560	13	2	1.19	93/248	1.0	7.3	16.0	15.8	1.5	0.25	39.0	11.0	110	670	
62	1250	0	0	0	33	600	12	4	1.15	93/198	1.27	4.6	20.0	15.7	1.4	0.25	37.5	11	100	920	
63	1500	0	0	0	34	580	14	10	1.13	93/170	1.48	4.6	19.4	13.1	18.0	2.5	39	11	380	710	
64	1500	0	0	0	34	640	13	10	1.14	93/175	1.44	5.7	24.4	16.9	1.4	0.25	34.5	8	140	1950	
65	2000	0	0	0	34	660	14	22	1.13	93/151	1.66	5.8	24.6	14.8	3.2	0.55	40.0	12	150	156	
66	2500	0	0	0	36	690	14	28	1.13	93/133	1.89	6.7	28.7	15.2	3.0	0.5	40	12	125	140	
67	3000	0	0	0	38	700	14	43	1.1	93/106	2.37	8.73	36.0	15.2	2.2	0.4	40	12	260	328	
68	3500	0	0	0	40	750	14	45	1.11	93/ 94	2.67	10.1	41.5	15.5	4.5	0.75	40.5	12.7	250	232	
69	4000	0	0	0	42	790	0	50	1.1	93/ 73	3.44	2.56	51.3	14.9	6.5	1.0	39.5	11.5	300	280	
70	1500	0	0	0	34	620	14	10	1.13	93/175	1.44	5.2	22.7	15.5	2.0	0.3	35.0	9.2	150	700	

IDLE ULTRASONIC CARBURETTOR

71	1100	0	0	0	38	500	14	4	1.1	93/262	0.96	3.2	13.2	13.7	2.0	0.4	38	10.5	100	355	
72	1500	0	0	0	24	620	14	20	1.17	93/145	1.73	2.8	25.5	14.7	1.0	0.25	37	9.7	110	170	
73	2000	0	0	0	23	640	14	22	1.17	93/115	2.18	3.51	31.7	14.5	3.0	0.5	37	9.7	150	500	
74	2500	0	0	0	29	700	26	30	1.15	93/120	2.1	3.8	33.7	16.0	1.0	0.25	37.5	10	140	280 350	
75	3000	0	0	0	34	750	14	40	1.11	93/ 82	3.06	4.6	39.2	12.8	8	1.2	40	12	150	300	
76	3500	0	0	0	37	800	14	40	1.12	93/ 80	3.14	6.3	53.1	16.9	1.0	0.25	38	10.5	120	600	
77	4000	0	0	0	31	800			1.14	93/ 65	3.86	5.86	51.1	13.2	3	0.5	40	12	150	280	
78	1200	0	0	0	36	620	11	6	1.12	93/198	1.27	9.4	20	15.7	1.0	0.2	39	13	150	183	
79	900	0	0	0	36	520	10	4	1.12	93/296	0.85	5.8	12.1	14.7	0.5	0.1	36.5	9.2	50	374	

IDLE: ORIGINAL CARBURETTOR ADJUSTED FOR LOW CO AND HC EMISSION AT EACH REV.

80	1100	0	0	0	30	500		5	1.15	93/217	1.1	5.7	13.1	11.5	2.0	0.3	39	13	100	443	
81	1900	0	0	0	32	700		16	1.14	93/146	1.7	10.9	24.9	14.5	3.0	0.5	40	14	120	200	
82	1400	0	0	0	33	620		7	1.14	93/205	1.2	8.1	18.5	15.4	2.0	0.3	39	13	120	199	
83	2800	0	0	0	33	730		36	1.14	93/115	2.15	14.4	32.9	15.3	2.0	0.3	39	13	200	177	
84	920	0	0	0	31	520		5	1.14	93/284	0.87	5.8	13.3	15.2	2.0	0.3	39	13	90	595	
85	1000	0	0	0	30	540		5	1.15	93/253	0.98	5.8	13.3	13.6	10/8	1.5 1.1	3.9	13	90	744	
86	1100	0	0	0	25	520		2	1.17	93/227	1.11	3.2	14.5	14.5	13	2	39.5	11.5	100	690	

IDLE, ORIGINAL ADJUSTMENT OF CARBURETTOR

	POWER				TEMP					CONSUMPTION				A/F	EMISSIONS						
NO	Rev	mV	Nm	kW	INL	Ex	p_m	IGN	γ_A	Fuel/time	kg/h	Air cm	kg/h		CO	%	CO_2	%	NO	HC	Remark
60	1100	0	0	0	25	520	14	2	1.17	93/227	1.1	3.2	14.5	14.9	13	2	39.5	11.5	100	690	
61	1000	0	0	0	33	560	13	2	1.15	93/248	1.0	7.3	16.0	15.8	1.5	0.28	39.0	11.0	110	670	
62	1250	0	0	0	33	600	12	4	1.15	93/198	1.27	4.6	20.0	15.7	1.4	0.25	37.5	11	100	920	
63	1500	0	0	0	34	580	14	10	1.13	93/170	1.48	4.6	19.4	13.1	18.0	2.5	39	11	380	710	
64	1500	0	0	0	34	640	13	10	1.14	93/175	1.44	5.7	24.4	16.8	1.4	0.25	34.5	8	140	1950	
65	2000	0	0	0	34	660	14	22	1.13	93/151	1.66	5.8	24.6	14.8	3.2	0.55	40.0	12	150	156	
66	2500	0	0	0	36	690	14	28	1.13	93/133	1.89	6.7	28.7	15.2	3.0	0.5	40	12	125	140	
67	3000	0	0	0	38	700	14	43	1.1	93/106	2.37	8.73	36.0	15.2	2.2	0.4	40	12	260	328	
68	3500	0	0	0	40	750	14	45	1.11	93/ 94	2.67	10.1	41.5	15.5	4.5	0.75	40.5	12.7	250	232	
69	4000	0	0	0	42	790	0	50	1.1	93/ 73	3.44	2.56	51.3	14.9	6.5	1.0	39.5	11.5	300	280	
70	1500	0	0	0	34	620	14	10	1.13	93/175	1.44	5.2	22.7	15.5	2.0	0.3	35.0	9.2	150	700	

IDLE ULTRASONIC CARBURETTOR

71	1100	0	0	0	38	500	14	4	1.1	93/262	0.96	3.2	13.2	13.7	2.0	0.4	38	10.5	100	355	
72	1500	0	0	0	24	620	14	20	1.17	93/145	1.73	2.8	25.5	14.7	1.0	0.25	37	9.7	110	170	
73	2000	0	0	0	23	640	14	22	1.17	93/115	2.18	3.51	31.7	14.5	3.0	0.5	37	9.7	150	500	
74	2500	0	0	0	29	700	26	30	1.15	93/120	2.1	3.8	33.7	16.0	1.0	0.25	37.5	10	140	280 350	
75	3000	0	0	0	34	750	14	40	1.13	93/ 82	3.06	4.6	39.2	12.8	8	1.2	40	12	150	300	
76	3500	0	0	0	37	800	14	40	1.12	93/ 80	3.14	6.3	53.1	16.9	1.0	0.25	38	10.5	120	600	
77	4000	0	0	0	31	800			1.14	93/ 65	3.86	5.86	51.1	13.2	3	0.5	40	12	150	280	
78	1200	0	0	0	36	620	11	6	1.12	93/198	1.27	9.4	20	15.7	1.0	0.2	39	13	150	183	
79	900	0	0	0	36	520	10	4	1.12	93/296	0.85	5.8	12.1	14.7	0.5	0.1	36.5	9.2	50	374	

IDLE: ORIGINAL CARBURETTOR ADJUSTED FOR LOW CO AND HC EMISSION AT EACH REV.

80	1100	0	0	0	30	500		5	1.15	93/217	1.16	5.7	13.1	11.5	2.0	0.3	39	13	100	443	
81	1900	0	0	0	32	700		16	1.14	93/146	1.72	10.9	24.9	14.5	3.0	0.5	40	14	120	200	
82	1400	0	0	0	33	620		7	1.14	93/205	1.2	8.1	18.5	15.4	2.0	0.3	39	13	120	199	
83	2800	0	0	0	33	730		36	1.14	93/115	2.15	14.4	32.9	15.3	2.0	0.3	39	13	200	177	
84	920	0	0	0	31	520		5	1.14	93/284	0.87	5.8	13.3	15.2	2.0	0.3	39	13	90	595	
85	1000	0	0	0	30	540		5	1.15	93/253	0.98	5.8	13.3	13.6	10/8	1.5 1.1	3.9	13	90	744	
86	1100	0	0	0	25	520		2	1.17	93/227	1.11	3.2	14.5	14.5	13	2	39.5	11.5	100	690	

TIGHTLY
BOUND
COPY

IDLE ULTRASONIC ATOMISERS IN INLET MANIFOLD

	POWER				TEMP					CONSUMPTION				A/F	EMISSIONS						
NO	Rev	mV	Nm	kW	INL	Ex	p_m	IGN	γ_A	Fuel/time	kg/h	Air cm	kg/h		CO	%	CO_2	%	NO	HC	Remark
87	1000	0	0	0	28	550		5	1.16	93/156	1.58	10.5	24.5	15.5	0.5	0.1	38	12	80	210	
88	2000	0	0	0	28	750		16	1.16	93/137	1.8	11.5	24.3	13.5	0.5	0.1	39	13	100	245	
89	2800	0	0	0	26	740		36	1.17	93/116	2.13	6.1	28.6	13.4	0.5	0.1	40	14	120	140	
90	2500	0	0	0	28	700		26	1.16	93/1262	1.95	5.5	25.6	13.1	0.5	0.1	39	13	120	56	
91	2500	0	0	0	29	740		36	1.16	93/1258	1.97	5.7	26.5	13.5	0.5	0.1	40	14	120	98	
92	1500	0	0	0	37	720		10	1.13	93/145	1.70	5.0	22.6	13.3	0.5	0.1	40	14	120	105	
93	3100	0	0	0	28	770		37	1.16	93/104	2.3	12.5	29.1	12.6	0.5	0.1	40	14	150	105	
LOAD ULTRASONIC ATOMISERS IN INLET MANIFOLD																					
94	2500			11.0	30	720		36	1.15	93/ 55	4.55	12.5	57.4	12.6	1.0	0.25	39	13	800	260	
95	2500			17.6	33	730		36	1.14	93/ 41	6.05	18.5	84.0	13.9	1.0	0.25	38	12	900	245	
96	2500	0	0	0	29	740		36	1.14	93/1258	1.97	5.7	26.5	13.5	0.5	0.1	40	14	120	98	
97	2500			14.3	31	750		36	1.14	93/ 59	4.2	13	59.5	14.1	1.0	0.25	40	14	1200	105	
98	2500			6.0	30	700		36	1.15	93/ 88	2.85	8.5	39.0	13.7	1.0	0.25	40	14	1300	175	
99	2000			7.0	35	-		25	1.13	93/ 73	3.4	13.4	60.5	17.5	1.0	0.25	36.2	9.5	300	210	
100	2000			14.2	35	680		25	1.13	93/ 47	5.3	14.5	65.6	12.4	1.25	0.3	38	12	1700	420	
101	2000			11.0	36	-		25	1.13	93/ 53	4.7	14.5	65.6	14.0	5.2	0.8	39	13	1500	120	
102	3000			10.9	36			40	1.13	93/ 57	1.35	16.0	72.5	16.6	3.0	0.5	38	12	1500	420	